The University of Sheffield
Department of Chemical and Biological Engineering

Mechanisms of food powder dispersion in an aqueous medium

W. Robert Mitchell

Thesis submitted in partial fulfillment of the requirements for the degree of Doctor of Philosophy

August 2015

Vorrei dedicare questa tesi alla mia nonna.

Abstract

Poor powder reconstitution is a major obstacle facing the food industry – if a powder does not rehydrate quickly and completely, it may be rejected by the consumer. Unfortunately, the mechanisms driving these dispersion phenomena are poorly understood; thus, an improved understanding may be key to the development of innovative solutions to reconstitution-related problems.

In the current study, a novel reconstitution rig was developed, consisting of a transparent stirred vessel, a video camera, and an FBRM (Focused Beam Reflectance Measurement) probe, which allows for an in-depth analysis of powder reconstitution, regardless of powder type. All steps of reconstitution (i.e. wetting/sinking, dispersing, and dissolving), can be observed as separate physical phenomena, and a new concept was proposed, i.e. that one step of reconstitution can be "rate-limiting."

Experiments were performed using a range of powders (different types of maltodextrin, dairy, and cocoa powders), under a wide range of conditions.

- In the first experimental chapter (Ch. 9), based on the total particle counts from FBRM measurements plotted over time, a novel kinetic hypothesis and model is presented, which is valid for completely water-soluble powders (e.g. maltodextrin) under good dissolution conditions. This model is capable of describing both the dispersing and dissolving of particles, as separate yet simultaneous phenomena, under various mixing conditions.
- In the second experimental chapter (Ch. 10), a mapping approach to describing the "rate-limiting regimes" of reconstitution is presented – this approach is also applicable

for conditions under which the aforementioned model (from Ch. 9) is invalid. Using maltodextrin (an amorphous polymer) as a model material, maps are constructed at different combinations of water temperature and impeller agitation speed, based on video recordings of the transparent vessel during reconstitution.

Using different types of maltodextrins, the influence of molecular weight and particle size, as well as temperature and agitation, is investigated. It was found that problems such as the formation of lumps and floating layers were most likely to occur for powders with a high molecular weight and small particle size; these problems could be mitigated by increasing the size via agglomeration. However for low-molecular weight powders, size enlargement did not have a large influence on dispersion behavior.

By equilibrating maltodextrin (a powder for which solid-phase crystallization is not an issue) to different water activities, it was determined that *increasing* water activity improved reconstitution. The results are in agreement with Dupas (2012) but contradict the logic of Marabi et al. (2007).

- In Ch. 11, similar regime maps are constructed for more complex, colloid-forming materials (cocoa and milk powders), with the camera being used to quantify the sinking time, and the FBRM sizing capabilities are used to describe dispersing quality. "Regime maps" are constructed in order to determine the influence of water temeprature, agitation rate, fat content (for milk) and lecithination (for cocoa).

  Results reveal that the water temperature *relative to the fat melting temperature* was of utmost importance in determining the *sinking rate*, as well as overall reconstitution. Results are not in agreement with the discussion of Marabi et al. (2008b). In fact, at temperatures above the fat melting temperature, powders with *greater* amounts of fat were faster to sink and reconstitute overall.

  Surprisingly, an increase in temperature was not always beneficial for powders. For instance for whole milk powder, under slow mixing, a high temperature led to the formation of lumps that were difficult to disperse – this is likely related to heat-induced damage of certain foodstuffs.

  In general, lecithination did help with particle dispersing; this may be due to greater electrostatic double layer repulsion between particles upon sinking. However, surprisingly, lecithination did not always improve sinking and overall reconstitution. For high temperatures (and low mixing rates), sinking was actually worse for the *lecithinated* powder. This may be due to imbibition and swelling taking place too quickly relative to dispersing effects.

In addition, it was discovered that by applying a heat treatment to the powders (above the fat melting temperature) and allowing the powders to cool before reconstitution, sinking (and overall reconstitution) was improved at 25 °C. Dispersion *at the liquid surface* was also better at lower fat content, and if a lecithination treatment was applied.

- In Ch. 12, the influence of various liquid properties is investigated. At increasing ionic strengths, *dispersing* was worse for milk and cocoa powders, related to colloidal phenomena, and *dissolving* was worse for maltodextrin, related to slower mass transfer. A decrease in surface tension was *worse* for particle sinking, due to reduced capillarity; results contradict the discussion by Schubert (1993), who mistakenly describe the theoretical behavior of food powders based on the physics of *single particles* rather than as porous beds. For viscosity experiments, powders were dissolved in solutions of the same material at increasing concentrations. Above a critical concentration, poor sinking occurs – this may be due to *both* wettability and viscosity effects.
- In Ch. 13, the effect of the vessel configuration is studied. For equivalent power draw, baffled conditions were consistently worse for reconstitution compared to unbaffled configurations – this was due to either sedimentation or floating problems, depending on the powder type. Comparing the Lightnin A100 vs. R100 impellers (axial vs. radial, respectively), R100 was slightly better than A100 at dispersing powders, for equivalent power draw. Positioning the impeller closer to the liquid surface, at the same agitation rate, improved powder downdraw for hard-to-sink powders. Scale-up criteria that best preserved reconstitution behavior depended on the "rate-limiting regime" of reconstitution. For sinking-limited behavior, constant tip speed was better; for dispersing-limited conditions, specific power draw was better. The results are explained based on the effects on the mixing characteristics upon scale-up.

Based on the empirical results, mechanisms of dispersion are proposed, taking into consideration principles from food chemistry, process engineering, material science, colloid technology, and fluid mechanics. It is believed that the results from the current study will help improve the understanding of food powder reconstitution fundamentals, allowing for a more targeted and effective product and process development in the industry.

Acknowledgments

I would like to start by thanking my primary supervisor, Prof Agba Salman. Agba, I can't express enough how grateful I am for having had the privilege of being part of your group, and for all of the opportunities I've had and skills I've learned while at Sheffield. I cannot think of a better or more appropriate place to have carried out this project, and I hope to stay in close contact in the years to come!

A huge « merci » also goes to Dr Laurent Forny (Nestlé Research Center, Lausanne), who was essential in establishing this collaboration, and helped develop my skills necessary for studying material science and powder technology. Thank you for all of the guidance over the past few years!

Next I would like to say „Danke" to Dr Tim Althaus (Nestlé Headquarters, Vevey) for the extremely helpful mentoring throughout the project. Thanks for the discussions regarding transport phenomena, rheology, and dimensional analysis, and for the advice regarding project management and written communication in general. It has been a pleasure working with you!

Thanks also goes to my secondary supervisor, Prof Mike Hounslow (Pro Vice Chancellor, Engineering Department). Thank you for taking time out of your (unbelievably) busy schedule to meet with me, and for showing me the fundamentals of mathematical modelling.

I also have to thank Prof Stefan Palzer (Nestlé Headquarters, Vevey & University of Sheffield Visiting Staff) for recruiting me for the PhD project, and for all of the discussions related to the subject. I admire how you are able to maintain such a strong presence in the academic community, and I am grateful that you take the time to recruit and develop young

professionals such as myself!

Thanks also goes to Dr Gerhard Niederreiter (Nestlé Research, Orbe) for helping to establish the Nestlé External Alliance with Sheffield, and for ensuring that I always had the proper training, funding, and equipment needed to make this project a success.

In addition to my supervisors, there were many other people at Nestlé and the University of Sheffield who helped me along the way. Thanks goes to Dr Marco Ramaioli, Dr Julien Dupas, and Dr Lennart Fries for discussions on material science fundamentals related to reconstitution. In addition, thanks to Dr Mauro Cavinato for the discussions on FBRM usage, and Dr Alessandro Gianfrancesco for the conversations on how drying parameters can affect particle properties. At Sheffield, I'd like to thank Dr Martin Pitt for his thought-provoking discussions, and for the entertaining lectures on chemical engineering concepts. Also a huge thanks to Dr Josselin Noirel for coaching me on Mathematica, and for answering, "literally" like a *Brazillion* questions about LaTeX.

Thanks to the post-docs in the Particle Products Group: Dr Kate Pitt and Dr Ranjit Dhenge, for the fruitful discussions, and for keeping the labs up and running. I really enjoyed working with both of you, in particular during the preparation of the 2013 and 2015 Granulation Workshops!

I'd also like to thank all of my fellow PhD students in the Particle Products Group for making Sheffield such a great place to work. In particular I have to thank Dine and Alê (Dr Christine Haider and Dr Alessandra Negreiros), who became a sort of "family" away from home, at least until they abandoned me during my final year! :-P Your positive energy is really contagious, and the number of inside jokes we have is incredible... if only there were some sort of dictionary.... Also a huge thanks to Syed Islam for always providing an extra set of hands when I needed help in the lab – thanks for being such a great colleague and friend! Thanks also to James, Washino, Ei Leen, Vikram, and Xavier for the good times during my first year, and to Chalak, Menan, Arthi, Mohammed, Sushma, Riyadh, William, Jian Kai, and Qing for being great coworkers during my second and third years – I will miss working with all of you! To the new students that started during my frantic write-up phase, it was great to meet you and best of luck! Thanks also goes to my two MEng students: Busayo Onasile and Wei Kang Tam. It was really a privilege to mentor you during your final year

projects, and I learned so much from having students of my "own" for the first time!

Possibly the people that deserve the most credit for this project actually being feasible is the technical staff at Sheffield. You guys are not only extremely competent and helpful, but also hilarious to work with. In particular thanks to Usman, Oz, and Mark for all of the help with computer/software-related issues, and Andy, Stuart, and Adrian for workshop-related requests, in particular for constructing the reconstitution vessel that was a central aspect of this project. Thanks to the PGR tutors: Dr Jags Pandhal and Dr Alan Dunbar for their support in keeping me on track for the PhD. Thanks also goes to the support staff in the Department of Chemical and Biological Engineering: cheers to Rhian and Nathalie for help in finance & procurement, and Marine, Deborah, Maria for the administrative support within the university. Thanks also to Dr Peng Zeng at the Kroto SORBY Center for the SEM training sessions!

In addition to the support I've had on my project itself, I have to thank my friends I've made in Sheffield for making my 3 years in England brilliant. In particular, a huge thanks to Sam, Laura, Ben, Lauren, Jane, Jordan, Gill, Danielle, Andrew, David, Sofía, Diana, Liz, Joe, Stephen, Katie, Nathan, Tom, Anna, Archer, Wes, Jake, Dan, Rachel, Becky, Emily, and everyone else – I will be back to visit as often as possible! Especially to those of you in my office during my final year, I don't think I'll ever have a more hilarious work environment ever again.

Thanks also to Nestlé Research for funding the current project as an External Alliance. I truly believe that such collaborations are extremely beneficial, both from a people development and innovation point-of-view, and I hope that similar projects will continue to exist in the future. Thanks also go to my current colleagues at Nestlé PTC Orbe in Switzerland for their flexibility during the final stages of the thesis submission!

Lastly, I have to thank my mom for all of her love and support. Thank you for putting up with me being so far from home, for adopting my dog when I moved to Europe, for helping pay for the (unbelievably expensive) flights back to the US, and for always being there for me my whole life, no matter what. You are truly an inspiration, and I don't know where I'd be without you.

Preface

The most exciting phrase to hear in science, the one that heralds new discoveries, is not "Eureka!" but "That's funny . . . "

Isaac Asimov

Powders are ubiquitous in the food industry for a number of reasons. When liquid foods are dehydrated, the volume is greatly reduced, facilitating transport and storage, and the reduction in water activity enhances the stability against degradative processes (Palzer et al., 2012). Food powders can be marketed directly to the consumer, they are often used on an industrial scale as ingredients (e.g. in Ready-to-Drink beverages), and they can be utilized in 'convenience' applications, e.g. in capsules or vending. Particularly in developing countries or for disaster-relief purposes, powdered, shelf-stable food is vital due to compromised local infrastructure necessary for quick food transport.

Prior to usage, food powders are (generally) reconstituted in an aqueous medium. However, these powders are not always easy to rehydrate, and thus the ease of reconstitution is one of the most important quality indicators of such powders (King, 1966). Problems like lump formation are not only frustrating to consumers, but can also cause problems on an industrial scale, for instance due to non-uniform heat transfer, improper dosing, pipe blockage or fouling, as well as serving a hurdle to the commercial launch of novel powdered products. According to Palzer (2013), such problems can also engender hygiene and safety concerns; food stuck to equipment surfaces could result in microbial growth if not properly cleaned, and lump

formation, particularly for infant formula, could pose a choking hazard. Food waste concerns may also be addressed (e.g. in capsule applications) if better dispersion can be achieved. Similar problems related to reconstitution are by no means limited to foods either; similar issues are also faced by the pharmaceutical, chemical, detergent, and paint industries, among others.

Such problems are also difficult to fix, partly because of a lack of fundamental understanding of the *mechanisms* of food powder dispersion. Studying such mechanisms is also challenging, due to the vast amount of complexity involved, with regards to the biochemical nature of foods, transport processes during reconstitution, interactions between particles once submerged, and mixing considerations. Moreover, in the author's opinion, the literature on the subject is insufficient – the analytical techniques used to study reconstitution have a number of flaws, and the vast range of food powders tested makes generalizations problematic. The current project was carried out in the framework of an alliance between Nestlé, the world's largest food, health and wellness company, and the Particle Products Group at the University of Sheffield, one of the leading particle research groups, well-known for its work on understanding and modeling particle behavior during processing. The main objects of the current study were to:

1. Dissect the literature on food powder reconstitution, focusing on the techniques used to monitor powder behavior, as well as the main conclusions of those studies.
2. Develop a novel analytical methodology that allows for studying *all* types of food powders and to monitor *all* of the main aspects of reconstitution.
3. Perform highly-controlled, carefully-selected experiments to better understand how variables related to the particles, liquid, and mixing affect reconstitution.
4. Challenge existing theories on the mechanisms of dispersion phenomena, and propose new explanations based on empirical results, taking into consideration the biochemical nature of foods, colloidal interactions, mechanical transport laws, and mixing characteristics.

The ultimate goal is to provide a knowledge foundation, based on which powder production and mixing operations can be improved.

Symbols and Acronyms

Greek symbols

Symbol	Meaning	Unit
γ	Surface Tension	$[\mathrm{N\,m^{-1}}]$
$\dot{\gamma}$	Shear Strain Rate	$[\mathrm{s^{-1}}]$
ϵ	Void Fraction	[-]
θ	Contact Angle	[°]
μ	Dynamic Viscosity	$[\mathrm{N\,s\,m^{-2}}]$
ν	Kinematic Viscosity	$[\mathrm{m^2\,s^{-1}}]$
π	3.14...	[-]
ρ	Density	$[\mathrm{kg\,m^{-3}}]$

Latin symbols

Symbol	Meaning	Unit
a_w	Water Activity	[-]
C	Concentration	$[\mathrm{mol\,m^{-3}}]$
d	Particle Size	[µm]
F	Force	[N]
g	Gravitational Acceleration	$[9.81\,\mathrm{m\,s^{-2}}]$
h'	Vortex Depth	[m]
k	Rate	(variable)
l	Height	[m]
m	Mass	[kg]
$\dot{m}$	Mass Feeding Rate	$[\mathrm{kg\,s^{-1}}]$
N	Impeller Agitation Speed	$[\mathrm{s^{-1}}]$
p	Pressure	$[\mathrm{N\,m^{-2}}]$
P	Power	[W]
r	Radius	[m]
t	Time	[s]
T	Temperature	[°C]
T_g	Glass Transition Temperature	[°C]
T_m	Melting Temperature	[°C]
v	Velocity	$[\mathrm{m\,s^{-1}}]$
v_p	Impeller Tip Speed	$[\mathrm{m\,s^{-1}}]$
v_{surf}	Particle Velocity at Liquid Surface	$[\mathrm{m\,s^{-1}}]$
V	Volume	$[\mathrm{m^3}]$

Acronyms

Acroynm	Meaning
db	Dry Basis
CMC	Critical Micellization Concentration
DE	Dextrose Equivalents
DLVO	Derjaguin, Landau, Verwey, Overbeek theory
DSC	Differential Scanning Calorimetry
EDL	Electrostatic Double Layer theory
ERT	Electrical Resistivity Tomography
FBRM	Focused Beam Reflectance Measurement
IDF	International Dairy Federation
IT	Instant (agglomerated maltodextrin)
LC	Lecithinated Cocoa
MW	Molecular Weight
NaCas	Sodium Caseinate
NMC	Native Micellar Casein
NMR	Nuclear Magnetic Resonance
NWPI	Native Whey Protein Isolate
NC	Non-lecithinated Cocoa
PSD	Particle Size Distribution
PVM	Particle Vision Microscope
RH	Relative Humidity
SEM	Scanning Electron Microscopy
SMP	Skim Milk Powder
USP	United States Pharmacopia
wb	Wet Basis
WMP	Whole Milk Powder
vdW	van der Waals interactions

Table of Contents

List of Tables

List of Figures

Part I

Literature Review

Chapter 1

Physics of Powder Reconstitution

Most studies on food powder reconstitution[1] divide this physical process into four more-or-less sequential steps (Fig. 1.1): wetting, sinking, dispersing, and dissolving (Forny et al., 2011). In the following four sections, these steps will be discussed in detail; the discussions to follow will be particularly useful when discussing the empirical results in subsequent chapters.

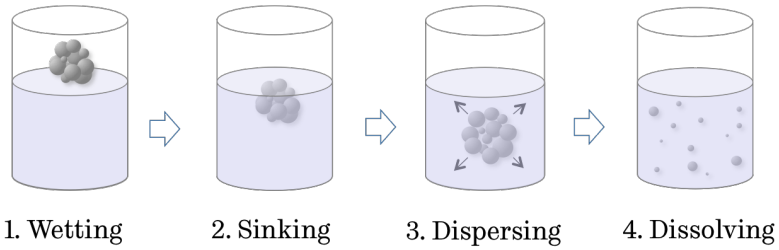

Figure 1.1: Four steps of reconstitution.

Contents

[1]The Merriam-Webster dictionary defines reconstitution, in this context, as: *"Returning (something, such as a dried food) to a former state by adding water."* Note that not all food powders originally exist in aqueous form (e.g. cocoa powders; § 6.3); nevertheless, this term is used throughout the current project to collectively refer to wetting, sinking, dispersing, and dissolving.

§1.1 Wetting

During the first step of reconstitution, the food powder comes into contact with an aqueous liquid in a process known as wetting. The ability of the liquid to adhere to the solid depends on the properties of both the liquid and the solid materials. For instance, water can more easily "wet" a hydrophilic substance than a hydrophobic surface, which has several implications during the production of food powders – as discussed in Chapter 2.

1.1.1 Adhesion & Cohesion

Wetting is driven by the interactions between molecules of the two phases coming into contact. As discussed in Israelachvili (2011), for this new surface to be formed, cohesive interactions within one phase must be displaced by adhesive interactions between the two phases.

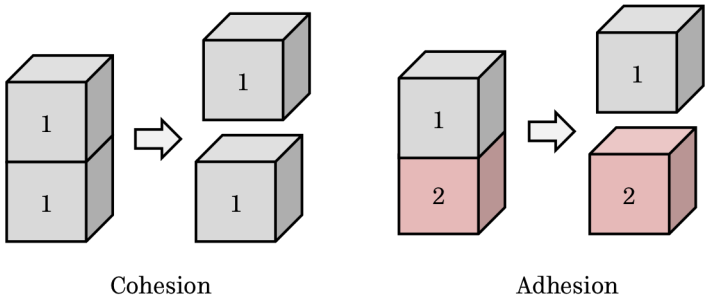

Figure 1.2: Work of cohesion and adhesion

In Figure 1.2 the cubes "1" and "2" are used to represent the two phases of interest, with each face assigned unit (i.e. = 1) area. The work of cohesion (left) for a single phase corresponds to the work required to split the phase in half, creating two new faces of the cube each with a surface energy equal to γ_1. Thus the work of cohesion (W_{11}) is equal to (Equation 1.1):

$$|W_{11}| = \gamma_1 + \gamma_1 = 2\gamma_1 \tag{1.1}$$

The work of adhesion (W_{12}) between two phases (right) can be interpreted as the work required to separate two different phases, which results in two new interfaces with surface energies γ_1 and γ_2. As a tension exists between the two phases (γ_{12}), this is subtracted, yielding the Dupré Equation (Equation 1.2):

$$|W_{12}| = \gamma_1 + \gamma_2 - \gamma_{12} \tag{1.2}$$

1.1.2 Droplet Spreading

In our case, if one considers phase 1 to be a droplet of water being deposited onto phase 2 (a solid), the droplet will spread, as determined by the respective quantities of W_{11} and W_{12}. If one assigns the subscripts $_S$, $_L$, and $_V$ to denote the solid, liquid, and vapor phases, respectively, spreading is determined by W_{SL} and W_{LV}. According to de Ruijter et al. (1999), the so-called "spreading coefficient" (S_c) is defined as the work of adhesion minus the work of adhesion:

$$S_c = W_{SL} - W_{LV} = \gamma_{SV} - \gamma_{LV} - \gamma_{SL} \tag{1.3}$$

If the work of adhesion is stronger than the work of cohesion (i.e. if $S_c > 0$), total wetting occurs. Otherwise partial wetting occurs, and a droplet (a spherical cap) forms on the surface. Additional work has been conducted on droplet spreading, e.g. by de Ruijter et al. (1999), who relates spread time to a friction coefficient between solid and liquid, and demonstrate that spreading time is faster if the liquid has a lower viscosity or higher surface tension.

A description of a droplet spreading to its equilibrium state is given by de Ruijter et al. (1999); they consider that spreading, which is driven by a decrease in free energy as the solid-liquid contact is increased, is opposed by viscous dissipation in the droplet core and friction between the solid and liquid near the contact line. They derive a universal equilibrium time ($t^\star$) for a small droplet (small Bond number (Eq. 1.20)), and thus neglecting gravity:

$$t^\star = \frac{\mu\, R_{\text{eq}}\, [\zeta_0/\mu + 8\, \ln(3\, v/\pi\, a^3\, \theta_{\text{eq}})/3\, \theta_{\text{eq}}]}{3\, \gamma\, \theta_{\text{eq}}^2} \tag{1.4}$$

Where v is the contact line velocity, ζ_0 is the friction factor between the liquid and solid, θ_{eq} is the equilibrium contact angle, γ is the liquid surface tension, and μ is the liquid dynamic

viscosity. The value of a describes the radius of a region near the center of the droplet that remains relatively stationary. Note that Equation 1.4 shows that droplet spreading (and wetting) improves (i.e. $t^{\star}$ is reduced) at greater values of γ, and lower values of μ.

1.1.3 Young Equation

Assuming that the solid surface is perfectly homogeneous and smooth, and that the liquid droplet has ceased to spread after reaching equilibrium, and assuming negligible influence of gravity, Young (1805) stated that the shape of the droplet is determined by the interplay of the three interfacial tensions γ_{SL}, γ_{SV}, and γ_{LV}, regardless of droplet size. The three tensions are depicted in Figure 1.3, with the angle formed between the droplet at the solid-liquid-vapor locus denoted as θ, known as the contact angle.

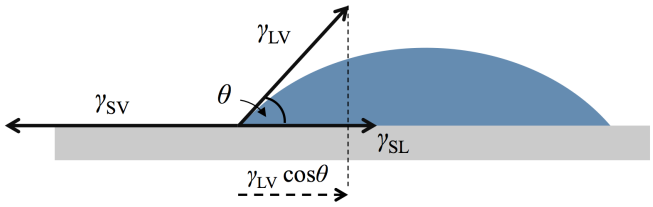

Figure 1.3: Force balance for Young's Equation

A simple force balance yields the classic Young equation:

$$|\gamma_{SV}| = |\gamma_{SL} + \gamma_{LV} \cos\theta| \tag{1.5}$$

By combining Equations 1.2 and 1.5, one obtains the Young-Dupré Equation (Eq. 1.6) to relate the work of adhesion W_{SL} to the contact angle θ and the liquid surface tension γ_{LV}:

$$W_{SL} = \gamma_{LV} \cos(\theta + 1) \tag{1.6}$$

1.1.4 Goniometry

One common technique to "directly" measure the contact angle θ is by depositing a droplet onto a solid material and measuring the contact angle using image analysis; this technique

is called the *sessile droplet method* (Lazghab et al., 2005). A goniometer can be used to measure the contact angle by using a video camera positioned from the side, adjusting the lighting to obtain good contrast between the droplet and the background (see Fig. 10.12). Image analysis can then be used to approximate the spherical cap to a sphere, and determine the contact angle formed at the baseline. In the case of powders, one common technique to obtain a "flat surface" is to compress the powders into a tablet; however, this introduces several complications, for instance related to the properties changing during compaction, the porous nature of tablets, etc. (Lazghab et al., 2005). The liquid is said to be *wetting* of the solid if the contact angle $\theta < 90°$, and *non-wetting* if $\theta > 90°$. If the water is liquid, some authors use this 90° cut-off to separate "hydrophilic" and "hydrophobic" powders; however, some authors describe powders as being hydrophobic even if $\theta < 90°$, e.g. Galet et al. (2009); Ren et al. (2003).

1.1.5 Imperfections of Food Powders

Unfortunately in reality surfaces are not ideal, and particularly of food powders, there are several factors that influence the measured, or *apparent*, contact angle, such as surface roughness, heterogeneous composition, component swelling of components such as starch or proteins, solubilization, or the orientation of the molecules (Forny et al., 2011; Cuq et al., 2011). As a result, measuring the contact angle is quite challenging.

1.1.6 Heterogeneous Surfaces

According to Israelachvili (2011), due to the heterogeneity of surfaces, there is not a single contact angle as assumed by Young (1805), but rather there exists contact angle hysteresis, where the *advancing* contact angle θ_a is larger than the *receding* contact angle θ_r, since the advancing end of the droplet can be hindered from movement by zones of low energy, and vice versa. The hysteresis H is defined as $H = \theta_a - \theta_r$, where $\theta_a > \theta_{\text{eq}} > \theta_r$, with θ_{eq} being the equilibrium contact angle. H can also be used as an indication of the cleanliness of surfaces.

The influence of surface roughness can be explained using different models. For a ho-

mogeneous, one-component, rough surface, the Wenzel model (Wenzel, 1936) is applicable:

$$\cos(\theta_w^\star) = r\cos(\theta) \tag{1.7}$$

where r is the roughness, equal to the ratio of the true surface area to the apparent (projected) surface area, thus $r > 1$, $\theta_w^\star$ is the apparent (Wenzel) equilibrium contact angle, and θ is the ideal contact angle. As r is necessarily > 1, according to Eq. 1.7 roughness exaggerates the wetting behavior determined by θ. That is, for $\theta < 90°$, roughness will improve wetting, and for $\theta > 90°$, roughness will worsen wetting (Forny et al., 2011).

The Wenzel Case (Fig. 1.4) is when the surface asperities are quite small, and the solid and liquid remain in close contact.

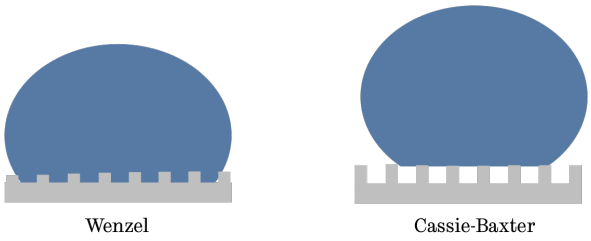

Figure 1.4: Wenzel and Cassie-Baxter conditions.

In the Cassie-Baxter state (Cassie and Baxter, 1944), asperities resemble taller "pillars" beneath which the droplet entraps air.[2] This Cassie-Baxter state is also called the "fahir state" due to the resemblance to fahir carpets (Afferrante and Carbone, 2010). The apparent contact angle θ_{CB} on such a heterogeneous surface can be described according to the Cassie-Baxter Equation for rough surfaces:

$$\cos(\theta_{\mathrm{CB}}^\star) = \phi\,(1 + \cos\theta) - 1 \tag{1.8}$$

where ϕ is the fraction of the surface area wetted by the liquid.

For a chemically heterogeneous surface, which is very much relevant for most food materials, the apparent contact angle, according to the Cassie-Baxter approach, predicts that $\cos\theta^\star$ is equal to the sum of the cosines of the ideal contact angles θ for each material multiplied by

[2] A transition from the Cassie-Baxter to Wenzel state can occur is the air pockets become thermodynamically unstable.

its fractional area f_i (i.e. its contribution), via:

$$\cos\theta^\star = \sum_{i=1}^{i_{\max}} f_i \cos\theta_i \tag{1.9}$$

1.1.7 Droplet Spreading on a Soluble Material

Another important consideration when discussing the wettability of food powders is the fact that many of them dissolve when in contact with water. As a result, a water droplet deposited on such a surface will not reach an equilibrium state, but rather the droplet will continue to spread, and the apparent contact angle continues to decrease. The mechanism involved in this type of spreading on soluble surface has recently been an area of focus, in particular within Nestlé Research, which collaborated with EPSCI in Paris to investigate the spreading of water on amorphous carbohydrate materials (Dupas et al., 2013, 2014). These studies utilized a unique setup to observe both the dynamic contact angle (from the side) as well as the behavior at the advancing contact line (from a tilted top view) of water, which is a volatile liquid, on thin layers of an amorphous food carbohydrate (maltodextrin, see § 8.1).

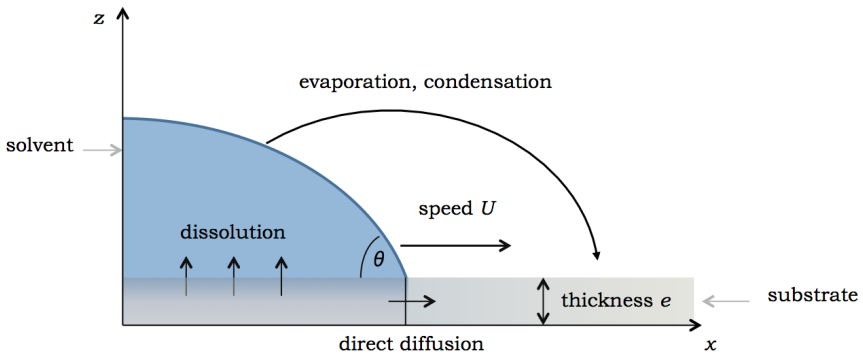

Figure 1.5: Mutual transfers during the spreading of a water droplet on a soluble surface (Dupas et al., 2013).

Figure 1.5 is a simplified diagram from Dupas et al. (2013) that shows a water droplet on a thin layer of thickness e and contact line speed U. These authors observed three different mechanisms for spreading, involving (1) mutual mass transfers between substrate and solvent, (2) the evaporation and condensation ahead of the contact line, and (3) the direct diffusion of solvent into the substrate as well as the dissolving of substrate into the solvent. They

conducted a number of experiments in order to investigate the influence of contact line speed U, water activity a_w, molecular weight M_w, and film thickness e, and they related these to the local water content (i.e. the hydration) of the film material, and they reported improved wettability (lower dynamic contact angle) with increased hydration of material. They also reported better wettability for a slower U (as water has more time to diffuse into the material), lower M_w (slower diffusion of water due to the higher viscosity of the resulting liquid solution), and smaller e (more of the water in the material is concentrated closer to the surface). They propose that a hydrated surface my exhibit improved wettability due to a preferential orientation of the carbon-dominant backbone of the carbohydrate at the film surface. They also observed (Dupas et al., 2014) that if the amorphous material is in a glassy state, then glass transition (induced by plastification by the water) would sharply accelerate the spreading of the droplet. Finally, they (Dupas, 2012) investigated the influence of supramolecular state of certain materials (crystalline vs. amorphous state)[3], by choosing a sugar material that can exist in either state (lactose). They explain that since water will not easily condense onto and penetrate *nor* diffuse through a crystalline material, then *only* dissolution of the material drives droplet spreading, leading to slower spreading and thus a higher contact angle, and worse wettability compared to if the material is in an amorphous configuration.

1.1.8 Capillary Rise (Wicking)

Another important consideration during the wetting of a powder in the possibility of liquid ascension into the porous powder bed, driven by capillary phenomena. If one considers e.g. an open glass capillary being placed into an infinite volume of water (Fig. 1.6), there will be a favorable interaction between the water and the capillary material ($\theta < 90°$) and the high surface tension will act to resist an extension of the exposed surface area of the liquid due to hydrogen bonding, thus forming a curved surface (a meniscus) to increase the contact surface.

The resulting curvature formation develops a pressure differential across the interface, which can be described by the Laplace (Young-Laplace) equation (Eq. 1.10) (Laplace, 1806),

[3]For further discussion of crystalline vs. amorphous states related to reconstitution, see § 1.4

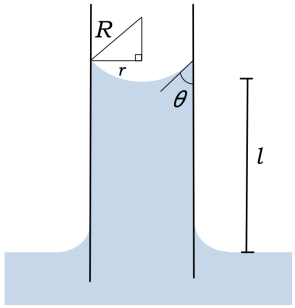

Figure 1.6: Open glass capillary placed into large volume of water

assuming a narrow capillary (i.e. with low Bond number, Eq. 1.20):

$$\Delta p = \gamma_{LV} \left(\frac{1}{R_1} + \frac{1}{R_2} \right) = \frac{2\,\gamma}{R} = \frac{2\,\gamma_{LV} \cos\theta}{r} \tag{1.10}$$

where Δp is the pressure drop, γ_{LV} is the surface tension, R_1 and R_2 are the radii of curvature (see Fig. 1.6); in this particular case, $R_1 = R_2 = R$, and r is the capillary radius, where $r = R\cos\theta$, as shown in the same figure.

1.1.9 Washburn Equation

The *rate* of ascension of a liquid into a capillary can be described using the (Lucas-)Washburn equation (Eq. 1.13) (Washburn, 1921). Washburn (1921) applies the (Hagen-)Poiseuille equation (Eq. 1.11), which opposes the capillary pressure and describes the pressure drop in fluid in laminar flow through a cylinder of which the length is much larger than the diameter:

$$\frac{\mathrm{d}l}{\mathrm{d}t} = \frac{r^2\,\Delta p}{8\,\mu\,l} \tag{1.11}$$

where l is the distance (height) traveled by the liquid, r is the hydrodynamic radius of the cylinder, μ is the dynamic viscosity, Δp is the pressure difference driving the flow, and t is time.

This pressure drop can then be thought of as the sum of the capillary pressure (Eq. 1.10) and the hydrostatic pressure, resulting in:

$$\Delta p = \frac{-2\,\gamma_{LV} \cos\theta}{r} + \rho\,g\,l \tag{1.12}$$

By considering only the very beginning of liquid ascension, one can neglect the influence of gravity ($\therefore \rho\,g\,l \approx 0$), and assuming the hydrodynamic and static radii of Equations 1.11

and 1.12, respectively, to be equivalent, by substituting these two equations and integrating[4] with the boundary condition that $l = 0$ at $t = 0$, one obtains the Washburn Equation for liquid rise into a single capillary:

$$\frac{l^2}{t} = \frac{\gamma\, r \cos\theta}{2\,\mu} \tag{1.13}$$

In the case of food powder wetting, according to Forny et al. (2011), one can also adapt Eq. 1.13 to a porous powder bed by assuming it behaves as a capillary network with parallel pores, obtaining:

$$\frac{l^2}{t} = \frac{c\,\gamma\,\bar{r}\cos\theta}{2\,\mu} \tag{1.14}$$

where $\bar{r}$ is the "mean pore radius", and c is an empirically determined form factor that takes into account the tortuosity of the network, and thus to apply Washburn's equation to powders, c would be highly dependent on the bulk density.

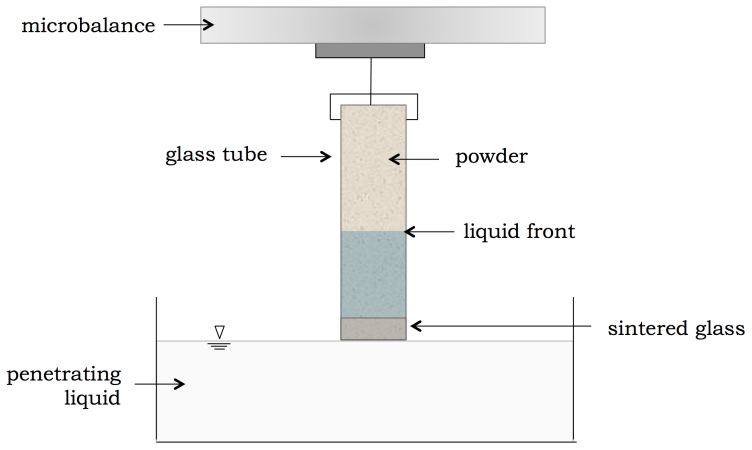

Figure 1.7: Tensiometer setup for wicking studies via Washburn method.

A setup such as the one depicted in Fig. 1.7 can be utilized to study the capillary rise of a liquid into a powder. It consists of a glass tube filled with a powder that allows liquid to penetrate through the porous bed. The tube is suspended from a microbalance that records the change in mass over time, that can be used to determine the liquid height (l in Eq. 1.13). This technique can be used for example to determine the contact angle between a powder and liquid by interpreting the initial rate of penetration.[5]

However in the case of food powders this may be difficult as water can dissolve the particles, resulting in a drastic change to the packing arrangement, due to swelling, which would

[4] $\int_0^l l\,\mathrm{d}l = \frac{1}{2}l^2$

[5] The form factor c can be estimated by first performing experiments with e.g. n-hexane, for which $\theta \approx 0°$.

reduce the "pore radius" ($l^2/t \propto r$), as well as material dissolution and a resulting viscosity increase ($l^2/t \propto \mu^{-1}$). Nevertheless, according to Forny et al. (2011), Eq. 1.13 can be useful to understand how liquid properties such as surface tension and viscosity can affect capillarity effects.

1.1.10 Jurin's Equilibrium Height

As the liquid continues to rise upward into a capillary, the influence of gravity will play an increasingly greater role, and if the capillary itself is tall enough, eventually the liquid will stop rising at a certain height, known as the Jurin height (Jurin, 1718), when the capillary pressure and hydrostatic pressure have the same magnitude. By combining Eq. 1.10 with the hydrostatic pressure and solving for the (equilibrium) liquid height l_{eq}, one obtains:

$$l_{\text{eq}} = \frac{2\,\gamma \cos\theta}{r\,g\,\rho} \tag{1.15}$$

It is important to note that the influence of pore radius on the *rate* and *extent* of capillary rise. Eq. 1.13 predicts faster penetration with larger capillaries ($l^2/t \propto r$), but the maximum vertical penetration possible decreases with increasing radius ($l_{\text{eq}} \propto r^{-1}$). As discussed in Chapter 2, the phenomenon of capillarity is exploited in powder processing by agglomerating powders to allow for faster wetting and sinking, and an optimum particle size may exist to obtain the best capillarity, due to the competing physical effects.

1.1.11 Geometric Effects on Wicking

There are other inaccuracies introduced when one considers the intra- and interparticle voids in a powder bed to behave similar to a network of parallel capillaries. In fact, particles may be stacked in such a manner that the path of the penetrating liquid is much more irregular than a cylinder, and the geometric considerations have important consequences for capillary rise. In another recent collaboration between Nestlé Research and EPSCI (Raux et al., 2013), the role of particle geometry in wicking was investigated. In that study, the authors hydrophobized glass capillaries and glass particles using silanization, and compared their wicking behaviors using liquids at different contact angles, using mixtures of water and ethanol, which each have respective contact angles θ of 105° and 35° with the silanized glass,

and a range of θ values was obtained based on the relative fractions of each liquid. They observed that a critical contact angle θ_{cr} exists, below which wetting is spontaneous and above which wetting does not occur. The value of θ_{cr} for the capillaries was 90° as predicted by Eq. 1.13. However in the case of particles, the system was more demanding, with a θ_{cr} of ca. 55°, which is close to the value they predicted with their model (not discussed here). They also demonstrated that other geometric considerations can affect θ_{cr} as well; e.g. wicking can be improved (θ_{cr} increased) by modifying the polydispersity of the system, by increasing the layer thickness of floating particles, and by introducing other "defects", e.g. gaps in-between spheres. Overall the project quite clearly demonstrated that the geometry of the powder bed is also important for powder wetting and sinking.

1.1.12 Darcy's Law

Another approach to describe the wetting of food powders is described by Schubert (1993) and Hogekamp and Schubert (2003). They relate the speed of liquid penetration to the porosity of the powder bed, using equations describing liquid flow through porous media. They combine the same principles used to describe liquid ascension as the Washburn approach described earlier, and consider the pressure drop encountered as liquid flows through a porous solid medium, according to Darcy's Equation (Darcy, 1856):

$$\Delta p = \frac{v\, l}{B\mu} \tag{1.16}$$

where B is the permeability, which can be described as a function of bed porosity via the Carman-Kozeny relationship (Kozeny, 1927; Carman, 1937), assuming the porous bed consists of identical spheres packed together and slow liquid movement ($\mathrm{Re} < 1$), and an even liquid front:

$$\Delta p = a\, \frac{\mu\, v\, l}{D_p^2}\, \frac{(1-\epsilon)^2}{\epsilon^3} \tag{1.17}$$

where a is a constant, D_p is the diameter of the particles, and ϵ is the porosity (void fraction). By rearranging Equations 1.16 and 1.17 to solve for $(\mu\, v\, l/\Delta p)$ and substituting in, one obtains the relationship:

$$B = a\, D_p^2\, \frac{\epsilon^3}{(1-\epsilon)^2} \tag{1.18}$$

Schubert (1993) combines these equations with those describing capillary pressure, and integrates to obtain:

$$\frac{l^2}{t} = \frac{D_p}{1.5} \frac{\epsilon}{(1-\epsilon)} \frac{\gamma \cos \theta_{\text{eff}}}{\mu} \tag{1.19}$$

The term θ_{eff} is used to describe the effective contact angle, as food powders contain "capillaries" with changing cross sectional radii, thus $\theta_{\text{eff}} > \theta$ for pure materials. They derived Eq. 1.19, which is similar to Eq. 1.13 but describes the case slightly more realistic for powders, although they did not consider the important effects of geometry, as explained earlier. Schubert (1993) also points out that increasing porosity can improve capillarity kinetics, which is related to powder agglomeration, as mentioned previously.

1.1.13 Polydispersity Effects

Schubert (1993) also briefly discusses the possible benefits of having a broad pore size distribution for adequate liquid penetration into a particle bed for good dispersion. If the distribution is too narrow, then for a submerged porous system, the wetting pressure of the penetrating liquid may not be able to surpass the pressure required for liquid drainage, and thus as a result air may remain inside of the agglomerates, thereby inhibiting complete wetting. However if there is a wider pore size distribution, liquid would quickly flow into the larger pores, displacing air that could escape through the smaller voids. Schubert (1993) uses this explanation as one reason to explain why jet agglomeration is preferred over tumbled agglomeration, for example, which would yield relatively uniformly sized agglomerates.

§1.2 Sinking

The second step of reconstitution is the sinking, or submerging, of the particles below the liquid/vapor interface. In the majority of food powder reconstitution studies, this step is unfortunately often ignored, as discussed in Chapter 5; however, this is not the case in the current thesis (cf. Chapters 10 and 11).

1.2.1 Single Particle Floating

In the case of relatively large non-porous objects, i.e. with a Bond number (Eq. 1.20) Bo $\gg 1$, one can predict whether a single object will float or sink by comparing the (effective[6]) densities of the object and the liquid – if the liquid is water, then if the object has a specific gravity < 1 it would be expected to float. The buoyant force (F_B) would be equal to the weight of the displaced water, which is equal in magnitude to the weight of the object (F_g). However at the length scales relevant to food powders, a low Bond number (Eq. 1.20) is possible, meaning that the surface tension effects can also play a role in supporting the weight of a floating object.

$$\mathrm{Bo} \equiv \frac{|\rho_s - \rho_l|\, g\, L^2}{\gamma} \tag{1.20}$$

where $|\rho_s - \rho_l|$ is the absolute difference between the solid and liquid densities, g is the acceleration due to gravity, L is the characteristic length (radius of the sphere), and γ is the surface tension. Thus, as explained by Kralchevsky and Denkov (2001) and Vella and Mahadevan (2005), even objects that would be expect to sink due a high density may still float on the surface if the surface tension γ is large enough[7], due to the vertical component of a capillary force (F_c). The force balance is given in Eq. 1.21:

$$|F_g| = |F_c + F_B| \tag{1.21}$$

In Figure 1.8, a single, small, hydrophobic sphere is floating at the surface of water (Vella and Mahadevan, 2005), where ϕ_c is the angle formed between the horizontal and the solid-liquid-vapor contact locus, z_c' is the distance between the undisturbed liquid surface and the depressed liquid at the contact locus, θ is the contact angle, R is the radius of the spherical particle, and ρ_s is the solid density.

The weight of the floating particle F_g of mass m is rather straightforward:

$$F_g = mg = \frac{4}{3}\,\pi\,\rho_s\,R^3\,g \tag{1.22}$$

The values of F_c and F_B are less obvious[8]. F_c is related to the perimeter of the circular contact locus between the solid and liquid, as well as the surface tension. Expressed in terms

[6] According to Schubert (1993), the *effective* density of food powders may be considerably lower than the *true* density, due to the inclusion of air into the particles.

[7] The surface tension is ca. $72\,\mathrm{mN\,m^{-1}}$ for water and ca. $25\,\mathrm{mN\,m^{-1}}$ for milk at 25 °C (Bertsch, 1983).

[8] For the derivations of F_c and F_B, refer to Vella and Mahadevan (2005).

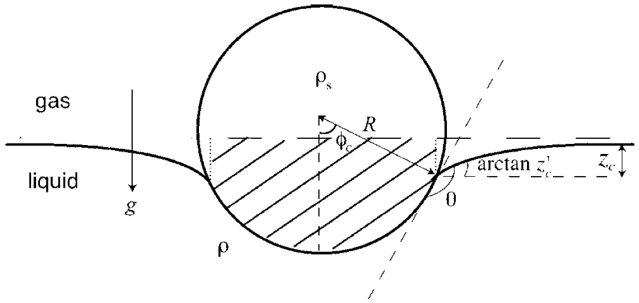

Figure 1.8: A heavy hydrophobic sphere being supported by the liquid surface tension (Vella and Mahadevan, 2005)

of particle radius, Vella and Mahadevan (2005) report:

$$F_c = \gamma\, 2\,\pi\, R\, \sin\phi_c \frac{z_c'}{\sqrt{1+z_c'^2}} \tag{1.23}$$

and the F_B is equal to the weight of the displaced water (the shaded region of Fig. 1.8). By observing that the shaded portion of the sphere used to express this displaced water looks like a cylinder attached to a spherical cap, Vella and Mahadevan (2005) derive:

$$F_B = \pi\,\rho\,g\,R^3\left(\frac{z_c'}{R}\sin\phi_c + \frac{2}{3} - \cos\phi_c + \frac{1}{3}\cos^3\phi_c\right) \tag{1.24}$$

In Eq. 1.23, one notes that decreasing the surface tension γ of the liquid would make sinking easier for a single particle. In fact, Schubert (1993) claims that the high surface tension of water is one hurdle to the sinking of food powders[9]. It is also important to note from this discussion that a hydrophobic particle would be expected to exhibit better floatability; Vella et al. (2006) observed that hydrophobic spheres (but not cylinders) are more likely to float as θ increases.

1.2.2 Interactions Between Floating Particles (Cheerios Effect)

One interesting phenomenon that occurs when particles are floating on the surface of a liquid is that they often spontaneously aggregate towards each other and towards the walls of the container. This has been named the "Cheerios Effect" (Vella and Mahadevan, 2005), due to quotidian observations of breakfast cereals on the surface of milk. These may also play an important role in the self-assembly of particles, for instance.

[9]The current author disagrees with this claim, as will be discussed in § 15.8.

Vella and Mahadevan (2005) demonstrate that if two very large plates are vertically suspended near each other in a liquid, a lateral capillary force can exist between them, causing an attraction or repulsion, depending on the wetting properties of each plate. If both cylinders have a low θ with the liquid, a similar case exists as in Fig. 1.6 where there is a lower pressure above the liquid surface due to meniscus (Laplace) effects, thus the atmospheric pressure could push these two plates together, as the surface tension drives to minimize the free surface to obtain a more energetically favorable state. However, if on the other hand, one plate is wetting and the other non-wetting, a repulsive interaction can exist. This is because if the two plates came together, the interface would need to greatly curve to "satisfy the needs" of each plate.[10] These interactions are explained mathematically in Vella and Mahadevan (2005).

Several authors have used these *lateral capillary forces* to explain the behavior of floating particles (Singh et al., 2010), etc. However, Vella and Mahadevan (2005) argue that this is a misconception about floating particle behavior, and argue that not all relevant forces are considered in such articles. They demonstrate using simple experiments that even for small particles, *buoyant* effects may actually be responsible for attraction and repulsion of floating particles. For example, if there are two heavy floating particles, they will "fall" into each others' menisci, and if there are light (or hollow) particles or bubbles, they may rise into each others' menisci due to a net upward force. However if two particles have opposite menisci (upward vs. downward), they will be repelled, as they do not satisfy the others' "needs". This is also explained mathematically in Vella and Mahadevan (2005). However, whatever the mechanism responsible, the current author does not believe that these Cheerios effects play a very important role in powder reconstitution.

1.2.3 Explosive Dispersion at the Liquid Surface

Singh et al. (2009, 2010); Gurupatham et al. (2011) describes an explosive dispersion of floating particles at a water-vapor interface immediately after they are added, and explain that these are related to capillary forces that *pull* particles downward into the interface. This

[10] However, if the plates are sufficiently close together there can be an attractive interaction, but the authors note one exception: if the two contact angles are the same number of degrees away from 90°, (i.e. $\cot\theta_1 = -\cot\theta_2$), there would be little curvature and thus they are always repulsive.

vertical acceleration is thus related to the particle weight F_g, the vertical capillary force F_c, and opposed by viscous drag F_D, via:

$$m\frac{\mathrm{d}v}{\mathrm{d}t} = F_c + F_D + F_g \tag{1.25}$$

where v is velocity and t is time.

They explain that due to a quick inertial suction into the interface during which the motion is inertia-dominated, the particle will overshoot its equilibrium position, and F_c will then act *upwards*, then when the particle once again overshoots its equilibrium position, F_c acts downwards again, etc. The result is an oscillating pattern, where the amplitude continually decreases due to the viscous dissipation of energy. The authors also suggest how to determine the velocity and frequency of oscillations. They explain that the resulting "waves" (which increase in frequency with surface tension γ, due to the importance of F_c) are the cause of the rapid hydrodynamic repulsion of particles radially from their point of impact at the liquid surface due to a lateral flow.

The same authors explain that increasing the number of particles causes a greater velocity of dispersion to occur, where the net flow is roughly equal to the sum of the flows for individual particles. The rate of dispersion also depends on the speed of impact (influencing oscillations), contact angle (stronger F_c result in a stronger initial pull into the interface), and size (smaller particles had a greater oscillation frequency). Singh et al. (2009) tested the dispersing of floating particles if a detergent (surfactants lower γ) is added *prior* to the particles being added to the surface. They observed that dispersing ability is greatly reduced, and explain this due to decreased F_c effects. The same authors also report that after the initial explosive dispersion, particles then slowly aggregate via the Cheerios Effect.

Gurupatham et al. (2012) then explain that a simpler mechanism is responsible for the breakup of floating particle clumps in order to form a dispersed monolayer. Particles on the outer periphery of the clumps are subject to the downward-pulling F_c that act against the cohesive forces between particles. Once the outer particle is brought into the interface and dispersed outwardly, a new particle is present at the periphery and may be subject to the pull of F_c, or alternatively larger clumps can break apart into smaller clumps, etc. Thus if γ is not high enough, the effect may not be strong enough to break apart particle clumps. The information in this section will be referred to in Chapter 11.

1.2.4 Particle Impact on the Liquid Surface

Another consideration for particle sinking is the impact a particle makes on the surface. For some objects (e.g. a paper clip) if dropped from a very large height it may pierce through the liquid-vapor interface, but if is delicately placed, it can float. Vella and Metcalfe (2007) investigated this phenomenon in order to relate the impact speed to sinking or floating conditions at low Weber numbers (We, Eq. 1.26, which indicates the relative importance of the impact to surface tension):

$$\mathrm{We} \equiv \frac{\rho U^2 r}{\gamma} \tag{1.26}$$

where ρ is the liquid density, U is the impact speed, r is the particle radius, and γ is the surface tension. The authors find that for a given U, there is a critical weight above which the particle sinks; they express this as a regime map where the dimensionless particle weight is plotted against the Froude number (Fr, see Chapter 3), which expresses the relative influence of impact speed to the speed of typical capillary-gravity waves. They show that the critical weight (for a given U) that they expected from calculations was actually less than what was observed empirically, possibly due to some of their assumptions (not discussed here). In the case of food powders, it is unclear how the feeding conditions of particles to the water will affect impact and thus sinking behavior. However, as discussed in Chapter 7, in the current report, food powders are dropped under highly defined conditions for reconstitution trials.

1.2.5 Sinking due to Water-logging

Vella and Huppert (2007) considers that floating objects may be porous in nature, thus due to porous flow discussed in § 1.1, objects may become waterlogged and sink as a result. They use the example of volcanic pumice rocks that float in the ocean and they relate imbibition both to capillary and Darcy flow to determine the sinking time. However in the case of a *powder* bed is also important to consider that individual particles may disperse once submerged (§ 1.3).

1.2.6 Sedimentation of Submerged Particles

Once particles make it past the liquid surface, if the effective density is greater than that of water, they will tend to sink to the vessel floor (assuming little or no mixing – cf. Ch. 3). Such sedimentation can be both visually undesirable to the consumer, and can lead to poor mass transfer for industrial applications. The speed at which a particle will sink to the vessel floor can be estimated by considering the relevant forces: the gravitational force (weight): F_g (Eq. 1.22), the buoyant force of the *submerged* particle F_b (Eq. 1.27)[11], as well as the drag force opposing particle movement F_d – Eq. 1.28 (D'arcy and Persoons, 2011).

$$F_b = -\left(\rho_p - \rho_f\right) \frac{\pi}{6} D_p^3 \, g \tag{1.27}$$

where ρ_p and ρ_f are the particle and fluid densities, respectively and D_p is the diameter of the spherical particle.

$$F_d = C_D \left(v_p - v_f\right) \tag{1.28}$$

where the drag coefficient C_D is multiplied by the slip velocity, which is the velocity of the particle relative to the liquid. The drag coefficient depends on factors such as particle shape, orientation, as well as the fluid speed, kinematic viscosity and particle diameter, which are incorporated into the dimensionless particle Reynolds number (Re_p):

$$\mathrm{Re}_p \equiv \frac{\rho_f \left|v_f - v_p\right| D_p}{\mu_f} \tag{1.29}$$

which relates the importance of inertial to viscous forces. For low Re_p values ($\mathrm{Re}_p \ll 1$), which would be expected for particle settling in a still liquid[12], the relationship for C_D as a function of Re_p of a spherical particle simplifies as follows (D'arcy and Persoons, 2011):

$$C_D = \frac{24}{\mathrm{Re}_p} \tag{1.30}$$

When food particles sink in a liquid, they will quickly reach a terminal velocity (settling speed, v_s) based on a balance of the relevant forces. By rearranging, one obtains Stokes' Law:

$$v_s = \left(\rho_p - \rho_f\right) \frac{D_p^2 \, g}{18 \, \mu} \tag{1.31}$$

[11] F_b is determined by the *volume* of the submerged particles, rather than the mass, as was the case for floating particles.

[12] At higher Re_p values ($\mathrm{Re}_p > 10^3$), it would be constant at $C_D = 0.44$, and for transitional regimes ($10^{-1} < \mathrm{Re}_p < 10^3$), a more complex empirical relationship can be used, cf. Eq. 1.61.

This equation demonstrates that the size of the particle will have a large impact on the settling rate – thus, if agglomerates are dispersed during sinking or reduced in size due to dissolving, they would sediment less quickly. Slower sedimentation would also be expected if the liquid viscosity μ is increased, which is one reason why ingredients like hydrocolloids are often added to food powder formulations (§ 6.1). In addition, if the effective particle density ρ_p is less than the density of the liquid ρ_f (e.g. due to the inclusion of air), a negative v_s would be expected, and the object would be expected to float (cf. Chapter 10). As explained in Chapter 3, the lift-off of sedimented material can be accomplished due to liquid movement induced by a spinning impeller. In the same chapter, the downdraw of floating particles due to agitation by the impeller (and vortex formation) will be discussed.

§1.3 Dispersing

The third step of powder reconstitution is dispersing; if the powder consists of agglomerated granules, this step may also be called de-agglomeration. It is often described as the breaking up of particle agglomerates and aggregates into smaller units, or possibly even primary particles. It occurs when the forces holding together the particles (cohesive interactions) are overcome by forces acting to separate the particles. For the vast majority of cases, for food powder reconstitution a complete dispersing is desirable, but there are some cases where an incomplete dispersing may actually be preferable. For instance, ColaCao®, a Catalan brand of chocolate beverage powder and a competitor to Nesquik, is known for leaving crunchy agglomerates at the bottom of the consumer's cup, which many prefer to a completely dispersed powder.[13] In any case, it is desirable for food manufacturers to be able to tailor the particle properties by controlling the formulation and production conditions, with the end-goal of producing particles that are strong enough to resist breakage and abrasion, but that also disperse well enough to obtain the desired degree of dispersing. In order to achieve such a goal, an improved understanding of the factors influencing dispersing may provide potential clues for improving the design of food powders.

[13] For those preferring complete dispersing, there is also a ColaCao "Turbo" brand.

1.3.1 Cohesion between Particles

One area of study in particle technology is determining the strength of interaction between particles. For example, strong particle-particle interactions may make it difficult to disperse powders in order to obtain reliable particle sizing data, both for dry dispersing (Calvert et al., 2013) and liquid dispersion (Tinke et al., 2009) applications. Simons et al. (1994) ranked the strength of these particle-particle interactions, with the strongest being solid bridges[14], followed by liquid bridges, then van der Waals, electrostatic, and finally magnetic interactions. As explained by Calvert et al. (2009), there are two key strengths to consider for describing the resistance to dispersing: tensile and shear, and the authors reviewed several models that describe the strength of an agglomerate in terms of these microscopic interactions. The most well-known of these is Rumpf's planar fracture model (Rumpf, 1970), in which a uniform particle cluster breaks apart into two halves (Fig. 1.9), giving the tensile strength σ_{tensile}:

$$\sigma_{\text{tensile}} = \frac{(1-\epsilon)}{\pi}\, k\, \frac{F_{\text{adh}}}{D_p^2} \tag{1.32}$$

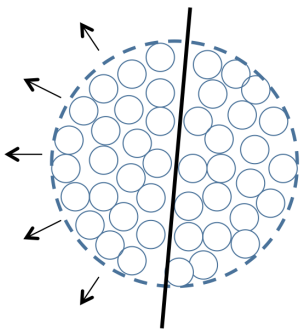

Figure 1.9: Depiction of the fracture plane for Rumpf's model of agglomerate dispersion.

where ϵ is the void fraction ($100\% - \epsilon$ is the packing density), $\pi \approx 3.14\ldots$, k is the coordination number (an indication of how particles are interconnected, i.e., where the force is transmitted between particles), F_{adh} is the adhesion force at particle-particle contact, and D_p is the primary particle diameter. Simplifications of Eq. 1.32 are also commonly encountered, by assuming $k\epsilon \approx \pi$ (Pietsch, 2002). As pointed out by Calvert et al. (2009) and Weiler et al. (2010), there are a number of issues with Rumpf's model when describing real powders.

[14]Strong solid bridges formed between particles during storage (i.e. caking) are detrimental to dispersion as well as other properties such as flowability. This is discussed in Ch. 2.

Due to the inhomogeneous distribution of stresses, particles will actually break apart at weaker coordination points – these studies propose improvements to Rumpf's model, as well as a "total dispersion" model, in which every contact within an agglomerate is considered. Nevertheless, Rumpf's model is widely employed in particle studies and does demonstrate that increasing the roughness of particles (lower k), increasing the particle size D_p, increasing porosity ϵ, and lower adhesion force F_{adh} all compromise tensile strength.

In order to estimate the adhesion force (F_{adh}), one must know the mechanism of contact – for example if a solid bridge exists, this may need to be dissolved or broken for complete dispersing, and the strength of the bridge itself will depend on the mechanical properties of the bridge material (Forny et al., 2011). For most studies of powder dispersing, especially those that use DEM (Discrete Element Method) modeling, e.g. Gopalkrishnan et al. (2007), it is assumed that the principle adhesion mechanism is van der Waals forces, particularly London dispersion forces (cf. Ch. 4).

1.3.2 Disruptive Forces – Spontaneous & Induced

The cohesive interactions mentioned above need to be overcome in order for dispersing to occur. When placed in a liquid (usually water), this dissociation can be spontaneous, or induced by some sort of agitation. According to Schubert (1993) when an agglomerate is submerged under water the van der Waals interactions between primary particles will become much weaker, and according to the same article, repulsive electrostatic double layers may also contribute to the dispersing of submerged particles (cf. Ch. 4 for more details). However the article provides no experimental evidence to demonstrate the importance of these phenomena. In most circumstances, some sort of agitation will be applied to assist in powder dispersing (Ch. 3) by applying mechanical stresses to the particles. Although in aerodynamic dispersing studies it has been reported that particle-particle collisions (impact stresses) are very important to disrupting cohesive particles (Calvert et al., 2009), in the case of dispersing in a liquid, these are not as important as *shear* in the liquid (Newman and Stolzenbach, 1996). These shear forces can be brought about using, for instance, an impeller or ultrasonic device (Ch. 3). A number of models have been described in the context of liquids breaking up particles in simple shear (Couette) flow. For instance Tinke et al. (2009) reviews a well-known model of a spherical particle being attached to a flat surface (or a much

larger particle). The fluid flow exerts both a lift force F_L which acts perpendicularly to the flat surface, as well as a drag force F_D which acts parallel to the surface:

$$F_L = \frac{10.15\ \mu\ D_p^3\ \dot{\gamma}^{3/2}}{\nu} \tag{1.33}$$

$$F_D = 2.55\,\pi\,\mu\,\dot{\gamma}\,D_p^2 \tag{1.34}$$

where μ is the dynamic viscosity, $\dot{\gamma}$ is the shear strain rate (see the article for more information), D_p is the particle diameter, and ν is the kinematic viscosity. In the case of *agglomerate* dispersing, one model used describes the breaking-off of a cap from a spherical agglomerate when exposed to shear flow; this has especially been used by the group of D.L. Feke at Case Western University (Boyle et al., 2005; Gopalkrishnan et al., 2005, 2007). The hydrodynamic forces (shear and normal forces) acting upon the cap at the plane of fracture are taken from (Bagster and Tomi, 1974), with Fig. 1.10 showing the coordinate notation.

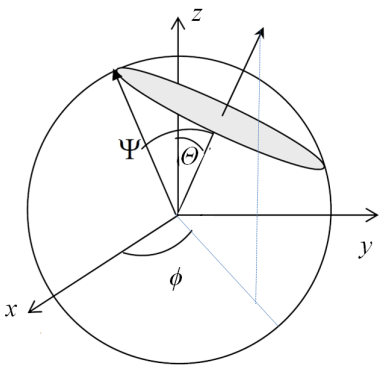

Figure 1.10: Three-dimensional coordinate system for the spherical cap.

According to their experimental results, the normal force (F_N) is more important than the shear force (F_S), as they reported that agglomerates are stronger in tensile strength compared to shear strength, by as much as two decimal orders of magnitude. The normal force (F_N) is given as:

$$F_N = \frac{5}{2}\,\pi\,\mu\,\dot{\gamma}\,R_{\text{agg}}^2\,\sin^2\psi\,\sin^2\Theta\,\sin\phi\,\cos\phi \tag{1.35}$$

where μ is the liquid dynamic viscosity, $\dot{\gamma}$ is the strain rate, R_{agg}^2 is the radius of the agglomerate, and Θ, ψ, and ϕ are given in Fig. 1.10. Moreover, their group apply DEM modeling to describe the dispersing of agglomerates in simple shear, using this F_N acting against the tensile strength (Eq. 1.32), assuming van der Waals attractions for F_{adh}.

1.3.3 Liquid Infiltration and the Effect on Tensile Strength

However, due to their experimental observations of agglomerate dispersing, in their model they also consider the influence of the surrounding liquid, which can *infiltrate* the agglomerate, as described in § 1.1, which they claim can have a significant effect on the dispersing mechanism, depending on the extent of infiltration. As per their description, when liquid penetrates into an agglomerate (with a dry center), it can influence the strength of interactions between two particles by forming a liquid bridge between them that introduces interfacial and viscous effects. Different (well-known) regimes for liquid saturation are: (i) the formation of adsorption layers on the particle surfaces, (ii) the pendular state, (iii) funicular state, (iv) capillary state, and finally (v) suspension. The three middle regimes (ii-iv) are illustrated in Fig. 1.11:

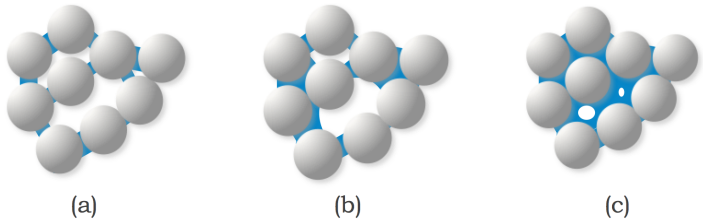

Figure 1.11: (a) Pendular state, (b) Funicular state, (c) Capillary state

where the saturation, S is calculated according to:

$$S \equiv \frac{V_{\text{liquid}}}{V_{\text{solid}} + V_{\text{liquid}} + V_{\text{void}}} \tag{1.36}$$

where V is the volume of the solid, liquid, and void fractions, as indicated. In their model, the group assumes a pendular state (Fig. 1.11a), which they define as $S = 13.6\%$, according to (Flemmer, 1991); they explain that this is the state during which the first significant change in interparticle interactions occurs. It has been shown that liquid bridges in their pendular state have a very significant effect on the flowability/cohesivity of powders (Althaus et al., 2012). Such an interparticle liquid bridge is shown in Fig. 1.12, where β is the half-filling angle, h is the minimum separation, R_1 is the primary radius of curvature of the bridge, and R_2 is the secondary curve, which is the secondary radius (radius of the neck of the bridge), by convention assigned as negative, and x is the particle radius.

Estimations for the volume of the liquid bridge can be found in Simons et al. (1994), and for R_1 and R_2 in Fisher (1926). In their model the group at Case Western University

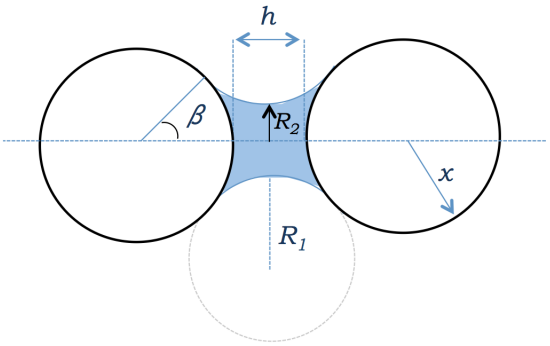

Figure 1.12: Liquid bridge between two particles (in pendular state).

approximate the instantaneous liquid bridge force F_{LB}, assuming quasi-static equilibrium, via:

$$F_{\mathrm{LB}} = F_{\mathrm{capillary}} + F_{\mathrm{viscous}} \tag{1.37}$$

where the capillary force, evaluated at the bridge neck via the Gorge method, is:

$$F_{\mathrm{capillary}} = 2\,\pi\,R_2\,\gamma - \pi\,R_2^2\,\Delta P \tag{1.38}$$

with ΔP being the Laplace pressure (Eq. 1.10). For the viscous force, the authors employ a thin-film model (using the Reynolds Equation for the toroidal shape) to describe a short-range force that opposes the dynamic separation of the particles:

$$F_{\mathrm{viscous}} = \frac{3\pi}{2}\mu\,x^2 \cdot \frac{1}{h}\frac{\mathrm{d}h}{\mathrm{d}t}\left(\frac{R_2^4}{(R_2^2 + xh)^2}\right) \tag{1.39}$$

where $\frac{\mathrm{d}h}{\mathrm{d}t}$ is the speed of separation. When the liquid bridge is present, the authors express the "wet" tensile strength (Eq. 1.32) in terms of F_{LB} for F_{adh}, since the liquid bridge would be expected to be stronger than van der Waals attractions F_{vdW}, as mentioned earlier.

1.3.4 DEM Model of Agglomerate Dispersing (Gopalkrishnan et al., 2005)

In their Discrete Element Method (DEM) model of agglomerate dispersing in a shear flow, Gopalkrishnan et al. (2005) divide up an agglomerate into seven segments (Fig. 1.13), with d being the infiltrated distance, and L being the separation distance between each fragment.

They model the motion of each segment according to Newton's second law with:

$$m\frac{\mathrm{d}^2h}{\mathrm{d}t^2} = \sum F_{\mathrm{vdW}} + \sum F_{\mathrm{LB}} + F_{\mathrm{N}} \tag{1.40}$$

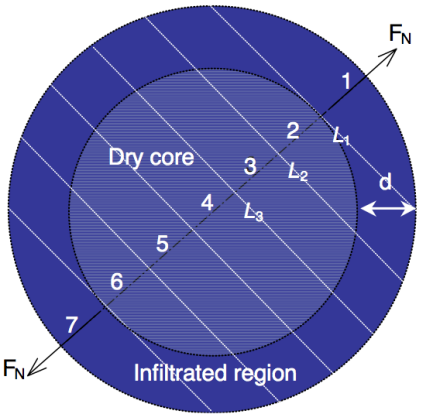

Figure 1.13: Segments of agglomerate (dry vs. liquid infiltrated) for DEM model (Gopalkrishnan et al., 2005).

where m is the mass. For the liquid bridge, rupture is assumed to occur at a critical separation distance (Eq. 1.41), which they use for their wet contact failure criterion; via the empirical estimation from Lian et al. (1993):

$$h_{\text{rupture}} = \left(1 + \frac{\theta}{2}\right) \sqrt[3]{V_{\text{LB}}} \tag{1.41}$$

where θ is the contact angle, and V_{LB} is the volume of the liquid bridge. At this distance, F_{vdW} is assumed to be 0. They also conducted experimental trials using the setups shown in Fig. 1.14 (Boyle et al., 2005).

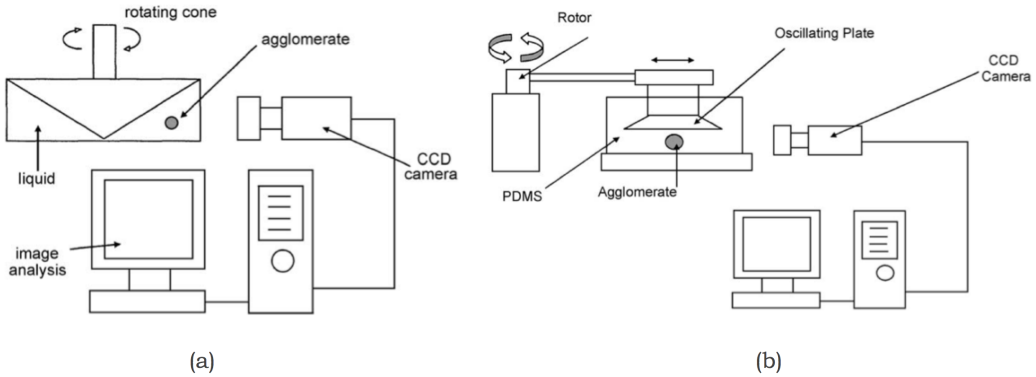

Figure 1.14: Shear devices used for dispersing analysis in D.L. Feke's group: (a) Cone-and-plate, (b) Oscillatory.

In the case of dry agglomerates, they describe two observed mechanisms for dispersing: (1) an erosion mechanism, in which particles slowly break off from the agglomerate surface, and (2) a rupture mechanism, where large fragments break off from the agglomerate. Both are said

to result from a cohesive failure mode. For infiltrated agglomerates they observed a particle rearrangement induced by the pressure of the advancing liquid, altering the cohesivity, and may lead to a "wet cohesive failure". They also describe a so-called "adhesive failure", which takes place due to poor adhesion between the wetted periphery and the dry core (Fig. 1.15).

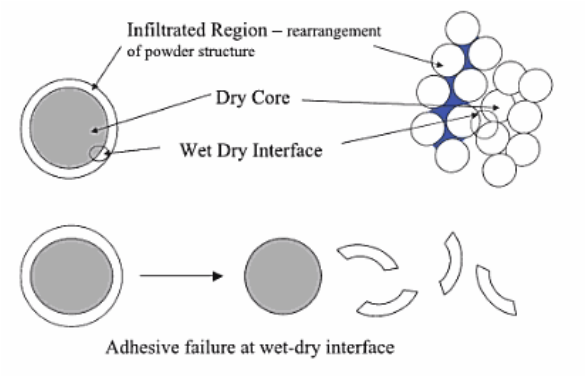

Figure 1.15: Adhesive failure mode for infiltrated agglomerates (Manas-Zloczower, 2009).

The work done by these researchers at Case Western University sheds new light on the complex dispersive mechanisms for powders in a shearing liquid.

1.3.5 Turbulence

It is of course important to realize that very often during powder reconstitution, turbulent (or transitional) flow (Ch. 3) is preferred over laminar conditions to promote dispersing and dissolving. According to Muthukumarappan (2009), there is no complete theory for turbulent flow phenomena; however, it is known that three-dimensional eddies are formed of different length scales, and the kinetic energy of these eddies is cascaded down to smaller and smaller eddies, until viscous dissipation to heat occurs in isotropic eddies of the smallest scale, known as the Kolmogorov length scale (λ) (Kolmogorov, 1941). This is said to depend on the rate of kinetic energy dissipation (ε) for turbulent flows, and the kinematic viscosity (ν), according to:

$$\lambda = \left(\frac{\nu^3}{\varepsilon}\right)^{1/4} \tag{1.42}$$

According to Doran (2013), fluid movement inside of the eddy is laminar, thus if the particle is smaller than the eddy, it will become entrained, and there will be little shear exerted on the

particle if the densities of the particle and liquid are similar. However if eddies are smaller than the particle, then an eddy can rotate the particle in the liquid, or if several eddies with different rotations simultaneously act upon a particle at once to dissipate the energy on a particle surface, significant stress effects may result. According to these authors, significant particle damage can occur, especially when $\lambda \approx \frac{2}{3}D_p$ or $\frac{1}{2}D_p$, with D_p being the particle diameter. The local dissipation rate of turbulent kinetic energy (ε) will increase with greater mixing, leading to a reduction in λ. While calculating ε is very challenging, Doran (2013) cite approaches used to estimate the order of magnitude of ε in a mixing vessel:

$$\varepsilon_{\text{vessel}} = \frac{P}{\rho V_L} \tag{1.43}$$

where P is the power draw (Ch. 3), ρ is the liquid density, and V_L is the volume of liquid in the vessel. As the turbulence is actually higher near the impeller, since energy dissipation is not uniformly distributed in the vessel, the authors give the following relationship for ε in the impeller region:

$$\varepsilon_{\text{imp reg}} = \frac{P}{\rho d^3} \tag{1.44}$$

where d is the impeller diameter. According to Barigou (2009), λ could simultaneously be $\approx$ 10 µm near the impeller and $\approx$ 30 µm in the bulk during mixing. These are calculated for the vessel used in the current report in Ch. 7.

§1.4 Dissolving

The fourth step of reconstitution is dissolving[15], during which thermodynamically compatible molecules (or ions) form solutes in the liquid solvent.

1.4.1 Bond Breakage and Formation

According to Yucel and Coupland (2010), dissolving is a thermodynamically driven process, but is kinetically limited. Whether or not it will occur spontaneously depends on the change

[15]Since many other studies in the literature use the term "dissolution" to refer to reconstitution overall, in the current report, "*dissolving*" is used to refer to this final step of reconstitution.

in Gibb's free energy (ΔG) when the solute and solvent come into contact:

$$\Delta G = \Delta H - T\,\Delta S \tag{1.45}$$

where H is the enthalpy, T is the absolute temperature, and S is the entropy (usually positive); spontaneous dissolving occurs if $\Delta G < 0$. From Eq. 1.45 one already sees that dissolving is more likely to occur if the involved processes result in a lower ΔH (the reaction more exothermic), the T is increased, or if higher entropy is obtained as a result of dissolving. The bonds that break and form are both within and between both the solute and the solvent phases (Syll et al., 2012). The breakage of solute-solute and solvent-solvent intermolecular forces are endothermic, and the formation of solute-solvent interactions (i.e. solvation, or hydration[16] if the liquid is aqueous) is exothermic. The overall enthalpy of solution (or "heat of dissolution") is the sum of the enthalpies of each reaction, according to Hess' Law.

1.4.2 Solubility

One commonly encountered word in dissolution studies is "solubility", which unfortunately is often misused, particularly in food reconstitution studies (§ 5.1). It is a thermodynamic (not kinetic) quantity, and it describes the maximum concentration of solute that can be added to the solvent, under given conditions, before precipitation occurs. According to Bhattachar et al. (2006), however, it is not so straightforward to determine, since equilibrium, which may require infinite mixing, is not easy to achieve. While such a definition is useful for studies of chemical or pharmaceutics, in the case of foods it is especially difficult to determine if a powder is "completely dissolved", especially if the resulting liquid is turbid. However, in general, solubility of organic molecules (most relevant for foods) tends to increase with temperature.

1.4.3 *Mass Transfer* is Rate-Limiting in Dissolving

On a larger length scale, dissolving also involves important mass transport considerations. According to Wang and Flanagan (2009), once solvation occurs, a slower (**rate-limiting**)

[16] During hydration of dissolved (or dispersed) materials, the water molecules form a more structured order, which may be important in non-DLVO interactions (Ch. 4) as well as NMR studies (§ 5.6).

process takes place, during which dissolved material moves from the solid-liquid interface into the bulk – it is slower due to the relatively large distances that must be covered by the molecules/ions of interest. The mass transfer itself can occur due to diffusion (due to a concentration gradient), convection (usually forced rather than natural convection, due to agitation – cf. Ch. 3), or a combination of the two, the relative importance of which can be expressed with the dimensionless Péclet number (Pe), which describes the ratio between the advection and diffusion rates of mass transfer:

$$\mathrm{Pe} \equiv \frac{v\,L}{\mathcal{D}} \tag{1.46}$$

where v is the flow velocity of solvent relative to the particle, L is the characteristic length scale, and $\mathcal{D}$ is the bulk diffusion rate (Parker et al., 2000).

1.4.4 Diffusive Models of Dissolving

As discussed in Dokoumetzidis and Macheras (2006), one of the most well-known mechanistic models of dissolving is the thin layer diffusion model. In this description, a thin, stagnant hydrodynamic boundary layer exists between the solid and the liquid bulk, across which diffusion occurs. The famous Noyes-Whitney Equation (Eq. 1.47, (Noyes and Whitney, 1897)) describes the dissolution rate (i.e. the concentration (C) of solute in the bulk per time (t)) as being driven by the difference between the solubility ($C_{\max}$) and the bulk concentration C:

$$\frac{\mathrm{d}C}{\mathrm{d}t} = k\,(C_{\max} - C) \tag{1.47}$$

where k is an empirical constant. This model was then further developed to account for Fickian diffusion: Fick's 1$^{\mathrm{st}}$ Law describes the flux according to the concentration, assuming steady state conditions:

$$J = -\mathcal{D}\,\nabla C \tag{1.48}$$

where J is the flux (concentration passing through an area per unit time), $\mathcal{D}$ is the diffusivity, and ∇ is the del operator.[17] Fick's 2$^{\mathrm{nd}}$ Law describes how the diffusion changes the concentration over time:

$$\frac{\partial C}{\partial t} = \mathcal{D}\,\nabla^2 C \tag{1.49}$$

[17] $\nabla = \left(\frac{\partial}{\partial x}, \frac{\partial}{\partial y}, \frac{\partial}{\partial z}\right)$

By applying Fickian diffusion to the thin layer model, Nernst and Brunner (Nernst, 1904) derive the expression:

$$\frac{\mathrm{d}C}{\mathrm{d}t} = \frac{\mathcal{D}\,A}{h}\,(C_{\max} - C) \tag{1.50}$$

where A is the exposed area, and h is the thickness of the thin layer. It is assumed that there is saturation (i.e. $C = C_{\max}$) at the interface of the solid and boundary layer. As can be seen, the model would suggest faster dissolution with a larger exposed surface area (i.e. smaller particles for larger *overall* surface area), greater solubility, and a thinner boundary layer. According to Wang and Flanagan (2009), the thin layer assumption is actually unrealistic hydrodynamically, but is widely used. As such, the layer thickness h probably cannot be determined without empirical fitting.

1.4.5 Sink Conditions

In the models described above, the concentration gradient was the driving force for dissolution (i.e. first order process). Under so-called "sink conditions", in which a very small amount of solute is added relative to saturation, and if the surface area and solvent are constant, dissolving behaves according to zero-order kinetics, and the dissolution rate simplifies to:

$$\frac{\mathrm{d}C}{\mathrm{d}t} = k \tag{1.51}$$

where the dissolution rate is independent of the amount of solute (Siepmann and Siepmann, 2008).

Another model by Hixson and Crowell (1931) is the "cube-root law", which is also applied under sink conditions, and accounts for the changing surface area during dissolution of spherical particles, and is derived as:

$$\frac{W_0^{1/3} - W^{1/3}}{\mathrm{d}t} = k \tag{1.52}$$

where W_0 is the initial particle weight, W is the weight of particle remaining at time t, and k is a constant.

1.4.6 Convective-Diffusion Model of Dissolving

Wang and Flanagan (2009) discusses a convection-diffusion model, which accounts for more realistic mixing conditions for powder reconstitution, due to the moving solvent. Molecular diffusion is said to occur at distances close to the solid surface (where liquid movement is slower and the concentration gradient larger), and convection at larger distances. The (simplified) convective-diffusive equation contains both a diffusive and convective term:

$$\frac{\partial C}{\partial t} = \mathcal{D}\,\nabla^2 C - v \cdot \nabla C \tag{1.53}$$

where v is the liquid velocity contributing to mass transfer. The boundary between regions of diffusion– or convective-dominant mass transfer is the "diffusion layer"[18], and mass transfer can also occur *parallel* to the solid surface (via convection). However, due to complex fluid dynamics, it is difficult to accurately apply the model (Wang and Flanagan, 2009).

1.4.7 Other Dissolving Models

In addition, there are other dissolving models as well (Dokoumetzidis and Macheras, 2006). For example, the "interfacial barrier model", in which the limiting step is not the diffusion through a thin layer, but rather the high interfacial transport activation energy, as well as the "surface renewal model", in which macroscopic "packets" of dissolving liquid reach the solid-liquid interface, absorb the solute via diffusion, and transport it to the bulk.

1.4.8 Mass Transfer for Particles Moving Through a Liquid

When considering the mass transfer that occurs for a spherical particle moving through water, additional interactions must be considered. According to Hartmann et al. (2006), the mass transfer is determined by a mass transfer coefficient k, where:

$$\dot{m} = k\,A\,(C_{\max} - C) \tag{1.54}$$

where $\dot{m}$ is the (convective) mass transfer between the solid and liquid phase, A is the surface area ($= \pi D_p^2$ for a sphere), $C_{\max}$ is the solubility, and C is the dissolved concentration. The

[18] Different from the Nernst layer described earlier, due to the presence of a velocity gradient.

value for k can be estimated from the dimensionless mass transfer coefficient: the Sherwood number (Sh), which relates the convective to diffusive mass transfer coefficients. One obtains:

$$k = \mathrm{Sh}\,\frac{\mathcal{D}}{D_p} \tag{1.55}$$

where $\mathcal{D}$ is the diffusivity. For typical mass transfer situations, Sh depends on two other dimensionless groups: the particle Reynolds number (Re_p, Eq. 1.29), and the Schmidt number (Sc), which is an indication of the liquid's capability of transporting momentum and mass by molecular means:

$$\mathrm{Sc} \equiv \frac{\nu}{\mathcal{D}} \tag{1.56}$$

where ν is the kinematic viscosity ($\nu = \mu/\rho$). According to D'arcy and Persoons (2011), this relationship can be predicted using the Ranz & Marshall equation:

$$\mathrm{Sh} = 2 + 0.6\,\mathrm{Re}_p^{\frac{1}{2}}\,\mathrm{Sc}^{\frac{1}{3}} \tag{1.57}$$

By combining Equations 1.29, 1.55, 1.56, and 1.57, one obtains (D'arcy and Persoons, 2011):

$$\frac{k\,D_p}{\mathcal{D}} = 2 + 0.6\left(\frac{\rho\,|v_f - v_p|\,D_p}{\mu}\right)^{1/2}\left(\frac{\mu}{\rho\,\mathcal{D}}\right)^{1/3} \tag{1.58}$$

The actual particle velocity (v_p) for transient flow would be obtained by the forces due to drag (F_D), buoyancy (F_b), liquid acceleration (F_a), and the Bassel history integral (F_{Basset}), the latter resulting from the resistance caused by unsteadiness of fluid flow (D'arcy and Persoons, 2011):

$$m_{p,\mathrm{app}}\,\frac{\mathrm{d}v_p}{\mathrm{d}t} = F_d + F_b + F_a + F_{\mathrm{Basset}} \tag{1.59}$$

The apparent particle mass ($m_{p,\mathrm{app}}$) would actually include the mass of liquid surrounding the particle within $\frac{1}{2}$ the particle volume:

$$m_{p,\mathrm{app}} = \rho_p\,\frac{\pi}{6}\,D_p^3 + \frac{1}{2}\left(\rho\,\frac{\pi}{6}\,D_p^3\right) \tag{1.60}$$

As the Re_p would be larger for such flow, the drag coefficient (C_D) for a spherical particle can be correlated to Re_p according to the empirical relationship (D'arcy and Persoons, 2011):

$$C_D = 3\,\pi\,\mu\,D_p\left(1 + 0.15\,\mathrm{Re}_p^{0.687}\right) \qquad \text{for } \mathrm{Re}_p < 300 \tag{1.61}$$

The fluid acceleration would be:

$$F_a = \frac{1}{4}\,\rho\,\pi\,D_p^3\,\frac{\mathrm{d}v_f}{\mathrm{d}t} \tag{1.62}$$

and the Basset force:

$$F_{\text{Basset}} = -\frac{3}{2} D_p^3 \sqrt{\pi \mu \rho} \int_0^t \frac{\frac{\mathrm{D}v_f}{\mathrm{D}t'} - \frac{\partial v_p}{\partial t'}}{\sqrt{t - t'}} \mathrm{d}t \tag{1.63}$$

where $\mathrm{D}/\mathrm{D}t'$ is the material derivative. Considering all of these equations, it is clear that increasing the mixing of the liquid will improve mass transfer during dissolving, in addition to aiding with dispersing.

1.4.9 Polymer Swelling

When the molecules dissolving are oligo- or polymeric in nature, their dissolving into the liquid bulk can become much more complex than the previously mentioned theories can describe. This is particularly true for powders such as hydrocolloids (§ 6.1), which are often used as thickening or gelling agents, as well as polymers native to food materials, e.g. starch in cocoa powders (§ 6.3) or certain proteins in dairy powders (§ 6.2). In addition, it is important for the pharmaceutical industry for controlled drug release (Siepmann and Siepmann, 2008).

According to Parker et al. (2000); Klein Larsen et al. (2003); Siepmann and Siepmann (2008), water will first penetrate into an (amorphous) polymer, which, when a critical water content is attained, will bring about a phenomenon called "polymer chain relaxation."[19]

This penetration and partial hydration may lead to swelling, or an increase in occupied volume, or a "viscous layer" (Chávez Montes et al., 2011b), which can impede both the water penetrating into the solid material, as well as the release of the entangled polymers from the swollen layer into the bulk. A more detailed model of these processes is described in Siepmann and Siepmann (2008). Moreover, some food polymers are able to form gels as well (§ 6.1) and this may play an important role in dissolving and lump formation (Parker et al., 2000). Particularly for a gel layer, shear-thinning behavior of the gel may call for violent mixing in order for complete dispersing to occur. The actual mechanical and thermal properties of such a gel would depend on the type of junction zones formed, the temperature, shear, and, if a polyelectrolyte, the ionic strength[20], and is highly dependent on the material properties (Klein Larsen et al., 2003; Saha and Bhattacharya, 2010).

[19] Essentially a glass transition, a relatively "rubbery" state, with more molecular mobility and greater free volume (Palzer, 2007) into which the solvent can penetrate.

[20] Or even ionotropic gelation effects, e.g. Ca^{2+} bridges for pectin, alginate, carrageenan, ...

1.4.10 Dissolving affects Wetting, Sinking, and Dispersing

As discussed in § 5.10, it is possible to isolate the dissolving step of reconstitution by focusing on the behavior of single particles. While this approach can provide useful information about the material behavior, by no means does faster dissolving of individual of particles guarantee faster powder reconstitution overall – particularly for materials that might swell when hydrated. In fact, as mentioned by Parker et al. (2000); Westergaard (2004), sometimes it is even desirable to delay the dissolving of individual particles in order to allow the first three steps of reconstitution (wetting/capillarity, sinking, and dispersing) to occur *before* dissolving. This is important because particle swelling (or dissolving to form a viscous solution) can hamper water transfer into the bulk material, which may result in lump formation. Parker et al. (2000) suggests for some gum powders, reconstitution should be performed at a lower temperature, otherwise dissolving may be too fast for proper wetting/sinking. Westergaard (2004) even suggests lecithinating (cf. Ch. 2) hydrophilic whey powders in order to make them more hydrophobic to delay hydration and thus swelling.

Another case in which this is true is with regards to the particle size. As shown in the Noyes-Whitney Equation (Eq. 1.47), a smaller particle size (larger surface area–to–mass ratio) would increase the dissolving rate; but due to tighter possible packing of smaller particles (higher bulk density), this may also inhibit proper liquid penetration. In fact, this is one reason why agglomeration (Ch. 2) is often needed for food powders.

1.4.11 Lump Formation

Lump formation during rehydration is one of the main quality defects of food powders. According to Szczesniak (2002), consumers may reject a food product if the perceived visual and oral-tactile texture of the product conflict with their expectations; for instance, a product may be dismissed[21] if it contains unexpected lumps, due to a sudden drying sensation in the oral cavity. According to Palzer (2013) there may even be health and safety concerns related to lumps – particularly for infant formula powders, improper powder dispersing could result

[21] According to the same authors, the preference may also depend on factors such as a consumer's cultural or socioeconomic background.

in a choking hazard, undispersed food masses that stick to vending equipment could present a microbiological hygiene issue, and powder lumps may affect heat transfer processes.

Unfortunately the term "lump" is not well-defined in the industry. According to the Merriam Webster's English dictionary, a lump in this context is a "*piece or mass of indefinite size and shape.*" Parker et al. (2000), for their discussion of lumps (or "fish eyes") of polymeric powders, arbitrarily define them as a visible mass on the order of 1 mm. As will be discussed in § 5.1, although the IDF[22] method for dispersibility does not explicitly refer to a "lump size", it uses a cut-off of 150 µm to determine a powder's "dispersibility"; however, it is not entirely clear why 150 µm was chosen as a cut-off. Lawless and Heymann (2010) reviewed studies that investigated the influence of particle size and shape on consumers' sensory perceptions. For instance they cite Tyle (1993) who suspended particles in syrups and reported that soft, rounded or soft, flat particles were perceived as gritty if the particle size was ≥ 80 µm, but angular particles were perceived as sandy at sizes as low as 11–23 µm.

With regards to the mechanism for lump formation, most of the work, to the author's best knowledge, has focused on polymeric additives such as gums and thickeners (§ 6.1). Parker et al. (2000) described lumps of such powders upon dissolution as "sacks" of dry particles encapsulated in a homogeneous gel-layer, which forms upon contact with water. This swelling and collapsing of particle structure then clogs interparticle voids and obstructs water penetration. These authors explain that lumps will *only* form if dissolving of the individual particles occurs *instantly*, otherwise lumps will not form at all as the particles disperse away from one another. Based on their explanation, they list some heuristic rules to minimize lump formation of polymeric powders:

1. Reduce the number of particle fines.
2. Factors that can accelerate dissolving (e.g. higher temperature) may exacerbate lump formation.
3. Slow powder addition can help separate individual particles and reduce the number or size of lumps.
4. A diluent (e.g. sucrose) can be dry-mixed with the powder (see Ch. 2).

However Parker et al. (2000) noted that there is a lack of experimental techniques appropriate

[22] International Dairy Federation

for studying lump formation (Ch. 5). Thus, they did not identify the *conditions* under which lumps may form, during actual reconstitution. This problem will be addressed in Chapters 10 and 11.

It is also worth noting that on an industrial scale, complete reconstitution of ingredients, such as thickeners, is often imperative, and if fish eyes form, then high shear or filtering of the solution may be necessary to remove them. However there have been recent developments in completely dissolving such problematic powders prior to dosing, with less energy required (e.g. the Quadro Ytron^{TM} ZC, Waterloo, Canada).

1.4.12 Not All Food Powders Completely Dissolve

It is also important to note that not all food materials will completely dissolve in water, even though many studies talk about the "dissolution" of e.g. dairy powders, for which the final step in reconstitution exists somewhere in-between dispersing and dissolving. In the case of milk, as will be discussed further in § 6.2, there are components that *will* dissolve in the aqueous media (e.g. lactose, serum proteins, and minerals), as well as components that become *suspended* to form a colloid (casein micelles and fat). As a result of these dispersed particles, light is diffracted and the beverage is turbid, which has major implications for Ch. 11. With regards to the "dissolution" of powders containing casein micelles (e.g. milk, milk protein concentration, and micellar casein powders; § 6.2), Mimouni et al. (2009) and Fang et al. (2011) propose two simultaneous mechanisms (Fig. 1.16): the first is the dispersing of agglomerates and aggregates into primary particles, and the second is the release of (nanometer-scale) casein micelles from the primary particles to be suspended in the aqueous medium. It should be noted that a similar final stage for cocoa powders may also exist, as these contain some components that dissolve and some that disperse (§ 6.3).

1.4.13 *Correlation* Between Exothermicity and Reconstitution Kinetics

It is well-known that some solid food materials can exist in either an amorphous or crystalline supramolecular state, such as lactose in milk (Palzer, 2007; Roos, 2010). It is also

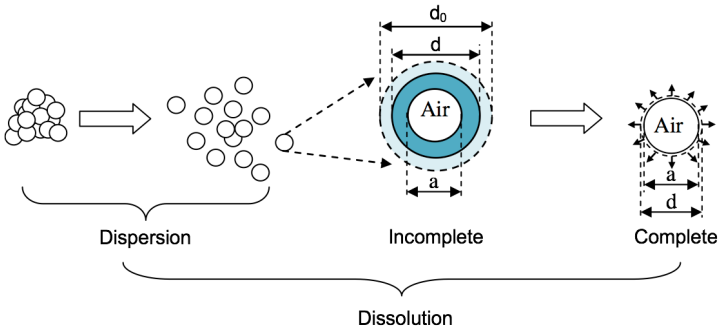

Figure 1.16: "Dissolution" of a food particle largely consisting of casein micelles (Mimouni et al., 2009; Fang et al., 2012). Note that for many food particles, a large vacuole (air) is located inside the primary particles, as will be discussed in Ch. 2.

widely accepted that the amorphous version of a material will dissolve more quickly than its crystalline counterpart (Schubert, 1993), thus maintaining the amorphicity of a food material in a powder can be desirable – this may lead to faster reconstitution overall, and for confectionery applications, the faster dissolving of sucrose may enhance its sweetness perception (Gianfrancesco et al., 2012). However, since water-soluble amorphous materials are hygroscopic, they can absorb humidity from the atmosphere, which can lead to issues such as solid-phase crystallization or glass transition, resulting in a number of issues (Ch. 2). To combat this sensitivity to environmental conditions, one group (Yazdanpanah and Langrish, 2013) proposed an "egg-shell" structure, where a crystalline shell surrounds an amorphous bulk – providing both fast dissolving as well as shelf stability.

As described by Bhandari and Roos (2012) whereas crystalline structure are repetitive and the molecules are well-aligned, in amorphous materials molecular orientation is more random, and have a higher energy level (i.e. less stable), with weaker intermolecular bonds that are easier to disrupt. The molecules also have a more open and porous structure, with more sites for solvent-solute interactions to occur. It is also widely accepted that increased (solid[23]) fat in particles, and particularly on the surface, is undesirable for rehydration, due to the increased contact angle with water, causing issues related to wetting (Kim et al., 2002, 2005b; Gaiani et al., 2009). However it is important to note that fat does *not* dissolve in water, but rather it becomes suspended, due to differences in polarity of the constituent molecules.

Some studies have demonstrated that there is a correlation between the solution enthalpy

[23] See Ch. 11

(§ 5.10) and the amorphous vs. crystalline content (Hogan and Buckton, 2000). They explain that the greater the amorphous content, the more exothermic the reaction due to the greater amount of sites available for solvent-solute interactions, which as explained before, is an exothermic interaction. In particular, it is the first few molecules to adsorb to the material surface that give the greatest exothermic response, as consecutive layers of water form afterwards. The authors thus suggest that solution calorimetry can be used as a tool to determine the amorphous content of a material after a calibration.

One project at Nestlé (Marabi et al., 2007, 2008a,b) noted that the "dissolution" kinetics are faster and the calorimetric response is more exothermic if powders are in an amorphous rather than crystalline state. They therefore argue that there may be a cause–effect relationship between the two phenomena, and that there may be a heat-mechanism that needs to be accounted for in dissolving studies. They also demonstrate, using a conductivity approach (§ 5.3) for reconstitution kinetics, that there is an increase in rehydration rate if the fat content is reduced, and there is also a more exothermic response[24] at lower fat contents. They once again suggest a cause-effect relationship between the exothermic response and faster rehydration. In a patent (Marabi et al., 2010), they propose that dissolving can be enhanced by creating a "microenvironment" in a single composite granule. The idea is that one component would dissolve exothermically, and the other endothermically; thus one material's heat of solution given off would be used to aid in the dissolving of the other material. They attempt to demonstrate this by creating a granule of chocolate beverage powder (endothermic) with maltodextrin DE21 (§ 8.1) that helps improve dissolving.

In the current author's opinion, there are a number of concerns to be addressed regarding Marabi et al.'s approach to dissolution studies. The first of which is, as mentioned earlier (cf. Wang and Flanagan (2009)), dissolving consists of both a solvation reaction *and* mass transfer, and it may very well be that the *latter* of these two is the rate-limiting step, but it is the former step which determines the enthalpic response.

The second issue, as pointed out by Syll et al. (2012), who directly challenge Marabi et al.'s work, is that there are some well-known examples of fast-dissolving species that dissolve *endothermically*, e.g. NH_4NO_3, $NaClO_2$, and $KClO_3$. Syll et al. (2012) also investigated the relation between rehydration (using a laser diffraction setup; § 5.4) and calorimetric responses,

[24] For greater fat content, there are less sites for water-solute interaction to occur.

and saw no correlation – they thus explicitly challenge Marabi et al.'s conclusions and argue that the dissolving mechanisms are more complex. They also suggest that the rehydration that Marabi et al. used (conductimetry) is not sensitive enough to appreciate the *end* of reconstitution, which is discussed further in Ch. 14.

A third concern is that Marabi et al. do not seem to consider other possible mechanisms to explain their results. For example they equilibrate skim milk powder to a high water activity[25] using a saturated salt solution of $Mg(NO_3)_2$, prior to performing rehydration experiments, and dissolution of single particles was slower after this equilibration process, likely due to the solid-phase crystallization of the lactose. However, in skim milk powders (Ch. 2), it is possible that residual fat may originally be encapsulated in the amorphous lactose matrix, but is expelled to the surface when the lactose crystallizes (Bhandari and Roos, 2012), and this might also have an influence on dissolving. If slower dissolving is due to the crystalline lactose itself, it might also simply be that the molecules are more difficult to remove from a crystalline matrix, as mentioned earlier, without necessarily involving the heat of solution as a causative mechanism.

Moreover, with regards to the correlation between fat content and the reconstitution time, it is possible that a mechanism other than heat of solution could be responsible. For instance, as discussed in § 1.1, a more hydrophobic surface may exhibit poorer wetting and capillarity, and thus this could limit the overall reconstitution rate due to a slow sinking rate. However the technique that Marabi et al. used to determine the kinetics was conductivity, which as will be discussed in § 5.3, would not be able to determine the *sinking behavior* of powders. It is thus possible that slower wetting/sinking, due to the presence of fat in the particles, may be an alternative explanation to the poorer reconstitution kinetics.[26]

With regards to Marabi et al.'s patent there are a number of reasons that adding a powder like maltodextrin DE21 to a composite particle of chocolate beverage powder (CBP) may improve the rehydration properties of CBPs. As will be shown in Ch. 9, maltodextrin DE21 exhibits good wettability and dissolves quickly. Thus it may be that the physical separation of

[25] They equilibrated the powder, containing mostly amorphous lactose, to a water activity (a_w) of 0.54 at a temperature T of 20 °C. This is surprising, as according to Vuataz (2002), the glass transition temperature T_g would be expected to be ca. 0 °C – thus one might expect that the powder would collapse at such a high $(T - T_g)$ value.

[26] Also, as pointed out before, fat does not dissolve in water.

the chocolate beverage powder components could allow penetrating water to wet the granule more easily, improving overall reconstitution.

Finally, Marabi et al. (2007) demonstrated that there is a less exothermic dissolving of (amorphous) maltodextrin DE21 when the powder is equilibrated to a higher a_w.[27] However for an unknown reason, the authors did not actually report any results regarding the influence of a_w on dissolving kinetics. This may be due to the fact that conductivity is not an appropriate technique to study the rehydration of such powders (Ch. 14), or that the dissolving of single particles might be too quick. In any case, according to their logic, they would expect *slower* dissolving at a higher a_w; however, as discussed in § 1.1 (cf. Dupas et al. (2013)), there is an improvement in wetting with an increase in a_w. In the current report (Ch. 10), the influence of a_w on rehydration was studied for maltodextrin powders, and results are in agreement with Dupas et al. (2013), but do not agree with the logic of Marabi et al.

[27] If more solute molecules are already hydrated prior to dissolving, then there would be less bonding sites available for water, thus one would indeed expect a less exothermic response.

Chapter 2

Food Powder Production & Storage

Particularly over the past decade, much attention has been paid to understanding how the functional properties of food powders (e.g. ease of reconstitution) are affected by particle properties, and how these properties, in turn, are governed by production and storage conditions of the powders. Of particular interest have been the particle microstructure and surface composition, and the use of advanced techniques is growing in popularity. The microstructure can be elucidated using e.g. X-ray tomography (Palzer et al., 2012), and the surface composition using X-ray photoelectron spectroscopy, which can examine the composition of the first 10 nm of the particle surface (Murrieta-Pazos et al., 2012a). The following discussion will give a brief overview of powder processing and how particle properties can be modified, as well as discussion of (generally negative) effects of powder aging during storage.

Contents

§2.1 Powder Formation

2.1.1 Drying Methods

There are a number of ways that food powders can be produced. For example in the case of cocoa powder (§ 6.3), a cocoa mass is pressed to remove most of the cocoa butter to obtain a cake, which is then pulverized. However most food powders are obtained by removing water from a concentrated liquid, and this area has received significant attention in the literature, especially for complex foods such as dairy products. There are a number of unit operations to dehydrate foods (Palzer et al., 2012) – two of the most common of which are spray drying and freeze drying. The basic concepts are that during spray drying, a pumpable liquid concentrate is atomized into small droplets, and water evaporates due to high temperatures and convection in a drying column, and during freeze drying, aqueous food is lyophilized: the

food is frozen and water is removed under vacuum via sublimation. The dried food can then be ground to produce granules.

In general it is said that freeze dried products are of higher quality compared to spray dried, for a number of reasons. The lower processing temperatures to remove water, compared to spray drying, translate to less flavor loss (e.g. for instant coffee), more homogeneous composition (Fyfe et al., 2011), and a better structure for wettability, since spray drying may result in small, hollow spheres that can be difficult to sink, whereas the voids left over from the sublimated water from freeze drying can provide better capillarity into the granules (Schubert, 1993). Haque and Roos (2006) also suggest that dissolving of freeze dried particles may be faster, as the microstructure allows for greater number of hydrogen-bonding sites for hydration to occur. Moreover, according to Palzer et al. (2012), for low-MW (molecular weight) polymers that can exist in either an amorphous or crystalline state, which affects dissolving, freeze drying is more likely to produce higher quantities of amorphous material. The same authors also discuss how the supramolecular structure can be impacted by the drying rate during spray drying – faster drying results in more amorphous content for such material, as less time is available for crystallization to take place as the water is removed. However despite the benefits offered by freeze-drying, spray drying remains popular as it is more energy efficient at present.

In addition, depending on the type of food at hand, other techniques may be used as well. For example, in the case of starch, extrusion may be used to produce the powder and simultaneously induce (pre-)gelatinization for better cold-water reconstitution (Schubert, 1993). Gas may also be incorporated into the liquid prior to drying to increase porosity, or possibly induce foam generation upon rehydration (Palzer et al., 2012). It has also been shown that energy efficiency and food powder quality may be improved by intermittent drying, i.e. where drying conditions are changed with time (Kumar et al., 2014).

2.1.2 Agglomeration

As discussed in § 1.1, smaller particles suffer from poor wetting/sinking due to ineffective capillary penetration – one reason that agglomerating powders is common in the food industry. Other reasons include to improve the flowability and floodability properties, to reduce dust

formation, prevent segregation, among others (Palzer, 2011). Essentially smaller particles are stuck to each other to create larger agglomerates, via a number of bonding mechanisms by using a different process techniques (see Palzer (2007)). For example, food powders can be agglomerated, e.g. by recirculating small fines recovered from a cyclone at the end of spray drying by choosing the right location to obtain optimal grape-like structures (Gianfrancesco et al., 2010), or by agglomerating in an external fluidized bed (Fries et al., 2013; Heine et al., 2013). The goal is to produce agglomerates that are strong enough to resist abrasion or breakage during transport and storage, but will not be too strong, otherwise they may be difficult to disperse upon rehydration (Schubert, 1993). According to Schubert (1993), agglomerates should not be too large as well, as these would exhibit poor dissolving properties (as predicted by Eq. 1.47), thus an optimum size may exist, although this optimum size probably is not universal for all food powders (Parker et al., 2000; Gaiani et al., 2007).

According to Richard et al. (2013), granulation should really only be employed if wetting and sinking are the limiting steps in reconstitution, and if the powder material is not damaged by the heat it will encounter during agglomeration. In addition, as the operations can be energetically expensive, unnecessary agglomeration should be avoided. These authors demonstrated that for a powder consisting of both casein and whey (§ 6.2), reconstitution of the granulated powder could take $2-3\times$ longer due to the "severe" thermal treatment that could damage protein and lead to insoluble structures. Gaiani et al. (2007) also reported that agglomeration only helped powder reconstitution if, and only if, wetting/sinking was the limiting step. Granulating (native) whey protein isolate powders (§ 6.2) improved rehydration, but had a detrimental effect for micellar casein powders. They explained that in the original non-granulated powder, micellar casein powder exhibited good wetting and sinking, followed by slower dispersion, while the whey protein isolate powder originally had poor wetting and sinking properties, but fast dispersing and dissolving. Thus the agglomeration *facilitated* the sinking of the whey powder, but the extra bridges formed between micellar casein powders *hindered* particle dispersing, and thus overall reconstitution.

2.1.3 Droplet Drying during Spray Drying

As mentioned before, spray drying is a very common technique for food powder production and, particularly in the past decade, there have been significant advances in understanding

how processing conditions affect surface composition, especially for dairy powders. There are now even efforts to *control* surface characteristics via the drying conditions (Nikolova et al., 2014). In addition, these properties can change due to aging effects during storage. In general the goal of the food manufacturer is to obtain the best quality powders by preventing undesired chemical reactions, or physical changes to components, by reducing the amount of fat on the surface, and by avoiding the development of "insoluble" material. The following discussion will elaborate on these points further, with a particular focus on dairy powders, as there is a wealth of information on such powders in the literature.

2.1.4 Damage to Components in a Drying Droplet/Particle

Firstly it is important to avoid damaging the heat-sensitive foodstuffs in the droplet during drying. If the temperature is too high then undesired changes can happen (Palzer et al., 2012), e.g. Maillard reactions between reducing sugars and proteins, which may cause an undesired change in flavor as well as a loss of nutrients (Schmitz-Schug et al., 2013), or the denaturation of heat-labile proteins, e.g. whey proteins (Anandharamakrishnan et al., 2007; Gianfrancesco et al., 2011), which would expose hydrophobic groups after the unfolding of secondary and/or tertiary polypeptide structure, or greater association between casein micelles[1], leading to more difficult water transfer during rehydration (Baldwin and Truong, 2007; Baldwin, 2010; Fang et al., 2012; Rogers et al., 2012). According to Baldwin (2010) the exact mechanism for casein-driven insolubility development is still subject to debate, but it may be due to greater association between and within the micelles via non-covalent bonds, such as hydrophobic interactions (Ch. 4). According to Fang et al. (2012); Rogers et al. (2012) it may be due to the "denaturation of casein", although this seems unlikely to be the dominant mechanism, given the higher stability against heat denaturation of casein compared to serum proteins (§ 6.2).

[1] See § 6.2

2.1.5 Damage during Preheat Treatments

It has also been shown that damage to dairy components *before* spray drying during preheating steps can contribute to insolubility development.[2] If the temperature is too high, undesired denaturation can occur, which as mentioned before, can worsen the reconstitution properties of e.g. emulsion-derived powders (Millqvist-Fureby et al., 2001) and of skim milk powder (Oldfield et al., 2005; Sharma et al., 2012). In the case of whole milk powder (WMP), high preheat temperatures can also denature sensitive proteins at the surface of fat globules (originally from the native fat globule membrane), which can bring about protein/protein interactions and ultimately the development of undesired "flecks" consisting of fat and protein. High preheat treatment of WMP can also induce "feathering" (coagulation), in high temperature–low pH environments, for instance in coffee whiteners added to coffee (Hui, 2006; Singh and Ye, 2010). On the other hand, the coffee stability of *skim* milk may actually be improved at higher preheating temperatures, since the denatured whey proteins can form disulfide bonds with κ-casein at the micellar surface, forming complexes and avoiding precipitation when added to the coffee (Oldfield et al., 2000).

In addition to damage to whey proteins (§ 6.2) *during* preheating or drying, damage can occur to whey protein isolate even after drying (Gulzar et al., 2011). This study showed that insolubility development depended on the pH of the concentrate prior to drying. Following a heat treatment, at lower pH values, aggregates were more soluble and were caused by intermolecular disulfide (S-S) bonds. At higher pH, the powder was more insoluble, due to cross-linking by other covalent bonds.

2.1.6 Component Migration inside a Drying Droplet

The reconstitution behavior of powders is very much affected by the *surface* composition of particles, which often is very different in composition from what one might expect based on the *bulk* composition of the powder, which could be determined by proximate analysis (Nielsen, 2014). The properties of spray-dried powders are influenced by the way that the

[2] High-temperature heat treating may be beneficial to the microbiological stability (Hui, 2006), but detrimental to the physical quality of the final product.

droplets form during atomization itself, and how different components migrate in the droplet as outward water transfer occurs (Kim et al., 2009b), even though the "lifetime" of the droplet is only on the order of milliseconds (Millqvist-Fureby and Smith, 2007).

There appears to be a ranking order of *which* components are most likely to appear at the particle surface: (1) hydrophobic materials, e.g. fat, (2) surface active materials e.g. proteins, which are amphiphilic, and (3) hydrophilic carbohydrates, e.g. lactose, followed by smaller minerals (Kim et al., 2009b). For instance, Kim et al. (2002) demonstrated that a much higher composition of fat appeared on the surface compared to the bulk in dairy powders (1 % total fat translated to 18 % on the surface, and 29 % fat in the bulk meant 98 % surface coverage). Nijdam and Langrish (2006) also reported that a small increase in the average fat content in milk powder (from 1 % to 5 %) lead to a sharp increase in the surface fat coverage (from $\approx$ 0 % to $\approx$ 35 %), with a more gradual rise in surface coverage at higher average fat contents. Vignolles et al. (2009) reported similar observations as well.

Kim et al. (2009b) explained that when a thin film of emulsified oil (as is the case for liquid milk) is atomized, the breakup of the stream into droplets is more likely to occur along the liquid-oil interface than elsewhere; and during drying, the droplet surface is to become the particle surface once water is removed. Nijdam and Langrish (2006) used similar logic to explain why whole milk particles are smaller than skim particles – as it is more frequent for the liquid stream to be broken up due to the greater oil-water interfacial area in the emulsion. Moreover, during drying, the dissolved and dispersed materials appear at the droplet surface (Nijdam and Langrish, 2006), as water diffuses out of the particle, there is a *migration* of material within the droplet, with the diffusivity through the water depending on both the polarity and the size of the components.

According to Fu et al. (2011), the mechanism for transport is still under debate. Kim et al. (2009b) argues that when water diffuses outward, there is a resulting concentration gradient, and a concomitant *inward* diffusion of material from the droplet surface, with the transport velocities being faster for more polar and/or smaller components. Thus, as a result, fat is the most likely component to be on the surface, especially those with a higher melting point (Kim et al., 2005b), followed by tensioactive proteins, then lactose, and finally minerals, as per the ranking order. On the other hand, Nijdam and Langrish (2006) argue against Kim et al. (2002)'s logic, since they noticed more lactose at the surface when spray drying took

place at *higher* temperatures, although the inward Fickian diffusion of lactose should be greater at higher temperatures. They therefore intimate that an *outward* diffusion of protein occurs towards the droplet surface and that the migration is quenched by fast drying due to the formation of a crust or skin. Whatever the mechanism of migration, the overall trend is the same in terms of surface composition gradient. Moreover, it has been shown that the relative position of the components takes place in the *early* stages of drying (i.e. during the *constant rate drying phase*), and the position is set before the onset of the *falling rate phase* (Kim et al., 2009b; Fu et al., 2011). In addition, Kim et al. (2009a) and Murrieta-Pazos et al. (2012b) have demonstrated that the surface composition is not significantly changed during agglomeration processes.

2.1.7 Crust & Skin Formation on Particle/Droplet Surface

According to Kim et al. (2009b), during the constant rate phase of droplet drying, saturation conditions are maintained and the temperature of the droplet is still relatively low, but as additional water is removed, solids begin to deposit at the droplet/particle surface, and the temperature will rise as the falling rate period begins, somewhat solidifying some of the deposited material (protein and lactose) as a "crust" possibly beneath a "skin" layer of fat molecules. These authors propose mechanisms for the formation of the crust. In the absence of fat, it is the surface active components that have surface priority (e.g. protein over lactose). However in the absence of both fat and tensioactive components the surface is determined by the solubility of dissolved materials – those that have the lowest solubility will precipitate first as water is removed, and is most likely to be located on the particle surface.

According to a number of articles (e.g. Nijdam and Langrish (2006); Kim et al. (2009b); Nikolova et al. (2014)), the composition of the surface also depends greatly on the *rate* of drying as well – the faster the drying takes place, the less migration of components possible due to the faster crust formation and as a result, the less difference between the surface and the bulk compositions (greater homogeneity). Nijdam and Langrish (2006) investigated the influence of the inlet spray drying temperature (T) and observed less protein and more lactose on the surface at higher T. Kim et al. (2009b) observed less protein and fat at the surface of skim milk powder at higher Ts, as well as at a higher feed solids content due to a higher viscosity and quicker drying (as less water needs to be removed), both of which

would hamper the migration of components in the droplet. However they also (indirectly) investigated the influence of droplet size (by sieving the powder and observing smaller and larger single particles) and saw no significant difference in the surface composition, even though one would expect a faster drying rate for smaller droplets.

Kim et al. (2009b) also investigated the influence of T and feeds solid content for *whole* milk powder and saw no significant difference, as the particle surface is largely covered in fat for all conditions. Nikolova et al. (2014) tested the influence of drying T on skim milk powder and also observed fewer lipids and proteins at higher drying Ts. They observed the influence of droplet size more directly by adjusting the nozzle pressure at atomization (higher pressure leads to smaller droplets), and for smaller particles, they saw a slight effect similar to that of higher T, due to faster drying (i.e. fewer lipids and proteins). With regards to feeds solid content, however, they observed no influence on surface composition, but it did affect powder moisture content (lower water activity if the feed was more concentrated).

Gaiani et al. (2011) compared the competitive surface adsorption between micellar casein and native whey proteins, and found higher amounts of casein on the surface at lower spray drying Ts, but not at higher Ts. They explain that the more surface-active caseins would have more time to migrate to the surface at lower Ts.

2.1.8 Morphology: Vacuole Formation (and Deflation)

Another property that is affected by the drying conditions is the morphology of single particles, especially for skim milk powder. According to Nijdam and Langrish (2006), once a crust develops on the drying droplet, the temperature of the particle will exceed the environmental temperature (in the falling state period), and the moisture will evaporate quickly. If the particle crust is hard and dry, then when the particle reaches a cooler zone of the drying chamber, the vapor will simply condense, leaving a spherical, **hollow** particle, as a result of the vacuole entrapped in the droplet during drying. However if the crust is still damp or not as sturdy, then the particle will deflate as it cools, leaving a **shriveled**, denser particle. Nijdam and Langrish (2006) demonstrated that higher spray dry temperatures yield more spherical particles, and lower temperatures result in more dimples. Similarly, Wu et al. (2014) observed more spherical particles at higher solids feed content, and explained this as being

due to a faster crust formation. In addition, these authors compared the "wettability" and "solubility"[3], and observed better wetting at higher feeds solids (attributed to larger size), but worse dissolving (possibly due to the denaturation of proteins, due to the faster temperature rise in the falling rate period as a result of the quicker solid crust formation).

Similar morphological observations were made by Muñoz-Herrera et al. (2010) using a much simpler system (maltodextrin DE20, a starch derivative (§ 8.1)). At higher temperatures *and* solids feed they observed more spherical particles, due to crust formation, and more deflated particles at lower Ts. These authors also were able to test the influence of morphology on "wettability" and "dispersibility" *without* the influence of component migration, as one would observe for dairy powders. With more spherical particles they observed worse "wettability" (in contrast to Nijdam and Langrish (2006)), possibly due to the poor sinking of hollow particles due to their low effective density (§ 1.2), however they saw improved "dispersibility", possibly due to the fact that the deflated particles would have a higher packing density, negatively influencing dispersing, due to greater possible contact between particles. However overall they report an improvement in reconstitution with spherical particles, which may be due to the fact that this type of maltodextrin material exhibits good wetting properties[4] making the wettability aspect less important for overall reconstitution.

On the other hand, the opposite effect of drying temperature on particle morphology was reported for milk protein concentrate (§ 6.2) by Fang et al. (2012). Particles were spherical at lower drying temperatures and deflated at higher temperatures – the reconstitution was also worse at higher temperatures. They explain that this may be due to damage to the proteins, as discussed before.

It should also be noted that with regards to surface composition and drying conditions obtained at a lab/pilot scale, spray dried powders may be significantly different when produced under similar conditions on an industrial scale (Fyfe et al., 2011).

[3] For a discussion about the ambiguity of these terms, see § 5.1.

[4] A similar maltodextrin powder is used in Ch. 9.

2.1.9 Fat on Particle Surface - Melting Considerations

With regards to high-fat powders, it appears that it is not only the amount of fat but also the type and mode of incorporation that determines a particles properties. Kim et al. (2005b) demonstrated that the properties, especially the wetting properties, of dairy powders is a function of the **melting** characteristics of the surface free fat/oil – wetting is vastly improved when the water temperature is high enough that it can melt the solid fat at the surface.

Milk fat is in fact a mixture of many different triacylglycerols, with melting temperatures ranging from $-40\,^{\circ}\mathrm{C}$ to $40\,^{\circ}\mathrm{C}$, depending on the esterified fatty acid residues (Kim et al., 2005b). These authors utilized a stepwise solvent extraction method to distinguish between different types of fat in the powder, e.g. surface free fat or fat encapsulated in the continuous matrix of amorphous lactose and protein. Using gas chromatography/mass spectrometry, they characterized the different fatty acid compositions and determined that higher-melting temperature fats (i.e. those with fatty acids with larger molecular weight and/or less unsaturated *cis*-double bonds) are more likely to be found in the surface free fat compared to encapsulated fat. They also demonstrated that the amount of solid fat is a function of the powder temperature: at $20\,^{\circ}\mathrm{C}$, ≈ 35 % of fat at the surface was solid, and 28 % of encapsulated fat was solid – the rest being liquid oil. In addition to the effects on rehydration of the powders, the authors (as did several authors, e.g. Nijdam and Langrish (2006); Vignolles et al. (2009); Fu et al. (2011); Nikolova et al. (2014)) discuss the implications of having high amounts of surface free fat, as these fats are "exposed" to the environment, whereas encapsulated fats that are "protected." Most notably is the possibility of off-flavor development due to oxidation (if O_2 is present) or lipolysis (enzymatically catalyzed) – thus, a higher degree of encapsulated fat is typically desirable (Vignolles et al., 2009).

2.1.10 Homogenization Effects

The amount of surface–free vs. encapsulated fat is also determined by the size of the fat droplet in the milk emulsion prior to drying; and this size distribution is affected by the extent of homogenization that the concentrate undergoes prior to drying. Kim et al. (2009b) investigated the number of passes through a homogenizer (2 vs. 6 passes), and observed

better encapsulation (less surface free fat) with a greater number of passes, especially at high drying temperatures. They explain that the smaller globules would be less likely to migrate towards the droplet surface during drying, and become entrapped in the lactose/protein crust. Similarly, Vignolles et al. (2009) dried high-fat dairy products both with and without homogenization (at 20 MPa). These authors also observed less surface free fat and smaller droplets in the homogenized dairy powder. They also reported better wetting/sinking the homogenized powder, due to less surface free fat.

§2.2 Aging during Storage

After a powder is manufactured, it typically needs to be transported and stored, often for many months, before final usage. However a number of changes can occur to the surface of food powders during this time; these aging effects typically deteriorate a powder's ability to reconstitute, as well as other functional properties. These effects are particularly strong when a powder is subjected to high temperatures, relative humidity and/or storage time. In the following discussions, some of the main effects are discussed (once again with a particular focus on dairy powders).

2.2.1 Fat Release during Storage

As already mentioned, fat on a particle surface can have a negative effect on powder wettability. During storage, low-fat dairy powders may see an increase in the surface hydrophobicity (and thus generally worse reconstitution properties) due to the migration of fat to the surface. Gaiani et al. (2007, 2009) explained that residual lipids in micellar casein powders, especially polar lipids originating from the native milk fat globule membrane, can migrate to the surface leaving behind pores and a higher amount of occluded air in the powder.

In addition, Kim et al. (2009c) reported that during long-term storage, the encapsulated fat (which, as previously mentioned tends to have a lower-melting temperature than the surface free fat), was released to the particle surface, thereby decreasing the melting point of the

surface fat, which would mean less solid fat on the particle surface.[5]

On the other hand, Vignolles et al. (2009), who as previously mentioned investigated the drying of homogenized vs. unhomogenized high–fat dairy emulsions, reported an increase in melting temperature of milk fat during storage, and related this to the polymorphic nature of milk fat – over time the fat could adopt more stable crystal structures, characterized by a signature change in thermal properties by DSC[6], which would lead to an increase in the melting temperatures of fats. They also report a *decrease* in surface fat for high-fat powders over time in their unhomogenized samples, and explained that the greater amount of free ("unprotected") fat was susceptible to deteriorative effects, such as oxidation or lipolysis – a hypothesis they corroborated using sensory tests.

2.2.2 Caking due to Fat Bridges

In addition, the presence of fat on the surface of food particles may lead to decreased flowability, or caking (a sort of undesired agglomeration (Palzer, 2005)), in which lipid bridges between particles are formed (Kim et al., 2005a; Nijdam and Langrish, 2006). According to Fitzpatrick et al. (2007), the increased stickiness leads to higher cohesivity between particles, which as discussed in § 1.3 may compromise the dispersing behavior of the powder. According to Bhandari and Roos (2012), such caking effects would be worse at higher pressures as well, which may be important for powders at the bottom of a bag, or if bags of powders are arranged in tall stacks.

2.2.3 Caking of Hydrophilic Crystalline Food Powders

Such caking phenomena are also posible for hydrophilic crystalline food materials. Langlet et al. (2013) and Dupas-Langlet et al. (2015) observed the effect of temperature (T) and relative humidity (RH) on the behavior of NaCl – they explain that at an RH above the deliquescent relative humidity (DRH) of the material, capillary condensation of water can occur on the material surface, dissolving the material in a saturated solution that can form

[5] The possible implications of this alteration in surface fat composition are discussed in Ch.11.

[6] Differential Scanning Calorimetry

a liquid bridge between particles. If the RH is then lowered below its efflorescence relative humidity (ERH), which is lower than the DRH due to a hysteresis, the spontaneous nucleation of material occurs, and the water is released into the atmosphere, leaving behind a solid bridge between the particles. Dupas-Langlet et al. (2015) also report that the DRH of mixtures of crystalline food materials can be lower than the DRH of the individual components: they observed deliquescence of sucrose-NaCl mixtures at RH = 64 %, even though the DRHs were 76 % and 85 % for NaCl and sucrose, respectively. Forny et al. (2005) also demonstrated that unexpected caking between (macroscopically) hydrophobic particles can even take place, if nano-sized hygroscopic salt crystals (like NaCl) are also present at the surface.

2.2.4 Caking of Hydrophilic Amorphous Food Powders

Even more susceptible to such caking effects during storage are hydrophilic amorphous food materials, as these will gradually absorb moisture from the environment if the relative humidity (RH) is greater than the material's water activity (a_w).[7] It has been shown by a number of studies that caking is determined by glass transition-related stickiness of amorphous materials (Palzer, 2005, 2009; Fitzpatrick et al., 2007, 2008, 2010; Hogan et al., 2010; Chávez Montes et al., 2011a; Hartmann and Palzer, 2011; Descamps et al., 2013).

Recently Haider et al. (2014) investigated the caking-related cohesion mechanisms between two single spherical particles of (amorphous) maltodextrin DE21, under controlled T and RH. Using a novel micromanipulation particle tester, they were able to control the contact between the particles in distance-controlled experiments in order to measure the cohesive strength of the particle-particle interactions, by measuring the force upon separation after a defined holding time. They determined that for two particles brought into contact, the cohesive strength and cohesion mechanisms were governed by the quantity $(T - T_g)$, i.e. the environmental temperature T compared to the material's glass transition temperature (T_g)[8] – the latter of which depended on the RH under equilibrium conditions, i.e. the material's water activity a_w.

[7] Hence, the "egg-shell" structures discussed by Yazdanpanah and Langrish (2013) discussed in § 1.4.

[8] They use the onset of glass transition with a heat ramp of 10 °C, and a double scan to eliminate thermal aging effects.

For two particles brought into contact, they report a greater viscoelastic flattening of particles as the $T - T_g$ increased, up until about 8.5 °C, due to a softening of the material. The increased contact zone allowed for greater cohesive forces (likely due to van der Waals interactions), and a stronger interaction up to a maximum at $T - T_g \approx 5.5$ °C. At higher values, however, the softer material streteched more easily upon separation, resulting in a weaker bond. In addition at higher $T - T_g$ values, (14 °C or 16 °C), they reported the formation of a low viscosity bridge, likely triggered by capillary condensation, that plasticize the material, causing a viscous material flow between the particles (i.e. sintering). While this bridge is weak upon separation, the authors demonstrated that if the T was reduced below the T_g of the material, the resulting glassy bridge was even stronger than the flattening-induced interactions. Thus, this study (as did the studies on crystalline materials), demonstrated not only the importance of T, RH, and the material properties on caking, but also *fluctuations* in ambient conditions on cohesive interactions, all of which may lead to a decreased dispersing ability of food powders upon reconstitution.

In addition, problems even worse than caking or sticking – the full-blown catastrophic collapse of the particle structure into a viscous liquid, could also occur if the humidity reaches even higher values (Palzer, 2009).

A number of anticaking agents also exist (Lipasek et al., 2012) – these generally act by absorbing moisture instead of the food powder, or possibly by coating the particles to reduce hygroscopicity.

2.2.5 Sub-T_g Relaxation of Amorphous Materials

For amorphous carbohydrate materials, there is also evidence that dissolving can become more difficult during storage, even if the T remains well below the material T_g. Descamps et al. (2009) investigated the sub-T_g structural relaxation, and explained that annealing of the molecules can lead to local order development that could affect dissolving. They also demonstrated higher sub-T_g temperatures hastened this aging effect, as did increased relative humidity, to a lesser extent. Syll et al. (2012) demonstrated that dissolution of amorphous sucrose was slower due to similar sub-T_g aging effects as well.

Zhou and Labuza (2007) also investigated the effect of storage conditions on the development of insoluble components in whey protein powders (§ 6.2). They observed no protein aggregation (solubility loss) for native whey protein isolate or β-lactoglobulin; however, they did observe significant solubility loss for whey protein hydrolysate, especially at high relative humidities. They explain that the hydrolyzed protein would have a lower T_g due to its lower molecular weight, and therefore would be more susceptible to molecular sub-T_g relaxation due to increased molecular mobility, which could lead to the formation of covalent disulfide bonds.

2.2.6 Solid-Phase Crystallization

As explained in § 1.4, for some low-molecular weight molecules, most notably lactose due to its presence in dairy powders, crystallization of amorphous molecules can occur if the molecules gain enough mobility through plasticization from moisture or an increase in temperature (Palzer, 2007). Not only is this undesirable due to the slower dissolving of crystalline materials compared to their amorphous counterparts, but it can have other serious repercussions as well. As previously mentioned, amorphous lactose is better at encapsulating other materials, such as water (and fat, etc.). If the lactose crystallizes, then these materials, including the water, can be expelled from the particle; this liberated water could then go on to plasticize other amorphous particles, possibly causing further crystallization, and even a sort of chain-reaction-like phenomenon throughout the powder bulk.

According to Kim et al. (2009c), the phase separation of fat can also be affected by the sharp crystal edges mechanically disrupting the membrane of a fat globule. Moreover, according to Thomas et al. (2004), proteins may be damaged due to the mechanical stresses caused by such physical changes, negatively affecting reconstitution properties. Thus, it is important to understand the factors that influence lactose crystallization.

Recently Gianfrancesco et al. (2011) demonstrated that lactose crystallization could be delayed during storage due to the presence of the whey protein β-lactoglobulin (β-LG), especially if this protein was denatured. However, micellar casein had no effect on crystallization delay. They explain that the more open structure of the denatured β-LG would be able to better interact with the sugar and prevent its movement (reduce its molecular mobility), thereby delaying crystallization.

2.2.7 Casein Aggregation during Storage

Another phenomenon that has gained considerable attention in the past few years is the decrease in reconstitution ability of dairy powders high in casein content, e.g. micellar casein (MC) powders, or milk protein concentrate (MPC), during storage. According to Mimouni et al. (2010), the main mechanism responsible is not due to the development of insoluble material (e.g. denatured proteins), but rather to stronger interactions between casein micelles, which would reduce water transfer and therefore delay reconstitution (as discussed in § 1.4, it is this release of casein micelles that limits the reconstitution of such powders.) The authors explain that a "monolayer skin" of aggregated caseins develops at the surface of the particles; however, the exact mechanism for the stronger interactions appears to be somewhat unclear. According to Havea (2006), it may be due to hydrophobic interactions, with some contribution of minor whey proteins (for MPC). According to Sikand et al. (2013) (for MPC), it could also be due to cross-linking between and within micelles via the micellar calcium phosphate, which serves as a sort of bridge that helps keep the micelles together, as well as possibly the effects of disulfide bonds.

Anema et al. (2006) observed the effects of storage temperature on the reconstitution properties of MPC, and attributed worse rehydration not to whey proteins, but to casein cross-linking as well; however, they also explained that particularly at higher temperatures, lactosylation of the casein proteins (which would be involved in the early stage of the Maillard reactions) was observed, and this could lead to different cross-link products as a result of actual chemical reactions (covalent bond formation). According to Haque et al. (2011), there may also be a limited unfolding of casein proteins that could favor casein–casein interactions.

Whatever the mechanism responsible, according to Fang et al. (2011), there may exist a threshold amount of aggregation at the surface, above which the reconstitution would steeply rise. In addition, a sub-T_g relaxation of these proteins may also occur, which would bring micelles into even closer contact, facilitating further interactions (Schokker et al., 2011; Haque et al., 2012).

2.2.8 Treatments to Disrupt Micellar Casein Structure Prior to Drying

Given the fact that the development of stronger casein interactions during storage can negatively impact reconstitutability of such powders, there have been a number of studies aiming to disrupt the micellar structure, thus releasing casein proteins into the serum prior to drying, in order to improve the powder quality.

Ionic Modifications

Some studies have demonstrated that changing the ionic nature of the concentrate prior to spray drying can influence micellar structure. For instance, according to Schokker et al. (2011); Augustin et al. (2012), if Ca^{2+} is removed, e.g. via ion exchange or a chelating agent, micellar structure will be loosened, as the divalent cation helps to cross–link between proteins. Havea (2006) explained that the removal of Ca^{2+} results in stronger electrostatic repulsive forces (Ch. 4) during rehydration. Conversely, Davenel et al. (2002), Schuck et al. (2002), and Schokker et al. (2011) demonstrated that adding $CaCl_2$ to micellar casein prior to spray drying worsened rehydration properties due to flocculation.

Addition of a Monovalent Ion

Some studies have demonstrated that the addition of monovalent cations (Na^+ or K^+) prior to spray drying improves rehydration properties, although the mechanism appears to remain unclear, or there may be more than one explanation for this effect. Both Schuck et al. (2002) and Sikand et al. (2013) explain that the ions will solubilize the Ca^{2+} bound to phosphoryl residues by an ion exchange, thereby weakening the micellar structure. Schuck et al. (2002) was also able to improve the reconstitution properties of micellar casein powders by *dry mixing* it with NaCl; instead of a modification to the micellar structure, they explain that this was due to the hygroscopic nature of the salt. A similar explanation was given by Davenel et al. (2002), even if it was co-dried (mixed before drying). Schuck et al. (2002), Davenel et al. (2002), Schuck et al. (2007), and Schokker et al. (2011) also demonstrated an improvement to

the "solubility"[9] of micellar casein by adding citrate or (to a lesser extent) phosphate prior to drying, again, by disrupting micellar integrity.

Mixing with Caseinate

Schokker et al. (2011) showed that the stability against this aging effect of micellar casein could be improved if it was mixed with a non-micellar casein (sodium caseinate[10]) in the spray dry feed – it was explained that this may have prevented cross-linking due to a spatial separation of micellar caseins, and non-micellar caseins may have adsorbed preferentially at the particle surface during drying due to a greater surface activity.

Conversion *to* Non-Micellar Casein

Instead of *adding* caseinate to micellar casein concentrates, Schokker et al. (2011) also demonstrated that it was possible to obtain a similar effect by inducing the formation of non-micellar casein *"in situ"*, by performing a heat treatment under alkaline treatment – see § 6.2 – or by applying high hydrostatic pressure to increase the amount of non-micellar casein. Similarly, Udabage et al. (2012) used a combination of both heat and pressure to improve the rehydration quality of milk protein concentrate. Huppertz and de Kruif (2007) also noted that if a high pressure treatment was applied long enough, caseins could reassemble into micellar structures, and that these interactions were unaffected by the presence of whey proteins.

Interestingly, however, Gianfrancesco et al. (2011) compared the rehydration of micellar casein and sodium caseinate powders, separately, and actually observed worse reconstitution of the *non*-micellar casein powder. They explained that these would exhibit more hydrophobic sites that would first contact water upon wetting. It should be noted, however, that they utilized a conductivity meter to monitor rehydration (Ch. 5), therefore it may be that micellar casein powder has better wetting/sinking properties, as the conductivity probe would only be able to detect the minerals in the powder once it is wetted/submerged.[11] Their technique

[9] See § 5.1.

[10] See § 6.2

[11] For problems associated with using a conductivity meter to monitor the rehydration of powders, see § 5.12

would have no way to assess the *extent* of particle and micellar dispersing (change in size distribution), and one might even expect better "solubility" of the *non*-micellar casein, even if the wetting/sinking is worse.

Gaiani et al. (2009) also indeed reported *slower wetting* of sodium caseinate (NaCas) compared to micellar casein (MC), but also a *better dispersing* of NaCas compared to MC.

High-Shear Pretreatment

It has also been shown that a shearing treatment of concentrates high in casein prior to drying can also disrupt micellar structure and improve the rehydration properties of the final powder during storage. Augustin et al. (2012) compared three different shear treatments: sonication, homogenization, and microfluidization. The sonication device causes cavitation bubbles that grow until they are no longer stable and collapse, inducing mechanical stresses due to localized shear. They explain that homogenization is a process where turbulence and cavitation is induced unto a liquid by pumping it through a small orifice. They explain that while casein micelles would normally be able to withstand homogenization processes aimed at reducing the size of fat globules (§ 6.2), at higher pressures ($> 100\,\mathrm{MPa}$) casein micelles can be disrupted as well. Finally microfluidization imposes impact, cavitation and shear forces as a liquid is forced into microchannels of defined arrangement. The study reported that microfluidics was the most successful at improving rehydration properties of milk protein concentrate (MPC).

Chandrapala et al. (2014) also saw an improvement in MPC powder quality following sonication, however they claim that the energy density used would not have been strong enough to alter the micellar structure (according to their previous work (Chandrapala et al., 2012)). Thus they propose that the responsible mechanism is rather due to a disruption of whey-casein aggregates. Liu et al. (2014) on the other hand did see a disruption of casein micelles in skim milk, particularly at higher pH values. They explain that this would be due to the fact that (negatively charged) casein micelles would have an increased negative charge under alkaline conditions. The resulting stronger repulsive forces would make the micellar structure weaker, and more vulnerable to disruption. The authors also reported improved

and Ch. 14.

disruption at *lower* sonication frequencies – as cavitation bubbles become smaller at higher frequencies, resulting in less force from the subsequent implosion.

Enrichment during the Production of High-Casein Powders

Some studies have also shown that mixing in other food molecules to micellar casein concentrate prior to drying can enhance reconstitution properties. Davenel et al. (1997) and Davenel et al. (2002) reported an improvement in reconstitution by adding either native whey protein concentrate or polydextrose (a soluble fiber), and explained that these additions sterically hindered the association of the micellar caseins via calcium phosphate bridges. However, they report that lactose and sucrose, smaller molecules, did not improve reconstitution.

Richard et al. (2013) on the other hand did observe an improvement in the behavior of micellar casein if dried with lactose – in fact the improvement was better than the improvement seen by co-drying with whey proteins. However it should be noted that while Davenel et al. (1997) used 12 % w/w lactose and freeze-dried the samples, Richard et al. (2013) used 30 % w/w and spray dried the samples. Richard et al. (2013) explain that the fast-dissolving lactose would favor quick solvent penetration. Gianfrancesco et al. (2011), however, performed similar experiments in a spray drier (25 % w/w lactose) and saw no significant difference. One possible reason could be due to the difference in drying conditions – as explained earlier, one might expect to see more lactose on the surface at higher drying temperatures due to quenched migration of components.[12]

Gaiani et al. (2007) also reported an improvement in micellar casein reconstitution if co-dried with native whey proteins; however, the reconstitution properties deteriorated if the two powders were dried separately and then dry-mixed, although they do not provide a clear mechanism to describe their observations.

[12]Unfortunately, Richard et al. (2013) did not report their drying temperatures. Although, if one assumes they applied the same heat conditions as in their previous publication ($T_{\text{inlet}} = 215\,^{\circ}\text{C}$), compared to Gianfrancesco et al. (2011)'s 180 °C, this mechanism could be relevant.

§2.3 Chemical Modifications

2.3.1 Use of Wetting/Dispersing Agents (Lecithination)

The reconstitution behavior of powders can also be altered by modifying the surface chemistry with the use of wetting/dispersing agents. Food grade surfactants, typically soya lecithin (Ch. 8.3), (usually < 5 %)[13] may be added to the surface. According to Hogekamp and Schubert (2003), the use of such agents is highly regulated; Freudig et al. (1999) claimed that lecithination of dairy powders was banned in Europe; however, the current author could find no evidence to support their claim. In fact, Westergaard (2004), based in Denmark, states that lecithination is common practice for whole milk powders, and Abdelaziz et al. (2014) in France says it is common for cocoa beverage powders. Lecithin is designated as E322 as a food additive by the European Union.

Lecithin contains phospholipids that are amphiphilic in nature; that is, they have both a hydrophilic and a hydrophobic end. According to Abdelaziz et al. (2014), when it is added to a lipophilic surface, the hydrophobic ends of the molecules will preferentially adhere to the solid surface, leaving the hydrophilic end exposed, which can then attract water. Thus in this particular case, it *improves* the wettability by water. According to Nijhuis et al. (2007), lecithin may also stabilize the final beverage against sedimentation/creaming once reconstitution is complete.

During whole milk powder processing, lecithin is often added in anhydrous milk fat (oil), and then sprayed on the powder surface (Westergaard, 2004; Kim et al., 2009a). For chocolate beverage powders (Ch. 6.3), lecithin can be directly sprayed onto the surface (Vissotto et al., 2006). For cocoa powders, lecithin can be added to the cocoa cakes (after cocoa butter is pressed from the cocoa mass, see Ch. 6.3) prior to pulverizing (Kamphuis, 2009).

There are also a number of **patents** filed regarding the use of wetting agents to improve powder wettability, demonstrating how competitive the industry is regarding powder rehydration quality. For instance, Ewing and Fisher (1982) atomized both lecithin and a fat emulsion

[13] Small amounts are added to prevent a negative flavor associated with lecithin (Schubert, 1993).

to be added to the surface of skim milk powders to obtain fat-containing dairy powder. Pray and Scott (1993) mixes the ingredients of cocoa beverage powder together, and grinds them to evenly disperse the emulsifier before agglomerating. Nijhuis et al. (2007) uses a solvent to reduce the fat content of cocoa powders, and this solvent also improves the uniformity of lecithin on the powder surface. Rogers (2011) uses lecithin from eggs to "instantize" powders high in whey protein content. In addition to published patents, there may very well be a wealth of trade secrets related to such processes as well.

Note that one patent (Colarow, 2009) actually claims, somewhat counterintuitively, that the wettability of cocoa products is actually improved by *reducing* the endogenous content of phospholipids. They claim that these phospholipids (released during fermentation), form a complex with the amylose of the starch granules, forming an insoluble film at the surface. Moreover, these granules would not be able to gelatinize (swell) during processing, and would result in insufficient amylose leaching and greater retrogradation during storage. They claim that the presence of the phospholipids increases hygrocapacity, worsening the swelling effects.

Freudig et al. (1999) demonstrated that the reconstitution of skim milk powder (which, as mentioned previously, may contain quite a high amount of fat on the particle surface compared to in the bulk) could be improved by dry-mixing with 1 % w/w powdered lecithin. They attributed this to improved wettability, as well as the development of an increased repulsive electrical double layer (Ch. 4) around the particles that improved dispersing; however, they provided no experimental evidence to support this claim.[14] Instead, they cited Schubert (1993) (one of the co-authors of Freudig et al.), who also provided no proof of this mechanism. Freudig et al. (1999) also reported improved reconstitution[15] if lecithin was added to the *water* before the milk powder is added, but the improvement was not as significant as if the lecithin had been dry-mixed with the powder.[16]

One interesting aspect of lecithination is that it does not always improve wettability with respect to water, but rather, it may be able to "reverse" the polarity of a surface. On a hydrophilic surface, the *hydrophilic* moiety of the amphiphilic molecule may preferentially attach to the surface, making the powder more hydrophobic overall. Westergaard (2004)

[14] See § 12.1.

[15] Unfortunately, Freudig et al. (1999) did not specify the water temperature of their trials, which as explained in Ch. 11 plays a major role in reconstitution properties.

[16] See § 12.2.

explained that this may actually be desired to *delay* water absorption in "very hydrophilic" whey proteins powders. They describe that if absorption of water is too fast, dispersing of the powder may become difficult, due to swelling (§ 1.4). However if absorption is slightly delayed, particles can be dispersed sufficiently before absorption. This description appears to contradict the patent of Rogers (2011), as well as Gaiani et al. (2009), who reported slow wetting/sinking of whey protein isolate.

Another example of lecithin being used to *hydrophobize* hydrophilic powders can be found in Millqvist-Fureby and Smith (2007). These authors added lecithin to skim milk concentrate, whey protein concentrate, and lactose, prior to spray drying (i.e. an "*in situ* lecithination"), in order to improve the dispersing of the hydrophilic powders in chocolate, a fat-continuous medium – the lecithin is added to stabilize the particles in chocolate against separation. By doing this, the researchers took advantage of the migration phenomena that occur inside of a drying droplet; this *in situ* lecithination is performed as a replacement to adding lecithin during the conching step of chocolate production. They report a "competition" between lecithin and other surface active molecules (i.e. proteins) for dominant presence at the surface, and this depended on how quickly they could adsorb to the droplet surface, with lecithin forming a monolayer at the air-liquid surface. It has also been shown that an *in situ* addition of surfactants to whole milk concentrate can also improve rehydration properties (Mather and Hollender, 1955). However, according to Tian et al. (2014), coating with lecithin *after* drying was more effective in improving the wetting/sinking properties of whole milk powder.

Parker et al. (2000) explain that mixing a surfactant to dry hydrocolloid (§ 6.1) powder can induce an explosive dispersion of particles at the surface of the water, which helped eliminate lump formation. They explain that this could be due to the Marangoni effect, which is that the surface tension at the point in the water where the surfactant dissolves will be reduced, causing a surface tension (γ) gradient with the surrounding interface. Mass transfer will then occur along the interface towards regions of higher γ, as γ is a contractile force, causing the explosive behavior. It is unclear if the change in downward capillary suction and oscillation-driven repulsion (§ 1.2) may also play a role as well. However, Parker et al. (2000) did not specify the amount of surfactant used, the powder used, the water temperature, etc.

Lastly, Kyaw Hla and Hogekamp (1999) reported a deterioration in wetting behavior of chocolate beverage powders during storage if the bags are left open during the storage. They

explained that this may be due to migration of lecithin away from the surface; however, in the author's opinion, this logic is hard to follow and surface analysis should have been performed to validate their claims.

2.3.2 Dispersion in Sugar

Particularly in the case of food hydrocolloids (§ 6.1), powder can be dispersed in sugar in order to improve their reconstitution properties, especially to prevent lump formation due to the physical separation of the grains (Klein Larsen et al., 2003). Kravtchenko et al. (1999) and Parker et al. (2000) even refer to so-called "dispersing" and "non-dispersing" conditions depending on whether or not the hydrocolloid powders are dry-mixed with sucrose prior to rehydration, with even as much as 19× more sucrose than hydrocolloid. It is important to keep this in mind when reviewing the literature. For instance, Klein Larsen et al. (2003) reported faster dissolution of alginate powders with decreasing particle size (under *dispersing* conditions), but it is unclear if the same results would be obtained under *non*-dispersing conditions, i.e. the powder by itself. Parker et al. (2000) reported a greater amount of lumps with decreasing particle size for various hydrocolloid powders under non-dispersing conditions, and also explained that characterizing the "end" of reconstitution (§ 14.3) is very challenging if long-lasting lumps form.

The addition of sugar to improve reconstitution properties is also common for chocolate beverage powders (CBPs). According to Abdelaziz et al. (2014), the cocoa powder (i.e. the signature ingredient of CBP) is mixed with sugar and/or milk powder, or sugar can be agglomerated together with the cocoa powder (Kowalska et al., 2011). The addition of sugar has been shown to improve the wetting/sinking properties as well as overall reconstitution (See § 6.3, cf. Kowalska and Lenart (2005) and Shittu and Lawal (2007)). Finally, Szulc and Lenart (2013) demonstrated an improvement in reconstitution of dairy powders if they were coated in lactose solution prior to drying.

2.3.3 Encapsulation

Finally, there are a number of encapsulation techniques to improve the solubility of incompatible ingredients (e.g. lipids) as well (Garti and McClements, 2012; Bhandari and Roos, 2012). These are especially useful for sensitive health-promoting substances (Davidov-Pardo and McClements, 2015), and can even be designed to promote the bioavailability of nutrients (absorption into the bloodstream following consumption), by protecting the ingredients until they reach absorption sites in the digestive tract (Parada and Aguilera, 2007). According to Drusch et al. (2012), the transport phenomena (discussed earlier) during atomization can also be exploited for microencapsulation purposes.

Chapter 3

Mixing

Contents

§3.1 Mixing for the Purpose of Powder Reconstitution

In order to hasten the mass transfer associated with reconstitution, mixing of the solids and liquids is nearly always performed. Ideally mixing should occur quickly and completely, with the absence of lumps, floating particles, or a sedimented layer, with minimum energy input (Richard et al., 2013).

3.1.1 Retail Mixing

There are many ways for mixing to come about: on a consumer level, for so-called "retail application", powder may be poured on top of the liquid and mixed with a spoon, or vice versa: the liquid could be poured over the solids. There may be other techniques as well, such as alternating adding the liquid and solid, as a sort of 'sandwiching' technique. In some cases, the consumer may even use a blender to exert high shear to disperse lumps. There is even one popular product amongst athletes – the Blender Bottle^{TM}, which consists of a canister with a metallic spring ball, which when shaken bounces around at high speeds to help reconstitute powders such as nutritional supplements (e.g. high-protein powders) for on-the-go reconstitution without the need for an electrical source.

3.1.2 Vending & Capsules

A number of 'convenience' applications exist as well to reconstitute powders, for instance vending machines. During vending, powder is mixed with a jet of water to reconstitute into a cup for immediate consumption. According to Schubert (1993), powders intended for vending purposes do not need to exhibit particularly good "instant properties", as do retail-intended

powders, as mixing is typically more intensive during vending-based reconstitution.

Other convenience beverage preparation machines at the consumers' homes or workplaces, e.g. Nescafé Dolce Gusto or Keurig (in the USA), operate by injecting pressurized water into a receptacle, such as a capsule or sachet, after piercing it (Dogan and Doleac, 2014). For beverages like tea or coffee, such a system can simulate brewing, by extracting the aroma compounds, and for powders such as Nesquik, inside the capsule reconstitution of the powder occurs to form a beverage. For coffee with creamer, or a cappuccino beverage, both an extraction and reconstitution may take place, therefore optimization of beverage quality requires knowledge of the food's reconstitution behavior when the liquid is injected.

3.1.3 Impeller-Agitated Mixing

On an industrial level, mixing of powders and liquids is a common unit operation in itself, as many ingredients for foods are transported in powdered form. For example RTD (ready-to-drink) beverages require reconstitution of ingredients, as do many products sold in solid form. According to Paul et al. (2004), such mixing applications can be very energetically expensive, and thus they emphasize the importance of understanding mixing fundamentals for process optimization. Generally industrial mixing is conducted using an impeller (or multiple impellers) that causes the liquid to move, and this movement in turn aids with the steps of reconstitution, as described earlier. There exists a vast variety of impeller types, depending on the specific mixing application at hand.

Compared to other methods of reconstitution, impeller-agitated applications offer the best ability of control the process, as the mixing unit can be adjusted to a well-defined geometry, and the mixing is well characterized (at least for Newtonian liquids). From a research perspective, the vast majority of powder reconstitution studies were performed in an agitated vessel, due to the amount of control the operator has, and for enhanced reproducibility. Thus such a set-up was also used in the current PhD (Ch. 7). Some other authors have used a magnetic stir-bar setup; however, the flows generated are not well-characterized, and the bar does not always move in a predictable manner. Moreover, some studies (although, unfortunately a minority) have also adhered to the **standard dimensions** for impeller-agitated vessels (Fig. 3.4) enhancing comparison between studies as well as reproducibility.

Most vessels, however, have rather arbitrary configurations (Ch. 5).

3.1.4 Sonication

Although not the focus of the current thesis, it is worth noting that ultrasounds can also be used to disperse particle agglomerates in a liquid. As briefly discussed in §1.3, an ultrasonic device causes sound waves to propagate in the medium, causing rarefaction and compression cycles. This can induce cavitation voids, that then violently collapse, causing high turbulence, pressure, and temperature when the bubble implodes. Kusters et al. (1993) gave a description for power characterization and the fragmentation of suspended particles. McCarthy et al. (2014) recently investigated the reconstitution of milk protein concentrate by combining a conventional overhead stirrer with a sonication system in a two-step process, and saw improved reconstitution than if only impeller-stirring was used. They attribute this to similar mechanisms regarding hydrophobic interactions of casein micelles discussed in Ch. 2. However, as ultrasounds rapidly increase the temperature and can damage food components, they had to use an ice bath around the mixing setup to dissipate the heat.

§3.2 Configurations of Impeller-Agitated Tanks

The type of flow in an agitated vessel depends largely on the vessel configuration, especially the impeller used, and whether or not the vessel is baffled.

3.2.1 Impeller Types

According to Tiwari and Cullen (2009), two main types of flow patterns are: axial, in which flow is mostly parallel to the impeller shaft, and radial, where flow is parallel to the impeller blade radius. An example of an axial-type impeller would be the Lightnin A100 marine-type propeller, and a radial-type impeller would be the Lightnin R100 Rushton-type turbine (Fig. 3.1), where Lightnin®, operating under SPX Flow Technology, is a company based in

Rochester, NY, USA.[1]

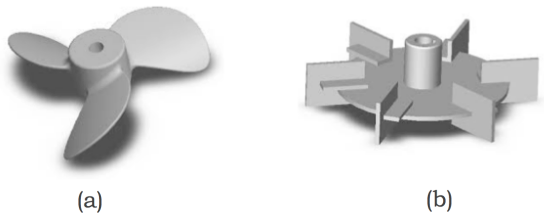

Figure 3.1: (a) Lightnin A100 and (b) Lightnin R100 impellers.

According to the manufacturer, the energy input given to these two impellers will be converted into flow differently, and it is important to understand as it will affect various mixing applications differently. The power will be converted into both a pumping effect Q, and a velocity head H, indicative of a shearing effect, such that:

$$P \propto Q\,H \tag{3.1}$$

where, for a given power input, axial impellers will produce more flow (higher Q), and radial impellers more shear. Fig. 3.2 highlights the difference in flow patterns, adapted from Roustan et al. (1999).

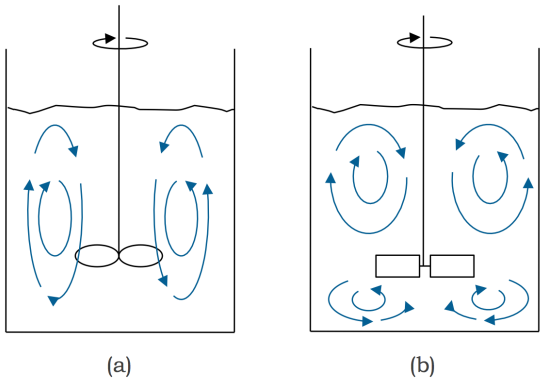

Figure 3.2: (a) Axial and (b) radial flows.

In addition, depending on the application, impellers can be placed at different vessel off-bottom clearances, or at different angles of tilt (see Roustan et al. (1999)); however, for the current study only the standard configuration is considered (Fig. 3.4). According to Fitzpatrick et al. (2000), in the case of food mixing, high shear from an impeller is desirable

[1] Additional information and impeller types can be found at `http://www.spx.com/en/lightnin/pc-impellers/`. However, these two impellers (A100 and R100) are the only ones used in the current PhD.

to aid with dispersing and dissolving; however, if the shear is too high, damage to the food (e.g. disruption of fat globules, resulting in creaming), may occur.

3.2.2 Baffling

Mixing performance also highly depends on the presence or absence of baffles along the side of the vessel. According to Dickey (2009b), these remove radial stratification, forming extensive vortices that can help improve mixing. However in unbaffled vessels, an air-cone vortex may form around the impeller shaft due to fluid swirling and centrifugal effects (Pakzad et al., 2008). According to Dickey (2009b), the swirling may result in poor mixing, and in particles settling towards the vessel center. In addition, if the vortex becomes too large that it extends past the impeller blades, it can incorporate air into the liquid (Busciglio et al., 2013), which may result in an undesired foam (Fitzpatrick et al., 2000). On the other hand, at higher viscosities, baffles may lead to the formation of "dead zones" in the vessel (Pakzad et al., 2008), and unbaffled vessels are easier to clean (Hörmann et al., 2011). There also appears to be a lack of consensus about whether unbaffled or baffled vessel are better at entraining floating particles (§ 3.4). One important consideration for this is that the liquid surface in a baffled vessel is relatively stationary, whereas the surface moves in a more circular pattern for unbaffled vessels (Fig. 3.3).

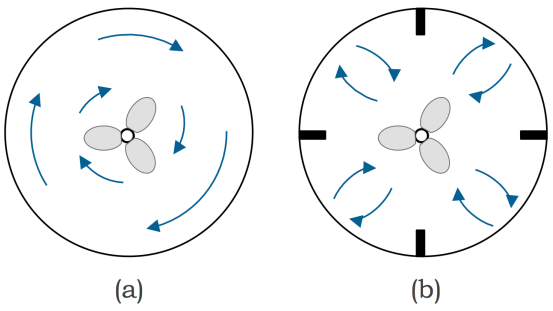

Figure 3.3: (a) Unbaffled and (b) baffled flows (top view).

In the case of unbaffled vessels, the *instantaneous liquid speed at the surface* will increase with agitation speed for a given configuration (discussed further in Ch. 7), which may influence powder entrainment, especially for slow-sinking powders (§ 15.2). Different numbers or types of baffles can be used to create different flows as well (Khazam and Kresta, 2008, 2009).

3.2.3 Characteristic Dimensions

The characteristic dimensions of the mixing vessel are shown in Figure 3.4, where d is the diameter of the impeller blade, h is the off-bottom clearance of the impeller (H' is the submergence), H is the liquid height, D is the tank inner diameter, b is the baffle width (if present), h' is the vortex depth measured from the depth of the surface of the *undisturbed* liquid, and N is the impeller speed.

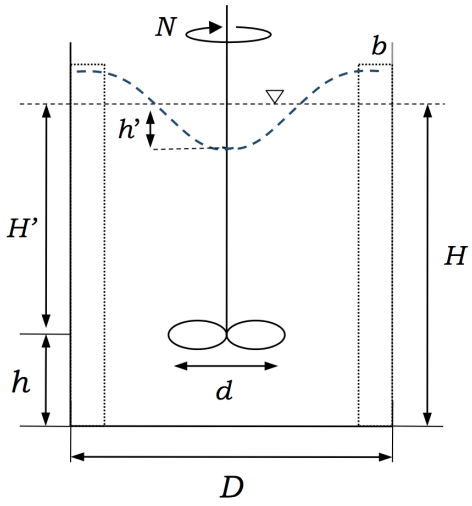

Figure 3.4: Experimental dimensions defined by Rushton et al. (1950). Note that the ratio of D:H:h:d is 3:3:1:1, and $h' = 0$ if $b \neq 0$.

Rushton et al. (1950) defined a standard vessel configuration, in which the impeller diameter d is equal in length to its off-bottom clearance h, and is $\frac{1}{3}$ of the vessel diameter D and the liquid height H. Baffles, if present, are $\frac{1}{10}$ the vessel diameter D in width, and there are four baffles for the standard baffled configuration. These dimensions have also been used by some other mixing studies as well (e.g. Forny et al. (2009); Freudig et al. (1999), etc.). Using these dimensions, one can also use the characteristic curves of Rushton et al.'s work (Fig. 7.2). Also note that Hosseini et al. (2010), who studied the suspension of glass particles at different impeller off-bottom clearances h, observed optimal dispersion at $h = \frac{D}{3}$. According to Waghmare et al. (2011), "non-standard" dimensions are also common, due to easier cleaning efforts.

§3.3 Energy Consumption of Stirred Vessels

According to Fagan et al. (2009), the power draw P (energy per time) is the most important measurement for mixing applications. This can be determined by measuring the torque τ [N m] on the motor during mixing using a torque transducer (Pakzad et al., 2008), according to the following relationship, where P is the power [W] and N [(rev) s^{-1}] the agitation rate:

$$P = \pi N \tau \tag{3.2}$$

ensuring that the torque is a result of fluid resistance and not from friction in the load bearings. The power can also be estimated based on the agitation rate and liquid properties if the vessel geometry is well characterized. According to Dickey (2009b), based on the Navier-Stokes Equation, which describes the momentum and mass balance of an incompressible Newtonian fluid, one can perform a dimensional analysis. Roustan et al. (1999) lists the variables that can influence liquid mixing:

1. The liquid characteristics: the surface tension γ [N m^{-1}], the volumetric mass ρ [kg m^{-3}], and the dynamic viscosity μ [Pa s],
2. The kinetic and dynamic characteristics, such as the agitation rate N, the acceleration due to gravity g (≈ 9.81 m s^{-2}), and the power dissipated P to overcome resistance,
3. At least ten geometric constants (see Fig. 3.4 for the symbols).

Together:

$$f(\rho, \mu, \gamma, N, g, P, d, D, H, h, w, b, l, p, n_p, n_c) = 0 \tag{3.3}$$

where w is the height and l the thickness of the blades, respectively, and p is the propeller pitch.[2] The numbers n_p and n_c are the number of blades and baffles, respectively. For the A100 impeller, $n_p = 3$, and the default case for the current study is an unbaffled vessel, with $n_c = 0$ (in §. 13.1, $n_c = 0$ or 4). These 16 variables can be expressed in terms of three fundamental units: mass, length, and time (not shown). By applying the Buckingham-Π theorem, this can be transformed in to a relationship with $16 - 3 = 13$ independent

[2] Pitch is the theoretical distance a propeller would travel after one revolution, assuming no slip, i.e. $p \equiv \pi\, d\, \tan(\alpha)$, where α is the blade incline with respect to the horizontal. For the Lightnin A100 propeller in the current study (Ch. 7), $\alpha = 18°$

dimensionless Π-terms, with d as the characteristic length:

$$f\left(\frac{d}{D}, \frac{d}{H}, \frac{d}{h}, \frac{d}{p}, \frac{d}{l}, \frac{d}{w}, \frac{d}{b}, n_c, n_p, \frac{\rho\, N\, d^2}{\mu}, \frac{N^2\, d}{g}, \frac{P}{\rho\, N^3\, d^5}, \frac{\rho\, N^2\, d^3}{\gamma}\right) = 0 \tag{3.4}$$

where Π_{1-9} (i.e. $\frac{d}{D}$ to n_p) are geometric relations.

Π_{10} is the impeller Reynolds number:

$$\mathrm{Re} \equiv \frac{\rho\, N\, d^2}{\mu} \tag{3.5}$$

which characterizes the relative importance of inertial to viscous forces. Re is used to characterize the different flow regimes, with laminar flow for $\mathrm{Re} < 10$, and turbulent flow for $\mathrm{Re} > 10^4$ for radial flow (e.g. using the R100 impeller) **or** $\mathrm{Re} > 10^5$ for axial flow (e.g. using A100 impeller), according to Roustan et al. (1999). In between laminar and turbulent flows exists transitional flow – according to Rielly and Gimbun (2009), it is common for turbulent-type flow to exist near the impeller blades, relaminarizing in the bulk. For flows with significant turbulence, eddies can help to destroy particles (§ 1.3).

Π_{11} is the Froude number, which compares inertial (centrifugal) to gravitational forces:

$$\mathrm{Fr} \equiv \frac{N^2\, d}{g} \tag{3.6}$$

Π_{12} is the power number (N_p), also called the Newton number (Ne), which is a sort of drag coefficient for the agitator in the fluid:

$$N_p \equiv \frac{P}{\rho\, N^3\, d^5} \tag{3.7}$$

Knowing the system geometry, one can obtain values for N_p from an empirically-determined characteristic curve, where $N_p = f(\mathrm{Re})$, see Fig. 7.2. As expected, and as can be seen in the characteristic curves, a radial-type impeller would have a larger N_p for a given Re compared to an axial-type impeller, due to greater fluid resistance as the blades are directed perpendicular to their movement with no blade incline. A combination of a radial-type impeller with vessel baffles results in a much larger N_p and greater power consumption at a given agitation rate N.

Π_{13} is the Weber number, which characterizes the inertial vs. surface tension forces[3]):

$$\mathrm{We} \equiv \frac{\rho\, N^2\, d^3}{\gamma} \tag{3.8}$$

[3]See also § 1.2 for a different usage of We.

where, for the current applications, it is expected that We $\gg 1$. According to Rushton et al. (1950), to calculate the power consumption (P):

$$P = \begin{cases} N_p \, \rho \, d^5 \, N^3 & \text{for } n_c > 0 \text{ and/or Re} \leq 300 \\ N_p \left(\dfrac{g}{N^2 \, d} \right)^{\left(\frac{\log \mathrm{Re} - a}{b} \right)} & \text{if } n_c = 0 \text{ and if also Re} > 300 \end{cases} \tag{3.9}$$

The separate expression for unbaffled tanks ($n_c = 0$) at Re > 300 is used to take into account vortex formation (via Fr). The constants a and b depend on the impeller and vessel configuration used. For the configuration used in the current study, for the A100 impeller, $a = 2.1$ and $b = 1.8$, and for the R100 impeller, $a = 1$ and $b = 40$ (Rushton et al., 1950). Note that Eq. 3.9 is extensively used in many of the later chapters of the current thesis.

§3.4 Other Hydrodynamic Considerations

3.4.1 Impeller pumping capacity

The volumetric flow rate Q [$\mathrm{m^3\,s^{-1}}$] of liquid passing through the area covered by the spinning impeller blades can be calculated according to (Roustan et al., 1999):

$$Q = N_Q \, N \, d^3 \tag{3.10}$$

where N_Q is the flow number. According to Pakzad et al. (2008), N_Q depends on the impeller type and the flow regime; N_Q quickly rises with N at low values of N, before becoming constant in the turbulent flow regime. According to Chudacek (1985), the "pumping efficiency" of an impeller can be determined according to $\frac{N_p}{N_Q}$, with a smaller number indicating greater pumping ability. The values for the A100 and R100 impellers in turbulent flow are obtained from Albright (2009): for the A100 impeller, $\frac{N_p}{N_Q} \approx \frac{0.35}{0.5} = 0.7$ and for the R100 impeller, $\frac{N_p}{N_Q} \approx \frac{5.75}{0.8} \approx 7.2$. Thus, the axial impeller is more efficient at pumping than the radial-type impeller for a given P (the radial impeller would convert more energy into *shearing* effects than pumping effects – cf. Eq. 3.1).

According to Wu et al. (2001), there is a correlation between the pumping capacity Q and the impeller speed required to "just suspend" solids (N_{js}), where $N_Q\, N_{\text{js}} = \text{constant}$.[4]

3.4.2 Average shear rate

In addition to effects due to eddy formation and pumping phenomena, impeller rotation can bring about shear effects that can help disperse particles. These shear forces exist because of a velocity profile of the liquid leaving the impeller blades, as well as friction between layers of liquid moving past one another (viscosity effects). The shear stress τ [Pa] is described by Newton's Law of Viscosity (Paul et al., 2004):

$$\tau = \mu\, \dot{\gamma} \tag{3.11}$$

where μ is the viscosity. The average shear rate $\dot{\gamma}_{\text{av}}$ can be taken as the time-averaged velocity gradient of the liquid, i.e.:

$$\dot{\gamma}_{\text{av}} = \frac{\partial \bar{v}}{\partial y} \tag{3.12}$$

where y is the vertical direction over which the velocity profile exists. According to am Ende (2011), one widely used approach relating $\dot{\gamma}_{\text{av}}$ to the impeller rotational speed is the relationship of Metzner-Otto (Metzner and Otto, 1957),[5] which is valid for laminar, transitional, and mildly turbulent flows:

$$\dot{\gamma}_{\text{av}} = k_s\, N \tag{3.13}$$

where k_s is a constant depending on impeller type. The shear rate will actually vary quite considerably within the tank, being much greater in the impeller region compared to the liquid bulk. Roustan et al. (1999) reports values for the A100 impeller: $k_s = 35$ near the impeller blades and $k_s = 10$ for the whole vessel, and higher values for the R100 impeller: $k_s = 60$ near the blades and $k_s = 13$ for the bulk. According to am Ende (2011), the $\dot{\gamma}$ is much higher and reaches a maximum near the blade *tip* (i.e. $\dot{\gamma}_{\text{max}}$), and reports a k_s value of 150, regardless of impeller type, for laminar and transitional flows. Methods to empirically determine k_s are discussed in Cullen and Connelly (2009).

[4] See the discussion on the suspension of solids later in the current section.

[5] This relationship to obtain average liquid shear rate is also used to obtain an apparent viscosity for non-Newtonian liquids for rheological analysis — see § 3.7.

Alternative correlations to Metzner-Otto are discussed in Pérez et al. (2006); these authors also suggest that $\dot{\gamma}_{\max} \propto N^{3/2}$ for turbulent flow. According to Paul et al. (2004), at high Re, as viscosity is no longer relevant to inertial forces with regards to momentum transfer, concepts related to shear and N become unimportant relative to the peripheral tip speed of the impeller blade v_p:

$$v_p = \pi \, N \, d \tag{3.14}$$

3.4.3 Vortex formation

In an unbaffled vessel, if a high stir rate is applied, a vortex may form on the liquid free surface due to the highly tangential liquid motion (Busciglio et al., 2013). According to that article, a number of studies have reported a linear dependency of vortex depth (h' from Fig. 3.4) on Fr, which as mentioned previously relates centrifugal with gravity effects. However, when at a critical Froude number Fr_c, the vortex extends below the impeller blades, incorporating gas and engendering mechanical vibrations. According to Gaddis (2010), the vortex depth will not only depend on the agitation rate (via Fr), but also on the impeller type. They report empirical relationships from Zlokarnik (1971) to calculate the dimensionless vortex depth ($\frac{h'}{d}$) for the A100 and R100 impellers:

$$\frac{h'}{d} = \begin{cases} 62.0\,\mathrm{Fr}\left(0.10 - \mathrm{Ga}^{-0.18}\right)\left(\dfrac{H'}{d}\right) & \text{for R100} \\ \\ 13.8\,\mathrm{Fr}\left(0.25 - \mathrm{Ga}^{-0.10}\right)\left(\dfrac{H'}{d}\right) & \text{for A100} \end{cases} \tag{3.15}$$

where H' (Fig. 3.4) is the liquid height (undisturbed) above the centerline of the impeller blades (i.e. the submergence of the impeller blades). In the current thesis, $\frac{H'}{d} = 2$. Ga is the dimensionless Galilei number:

$$\mathrm{Ga} \equiv \frac{\mathrm{Re}^2}{\mathrm{Fr}} \tag{3.16}$$

In the vessel characterization section of the current report (§ 7.3), the estimated vortex is compared with the measured time-averaged values. From these equations above, one would expect that as the water temperature increases, and the viscosity decreases, the vortex depth would increase. Conversely, if the viscosity increases, e.g. due to the addition of a food powder,

the vortex depth would decrease. The range of validity for these empirical relationships (see Gaddis (2010)) are appropriate for the vessel dimensions, Fr, and Ga for the current report.

In addition to these empirical relationships, there have also been attempts to model vortex formation directly Ciofalo et al. (1996); Cartland Glover and Fitzpatrick (2007); Busciglio et al. (2012). Hörmann et al. (2011) reported good experimental agreement with Zlokarnik (1971)'s equations.

3.4.4 Downdraw of floating particles

As mentioned in § 1.2, particles can remain floating at the liquid surface for a number of reasons, e.g. due to buoyant effects if the true density ρ_t is less than that of water ρ_{H_2O}, or even if $\rho_t > \rho_{H_2O}$, if the bulk density of the powder $\rho_b < \rho_{H_2O}$, due to air entrapment inside of particles due to the formation of hollow spheres, or air trapped between particles (Ch. 2). Sinking can also be inhibited by surface tension effects if there is poor wetting of the solid by the liquid (i.e. high contact angle θ), and a large enough contact area exists. In a stirred vessel, once the impeller is turned on, additional forces will exist that will help draw the particles down into the liquid (Khazam and Kresta, 2008) – see Fig. 3.5.

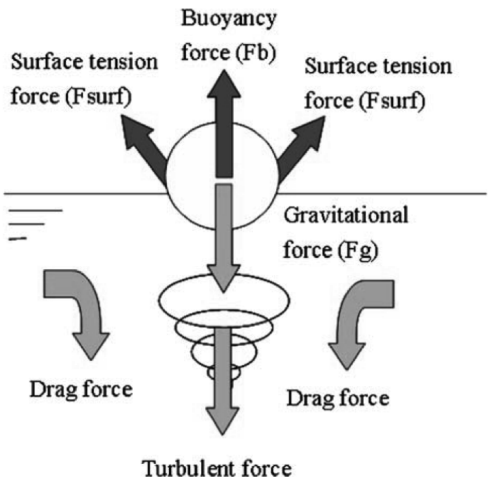

Figure 3.5: Forces acting during the downdraw of floating solids (Khazam and Kresta, 2008).

Khazam and Kresta (2008) suggest, based on CFD[6] simulations and experimental work using polystyrene beads, that there are three different mechanisms for downdraw: (1) vortex formation, which breaks up stagnant zones and pulls solids into the liquid, (2) turbulent engulfment, where fluctuating surface eddies larger than the particle entrain them in small packets, and (3) mean drag (the vertical component), involving surface waves and swirls intermittently disrupting stationary zones on the surface. As mentioned previously, the mean drag will depend on the particle slip velocity, and therefore also on the liquid mean velocity (Waghmare et al., 2011). Khazam and Kresta (2008) explain that there may also be a combination of responsible mechanisms; although, one of them usually dominates over the others. For instance, the first mechanism (vortex formation) is not applicable for baffled vessels, and within baffled vessels the mechanism may depend on the impeller submergence (H' in Fig. 3.4). That is, at large H' (impeller blades close to the vessel floor), mean drag is the dominant mechanism, but at low H', turbulent engulfment dominates.

Khazam and Kresta (2008) also looked at the influence of H' on the downdraw behavior and vortex formation in *unbaffled* vessels with different impellers. They report that when the impeller is close to the liquid surface (low H'), a lower agitation speed is needed to "just downdraw" particles, i.e. there is a lower N_{jd}. Also at this lower N_{jd}, the vortex depth h' is smaller in magnitude. **Therefore, downdraw is better when the impeller is closer to the base of the vortex.** Thring and Edwards (1990) also compared the downdraw behavior of axial and radial impellers, and reported a higher N_{jd}, but a lower power draw, for the axial impeller.

For *baffled* tanks, and assuming that mean drag is the only relevant mechanism for downdraw, Waghmare et al. (2011) correlated the downdraw rate (i.e. the inverse of the particles' residence times at the surface) to the average surface velocity of the liquid, which is an indication of the strength of the velocity field. Moreover, they also observed that in this case, particles tend to travel to the vessel wall before being drawn under, as this is where CFD simulations showed a downward velocity. Thus, with regards to scale-up effects, particles would need to move further at the surface before reaching a wall, and as a result, increased tank diameter would inversely correlate to downdraw rate. According to Khazam and Kresta (2008), the particle properties also play a significant role in determining N_{jd}, although most correlations only consider density differences (not wettability traits), and also

[6]Computational Fluid Dynamics

do not consider powder agglomerates or bulk beds, which may also exhibit capillarity and water-logging effects (§ 1.1 and 1.2).

Regarding whether or not baffles facilitate or hinder the downdraw of floating solids, Khazam and Kresta (2008) and Waghmare et al. (2011) agree that vortex formation should be *avoided*[7], as the whirlwind will act more as a centrifuge that does *not* suspend particles throughout the vessel well, and keeps particles near the vortex free-surface. Meanwhile, baffling would increase mean and turbulent downdraw, and promote top-to-bottom liquid flow. Khazam and Kresta (2009) even proposed a partially baffled configuration (including half– and surface–baffles) to improve turbulent downdraw but prevent bottom-to-top transport of particles already suspended.

On the other hand, when it comes to food powder downdraw, it appears that an *unbaffled* configuration is preferable, as the process is more complicated than it would be for negatively buoyant, non-sticky, free-flowing particles like polystyrene beads. Freudig et al. (1999) compared the downdraw behavior of skim milk powder in both baffled and unbaffled configurations. They observed superior reconstitution behavior for the unbaffled vessel (even though the power draw-per-volume (P/V) was lower), because as particles were added (which they controlled using a vibratory feeder), the particles were carried away by the circulating liquid from the point of impact, so that following particles would also make contact with the liquid. However, in a baffled vessel, the particles remain relatively motionless at the surface, and particles fall on top of one another, forming a particle heap, with limited water-solids contact; this heap also did not readily sink, possibly due to swelling and stickiness effects, that would have made it difficult for turbulent and drag forces to act upon particles.

As this heap formation was the rate-limiting step of overall reconstitution, the *shape* of the heap may also play a role. For poorly flowable powders, a steep heap with a large angle of repose may form; however, more flowable powders would more likely avalanche, possibly forming better solid-liquid contact. Hogekamp and Schubert (2003) also demonstrated the importance of the feed rate for powder reconstitution – slower particle addition (particularly if the vessel is unbaffled), may lead to better reconstitution overall because of less heap formation and thus better sinking ability. This may partly be because capillary rise and water-logging would be easier for a *thin* layer of particles, as the speed of capillary rise decreases with height,

[7] See Ch. 13.1 for a discussion on the problems with their claim.

as predicted by Eq. 1.14. These studies thus demonstrate the importance of controlling the feed rate of particles when studying powder reconstitution. Unfortunately, as discussed in Ch. 5, most studies on particle reconstitution fail to specify how powder is added. For instance, the height from which the powder is dropped; as discussed in § 1.2, the speed of impact may affect the sinking behavior of particles. Freudig et al. (1999) also point out one complication when controlling the feed rate ($\dot{m}$) of powders for reconstitution study – if a powder is agglomerated, it will have a lower bulk density, and thus to achieve a constant rate of addition, a large overall bulk volume will be added to the liquid, which may result in an even worse particle heap than the unagglomerated powder, thus a slower $\dot{m}$ may be necessary for such large granules for decent reconstitution.

Schober and Fitzpatrick (2005) investigated the influence of mixing in an unbaffled vessel to the downdraw and vortex formation for whole and skim milk powders to high solids concentration (above 40% w/w). They continually added increasing amounts of powder, and used a stopwatch to determine the sinking time. Since the viscosity of the liquid increases, the vortex would decrease in magnitude (as explained earlier in this section), thus they increased the impeller speed to maintain the same vortex depth (h'), as they (wrongly) assumed that h' determines the downdraw. Instead, they saw *faster* downdraw at higher concentrations, presumably because a much larger agitation speed, and thus pumping capacity ($Q \propto N$, Eq. 3.10), was necessary to maintain such a vortex at high viscosities. In addition, as the total volume of liquid significantly increased with such high amounts of added powder, the distance between the impeller and the vortex bottom increased. However by continually raising the impeller to be closer to the vortex bottom with each increment of powder added, they observed improved downdraw, in agreement with Khazam and Kresta (2008). These authors also noted that for high solids content, age thickening (i.e. gel formation due to a protein network forming) may occur, resulting in an increase in viscosity as well.

According to Hörmann et al. (2011), if vortex-feeding of powders is desired, but particles may stick to the impeller shaft, there are ways to offset the vortex, for instance using a single baffle, in order to circumvent this problem.

3.4.5 Suspension of sedimented solids

As discussed in § 1.2, another role of impeller movement in a stirred vessel may be to lift off solids from the vessel floor. This may be particularly relevant if a powder wets and sinks easily, but does not disperse and/or dissolve sufficiently before settling to the vessel floor (Ch. 10). According to Khazam and Kresta (2008), such particle suspension off the bottom of the tank is much better understood than the mechanisms of downdraw, due to the free surface no longer contributing to complex effects. According to Barigou (2009), there are different regimes of suspension – e.g. a filleting regime, complete particle motion, complete off-bottom suspension, and uniform suspension. It is this third regime that gains the most attention in the literature for solid-liquid mixing – the minimum agitation speed to achieve this "just suspended" state (N_{js}) can be determined empirically in a transparent vessel, by determining when no particle remains at the vessel floor for more than one or two seconds. According to Ibrahim and Nienow (1999), N_{js} can be used, e.g. to compare the performance of impellers. The value of N_{js} will depend on a number of factors, including the solids' and liquids' properties, the impeller type, vessel configuration, etc. One well-known correlation to estimate N_{js} for low-viscosity liquids is Zwietering's correlation (Eq. 3.17). Zwietering (1958) performed a number of experiments with varying solids and liquid properties, impeller types, etc., and used dimensional analysis to obtain Eq. 3.17.

$$N_{\mathrm{js}} = S\,\nu^{0.1}\,D_p^{0.2}\left(\frac{g\,\Delta\rho}{\rho_L}\right)^{0.45} d^{-0.85}\,X^{0.13} \tag{3.17}$$

where ν is the kinematic viscosity, D_p is the particle diameter, d is the impeller diameter, and X is the solids concentration by mass in percent. S is a dimensionless shape parameter depending on a number of geometric factors. For example, as discussed earlier, S would be larger for the A100 impeller compared to the R100, due to greater pumping capacity. In fact, according to Barigou (2009), axial flow impellers (in down-pumping mode) are the most energy efficient for suspending solids. According to Paul et al. (2004), for the vessel geometry used in the current study (Fig. 3.4), for A100, $S = 6.9$ and for R100, $S = 4.4$. Estimations for N_{js} for the current report are given in Ch. 14, assuming maltodextrin DE21 (§ 8.1) as the particle.

§3.5 Mixing Scale-Up

Another important consideration for mixing studies on a lab-scale is how similar behavior could be replicated for larger (e.g. pilot or industrial) scale. According to Hörmann et al. (2011), however, scale-up is complicated because of the different effects that need to be balanced. While it is impossible to keep all mixing aspects constant on scale-up, Dickey (2009a) explain how similar conditions can be obtained, based on the specific objective of the mixing application.

For most scale-up purposes, if feasible, geometric similarity of the mixing vessels is advised, as this greatly simplifies scale-up efforts. In the current thesis, discussed in Ch. 13, the same linear ratios are used in the scaled-up vessel as in Fig. 3.4, i.e. standard configurations, with a similar A100 impeller. Other concepts of similitude are kinematic and dynamic similarity (Roustan et al., 1999). Kinematic similarity refers to similar liquid motion in the vessel (e.g. liquid velocities relative to the impeller tip speed v_p), resulting in similar flow patterns. Dynamic similarity refers to similar relationships between forces within the vessel. For example, for high Re (turbulent flow), fluid forces are dominated by inertial flow, driven by a pressure differential across the impeller blades, but at low Re, viscous drag will be more important (Dickey, 2009a).

If geometric similarity is maintained, then the agitation speed (N) is the only mixing characteristic that needs to be changed upon scale-up; this N then can be determined based on the scale-up factor and the exponent n, via the inverse length ratio (Eq. 3.18).

$$N_2 = N_1 \left(\frac{d_1}{d_2}\right)^n \tag{3.18}$$

where N_2 is the agitation rate of the scaled-up vessel, and (d_1/d_2) is the ratio of the diameters of the small and large vessels, respectively, i.e. the scale-up factor. The value of n depends on what mixing characteristic will be held constant. For example, for equal blend time (same agitation rate), $n = 0 \therefore N_2 = N_1$. However as $P \propto d^5$ (Eq. 3.9), this is not practical, thus typically $N_2 < N_1$ (Dickey, 2009a). For equivalent Re, $n = 2$, although according to Dickey (2009a), N_2 would be too low, and would never be used as not enough liquid motion would be generated for mixing. For equivalent Fr, $n = \frac{1}{2}$, which could be use to maintain constant vortex depth upon scale-up. However, N_2 would be too large, and also is generally not used

Table 3.1: Examples of how mixing characteristics change depending on scale-up criterion.

S-U criterion	d_2/d_1	$\mathrm{Re}_2/\mathrm{Re}_1$	N_2/N_1	v_{p_2}/v_{p_1}	$(P/V)_1/(P/V)_2$
v_p	10	10	0.1	1	0.1
P/V	10	21.5	0.22	2.2	1

(Dickey, 2009a).

According to Dickey (2009a), the practical values for n are usually in the range of $0.\bar{6} \leq n \leq 1$. An $n = 1$ would represent equivalent tip speed (v_p), which under turbulent conditions would result in similar local liquid velocities. At $n = \frac{2}{3}$, a constant specific power draw (i.e. power-per-unit-volume (P/V)), would be maintained, under turbulent conditions. Rieger et al. (1988) recommends using P/V for the scale-up criterion for weakly homogeneous, and v_p for highly homogeneous systems. Paul et al. (2004) illustrates how some other mixing characteristics are affected if a 10× linear scale-up ($d_2/d_1 = 10$) is used ($V_2/V_1 = 1000$).

In the current report, both P/V and v_p are tested as scale-up criteria in Ch. 13.

As discussed in § 3.4, shear effects may be important for particle dispersing, and the shear rate $\dot{\gamma}$ will depend on the distance from the impeller. In a scaled-up tank, these effects are even greater. For constant P/V, there will be an overall decrease in the average shear rate $\dot{\gamma}_{\mathrm{av}}$ in the tank due to a much larger volume involved, as well as a broad distribution of $\dot{\gamma}$. On the other hand, as the tip speed will increase at constant P/V, the *maximum* shear rate $\dot{\gamma}_{\mathrm{max}}$ will increase (Paul et al., 2004).

3.5.1 Scale-up for solids suspension

According to Eq. 3.17, the N_{js} for solids suspension would also change upon scale-up. The parameter S is dimensionless, and would thus remain constant if geometric similarity is preserved. As the impeller diameter d increases, N_{js} would decrease, as $N_{\mathrm{js}} \propto d^{-0.85}$. Roustan et al. (1999) also discuss the importance of chemical similarity upon scale-up as well; i.e. similar

concentrations in the vessel. Thus the parameter X from Eq. 3.17 would remain constant upon scale-up as well. According to Dickey (2009a), if the main objective of scale-up is solids suspension, different values of n can be used for scale-up design based on the particle slip velocity.

3.5.2 Scale-up for solids drawdown

Lastly, according to Waghmare et al. (2011), the effect of scale-up on particle drawdown has rarely been studied, and the effect is unclear. Özcan-Taşkin (2006) reported that maintaining a constant P/V, v_p and Fr all failed to preserve drawdown behavior of floating plastic particles for an axial impeller and a pitched-blade turbine for down-pumping conditions. However P/V was successful for *up*-pumping configurations. They propose that the mechanisms for downdraw in a down-pumping configuration were more complex than for up-pumping. As for the downdraw or sinking behavior of food powders in a scaled-up tank, the author could not find any relevant studies.

3.5.3 Scale-up simulations using CFD

It is worth mentioning that in recent years, there have been advances in simulating particle dissolution using CFD.[8] This line of research is particularly strong in the pharmaceutical field, as such *in silico* techniques would significantly reduce the amount of expensive materials that would be needed for research purposes, as well as the time needed to conduct the trials. For instance, McCarthy et al. (2014) modelled the dissolving of tablets in USP dissolution apparatuses (Ch. 5). Hartmann et al. (2006) and Hörmann et al. (2011) investigated the dissolution of powders in a stirred vessel, modeling dissolution based on the mass transfer equations discussed in § 1.4. Hörmann et al. (2011)'s vessel was unbaffled, as they incorporated vortex formation into their model, and they used PIV (Particle Image Velocimetry) to validate the liquid flow in the vessel against their simulations, and took turbulent effects into account using a turbulence model. However, in both studies they assume that wetting, sinking and dispersing of the particles was negligible compared to the mass transfer involved in dissolving,

[8] For details about CFD, the reader is referred to Rielly and Gimbun (2009).

which, as will be shown in the experimental chapters of the current report, generally is not true for food powders (although it may be true for pharmaceutical powders). A similar CFD approach was taken by Koganti et al. (2010), and they reported good agreement in dissolution time ("t_{95}", or time to reach 95 % max. concentration), when P/V was used for the scale-up criterion; however, similar assumptions about the powder behavior was made.

Koganti et al. (2010) compared the dissolution of propylparaben in a lab (2 L) and commercial (4000 L) scale tank, taking regular samples of the dissolution medium and using spectroscopy (§ 5.10) to determine the "dissolution time" (t_{95}). They reported good agreement between lab- and commercial scales using P/V as the scale-up criterion.

§3.6 Dimensional Analysis Applied to Rehydration

According to Jeantet et al. (2010), a number of models exist regarding powder rehydration, both empirical/semi-empirical and mechanistic (see Ch. 5); however, they argue that there are huge discrepancies between theory and experiments, due to the complex nature of food powder rehydration. These authors argue that there is still a need to understand the quantitative importance of factors like temperature T, agitation rate N, and concentration of particles X on rehydration kinetics. As with any such complex physical process, there is a desire to simplify the relationship between input (process conditions) and output (rehydration time), using dimensional analysis. Jeantet et al. (2010) performed rehydration experiments with micellar casein powders (§ 6.2), using a laser diffraction technique (§ 5.4), reconstituting powders at different combinations of T, N and X (i.e. each trial had a different [T, N, X]).

For a given T, they identified that the rehydration time t_{90} (time to reach 90 % maximum reconstitution), depended on the properties of the solids (i.e. X, density ρ_p, and diameter D_p), the liquid (ρ_l, μ), the diffusivity ($\mathcal{D}$), gravitation acceleration g, and N. They obtain:

$$F_1 = (t_{90}, d, D, H, w, h, D_p, \rho_p, \mu, \rho_L, X, \mathcal{D}, N, g) = 0 \tag{3.19}$$

where w is the blade thickness of the impeller, and the other geometric constances are detailed in Fig. 3.4. By dimensional analysis with d as the characteristic length:

$$F_2 = \left(\Theta_{90}, \frac{H}{d}, \frac{D}{d}, \frac{w}{d}, \frac{h}{d}, \frac{D_p}{d}, X, \mathrm{Re}, \mathrm{Fr}, \mathrm{Sc}\right) = 0 \tag{3.20}$$

where Θ_{90} is the number of impeller revolutions ($\Theta_{90} = N\, t_{90}$), and Sc is the Schmidt number (Eq. 1.56). For a single powder, vessel geometry, T, and assuming no vortex formation, Jeantet et al. (2010) simplify the relationship to:

$$F_3 = (\Theta_{90}, X, \mathrm{Re}) \tag{3.21}$$

It should be noted that particle morphology, polydispersity, and the shrinking size associated with dissolution, as well as complex wetting effects, are not included in this analysis. Nevertheless, Jeantet et al. (2010) observe for a given [X, T], the t_{90} decreases linearly with N, and Θ_{90} was independent of N. Similar results were reported by the same group in Richard et al. (2013), using different dairy powders and impeller types. Thus they suggest that it is a general rule that the number of impeller revolutions (Θ_{90}) governs rehydration time. The *effects* of T, and X from the cited studies will be discussed in § 6.2.

§3.7 Non-Newtonian Complications

One major complication associated with food mixing, particularly at higher solids concentrations, is that the rheology of the system can become quite complex. Many liquid foods exhibit non-Newtonian behavior due to complex structure formation, i.e. the viscosity of the liquid is *not* independent of the applied shear rate, thus predicting mixing behavior, and mixing itself, can be quite challenging. For example, for shear-thinning liquids, a cavern might form around the impeller region, as the shear rate (and thus apparent viscosity) is different where the shear rate is higher (Pakzad et al., 2008). According to Venneker et al. (2010), there is not much literature on the flow behavior of non-Newtonian fluids, but these authors (using Rushton's configuration) used CFD to investigate the flow of xanthan gum solution (§ 6.1), which is shear-thinning. Pakzad et al. (2008) and Pakzad et al. (2013) also used CFD for xanthan solutions, and used ERT (Electrical Resistivity Tomography, § 5.8) to validate the flow patterns; they preferred this technique over PIV as it can be used for *opaque* liquids. In light of the complications associated with food rheology during mixing, in the current thesis, a low solids concentration (2 % w/v) is used as a default condition (§ 7.2).

Chapter 4

Particle Interactions in Aqueous Media

Once the particles are submerged in the aqueous medium there are a number of intermolecular interactions that may influence dispersing behavior, and dispersion stability. Colloids are dispersions of particles in a continuous medium, in which the size of the particles falls within the range of 0.005 to 100 µm (Israelachvili, 2011), which is relevant for food powder primary particles, as well as subcomponents, e.g. casein micelles for dairy powders. According to Liang et al. (2007), the main colloidal forces between particles in an aqueous medium are: London-van der Waals, electric double layer, hydration, hydrophobic, and steric forces.

Contents

§4.1 van der Waals Interactions

van der Waals (vdW) forces between particles, as mentioned in §1.3, may be one of the key ad/cohesion mechanisms between dry particles, contributing to their strength resisting dispersion. According to Tadros (2011), these vdW forces include three types: (1) Keesom: interactions between two particles with dipoles, (2) Debye: between one with a dipole and the other with an induced dipole as a result of the presence of the first particle, and (3) London: the electrodynamic, fluctuating dipole/induced-dipole interactions. According to van Oss (2006), these London-vdW forces are universal, as no permanent dipole is needed.[1] The typical range for these interactions is relatively short (1 – 50 nm), with the force decreasing with separation distance to the 6^{th} power, very quickly dying off.

In order to estimate the vdW forces (F_{vdW}) between two smooth spheres (Tinke et al., 2009):

$$F_{\text{vdW}} \approx \frac{A\, D_p}{12\, x^2} \tag{4.1}$$

where D_p is the diameter of the sphere; for two spheres of different sizes, the Derjaguin approximation can be used: $D_p \approx \frac{(D_{p,1})(D_{p,2})}{D_{p,1}+D_{p,2}}$. According to Tinke et al. (2009), F_{vdW} tends to be overestimated, as real particles are not smooth. The variable x is the minimum surface-to-surface separation distance, and A is the Hamaker constant that is dependent on the material, but independent of geometry.

According to Liang et al. (2007), there are two main approaches to obtain the Hamaker constant of a material, either (1) Hamaker's microscopic approach, which is a sort of "bottom-up" approach that adds up the interactions between molecules, or (2) the macroscopic (Liftshitz) approach, where the atomic structure is ignored and particles are treated as continuous, and A is determined based on the bulk properties such as the refractive indices and dielectric constants, thus it takes screening effects into account. According to Somasundaran et al. (2009), most studies have used the Hamaker rather than the Liftshitz approach.

As alluded to in § 1.3, the Hamaker constant A of a dry food particle will decrease when

[1] For the remainder of this thesis, these *London*-van der Waals forces are assumed whenever discussing van der Waals interactions.

it is placed into an aqueous medium. According to Achebe (2013), in order to estimate A between two particles of materials "1" into a medium "3", the following expression can be used:

$$A_{131} = A_{11} + A_{33} - 2A_{13} \tag{4.2}$$

where A_{131} is the Hamaker constant between the two particles of "1" in the medium "3", A_{11} is the Hamaker constant between the two particles in a vacuum, and A_{33} between the medium and a vacuum. By assuming that $A_{13} \approx \sqrt{A_{11}\,A_{33}}$, one can express A_{131} simply in terms of A_{11} and A_{13}:

$$A_{131} = \left(\sqrt{A_{11}} - \sqrt{A_{33}}\right)^2 \tag{4.3}$$

According to Shimada et al. (2002), the A_{11} for a hydrocarbon is generally ca. $4-10\times10^{-20}$ J, and according to Tinke et al. (2009), A_{33} for water is $3.7-4.4\times10^{-20}$ J. Eq. 4.3 clearly demonstrates that the Hamaker constant (and $\therefore F_{\mathrm{vdW}}$) for food materials would be greatly reduced when placed in water or another aqueous medium, which may help contribute to *spontaneous* dispersing (§ 1.3). Note that between identical particles, vdW forces are *always* attractive; although, according to van Oss (2006), vdW interactions between two different materials *may* be seen as repulsive depending on the medium properties (if the Hamaker constant of the medium is in-between the Hamaker constants of the two materials).

§4.2 Electrostatic Double Layer Repulsion

In addition to a decrease in van der Waals attractions upon submersion into an aqueous medium, according to Schubert (1993) and Freudig et al. (1999), the development of a double layer of counter-ions around charged surfaces may help the particles spontaneously disperse during reconstitution. Freudig et al. (1999) even claims, as discussed earlier, that dry mixing lecithin with a food powder may help promote such repulsive forces to aid in dispersing. According to Israelachvili (2011), particle surfaces can become charged in a liquid medium that has a high dielectric permittivity ε_r, such as water, due to three charging mechanisms: (1) the ionization or dissociation of surface groups, (2) the adsorption of ions onto an uncharged surface, or (3) short-range acid/base-type adhesion forces. These charged surfaces will attract ions of opposite charge (counter-ions) and repel like-charged ions (co-ions), resulting in the

development of an electrostatic double layer (EDL), with the charge separation greatest near the surface. The double layer model is illustrated in Fig. 4.1 (Somasundaran et al., 2009).

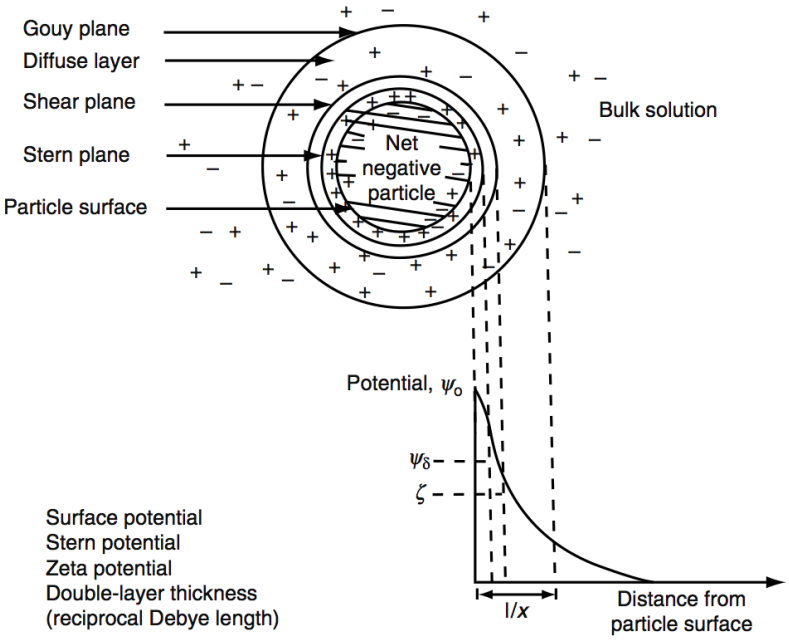

Figure 4.1: Electrostatic double layer around a charged particle (Somasundaran et al., 2009).

According to this EDL theory counter-ions at the solid surface are tightly bound to the surface in the *Stern* layer. The second layer is the *diffuse* (or *Guoy*) layer, where ions are less tightly bound, but still contribute to a particle's behavior, and the plane separating these two layers is called the Stern plane (sometimes described in terms of the inner and outer Helmholtz planes (Parsons et al., 2011)). As the distance x from the particle surface increases, the electrostatic potential ψ decreases; here ψ_0 is denoted as the surface potential. Across the Stern layer, this decrease in ψ is relatively linear, and across the diffuse layer, it decays exponentially (see Israelachvili (2011)). The Boltzmann equation (Eq. 4.4) describes the ion distribution in the electric field, by balancing Coulombic interactions and thermal energy kT:

$$n(x) = n_{i,0} \exp\left(\frac{-z_i e \psi(x)}{kT}\right) \tag{4.4}$$

where $n(x)$ is the concentration of ions at a distance x, $n_{i,0}$ is the bulk concentration of ion i, z_i is the valence charge of ion i, e is the elementary charge (of a proton), where $e = 1.6 \times 10^{-19}$ C, ψ is the potential (in units of $\mathrm{J\,C^{-1}}$), k is Boltzmann's constant ($1.38\times\ 10^{-23}\,\mathrm{J\,K^{-1}}$), and T is the absolute temperature (K). The Poisson Equation (Eq. 4.5, expressed in one-dimension),

on the other hand, describes how ψ decreases with the ion density:

$$\frac{\partial^2 \psi(x)}{\partial x^2} = -\frac{\rho(x)}{\varepsilon_0\, \varepsilon_r} \tag{4.5}$$

where ρ is the charge density ($\mathrm{C\,m^{-3}}$), with $\rho(x) = \sum_i z_i\, e\, n_i(x)$, ε_0 is the permittivity of free space ($\varepsilon_0 = 8.85 \times 10^{-12}\,\mathrm{C\,N^{-1}\,m^{-2}}$) and ε_r is the relative dielectric constant of the medium (unit-less), with $\varepsilon_r \approx 78$ for water at 25 °C (Malmberg and Maryott, 1956). Using the linearized Debye-Hückel assumption[2], with $z\, e\, \psi \ll kT$ (Liang et al., 2007):

$$\frac{\partial^2 \psi(x)}{\partial x^2} = \kappa^2\, \psi(x) \tag{4.6}$$

where ...

$$\kappa = \sqrt{\frac{\sum_i z_i^2\, e^2\, n_{i,0}}{\varepsilon_0\, \varepsilon_r\, k\, T}} = \sqrt{\frac{e^2\, N_A}{\varepsilon_0\, \varepsilon_r\, k\, T} \left(\sum\nolimits_i z_i^2\, c_{i,0}\right)} = \sqrt{\frac{e^2\, N_A}{\varepsilon_0\, \varepsilon_r\, k\, T} \cdot 2I} \tag{4.7}$$

where $c_{i,0}$ is the bulk ion molar concentration, N_A is Avogadro's number, and I is the ionic strength[3]:

$$I = \frac{1}{2} \sum z_i^2\, c_{i,0} \tag{4.8}$$

Combining Equations 4.4 and 4.5, one can solve for the (linearized) Poisson-Boltzmann Equation (PBE):

$$\psi(x) = \psi_0\, \mathrm{e}^{-\kappa\, x} \tag{4.9}$$

The reciprocal of κ (i.e. κ^{-1}) is called the *Debye length*, and according to Eq. 4.9, it is the distance at which $\psi = \frac{\psi_0}{\mathrm{e}} \approx 0.37\, \psi_0$, and κ^{-1} is often referred to as the double-layer "thickness", corresponding to the Guoy plane in Fig. 4.1. Thus it gives an indication of how neighboring particles will interact with one another, because an overlapping of these double layers results in a repulsive force. Using the linear superposition approximation, and assuming two particles with the same surface charge and radius:

$$F_{\mathrm{EDL}} = 2\pi\, \varepsilon_0\, \varepsilon_r\, \kappa\, R\, \psi_0^2\, \mathrm{e}^{-\kappa\, x} \tag{4.10}$$

In Fig. 4.1, the "shear plane" (or slipping plane) refers to the distance that would correspond to the zeta potential (ζ), which can be determined experimentally, and this shear plane is close to the Stern layer, but may be slightly further away from the surface (Tinke et al., 2009). One important aspect of the EDL repulsion is that it is influenced by the salt content

[2] That is, assuming that ions are point-charges; thus, it may only be acceptable in dilute solutions.

[3] For a further discussion of ionic strength, see Ch. 12.

in the medium. According to Equations 4.7 and 4.10, as the ionic strength (and salt content) increases, κ^{-1} would decrease, meaning that the double layer would have less of an influence on neighboring particles, i.e. the EDL effects would be *screened*. In addition, the dielectric constant of water ε_r would also descrease with increasing concentration of NaCl (Gavish and Promislow, 2012).

§4.3 DLVO Theory & non-DLVO Interactions

One very well-known theory regarding the stability of colloidal systems is the DLVO theory, named after the credited researchers: Derjaguin and Landau (1941) and Verwey and Overbeek (1948). As explained by Liang et al. (2007), this theory for interactions between neighboring colloidal particles is determined by the additive balance of the (attractive) van der Waals interactions E_{vdW}, and the (repulsive) double layer interactions E_{EDL}:

$$E_{\text{total}} = E_{\text{vdW}} + E_{\text{EDL}} \tag{4.11}$$

As the distance between the particles x decreases, these two contributions both increase, but to a different degree. $E_{\text{vdW}}(x)$ is a power-law function and will be greater in magnitude at very small distances, but further out, E_{EDL} is stronger, and E_{total} is illustrated in Fig. 4.2.

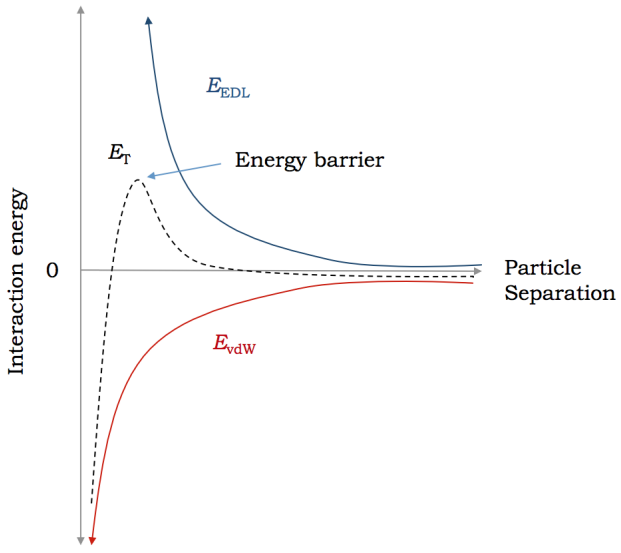

Figure 4.2: Illustration of total DLVO interactions as a function of distance; adapted from Israelachvili (2011).

The peak of E_{total} in the repulsive region can be thought of as an energy barrier separating

the two particles. Thus an increase in salt content (or a change in pH) can affect the strength of E_{EDL} and thus E_{total} (with E_{vdW} largely unaffected). An increase in salt content or a charge-neutralizing effect of a pH change (e.g. if the surface charge is *negative*, then a *decrease* in pH, and vice versa) will reduce the repulsive reactions. According to Vallar et al. (1999), if the $\frac{E_{\text{total}}}{kT} \gtrapprox 10$, the colloid will remain stable, but if E_{total} is reduced enough, a coagulation can occur, assuming these are in fact what determines stability. If enough salt is added to reduce E_{EDL} such that $E_{\text{total}} < 0$, a very rapid coagulation occurs, and the "critical coagulation concentration" is said to have been reached. According to the same authors, the zeta-potential ζ is also a good indication of stability, with colloids stable in the range $\zeta \gtrapprox 20\,\text{mV}$. However, as the DLVO theory is a continuum model and assumes no solvent structure, the theory's assumptions become increasingly problematic where solvation effects may actually be quite important (Collins, 2012).

Water structuring becomes important especially at small separations between particles, and also if the particles are hydrophilic ($\theta \lessapprox 15°$), where repulsive "**hydration**[4] forces" can be relevant, and for hydrophobic surfaces ($\theta \gtrapprox 65°$), attractive "**hydrophobic** forces" can become a major driving force for determining the colloidal stability (Israelachvili, 2011). According to Liang et al. (2007), the exact nature of these two structural forces is still unknown and quite controversial. According to Hoek and Agarwal (2006), the DLVO theory can be modified to include these "non-DLVO" interactions to form an "extended DLVO theory" (or XDLVO) via:

$$E_{\text{total}} = E_{\text{vdW}} + E_{\text{EDL}} + E_{\text{structural}} \tag{4.12}$$

Some authors call these structural interactions "polar" or "Lewis acid/base" interactions (e.g. van Oss (2006)); however, in the current author's opinion calling these Lewis acid/base interactions is confusing, as there is no actual net transfer in electrons. In any case, van Oss (2006) explains that hydration forces exist as water forms hydrogen bonds to hydrophilic or ionic surface groups, and hydration layers form as a result. Repulsion occurs at short separation distances where these layers could overlap (according to Briscoe (2010), these can exceed E_{vdW} or E_{EDL} below $\approx 30\,\mu\text{m}$). According to Liang et al. (2007), this strong short-range force exponentially decays with distance according to:

$$F_{\text{structural}} = k\,\mathrm{e}^{-(x/\lambda)} \tag{4.13}$$

[4] Or "solvation" if the medium in question is non-aqueous

where $k > 0$ means the force is repulsive (hydration force) and $k < 0$ makes it attractive (hydrophobic force), x is the distance, and λ is the correlation length of the ordering of molecules. According to Somasundaran et al. (2009), $\lambda = 0.6\,\text{nm}$ for water molecules, i.e. $3\times$ the dimensions of a water molecule, as these tend to form clusters via hydrogen-bonding of ≥ 3 molecules.

According to these authors, **structural undulation forces** can also exist for smooth surfaces (probably not so relevant for food materials), where the force oscillates between being attractive and repulsive as the surfaces approach. This is due to their favorable ordering of integral (1, 2, 3, ...) number of solvent molecules, with destructively overlapping density profiles at intermolecule (non-integral) distances.

As for hydrophobic forces, the exact origin is still debated (Liang et al., 2007; Somasundaran et al., 2009), but it is generally said to arise from water structuring as well. As it is more entropically favorable for water to interact with other hydrogen-bonding species (like other water molecules) rather than with hydrophobic surfaces, to reduce the total Gibbs free energy, molecules near these surfaces can be expelled away from the surfaces where they would have more freedom to accommodate water's tetrahedral structure. As a result, a net attraction between the hydrophobic surfaces is perceived. According to Liang et al. (2007), these hydrophobic forces are actually quite long-range, and can be stronger than F_{vdW}, particularly if there is a strong Hamaker constant. According to Mao (1998), the force can be represented by a double exponential function, where the long-range term is subtracted from the short-range term, or possibly even as a power-law decay, depending on the case.

According to Hussain et al. (2012), hydrophobic effects are greater at higher temperatures, as it is entropic in nature (Eq. 1.45). According to Owusu-Apenten (2005), this effect is true up to about 70 °C for food proteins.

§4.4 Effects of Adsorbed Polymers

Another "non-DLVO" interparticle interaction is **steric** effects, particularly if a polymer exists (e.g. κ-casein on micellar surface for dairy; § 6.2), or is adsorbed onto a particle (Somasundaran

et al., 2009). According to Liang et al. (2007), no single, simple comprehensive theory exists to describe these, as they are complex in nature. Somasundaran et al. (2009), however, presents a model based on Flory's liquid lattice model. The general concept for these steric interactions is that adsorbed polymers dangle into the solution and move due to thermal effects. If two such coated surfaces come close to one another, the unfavorable entropy of entanglement of the chains induces a repulsive effect, helping to stabilize colloidal systems (Liang et al., 2007). However, if one polymer becomes adsorbed onto two neighboring particles, an attractive "bridging" interaction may exist (Somasundaran et al., 2009).

Non-adsorbed polymers in between two surfaces can cause an attractive "**depletion**" interaction; if the two surfaces approach to the extent that the gap can no longer accommodate the polymer molecules, this "depletion zone" can be seen as a sort of semi-permeable membrane – it drives water out of this polymer-depleted area via osmotic pressure into the bulk where the concentration is higher. The depletion of water thus drives the surfaces together (Israelachvili, 2011).

§4.5 Salt Effects

Adding a salt during food powder reconstitution can have a number of effects on the process, and these effects may be linked to some of the colloidal interactions mentioned in this section. As discussed in Ch. 2, adding NaCl to powders rich in micellar casein prior to reconstitution may enhance their rehydration behavior. On the other hand, the effect of salt dissolved in the *medium* prior to powder addition has not yet been discussed in this literature review. This is an interesting area to explore not only because it may help elucidate the role of such colloidal interactions vis-à-vis powder dispersing, but it may also be worth studying because, unlike the majority of experiments performed in the current thesis (using deionized water, § 7.2), in reality, consumers around the world are much more likely to reconstitute powders into aqueous media with higher (and variable (WHO, 2003)) mineral contents, which may, at least to some extent, play a role in a powder's behavior upon rehydration.

As expected from Eq. 4.7, the Debye length κ^{-1} would decrease, depending on the concentration of salt added, as well as the valency of the ions. This **screening** effect would reduce

repulsive interactions between particles that may play a role in dispersing.

In addition, particularly at higher concentrations, salts can affect the structuring of water, which would affect "structural interactions," particularly the long-range hydrophobic interactions (Mao, 1998). According to Owusu-Apenten (2005) and Zhou (2005), salts that have an anti-surfactant effect, i.e. those that increase the surface tension (such as NaCl in water (Pegram and Record, 2007)), will enhance hydrophobic interactions. This phenomenon of ions affecting water structure has particularly been studied in relation to protein stability, and the effect is specific to which cations/anions are involved. According to Bye and Falconer (2013), smaller ions with a higher charge density (called "kosmotropes") will tightly bind to neighboring water molecules, preventing them from moving about. However larger ions with lower charge density ("chaotropes") would make water molecules more mobile. According to Bye and Falconer (2013), these smaller kosmotropes would decrease the solubility of a protein, making it more likely to precipitate ("salt-out"). A ranking order for the ability of ions to bind with water is known as the lyotropic series (or Hofmeister series) – see Collins (2012) – and the effects they have are called "**Hofmeister Effects**", or "specific-ion effects."

In the case of NaCl, according to Collins (2012), Na^+ is slightly kosmotropic and Cl^- is slightly chaotropic, thus it would have a relatively neutral effect on water structuring. The effect that this would have on a protein thus depends on the type and concentration of the salt, as well as the protein structure – according to Albarracín et al. (2011), in an aqueous medium, proteins tend to fold such that the hydrophobic side chains of the amino acids would be "protected" from the bulk, with hydrophilic groups exposed and interacting with the water molecules. Thus if the solvent becomes less available to interact with these side chains, protein-protein interactions (via hydrophobic effects) would be stronger than solvent-solute interactions. These authors also explain that at lower salt concentrations, the electrostatic shielding effects can actually help to *enhance* solubility of proteins ("salting-in"), as hydrophilic interactions *within* the protein would be disrupted, but salting-out would still occur at higher concentrations. According to Pegram et al. (2010), in general, salts at lower concentrations ($< 0.1\,\mathrm{M}$) have a greater non-specific effect (Coulombic), but at higher concentrations ($\geq 0.1\,\mathrm{M}$), these effects are more specific to the ion (Hofmeister). Parsons et al. (2011) and Collins (2012), on the other hand, put this "threshold" range at closer to $0.01\,\mathrm{M}$. Boström et al. (2006) also proposes methods to quantify these effects.

Hussain et al. (2011) and Hussain et al. (2012) investigated the effect of adding salts to the reconstitution medium before adding micellar casein powder or native whey protein isolate (§ 6.2), using their turbidity method (§ 5.2). In the case of **whey**, they observed slower wetting when salts were added, as well as slower dispersing, which they attributed to electrostatic shielding and specific-ion hydrophobic effects. In the case of $CaCl_2$, they reported that a greater effect was observed compared to NaCl at the same concentration, due to higher valency of the Ca^{2+} cation compared to Na^+, as well as the "bridging" ability of divalent cations between two negatively charged groups. It should be noted that even though a salting-in effect might be expected at lower salt concentrations (better solubility), the powder had worse reconstitution properties. This may demonstrate a flaw in a Noyes-Whitney approach (Eq. 1.47), which assumes that a greater solubility (an equilibrium value) necessarily determines kinetics; the process is more complicated due to dispersing effects.

In the case of the micellar **casein** powder, they also observed slower wetting when salt was added. As for the effect of NaCl or $CaCl_2$ on casein powder, the effects were more complicated. At low concentration (0–3 % for NaCl or 0–0.75 % for $CaCl_2$), they observed poor dispersing of micelles with increasing salt concentration, which they explained according to the findings of Huppertz and Fox (2006), who observed that NaCl reduces the net negative charge of caseins in fluid milk.

However, at even higher concentrations ($\geq$ 6 % for NaCl or $\geq$ 1.5 % for $CaCl_2$), they actually report a reversal in effects, where dispersing apparently improves. They attribute this to similar structural changes to the micellar structure as discussed in Ch. 2. However, the author is not aware of any studies that investigate the effect of salt in the rehydration medium on milk powders or *non*-micellar casein powders (see Ch. 12).

As for the effects of salt in the rehydration medium, similar results have been reported (i.e. worse behavior) for hydrocolloid materials; however, the mechanisms proposed are much different. Klein Larsen et al. (2003) used a rheological approach (§ 5.5) to investigate the dissolution of alginate (a hydrocolloid; § 6.1), in salt solutions of varying types and concentration. They explained that the slower dissolution of alginate in solutions with a monovalent cation was due to the attraction between the polymer (a polyanion – a type of polyelectrolyte), and the much smaller counter-ions. They explain that this attraction during the diffusion step of dissolving (§ 1.4) creates a drag force on the molecules, hindering

reconstitution. In their explanation, they do not discuss colloidal effects. Unfortunately their viscosity-based technique would not reveal whether reconstitution overall was dispersing-limited (salt effects may influence dispersing), or dissolving-limited. This issue with their method will be discussed in Ch. 5. For the same powder in solutions of $CaCl_2$, they not only report slower dissolution but also lump (fish eye) formation, and explain that this is due to a gel formation.[5] To et al. (1994) also used a rheological approach to investigate the dissolution of xanthan gum (also a hydrocolloid) in NaCl solutions, and saw slower dissolution at high salt concentrations. They explain that this is due to a configurational transition from random coils to stiffer structures when salt is added. Thus they propose two possible mechanisms for slower reconstitution – the less flexible molecules would have more trouble disentangling from the swollen layer upon dissolving, or there would be less entropy to gain from dissolving, and thus less of a drive for the process to happen.

[5]It is well known in food science that for some carbohydrates, divalent cations can induce "egg-box structures" (Damodaran et al., 2008).

Chapter 5

Analytical Techniques

You have to learn the rules of the game. And then you have to play better than everyone else.

Albert Einstein

A number of techniques are used in the literature to evaluate the reconstitution behavior of food powders. These techniques are very diverse, with some arguably superior to others, and the information obtained highly depends on the method used, and its limitations. For the following discussion, the general assumption is that powder is added *onto* the liquid surface – as this is the case in the vast majority of studies, as well as in the current thesis.

Contents

§5.1 "Instant Properties"

Schubert (1993) describes terms such as "wettability," "dispersibility," and "solubility" to refer to different aspects of reconstitution (wetting, sinking, dispersing, and dissolving). In the current author's opinion, these terms are highly ambiguous and confusing; however, as they appear throughout the literature, they will be discussed in the current section. For many studies, these terms refer to procedures defined by the IDF (International Dairy Federation), and are sometimes (confusingly) cited as GEA Niro methods, as this company has incorporated several IDF standards into their own standards. Such standards will be discussed in the following subsections. Although they are defined by the IDF, they have also

been used for non-dairy powders as well. For instance, according to Meursing (2009), there are no well-established methods for cocoa powders, thus these IDF standards are often used, possibly with slight modifications.

5.1.1 “Wettability”

As discussed in § 1.1, the term wettability refers to the molecular interactions between a liquid and a solid. However, unfortunately, with regards to food powder reconstitution, this term has come to take on a very different meaning, and the techniques used to determine the so-called “wettability” generally involve determining the amount of time powder floats on a liquid surface. Thus perhaps a more appropriate term might be the “wetting/sinking time” (see Ch. 11).

The most basic technique to determine “wettability” is to **sprinkle** powder onto a static water surface and use a stopwatch to determine when the powder sinks. Each study appears to define its own conditions, e.g. for chocolate beverage powders (§ 8.3), Selamat et al. (1998) performs measurements at 60 °C, 1 % w/w powder whereas Shittu and Lawal (2007) uses 27 °C and 10 % w/w for the same type of powder. Park et al. (2001) performs measurements at 70 °C, 1 % w/w for micronized green tea powder. None of the studies specify *how* the powder was added (e.g. from what height, etc.).

The **IDF** standard for “wettability” (IDF, 1979) operates on a similar concept, but feeding of powder is better defined. In the method 10 g of powder is added to a steel tube with a glass plate at the bottom, and this is positioned over a glass beaker with 250 ml of water at 25 °C. The glass plate is withdrawn by hand and a stopwatch is used to determine when the powder has sunk. It has been used in the literature for non-dairy powders as well, e.g. maltodextrin (Muñoz-Herrera et al., 2010). GEA Niro has incorporated this IDF standard into their own (Method No. A5b), but they also have their own standard which operates based on a very similar principle (Method No. 5a). Instead, 100 ml of water at 20 °C is used, and the powder is added using a funnel rather than a cylindrical tube. The amount of powder added depends on the powder type: 13 g for baby food, 10 g for skim milk powder (SMP), 13 g for whole milk powder (WMP), or 6 g for whey. The temperature used also depends on the powder type: 20 °C for SMP, “instant” WMP, or whey, or 40 °C for whole milk or baby food. The method

described by Schuck et al. (2012) is almost identical to this Niro method, except that they fail to mention that the temperature is supposed to change depending on the powder. This is just one example of many to demonstrate the confusion regarding the term "wettability" between studies. Schuck et al. (2012) also describes a "wettability index" (WI) for different powders, and explains that in the dairy industry a powder is "wettable" if "WI" $< 60\,\mathrm{s}$. They also report the "WI" for different food powders, although as these can highly depend on the conditions used to make the powders (Ch. 2), these values will not be reported here.

There are also a number of more **advanced** setups to determine "wettability" of powders, e.g. those described by Hogekamp and Schubert (2003). The methods described in the previous paragraph are known in this article as "slider methods", and the authors also describe methods such as the "cone" and "improved slider" methods, as well as dynamic methods such as a "straight flow channel" or "annular channel." The dynamic methods are interesting as the liquid is moving and powder is added at a defined rate, which as discussed in Ch. 3 may affect heap formation and therefore drawdown.

The "wettability" can also be determined during **actual reconstitution** experiments in a stirred vessel. This was the focus of Schober and Fitzpatrick (2005) who used a stopwatch at defined impeller speeds. Gaiani et al. (2009) used a turbidity meter (§ 5.2) and inferred the "wetting time" based on the resulting turbidity profile. In the current report (Ch. 7), the wetting/sinking time is determined more *directly* using video recordings of the liquid surface, and controlled feeding rate using a vibratory feeder, both of which eliminate manual bias.

5.1.2 "Dispersibility"

Another poorly defined concept is that of "dispersibility." Pietsch (2002) describes this as the "*measure for the ease with which, under specific conditions, e.g. in liquids, an agglomerate breaks down into primary particles.*" Tamime (2009) on the other hand defines it as the "*ability to disperse in water by 'gentle stirring'.*" In terms of quantifying this property of a powder, the definitions become even more confusing.

Several authors use **sedimentation** analyses to determine the "dispersibility" e.g. Park et al. (2001); Ren et al. (2003); Shittu and Lawal (2007). However there are many problems

with this technique in the author’s opinion. While sedimentation may be *influenced* by particle dispersing (cf. Eq. 1.31), there are many other factors that affect sedimentation as well, such as density, etc., thus it is not a direct measurement of dispersing ability. Ideally a method would take particle size directly into account, as larger agglomerates disperse into smaller units.

According to Fang et al. (2007), the most common method to measure a powder’s “dispersibility” is the **IDF standard** (IDF, 1979), which is the same as the GEA Niro Method A6a. This method requires a vessel and a steel spatula of defined dimensions. Essentially the user stirs the powder (26 g for SMP, or 34 g for WMP) by hand into 250 ml deionized water at 25 °C in a defined manner for 15 s, then it is allowed to stand for 30 s, and the beverage is poured through a 150 µm mesh sieve, and the filtrate is dried in an oven at 102 °C. The “dispersibility” D in % can be determine according to:

$$D = \begin{cases} \dfrac{962\,T}{100 - (W + T)} & \text{for SMP} \\ \dfrac{735\,T}{100 - (W + T)} & \text{for WMP} \end{cases} \tag{5.1}$$

where T is the total solids of the filtrate per 100 g of starting liquid, and W is the moisture content (% wb) determined from an IDF method (GEA Niro Method A1b). According to Tamime (2009), “dispersibility” is considered good if $D \geq 95$ % for SMP or $D \geq 90$ % for WMP.

However, this method has been often misquoted. For instance, Schuck et al. (2012) claims that the same method requires a 200 µm mesh sieve, Gaiani et al. (2011) claims it is 210 µm, and Bhandari and Roos (2012) claims it is 250 µm, once again adding to the confusion when comparing studies. According to Tamime (2009), this technique is labor-intensive, and the reproducibility is poor, even for skilled technicians, due partly to the high amount of manual manipulation required. Moreover it only yields a single value and does not demonstrate the *kinetic* aspects of dispersing. Nevertheless it has been used by Wang et al. (2008b); Muñoz-Herrera et al. (2010) and a modified approach was used by Fitzpatrick et al. (2000).

Another “dispersibility” method is presented in GEA Niro method No. A7a for slow-dispersing agglomerated milk powders. This technique mirrors method A5a for “wettability” discussed before: 10 g for skim milk in 100 ml water at 20 °C, or 13 g whole milk powder in

40 °C (or 20 °C if the whole milk powder is lecithinated). For some reason, this method is with tap water, even though the rest are with deionized water. Essentially, a teaspoon is used to stir the powder in a circular fashion for ≈ 20 s before filtering in a Büchner funnel.

5.1.3 "Solubility"

As discussed in § 1.4, the term solubility is an equilibrium term to describe the saturation concentration of a material in a solvent. However, similar to wettability, this term has unfortunately also had its meaning distorted in dairy research. According to Granizo et al. (2007), the "solubility" of powder can be determined with techniques such as HPLC (High Performance Liquid Chromatography), filtration and drying, or spectroscopy. However, according to Walstra et al. (2006), the most common technique involves centrifuging samples after reconstitution at high agitation speeds. Bisig et al. (2005) describes three different standards involving centrifugation:

1. The IDF method 129A (IDF, 1988), which is equivalent to the GEA Niro A3a, determines the so-called "insolubility index" where powder (6 g whey, 10 g SMP, or 13 g WMP) is reconstituted at high agitation (≈ 4000 rpm) for 90 s in 100 ml water at 24 °C with a defoaming agent, then let to sit for 15 min, centrifuged, decanted, refilled with water to redisperse the sediment, then centrifuged again for 5 min, and the amount of sediment is read in milliliters. According to Schuck et al. (2012) the sediment amount is the "insolubility index" (II), and the "solubility index" (SI = 100% - II); a powder is said to be "soluble" if SI ≥ 99 %. This technique has been used for many studies, many of which were discussed in Ch. 2, e.g. Schokker et al. (2011); Chandrapala et al. (2014).
2. For high-protein powders, Bisig et al. (2005) states that the IDF method standard 173 IDF (1995) can be used. Essentially powder is reconstituted at 22 °C using a magnetic stir-bar and the pH is adjusted to 7.0; the Kjeldahl method[1] is used before and after centrifugation; the ratio of the two nitrogen contents gives an idea of the "solubility"; this technique was used e.g. by Udabage et al. (2012).
3. The ADMI (American Dairy Milk Institute) method – a similar method to that of its European counterpart (IDF, which is based in Brussels), the technique also involves

[1] A well-known method in food science to determine nitrogen content, which is related to protein content – see Nielsen (2014).

centrifugation. It was used by Fitzpatrick et al. (2000).

There have also been similar techniques used in the literature but do not follow any of these standards, e.g. see Shittu and Lawal (2007); McCarthy et al. (2014).

As mentioned in § 1.4, not all powders completely dissolve, thus using the word "soluble" to describe powders like milk or cocoa is somewhat confusing. Moreover, if one is actually interested in the *kinetics* of dissolving of a soluble material, a better term may be the "dissolving rate."[2] In addition, according to Fang et al. (2012), using an *in situ* probe technique like FBRM (§ 5.9), one may be able to quantify the "insoluble material" without the need for such off-line manipulations.

§5.2 Optical Backscatter (Turbidity)

While the previously-mentioned measurements of "instant properties" are performed off-line and have a number of flaws, it is also possible (and advisable, in the author's opinion) to follow powder reconstitution *in situ*; that is, in real-time during actual reconstitution trials in a stirred tank. This allows the researcher much more flexibility in terms of the conditions used (e.g. impeller speed N, impeller type, etc.) and yields information about the *kinetics* of reconstitution.

One commonly used approach utilizes a probe that emits light into the suspension and also detects light that is backscattered from the particles (due to the Tyndall effect). This is a measurement of turbidity of the sample – which is a concept often exploited for water quality analysis (ISO standard 7027). While turbidity can be measured based on the attenuation of light shown through a sample, these probes operated based on the scattering instead, which is related to nephelometry. There are several units for turbidity, depending for example on the type of light emitted (e.g. white vs. monochromatic near infra-red, etc.), but in the literature relevant to powder reconstitution the signal is often simply calibrated to concentration via a (linear) standard curve, and/or normalized against the minimum and maximum values ($0 \rightarrow 1$).

[2] See Ch. 9 for a discussion about different *types* of dissolving rates, defined in the current thesis.

The reconstitution profile obtained after the trial highly depends on the type of powder utilized. For example, L. Galet's lab at the Ecole des Mines d'Albi in France used an optical fiber sensor to monitor cocoa powder (Vu et al., 2003; Galet et al., 2004) as well as talc powder (Goalard et al., 2006; Galet et al., 2009; Lefebvre et al., 2011a,b). For both powder types, the reconstitution curve was simple: the turbidity signal rises similar to an increasing exponential decay to maximum, e.g. Fig. 5.1.

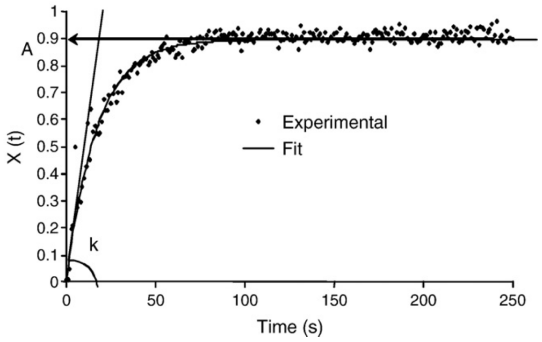

Figure 5.1: Typical normalized curve obtained with turbidity measurements for powders such as talc (Galet et al., 2009).

These studies have then interpreted this type of curve, for example by reporting the time to achieve 90 % the maximum value (i.e. the "t_{90}" value), or performed simple first-order reaction-analogous curve fitting (empirical modeling), according to:

$$X(t) = A\left(1 - \mathrm{e}^{-k\,t}\right) \tag{5.2}$$

where $X(t)$ is the extent of dispersion as a function of time, A is an indication of the final extent of dispersing, and k [s^{-1}] is the "dispersion rate." It should be noted that the turbidity signal not only depends on the amount of material on a weight basis, but the turbidity also increases with decreasing size (Gaiani, 2006). Thus using such a technique, it is difficult to determine purely from a turbidity profile if an increase in $X(t)$ is due to sinking or dispersing, as both would result in an increase in turbidity. Using their setup (Fig. 5.2), one cannot visually view (or record) the powder behavior at the liquid surface to determine if sinking or dispersing is responsible for the rise in signal.

More complex turbidity profiles were demonstrated for dairy protein powders in a series of papers by C. Gaiani's group at the Université de Lorraine in France (Gaiani et al., 2005, 2009; Hussain et al., 2011). For micellar casein and native whey protein powders, they report different "stages" in reconstitution, depending on the powder type, e.g. Fig. 5.3.

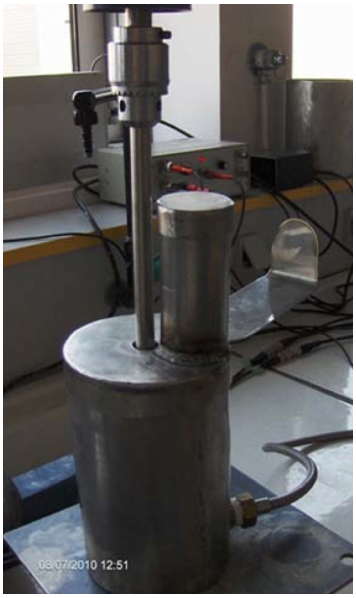

Figure 5.2: Setup used by the group of L. Galet (Lefebvre, 2010).

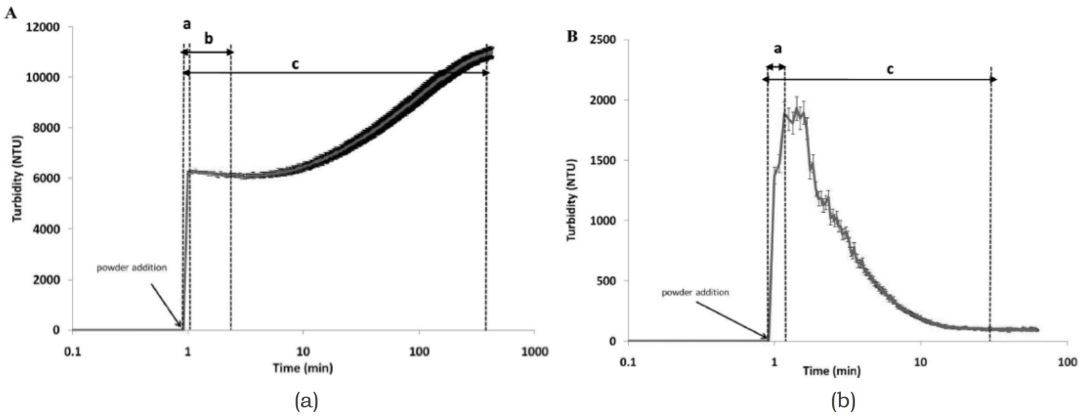

Figure 5.3: Typical turbidity profiles for (a) micellar casein and (b) whey protein isolate (Hussain et al., 2011).

In the case of micellar casein, the authors report a wetting time (a), swelling time (b), and a total rehydration time (c). As mentioned previously, when casein micelles are released during rehydration, they do not dissolve – thus the turbidity increases as more individual micelles disperse and diffract light. However, native whey protein isolate (Fig. 5.3) *is* water-soluble; thus, they infer a wetting phase (a), no swelling, and a total rehydration time after the powder has mostly disappeared (dissolving leads to a *decrease* in turbidity). The y-axis for both curves is NTU (nephelometric turbidity units), which was the default for their probe, even though light detected was *back*scattered at 180°, not 90°. It should be noted that, as far as the author is aware, no video recording device was used to confirm that the "wetting time" actually corresponds to wetting and sinking. In the author's opinion, these curves are also difficult to interpret, as they plot the time on a logarithmic scale. Unlike techniques such as laser diffraction or FBRM (discussed later in the present chapter), turbidity is not a direct measurement of size distribution; thus, one cannot *directly* study dispersing, which of course involves a shift in size distribution. However, this technique has the advantage of being an inexpensive, *in situ* measurement, and does give the operator some information about concentration of dispersed particles.

§5.3 Electrical Conductivity

A (somewhat) similar approach to turbidimetry is the use of a conductivity meter, which also can be applied *in situ* to (theoretically[3]) track the progression of powder dissolution. The probe operates by applying an electrical potential (voltage) across two electrodes (an anode and cathode) and measuring the current, which is proportional to the concentration of conducting ions (Jenway 4510 User Manual, see Ch. 7). The resistance R can be calculated according to:

$$R = \frac{V}{I} = \frac{I}{G} \tag{5.3}$$

where V is the voltage [V], I is the current [A], and R is the resistance [Ω]. The inverse of resistance R is conductance G, which depends on the geometry of the probe used; this can be taken into account by introducing the cell constant k_c where:

$$k_c = \frac{d}{a} \tag{5.4}$$

[3]See Ch. 14.

where d is the separation between the electrodes (generally given in cm), and a is the effective surface area of the electrode (cm^2), thus the units for k_c are given in units of cm^{-1}. The conductivity C is then calculated according to:

$$C = G\, k_c \tag{5.5}$$

where the units for C are generally given in $S\,cm^{-1}$, with S being the S.I. unit Siemens. Generally for food powder reconstitution studies, conductivity is converted to concentration (via a linear standard curve) or normalized, like with turbidity in the previous section.

The curves obtained after reconstitution trials tend to be quite straightforward – they look similar in shape to Fig. 5.1 for turbidity, and the curves can be interpreted similarly, obtaining a value such as the "t_{90}" or the slope of the initial curve can be used for the "dispersion rate", etc. For instance Marabi et al. (2008b) used this approach to investigate the effect of fat content on the "dissolution rate" of dairy powders, and observed slower reconstitution with higher fat contents (at 20 °C). However it should be noted that their technique had no way of reporting if the slower behavior with increasing fat content was due to slower wetting/sinking, dispersing, etc. Moreover, the probe would only detect the presence of electrically conducting materials, which in the case of dairy powder is mostly minerals/salts that are present in relatively low concentration (§ 6.2), and probably do not significantly contribute to phenomena such as lump formation. As pointed out by Syll et al. (2012), who criticized the approach by Marabi et al. (2008b), conductivity meters do not yield information about particle size, thus making them ineffective at determining the *extent* of dispersing, and could therefore give a misleading result in terms of when reconstitution is "finished" (see § 14.3). Nevertheless it is still often used for studies involving powder reconstitution.

Another consideration for using conductivity is that rapid mixing is required to ensure quick convective transport of ions throughout the vessel, and to the probe measurement site, thus it may not be appropriate for slow mixing applications.

§5.4 Laser Diffraction

Laser diffraction, also known as "static light scattering (SLS)", or "low angle light scattering", among other names, is a particle sizing technique that has also been used quite frequently during food powder reconstitution analysis. A number of different units exist that operate on this principle; for instance Malvern Instruments (UK) offers three devices: (1) Spraytech, which works for dry dispersion or spray applications, (2) Mastersizer, which can be used for wet suspensions or dry applications, or (3) Insitec, an instrument that could be used for all three applications. According to Malvern, the Mastersizer is the world's most popular particle sizing device, and as it can be used for wet applications, it has been used for rehydration purposes.

A full description on the principle of a laser diffraction unit is given elsewhere (Merkus, 2009, Ch. 10). The basic principle considers that light can interact with a particle via four interactions: edge diffraction and refraction at the interface (which can both be measured), as well as reflection off the surface and absorption (which make interpretation more difficult). During measurements particles are presented in front of a laser beam; spherical particles will produce a diffraction pattern related to the particle size, with larger particles diffracting light at smaller angles (smaller distances between concentric rings of the diffraction pattern), and at higher intensity than for smaller particles. If the powder suspension is **dilute** enough (low obscuration), then one can assume that each particle produces a separate diffraction pattern, and that light is not diffracted by more than one particle. The Mastersizer can interpret and convert the patterns to size distributions (for several laser sweeps) using one of two theories: Fraunhofer or Mie theories. According to Merkus (2009), Fraunhofer's theory assumes that particles behave as opaque, two-dimensional circles, and becomes invalid particularly at smaller sizes or greater transparencies. Mie's theory incorporates knowledge about the optical properties of the particles and the medium, expressed using a complex number for the ratio of refractive indices between particle and medium: the real component is related to refraction, and the imaginary component corrects for absorption – as shown in Fig. 5.4, backscatter detectors can also be used to correct for reflection.

Note that both theories assume dilute suspensions and spherical, non-porous particles, which are generally **not true** during food powder rehydration.

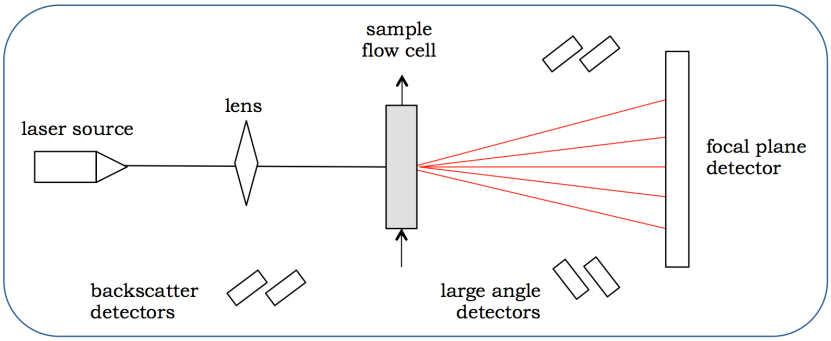

Figure 5.4: Sketch of the laser diffraction principle.

The Mastersizer has been used for powder reconstitution studies, particularly for dairy powders, to monitor the changes in size distribution, which is not possible using the previously-mentioned techniques in the current chapter. The way this is generally performed is that an **aliquot** will be taken from the medium at regular intervals, diluted until an acceptable obscuration is obtained, and then values such as the $d_{50,3}$ (volume-based median size) are plotted over time (Gaiani, 2006), a surface plot of population balance (particle size vs. time) is constructed (Mimouni et al., 2009), the d_{50} can be normalized against the final $d_{50,\infty}$ to plot the "extent" of dispersion ($d^\star$) vs. time (Jeantet et al., 2010), etc.

For some studies (e.g. Richard et al. (2013)), instead of manually sampling, the researchers have a series of **tubes** connected to a peristaltic **pump** that continuously takes samples and dilutes them for analysis. There are some clear advantages to observing size changes during reconstitution: one may be able to see if the conditions chosen has an effect on the *extent* of dispersion, not only the kinetics of reconstitution overall.

However, there are some serious **drawbacks** of the laser diffraction approach. Measurements are performed off-line (or, at best "in-line"), but not *in situ*, and the dilution and/or pumping action required to obtain a measurement may in fact destroy larger structures such as lumps or agglomerates, which may be, themselves, the most interesting features of dispersion for the researcher. Depending on the size of the hoses, for instance, lumps may not even be able to fit into the measurement device.

A possible alternative is the Malvern Insitec, which according to the Malvern website uses "multiple scattering algorithms" to correct for the fact that at high concentrations neighboring

particles could re-scatter diffracted light. However measurements would unfortunately not be able to be performed *in situ*. In the literature search only one article was found that used this technique (Goalard et al. (2006) for talc powders) but the sampling technique was not specified.

Thus, a more powerful tool would be a technique that can perform size distribution measurements (and concentration measurements, which laser diffraction cannot do), *in situ*, without the need for sampling or dilution.

§5.5 Rheological Approach

Another approach to study food powder reconstitution is to take advantage of the fact that the liquid medium may become more viscous during dissolution; this is especially true for hydrocolloid powders (§ 6.1) – as a result the torque on the impeller/stirrer may measurably increase. Rheology itself is the study of how a material will flow (or deform) when a stress is applied, and has many applications in food technology (Rao, 2007). This study is often performed under shear flows with the use of a rotational rheometer, which is similar to a viscometer, but can perform measurements under different flow conditions. Such a rheometer operates by placing a sample in between a rotor and a stator (of which there are several geometries), and the machine can shear the sample by rotating the rotor at a defined speed (assuming strain-rate controlled conditions), while the torque required to cause the rotation is recorded. Knowing the geometry used, the speed of rotation may be converted to shear strain rate $\dot{\gamma}$ [s^{-1}] and torque can be converted to shear stress τ [$N\,m^{-2}$]. For example, for the **cone-and-plate** geometry, which has a well defined, even shear field (Rao, 2007)[4] the following relationships can be used (Dogan and Kokini, 2007):

$$\dot{\gamma} = \frac{\omega}{\alpha} \tag{5.6}$$

where ω is the frequency of rotation [s^{-1}], and α is the angle of the cone slope from the horizontal (in radians), with:

$$\tau = \frac{3\,T}{2\,\pi\,R^3} \tag{5.7}$$

[4] And which will be used in § 12.3

where T is the moment of force [N m], and R is the radius of the stator plate [m].[5] The values for $\dot{\gamma}$ and τ are related via a coefficient of proportionality, for liquids called dynamic viscosity μ [Pa s]:

$$\tau = \mu \dot{\gamma} \tag{5.8}$$

For Newtonian liquids, e.g. water, for a given temperature, μ will be independent of $\dot{\gamma}$ (i.e. τ will increase linearly with $\dot{\gamma}$). However, many liquid foods exhibit non-Newtonian behavior, as mentioned in § 3.7, where τ will change with $\dot{\gamma}$, often in a non-linear way. According to Rao (2007), many foods exhibit shear-thinning (pseudoplastic) behavior, where the structure of food begins to align with the flow as $\dot{\gamma}$ increases, providing less resistance. Some materials exhibit shear-thickening (dilatant) behavior, and some behaviors can change with time at a defined $\dot{\gamma}$ as well, or exhibit a yield stress, below which no flow occurs. Thus an "apparent" viscosity μ_{app} at a specified $\dot{\gamma}$ must be reported in these cases.

For food powder reconstitution, a different geometry is used: one that must be able to hold a low-viscosity liquid, and for which the rotor should (theoretically) mix the powder. For instance Gaiani et al. (2006) used a **vane** (paddle) geometry to study dairy protein powders (Fig. 5.5). They perform measurements at a constant rotational speed, and also claim a "constant shear (strain) rate"; however, as discussed in Rao (2007), this is not actually true, since the shear rate can vary quite considerably from point-to-point for such a geometry. To obtain the viscosity over time, Gaiani et al. (2006) compared the profiles with cone-and-plate data. Some other studies used custom-made geometries; e.g. Kravtchenko et al. (1999) and Parker et al. (2000) used a sort of paddle of which the shaft does not become submerged, preventing rubbery hydrocolloids from sticking to the dry shaft surface. However this geometry is so poorly defined that they simply report the raw torque, or convert the torque to a concentration via a standard curve. Other studies (To et al., 1994; Klein Larsen et al., 2003) use a lab mixer/impeller and report shear stress or concentration over time.

There are some serious drawbacks to such an approach, if not used in conjunction with another approach. Rheological measurements give no information about wetting/sinking behavior, or dispersing, as no size measurements are obtained. In the framework of the current PhD, experiments were attempted (results not shown) using the vane geometry for different

[5] While the cone-and-plate geometry is useful to characterize the rheology of liquids, it is not appropriate for *monitoring* powder reconstitution.

Figure 5.5: Vane geometry used by Gaiani et al. (2006) for "rheological approach."

food powders during rehydration, but the mixing was too unrealistic for real applications. Some powders did not sink, even at high shear rates, and those that did sink were simply pushed along in a circular pattern without dispersing. The data obtained if the torque from an *impeller* would be quite interesting, but the other issues discussed (no size distribution, etc.) still remain.

§5.6 Nuclear Magnetic Resonance

Nuclear Magnetic Resonance (NMR) is a phenomenon that has occasionally been used to study food powder rehydration. It exists for nuclei with non-zero spins, i.e. nuclei of isotopes having an odd number of protons and/or an odd atomic mass number. As explained by Figura and Teixeira (2007), when these nuclei are placed into a magnetic field they will absorb a quantum of energy corresponding to their resonance frequency, causing the nucleus to become 'excited.' The excited nucleus will eventually 'relax' to its equilibrium state, thereby emitting electromagnetic radiation at radio frequencies that can be detected using an NMR spectrometer. Figura and Teixeira (2007) explains that these instruments generally operate by emitting short ($\approx 10\,\text{ms}$) pulses of electromagnetic radiation to excite the nucleus then the re-emitted radiation is detected with a receiver coil. The shape of the decay signal is affected by two components: the 'spin-lattice' or 'longitudinal' magnetic relaxation (T_1) and the 'spin-spin' or 'transverse' relaxation (T_2) – see Brown and Semelka (2010) for more details about the complex relaxation process. According to Figura and Teixeira (2007), the duration of the NMR signal is ultimately limited by T_2. NMR techniques can follow different non-zero spin nuclei such as ^{13}C, ^{19}F, or ^{31}P; however, the most commonly used isotope for food (and medical) applications is ^{1}H, as it is present in water molecules (Marcone et al., 2013).

5.6.1 NMR Relaxometry

NMR spectroscopy has recently become a powerful tool for food technologists, with diverse applications, such as composite analysis, quality and authenticity assurance, and on-line monitoring during food production (Minoja and Napoli, 2014; Marcone et al., 2013). For instance it has been used to monitor the chemical stability of food powders (Schmitz-Schug et al., 2013). It has also been used for food rehydration studies (Davenel et al., 1997, 2002; Schuck et al., 2002, 2007; Granizo et al., 2007). As explained by Granizo et al. (2007), low-field NMR measurements are performed by monitoring the T_2 over the course of reconstitution (the reconstitution vessel is surrounded by magnets – see Davenel et al. (2002)). As the powder rehydrates, water molecules will form multi-layers around food macromolecules (see § 1.4) and as a result, these 'restricted' or 'bound' water molecules have less mobility than 'free water'. These nuclei of restricted water molecules would then have faster relaxation times (lower T_2 values), which, when plotted over time, demonstrates the speed of dissolution.

While NMR-relaxometry has the advantage that measurements are performed non-intrusively, it does not yield very much information on its own. It yields no direct information on wetting/sinking, nor does it show how particle sizes might evolve. According to Saggin and Couplan (2002), it may also be difficult to use in metallic containers, thereby restricting applicability, and measurements are slow and expensive to perform (Yucel and Coupland, 2010).

5.6.2 Magnetic Resonance Imaging

A more advanced application of NMR phenomena is (nuclear) magnetic resonance imaging (MRI).[6] As explained by Brown and Semelka (2010), this imaging is performed by applying additional radio frequency fields to alter the alignment of the magnetic nuclear field, causing nuclei at different spatial locations to behave differently, with the frequency of the released signal being dependent on its origin. Thus, the geometric source can be deconvoluted. MRI has applications in many fields, not only medicine, and is beginning to have several

[6]The "nuclear" part of the name is usually emitted largely due to reasons related to public misconceptions, since MRI is often used for medical analysis.

applications in the food industry (van Duynhoven et al., 2009). According to Marcone et al. (2013), it is particularly attractive as it can monitor the *internal* structure and composition of foods, whereas most techniques focus on external properties.

MRI has also been gaining attention in rehydration studies as well, due to the fact that it can monitor both solids and liquids, even in an opaque system. For instance it has been used by Vergeldt et al. (2014) (in collaboration with Unilever) to observe the imbibition of water into freeze-dried carrots. In the pharmaceutical industry it has also been used to monitor the dissolution of tablets in a flow cell (Langham et al., 2012). While using MRI for such applications may present a major advantage over techniques such as optical image analysis, since one can monitor the 3-D tablet instead of a 2-D projection, the equipment required is much more expensive.

Chen et al. (2010) at Cambridge used an **ultra-fast MRI**, which can characterize dissolution phenomena at smaller time scales than would otherwise be possible, such as tablet swelling and rapid release. According to van Duynhoven et al. (2009), MRI in general would not typically have good enough temporal and spatial resolution for applications like *powder* reconstitution. However the same group at Cambridge (in collaboration with Nestlé) has recently employed ultra-fast MRI to monitor the suspension of inert, non-dissolving particles (Peng et al., 2013). What is particularly interesting about their approach is that **water can be added to the powder** which cannot reasonably be done using the other techniques discussed in the current chapter. The authors up-injected liquid into a bed of poppy seeds, and reported two regimes: either the formation of a liquid "jet" in the middle of the particle bed (at lower powder amounts, higher flow rates, or lower solid-liquid contact angles θ), or a "lifting" regime where the bed is lifted upwards. However in terms of powder wetting, capillarity, dispersing, and dissolving, it appears that the technology still needs to be improved for better resolution. Another clear disadvantage of such an approach is the huge cost involved; thus it is currently more appropriate for academic research applications.

§5.7 Ultrasonic Spectroscopy

One interesting technique that has attracted quite some attention over the past few years is acoustic spectroscopy. As mentioned previously (Ch. 2), ultrasounds can be used to destroy casein micellar structure as a pre-treatment, or as a dispersion/mixing method during reconstitution (Ch. 3). Here, however, when used as an analytical tool, the power density and amplitudes of deformation are much lower, and according to Bonacucina et al. (2009) they have no permanent effect on the structure of the dispersed system, making the technique non-intrusive.

As described by Richard et al. (2012), the way an ultrasonic spectrometer works is that it utilizes a piezoelectric transducer to emit compressional longitudinal sound waves (the frequency of which is above the frequency audible to humans i.e. $> 20\,\text{kHz}$) into the analytical chamber, and another transducer on the other side (usually) receives the signal. According to Bonacucina et al. (2009), there are six different mechanisms for how this mechanical wave can interact with dispersed particles:

1. Viscous dissipation from the drag resulting from density differences between oscillating dispersed and continuous phases,
2. Thermal effects due to gradients in temperature near the particle surface,
3. Scattering/diffraction, similar to the effects discussed in § 5.4,
4. Intrinsic absorption energy,
5. Oscillations of a structural network, if it exists,
6. Electrokinetic (which would be negligible for overall attenuation).

The equipment generally (nowadays) measures *both* the attenuation of the signal (loss of energy due to a decrease in amplitude, measured in dB), as well as the velocity (related to propagation time) (Buckin et al., 2003). By performing measurements over a wide range of frequencies, one can use a model that predicts the magnitude of scattering mechanisms to convert to a particle size distribution (see McClements (1996) or Pinfield (2014) for details). According to Allen (2003), if the particle size is much smaller than the wavelength, it will move *in synch* with the oscillation. However, if the particle size or frequency increases, additional drag between the medium and particle will occur, which is exploited for the conversion to

particle size distribution.

According to Povey et al. (1999), measurements can be performed at **high concentrations** as well, using a multiple scattering theory that gives good estimates of size without the need for dilution (analogous to the discussion in § 5.4, cf. Insitec), and thus has the advantage that measurements can be performed in opaque suspensions and for large size ranges. As such, this technique has recently attracted interest for **on-line particle size distribution (PSD) measurements** for particle suspended in liquids; Meyer et al. (2006a) at Nestlé used this technique for on-line characterization of milk, and reported that this technique is more promising than laser diffraction.

Not surprisingly, this technique has also been used to characterize the reconstitution of food powders, although interestingly, none of the papers found in the literature search used the technique to actually monitor the evolution of PSD during reconstitution. Meyer et al. (2006b) compared the attenuation and velocity signals during reconstitution of milk powder to a "visual reconstitution test" and reported good correlation to *attenuation* but not to signal velocity. They explained that this is due to the fact that the main mechanisms for attenuation is scattering, which is related to particle size and volume fraction, which of course are important for reconstitution quality. Velocity, on the other hand, is related to the physical state of the milk components, which are less relevant.

Richard et al. (2012) investigated the effect of adding dairy protein powders to water on the amplitude of the received signal, and observed the evolution of a normalized attenuation parameter. They saw a sharp decrease when the powder was added, followed by a gradual increase back to the original value; the "t_{90}" value is referred to as the "relaxation time." They compared results from these tests with those simultaneously performed using a laser diffraction approach (§ 5.4) and observed a difference in the results; even after the acoustic results had stabilized, the particle size continued to decrease, indicating that reconstitution was not yet completely over. They explain that the loss in signal when powder was added is **due to the presence of air** incorporated with the powder, and as the water penetrates primary particles (which may be hollow – Ch. 2), air is released and as more air is released, the normalized parameter returns to its original value.

Yucel and Coupland (2010) on the other hand observed both the attenuation and velocity

during lactose dissolution and reported that the velocity was related to the concentration of both dispersed *and* dissolved lactose, but the attenuation was related only to suspended (not dissolved) material. Thus, they proposed it is a useful technique for on-line control of crystallization and dissolution of such sugars, and suggest it could also be used to monitor the mixing of opaque suspensions (e.g. during chocolate conching).

Bonacucina et al. (2009) used acoustic spectroscopy to monitor the dissolution and solvation of hydrocolloid food powders (§ 6.1), which are often used as thickening agents, and thus of course the rheology of the system may be interesting to monitor (§ 5.5). According to these authors, acoustic spectroscopy can be used for a sort of **"microrheological approach"** to monitoring reconstitution, as the velocity and absorption are related to the extensional modulus[7] of the liquid. The storage modulus G', which describes the elastic component of deformation, and the loss modulus G'' (non-recoverable) [Pa] can be determined according to:

$$G' = \rho\, v^2 \tag{5.9}$$

$$G'' = \rho\, v^3\, \frac{\alpha}{\omega} \tag{5.10}$$

where v is the sound speed, α is the attenuation, ω is the frequency, and ρ is the density of the system. The authors monitored these moduli during solvation of gums and reported a sort of first-order-like increase in G' to a maximum value, and a similar decay in G''. As the attenuation correlated linearly with ω, they claim that the curves obtained would be valid at any ω. The increase in G' was explained due to structural changes in the system – as water hydrates the molecules, less free water is available, and the sound velocity increases, as does G' (Eq. 5.9). G'' on the other hand depends on attenuation. Thus they use the initial slope of the G' as a way of comparing hydration at different conditions, e.g. temperature, ...

One major disadvantage with the setups used in the literature is that measurements are performed in a flow cell, meaning that samples must be taken away from the vessel for analysis – even if measurements are performed on-line with a pumping system, this is not ideal, as discussed in § 5.4. Richard et al. (2012) used a sort of U-shaped probe containing both transducers; however, as can be seen in Fig. 5.6, there is an enormous baffling effect, making

[7] Different than shear effects discussed in § 5.5 as the stress is applied not tangentially but normally.

it impractical if one is interested in studying the influence of liquid flow on reconstitution mechanisms.

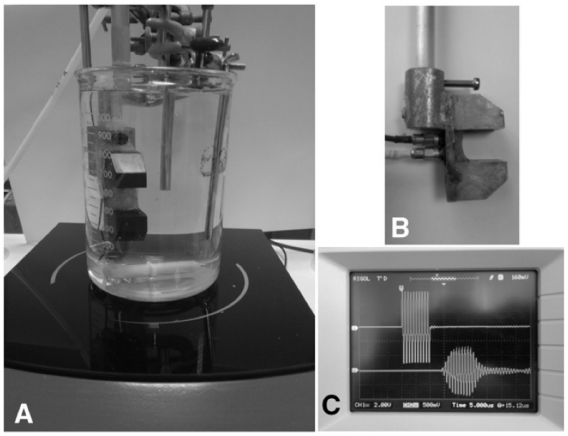

Figure 5.6: U-shape ultrasonic probe used by Richard et al. (2012).

However, Weser et al. (2013, 2014) present an ultrasonic *backscattering* approach that could monitor particle size distribution as well as concentration, and may be positioned such that it would not disturb the liquid flow; however, to the author's best knowledge this technique has not been used for reconstitution. It should also be noted, that like every other technique discussed thus far, that this approach would also yield no direct information about the wetting/sinking stages of reconstitution.

§5.8 Electrical Tomography

Recently, electrical resistivity tomography (ERT)[8] has become popular for liquid and solid-liquid mixing applications. According to Kowalski et al. (2010), for this technique, electrodes are placed on the inside wall of a mixing vessel in a circular pattern at different heights in the vessel to form cross-sectional 2-D slices or planes. As described by Pakzad et al. (2008), these electrodes are connected to a data acquisition system (DAS), which controls the applied electrical current between different combinations of adjacent electrodes per plane, also measuring the voltage between all other pairs of electrodes in the plane. A computer then uses an image reconstruction algorithm to create a 2-D tomogram for each slice, or a 3-D image from information from all slices.

[8] And closely-related electrical impedance technology (EIT), or electrical capacitance tomography (ECT).

According to Shirhatti et al. (2005), for a conducting liquid medium (e.g. tap water), the addition of a non-conducting material would decrease the conductivity (according to Maxwell's equations – not shown), and thus could also be detected with ERT. According to Sharifi and Young (2013), ERT has many applications for engineers, e.g. flow analysis in pipes, on-line monitoring of phase distributions, etc. Pakzad et al. (2013) used ERT to measure the formation of caverns around the impeller in solutions of shear-thinning xanthan gum, and used the results to validate their CFD model. Hosseini et al. (2010), Tahvildarian et al. (2011), and Tervasmäki et al. (2014) used ERT to determine the N_{js} (Eq. 3.17) of glass beads, latex particles, and sand, respectively. Kowalski et al. (2010) at Unilever demonstrated that it can be used to monitor the physical stability of colloidal liquid food systems against processes such as creaming or coalescence. Sharifi and Young (2011) demonstrated its use in milk holding tanks, as it can be used to identify defects such as aeration or even adulteration. They even used it to **detect lump formation** resulting from poor reconstitution of milk powders, whereas such lumps may otherwise be left undetectable due to the opaque nature of milk. As a result, ERT may be an attractive technique for food powder rehydration studies. However, the only study that was found in the literature search that used ERT for such a purpose was Shirhatti et al. (2005); however, in this study the powders used were unspecified (due to confidentiality) and the full potential of the technique was not realized in the report, in the current author's opinion.

The **advantages of ERT** that should be pointed out are that the technique would not obstruct flow patterns as it is non-intrusive, it can be used for opaque systems (unlike Particle Image Velocimetry (PIV), according to Pakzad et al. (2008)), and gives 3-D information that most other techniques could not, with the possible exception of MRI.

In the framework of the current PhD project, at the beginning it was planned to use the ERT setup at the Nestlé Research Center in Lausanne, Switzerland (ITS – Industrial Tomography Systems, Manchester, UK); results not shown. However it was determined that the spatial resolution was not high enough for the systems tested, and the electrodes placed around the vessel made it difficult to obtain high-quality images in the transparent vessel (Ch. 7). Thus, the ERT project was abandoned in favor of another approach (Ch. 7). However, it is possible that ERT will find useful applications in the near future for powder reconstitution studies.

§5.9 *In situ* Laser Backscattering

5.9.1 Theory of FBRM

One very attractive approach to study powder reconstitution is the use of laser backscattering. The most commonly used equipment that employs this concept is FBRM (Focused Beam Reflectance Measurement) technology, which was patented by Lasentec, a company acquired by Mettler-Toledo in 2001. The technology operates by use of a probe (Fig. 5.7, from the product manual) that can be placed directly into a process. As explained by Höpfner et al. (2010), a diode emits a laser beam that is carried to the probe tip via fiber optics. A lens focuses the beam a fine point at the sapphire window, and this lens rotates at high speeds (≈ 75 Hz) in a circular pattern, and as a result, so does the focused laser point.

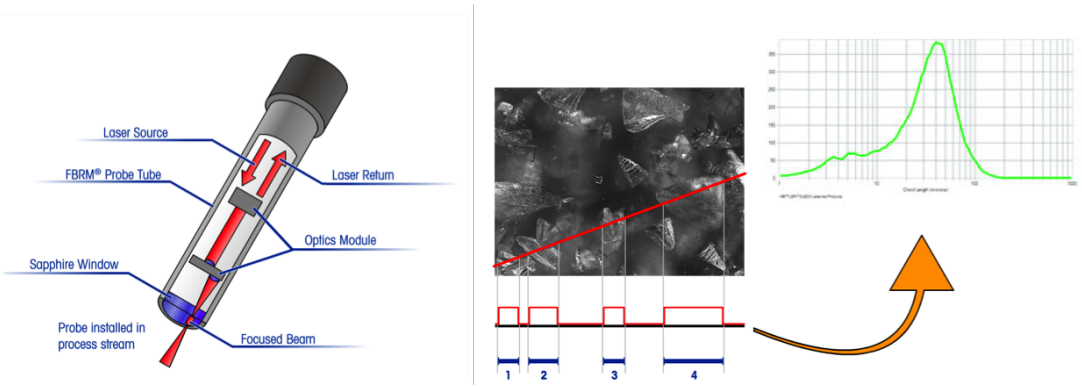

Figure 5.7: Diagram of FBRM probe and depiction of backscatter from rotating beam being converted to chord length distribution (FBRM G400 User Manual, 2011).

When the laser light contacts a suspended particle, it is scattered in several directions, but the light that is scattered at 180° (i.e. backscattered) is transmitted back through the probe, and a beam splitter separates the received light from the light being emitted, and a detection unit determines the duration of the backscatter pulse. A discrimination circuit is used to ignore particles that are out of focus (using a chord selection method (CSM), where if the rise and fall in signal is too gradual, it is discarded). Since the laser beam is moving very quickly compared to the particles, and since the instantaneous focused laser speed is known ($2\,\mathrm{m\,s^{-1}}$ for the G400 model – see Ch. 7), the chord length of a particle can be calculated. Höpfner et al. (2010) explains that thousands of particles can be measured each second, and that the information is stored in 1,324 channels, ranging from 0.25 µm and 1024 µm; the lower

400 channels have a resolution of 0.25 µm and the 924 larger channels have a resolution of 1.0 µm – all of this information is used to create a chord length distribution (CLD) for each measurement.

5.9.2 Alternatives to FBRM

A very similar technique to FBRM is the "3-Fold Dynamical Reflectance Measurement," or "3D ORM," which has been developed by Sequip GmbH in Germany. As explained by Peda et al. (2010) and Peda et al. (2011), this technique also uses a rotating focused laser beam in a probe to obtain a CLD for particles; however, the probe also contains a fiber optic coupler that allows for a "dynamic focus," where the focused laser can be applied in a 3-D spiral pattern (rather than a 2-D circle, like for FBRM). According to Peda et al. (2011), this gives 3D ORM better resolution than FBRM, thus it is better equipped for studying nucleation in crystallization studies. It has also been by Hahn et al. (2013) to study the size of microgels during fresh cheese production. However, to the author's best knowledge, it has not been used for powder reconstitution study.

Another technique that uses laser technology to obtain a CLD of particles *in situ* is the Parsum, by Malvern Instruments (UK). In the technique, particles flow through a slit in the probe, through which a laser beam is shone, and particles thus cast a shadow. The light interruption is converted to CLD – but only for relatively large particle sizes (50 – 6000 µm), thus it is not appropriate for food reconstitution studies.

As 3D ORM and Parsum have not been used for reconstitution study, and since FBRM *is* the main technique used in the current report (Ch. 7), it will be considered exclusively for the remainder of this section.

5.9.3 Uses of FBRM

FBRM has recently gained considerable attention in several different industries as a PAT (Process Analytical Technology) tool, due to its inline measurement capabilities (Li et al.,

2013). It has been used to monitor the growth kinetics during granulation processes (Cavinato, 2010), droplet sizes in emulsions (Boxall et al., 2011), biomass concentrations (Whelan et al., 2012), size of ice crystals in frozen sorbet (Arellano et al., 2012), and also tablet disintegration[9] (Coutant et al., 2010). FBRM has also been used to study nucleation, growth, and dissolution of crystals (Markande et al., 2013), and according to Barthe et al. (2008), a change in the form of a chord length distribution can be linked to morphological changes to crystals.

5.9.4 Analyzing powder reconstitution using FBRM

Despite its promising applications across several fields, FBRM has rarely been used as a technique for reconstitution studies. Shirhatti et al. (2005) demonstrated that the technique can be used, but disappointingly they only used the technique to report the total counts vs. time, without taking advantage of the sizing capabilities; the study also does not even specify the type of powder used.

The group that has done the most[10] work with FBRM for food powder reconstitution is a group at Monash University in Australia. Fang et al. (2010), Fang et al. (2011), and Fang et al. (2012) studied the reconstitution behavior of milk protein concentrate (MPC; § 6.2), and unlike Shirhatti et al. (2005), they *did* take advantage of the sizing abilities of FBRM. MPC contains high levels of casein, which does not completely dissolve in water (Ch. 2), and Fang et al.'s group observed an increase in total counts over the course of reconstitution, similar to what Gaiani et al. observed using turbidity (§ 5.2). However the main focus of their reconstitution studies was the **mean particle size**, which as illustrated in Fig. 1.16 decreases as powders and individual particles disperse.

To describe the kinetics of the process via mean size evolution, they developed a model based on the Noyes Whitney Equation (Eq. 1.47). Assuming a constant surface area, the concentration can be converted to the mass of dissolved material (W), and by integrating

[9] This technique would *not* be appropriate for tablet erosion; it requires a disintegration because it would detect particles that break off of the tablet – see Brielles et al. (2008) for a discussion about disintegration vs. erosion regimes for tablets.

[10] To the author's best knowledge.

one obtains:

$$W = W_{\mathrm{E}} \left(1 - \mathrm{e}^{-k\,t}\right) \tag{5.11}$$

where W is the mass of "dissolved" material, W_{E} is the mass at the final stage, k is a rate constant, and t is time. As FBRM measures the size of particles that are *not yet* dissolved, Eq. 5.11 can be rewritten to:

$$W_0 - W_t = (W_0 - W_\infty) \left(1 - \mathrm{e}^{-k\,t}\right) \tag{5.12}$$

with $W = W_0 - W_t$ and $W_{\mathrm{E}} = W_0 - W_\infty$, where W_0 is the initial particle mass, W_∞ is the amount of particle still "undissolved" at the end of the measurement, and W_t is the amount undissolved at time t. By assuming spherical particles and uniform density, they express Eq. 5.12 in terms of mean size from FBRM measurements:

$$d^3 = \left(d_0^3 - d_\infty^3\right) \mathrm{e}^{-k\,t} + d_\infty^3 \tag{5.13}$$

where d_0 is the initial particle size (which they assume to be equal to the $d_{90,3}$ from dry laser diffraction measurements), and d_∞ is the final "particle" size, with $d_\infty \leq d_0$ (see Fig. 1.16). These studies monitor both values of k and d_∞ in order to study the effect of different parameters (e.g. water temperature) and storage conditions (e.g. storage temperature & time, spray drying temperature, etc.), on the *kinetics* and *extent* of reconstitution, respectively.[11] In one graph the authors demonstrate that over the course of reconstitution, counts measured per second can be divided into different size classes; they show that "small" counts (1–10 µm) increase to a maximum value, but larger particles (150–300 µm) have a sharp rise at the beginning, but decrease over time (Fig. 5.8). However the authors do not explain why they ignored particles between 10 and 150 µm.

While Fang et al.'s work did demonstrate some powerful advantages of FBRM for reconstitution study, there are a number of concerns with their overall approach. Firstly, the placement of the FBRM probe in the vessel is done from above (Fig. 5.9), which would create a baffling effect significantly disrupting liquid flow.

Secondly, the vessel they used appears to have arbitrary configurations, and does not appear to adhere to any sort of standard. Thirdly, the method of powder addition was left unspecified,

[11] In the author's opinion, this is quite a refreshing distinction to draw, as most other studies in the literature focus on one aspect of reconstitution without considering the others. However FBRM is able to determine both kinetics *and* extent of dispersion.

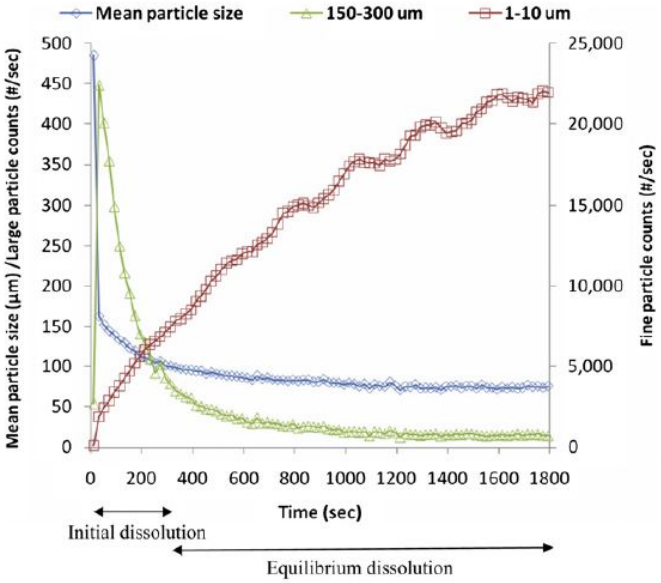

Figure 5.8: Using FBRM to show evolution of small and large populations (Fang et al., 2011).

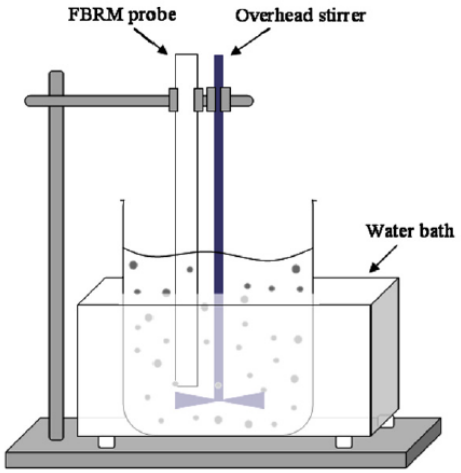

Figure 5.9: Setup used by Fang et al. to study powder reconstitution (Fang et al., 2010).

and the approach did not consider how *long* powders take to wet/sink. Moreover, the studies only used one type of powder under a very narrow range of reconstitution conditions (only one rotation speed, N, etc.); therefore, there is quite a bit of room for improvement with regards to using FBRM for reconstitution studies, as will be the focus of Ch. 7 in the current dissertation.

5.9.5 (Dis)advantages of FBRM for reconstitution analysis

As discussed by Höpfner et al. (2010), FBRM has a major advantage over *ex situ* techniques, like laser diffraction, for particle sizing as it can be applied *in situ* without the need for dilution, and it also yields total counts, counts within a specified size range, as well as a number of other statistics. However some disadvantages have been reported as well. According to Tok et al. (2008) and Wilson et al. (2012), FBRM probes can be susceptible to fouling as particles stick to the probe window, blocking measurement. However, Huang et al. (2010) presented a scraper that can be attached to the probe tip to remove stuck particles, and according to Mettler-Toledo, the newest line of FBRM probes (the G-series, see Ch. 7) also includes a "stuck particle correction" algorithm in the measurement software that recognizes if a particle is being repeatedly measured and ignores the measurement. If too much of the probe window becomes "dirty", an error message appears to warn the operator.

Another disadvantage is that FBRM only measures particles that pass directly in front of the probe window, and gives no indication of the 3-D distribution of particles in the vessel (as would ERT or MRI, for instance). In the current PhD, this is mostly accounted for by using a video camera (Ch. 7).

5.9.6 Chord Length vs. Particle Size

One common concern when using FBRM is that it yields a chord length distribution (CLD) rather than a "particle size distribution" (PSD), which, as discussed in § 5.4, is based on the assumption that all particles behave like spheres to interpret the laser diffraction pattern. Characterizing the size of a particle is especially challenging for the study of crystallization

where particles can have high aspect ratios, which is one reason why FBRM is often used in conjunction with an *in situ* image analysis technique (Larsen et al., 2007) – see § 5.10.

Li et al. (2013) reviewed much of the relevant literature regarding the use of inversion procedures to estimate PSD from FBRM measurements, and discusses the challenges associated with these procedures. They refer to a "geometric model" for CLD, where the chord length is defined as a straight line along the 2-D projection (silhouette) of a suspended particle as it is hit with the moving focused laser beam. Thus this model assumes that particles are opaque, do not overlap, and that the laser beam remains focused, and an algorithm can be used to obtain CLDs from the projections by analytical calculations (in the case of sphere-like particles) or using Monte Carlo simulations (numerical approach) for other geometries. However the authors note that this model may be invalid for transparent particles (e.g. many crystals), and propose a solution via an empirical relationship. However, in the case of powder reconstitution for the current study, it does not appear necessary to convert CLD to PSD, particularly if one wishes to demonstrate a qualitative difference in dispersing ability between powders (see Ch. 11). For a further discussion about issues with *quantifying* dispersing/dissolving phenomena using FBRM, see Ch. 9.

§5.10 Other Analytical Techniques

In addition to the main techniques discussed earlier in the present chapter, there are some other techniques worth mentioning as well, such as solution calorimetry, compendial test methods, and image analysis approaches.

5.10.1 Solution Calorimetry

Dissolution (ampoule-breaking) calorimetry is one technique that has occasionally been used in relation to powder reconstitution studies. It is one application of isothermal calorimetry, which is a technique where the heat change is measured during a chemical or physical change, at a constant temperature (O'Neill and Gaisford, 2011). As described by O'Neill and Gaisford (2011), during solution calorimetry, the solid and liquid are brought into contact by piercing a

membrane that separates them, then mixing of the two phases occurs, and the resulting heat change can be directly measured or converted from a temperature change – see Kayaert et al. (2010) for details. The enthalpy change ΔH for a pure material dissolving into a solvent is due to the breakage of a crystal lattice (if there is one) and the formation of solvation interactions, as discussed in § 1.4, via:

$$\Delta H_{\text{solution}} = \Delta H_{\text{lattice}} + \Delta H_{\text{solvation}} \tag{5.14}$$

where the $\Delta H_{\text{solution}}$ can be positive (if the reaction is endothermic), or negative (exothermic). According to O'Neill and Gaisford (2011), for a purely amorphous material, $\Delta H_{\text{lattice}} = 0$; however, in reality even local order formation can be detected. As such, this technique has been widely been used to determine the crystallinity/amorphous content of materials (Terada et al., 2000; Katainen et al., 2005; Gaisford and Saunders, 2012), and can also yield information regarding aging effects of food powders due to structural relaxation (Syll et al., 2012) – see Ch. 2. Terada et al. (2000) even reported a strong correlation between the dissolution rate to the $\Delta H_{\text{solution}}$, explaining that slower dissolution was related to the *crystallinity* of the sample. Marabi et al. (2007) and Marabi et al. (2008b) performed similar experiments and also reported a correlation between dissolution kinetics and $\Delta H_{\text{solution}}$, but went so far as to suggest an important contribution of a "local heat transfer" in dissolving; a hypothesis that was challenged in more detail in § 1.4.

Solution calorimetry has also been used to *directly* monitor the progression of dissolution by plotting (normalized) heat flow vs. time. For instance Conti et al. (2006) monitored the dissolution of powdered polymers, and fitted the dissolution profile to a power law function ($y = k\,t^n$), where k is a constant, and n is a fitting parameter that, they claim, yields information on the swelling behavior. Kayaert et al. (2010) monitored the dissolution of nano-suspensions, which they explain dissolve so quickly that other techniques would have difficulty monitoring the progression. According to Conti et al. (2006) this technique also has the advantage that it can be used for opaque liquids.

However, there are a number of disadvantages compared to other techniques. As one cannot visually see the reconstitution taking place, it is difficult to obtain wetting/sinking information, feeding/mixing cannot be varied as they can be when a stirred vessel is used, and one obtains no direct information about the size evolution related to dispersing.

5.10.2 Compendial tests

Quite a bit of the literature about dissolution is rather specific to the pharmaceutical industry, but it is still worth discussing as many concepts are transferable to foods, and some of the materials are similar or even the same; particularly hydrocolloids (§ 6.1). However, unlike food dissolution, which lacks any sort of strict regulatory standards for how tests are performed, drug dissolution studies are much more strictly regulated. The history of the research on pharmaceutical dissolution was reviewed by Dokoumetzidis and Macheras (2006); in the 1950s it became understood that it was the *dissolution*, rather than the disintegration, of oral doses that was related to the bioavailability of drugs, and as a result, a number of standardized tests were developed that are used in both research and development (R&D) and quality control (QC) applications. The most well-known methods (called "compendial tests") are defined by the United States Pharmacopeia (**USP**), but other pharmacopeiae also exist (British, European, Japanese, ...).

According to Azarmi et al. (2007), there are six main USP apparatuses for dissolution study, which include, e.g. USP 1 (a rotating backet), USP 2, paddle, etc. The authors state that these USP tests are generally used for tablets and capsules, but there are some studies that have used the same set-ups for powder dissolution study. They also state that when such tests are performed for QC purposes, it is to screen for variations between batches, but for R&D these *in vitro* tests supposedly provide a predictive tool for *in vivo* applications; although, according to Rosanke and Brown (1996) there is some controversy about whether an approach is truly valid. Azarmi et al. (2007) also proposes some other "non-conventional" techniques (modifications) for R&D purposes. Another concept used in drug dissolution research is the so-called "Intrinsic Dissolution Rate" (IDR), which is supposedly characteristic of a certain material, as studies are performed on tablets of the material in question at constant surface area, pH, ionic strength, and stir speed (Mauger et al., 2003). Generally during such compendial tests, the amount of active pharmaceutical ingredient (API) dissolved in the medium is determined over time by taking samples of the liquid and analyzing them with spectrophotometry (e.g. Ultraviolet (UV)/visible light, at the appropriate wavelength) (Ring et al., 2011; Han et al., 2011). Tsinman et al. (2009), on the other hand, instead used a dip probe fiber optic UV method in order to determine the "IDR" *in situ*.

According to Marabi et al. (2008a), such an approach would not be appropriate for food powders, as they are too complex in composition, with components absorbing light at different wavelengths. In addition, there is not necessarily one component of interest (like an API) but rather, the powder as a whole needs to be dispersed and/or dissolved. Nevertheless, Hellborg et al. (2012) used spectrophotometry (with sampling, i.e. *ex situ*) to study the rehydration of different dairy powders (and methyl cellulose) at 225 nm for absorbance.

It is also worth mentioning that, according to the USP website (`http://www.usp.org`), over the past few years, there has been an effort to harmonize the methods across different phamacopeiae through bilateral agreements, and a number of summits have recently taken place; thus the use of such techniques may be undesirable as these standards may be subject to change.

5.10.3 Image Analysis

Another technique that has been utilized in reconstitution studies is the processing of images taken of dissolving particles, and a few approaches have been taken.

Single Particle Analysis

A few studies have concentrated on the dissolving of individual particles in order to separate the final reconstitution step from wetting/sinking and dispersing effects. Marabi et al. (2008a) used a simple setup where a spherical sucrose[12] particle is placed in stationary water and a video camera monitors dissolution, and the area of the projection is converted to volume (assuming the particle remains spherical), and plotted over time, and a simple empirical equation ("shrinking sphere model") is used to extract the dissolution rate.

Börjesson et al. (2013) uses a similar concept with a light microscope with image processing software to determine the swelling and dissolution behavior of sodium caseinate (§ 6.2) particles, using a more sophisticated approach. Measurements are performed in a flow cell

[12]Presumably amorphous, or with some sort of other filler material, since crystal spheres of sucrose are unlikely to exist, to the author's best knowledge.

(Fig. 5.10) where the water flow velocity can be controlled. They observed quite a bit of variation between results due to morphological differences in particles, but on average the dissolution rate improved at higher flow velocities, and they related the trend to the common dependence of mass transfer coefficients to Reynolds (Re) and Sherwood (Sh) numbers (see § 1.4). However, they did not observe an effect of flow velocity on the *swelling* of particles.

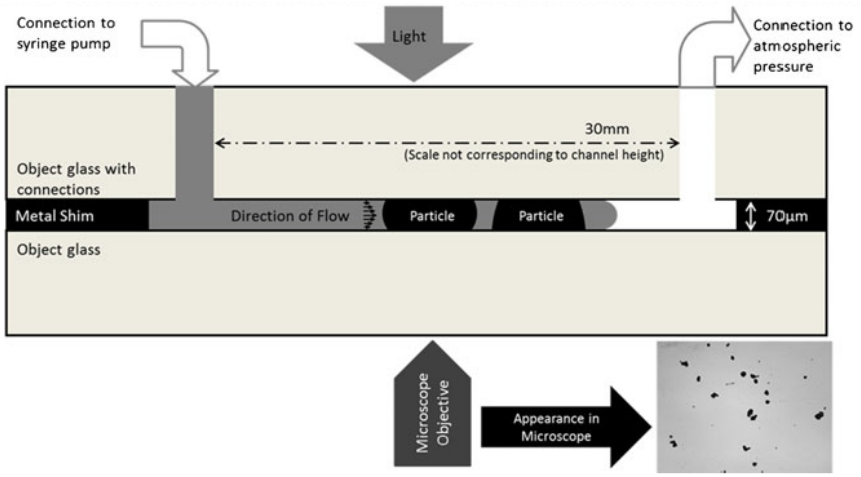

Figure 5.10: Flow cell used by Börjesson et al. (2013).

While Marabi et al. (2008a) criticizes a "bulk approach" to powder reconstitution in favor of a single particle approach, it is important to consider how the dissolving of individual particles will affect bulk (overall) reconstitution. As discussed in § 1.4, under some conditions a faster dissolving of single particles may actually be undesirable, particularly if the dissolving material has a strong viscosity-building effect, as this may lead to the formation of lumps that resist dispersion (Parker et al., 2000), or that inhibits wetting/imbibition (Hellborg et al., 2012).

Use of a Granulomorphometer

A very different application of image analysis has been used in conjunction with dissolution experiments in a stirred vessel, using a granulomorphometer. Such a technique, in this context, operates by passing a suspension of particles in a liquid through a measurement stage, and a camera takes many images of the back-lit suspension. An automated image analysis software can interpret the 2-D projected images of the particles. Such an approach can reveal information about the size distribution – generally the "EQPC" (equivalent projection

area of a circle) is used, but other size parameters can also be extracted, e.g. Feret (caliper) diameters, chord lengths, etc. It can also enumerate particles to give an idea of the particle concentration, and shape factors (e.g. sphericity) can also be reported, as well as actual binarized images of particles for qualitative analysis.

Wilson et al. (2012) uses such a device (the QicPic from Sympatec GmbH, Germany) to monitor both the disintegration and dissolution of immediate release tablets in a USP vessel (paddle geometry). The vessel was connected to the QicPic using hoses and a peristaltic pump to feed particles from the dissolving medium that had **broken off of the tablet** for analysis. They then used population balance modeling (PBM) to relate the competing rates of particle release from the tablet to the dissolving of the released particles, and compared the result to compendial tests.[13] While the results did agree, they cite the many advantages of their novel approach.

Richard et al. (2012) and Richard et al. (2013) employed a similar technique to study the reconstitution of different dairy powders in a stirred vessel, with hoses and peristaltic pump used to lead particles into a similar device (Flow-Cell 272 2005 - M, Occhio, Belgium). Abdelaziz et al. (2014) used an analogous approach (with QicPic) to study the behavior of chocolate beverage powders (§ 6.3), and called their approach a "dynamic method" and compared their results to so-called "static methods," i.e. the IDF standards for "wettability", "dispersibility," and "solubility" (§ 5.1). They reported that both types of tests are in agreement, but that one obtains more useful information from the "dynamic approach." The authors also claim that their approach is an "*in situ*" method; however, this is not true as measurements are *not* performed in the vessel itself. Moreover, similar to the discussion given for laser diffraction (§ 5.4) regarding the use of pumps and hoses for measurements, it cannot be argued that this approach is non-invasive.

In situ Microscopy

Another interesting possibility for image analysis of dissolving particles is using an *in situ* microscope, which (by definition) could capture images of particles directly in the mixing vessel.

[13] For the USP test for tablet disintegration, tablet fragments would need to pass through a 2 mm mesh basket, and UV-absorption is used for dissolution analysis.

According to Höpfner et al. (2010), two such techniques would be the **PVM** (Particle Vision Microscope) by Mettler Toledo, which uses an incident light, and ISM (*In Situ* Microscope) by Sartorius, which uses transmitted light. According to Höpfner et al. (2010), a PVM probe consists of a CCD (charge-coupled device) camera, and six laser sources equally spaced apart that are focused by lenses on the opposite side of a sapphire window to illuminate an area of interest (Fig. 5.11).[14]

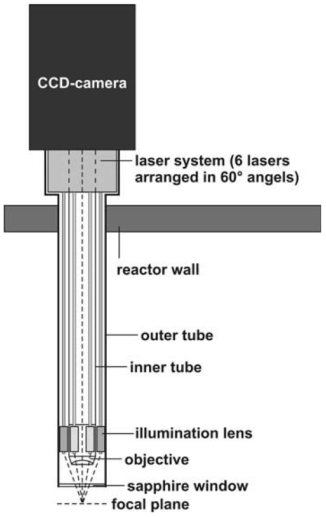

Figure 5.11: PVM probe (Höpfner et al., 2010).

The PVM probe is typically used in conjunction with an FBRM probe (from the same manufacturer) and can be used as a complement to the data – the iC FBRM software (Ch. 7) can even directly link the two measurements to show images at each point in time. The two techniques have been used together to study emulsion droplet sizes (Boxall et al., 2011), crystal formation/dissolution (Zhao et al., 2013), and PVM is particularly interesting to consider if needle-shaped crystals are present (Leyssens et al., 2011). With regards to obtaining size information from such images, according to Larsen et al. (2007), the segmentation (thresholding) could be quite challenging, especially for crystals, due to non-uniform density and color, making edge detection difficult. Nevertheless the images themselves may be quite interesting, at least from a qualitative point of view.

However, to the author's best knowledge, PVM (or similar techniques) **have not yet been used for food powder dissolution**. In the framework of the current PhD, a PVM probe

[14]The PVM V819 model used in the current report (see Appendix) has a field range of 1075 × 875 µm, with a spatial resolution of ca. 2 µm, according to Mettler Toledo.

was used to monitor the effect of temperature and agitation speed on powder dispersion – results are shown in the Appendix. While the results were interesting, particularly as image analysis approaches can also give information about the *morphology* of particles during dispersion, experiments were performed during a demonstration with a representative from Mettler Toledo. As the probe was quite expensive (quoted at about £80,000), it was decided to proceed without PVM in favor of the setup described in Ch. 7. For most cases, it is argued that the use of a video camera (ca. £50) revealed enough information that PVM was not necessary for the study and may even reveal more interesting phenomena (floating, sedimentation, etc.) that PVM might miss (Ch. 10).

5.10.4 Stopwatch Method

While there are several advantages and disadvantages for the techniques discussed heretofore, the "stopwatch method" is arguably the least advanced and may be inadequate for studies on dispersion mechanisms. Essentially, a person with a stop-watch in hand records the amount of time until the powder has "completely dissolved": while this might be acceptable as a quick quality control test, it has unfortunately appeared in research literature as well, e.g. for maltodextrin (Takeiti et al., 2008; Ziyani and Fatah, 2014), or even chocolate beverage powder (Omobuwajo et al., 2000). It should be remembered that defining the "end of reconstitution" is quite subjective (Ch. 14).

§5.11 Interpretation (Modeling) of Rehydration Profiles

Following a reconstitution experiment, normally one obtains a dissolution profile similar in shape to Fig. 5.1, where the y-axis gives an indication of concentration, and the x-axis is time. In an attempt to concisely describe the results using a few parameters, a number of studies have focused on which (semi)-empirical model best fits the curve – and quite a few of such models can be found in the literature, particularly for hydrocolloid (§ 6.1) powders (Wang et al., 2008a). Such models are particularly important to keep in mind whenever the word "rate" is used in Ch. 6. Similar modeling studies have also been performed to study the imbibition of water into larger food particulates, and by weighing them at regular intervals,

one obtains a graph similar in shape to Fig. 5.1, with weight (or mass) on the y-axis (Saguy and Marabi, 2011). A few models, such as those based on chemical reaction kinetics, or power law were already discussed in previous sections, as was the "t_{90}" model from normalized data. Another model that has been used in many applications (e.g. describing the shape of cumulative particle size distributions (Cheong et al., 2004)) is the Weibull function:

$$X(t) = 1 - \mathrm{e}^{(-t/\alpha)^{\beta}} \tag{5.15}$$

where X is the amount dissolved (or water imbibed, etc., depending on the context), t is time, α is a fitting parameter that describes the *time scale* (when $t = \alpha$, $X(t) = 1 - (1/\mathrm{e}) \approx 63\,\%$ complete), and β is the other fitting parameter that determines the *shape* of the curve. Marabi et al. (2003) claims that for imbibition into freeze-dried carrots, β also yields information regarding the mechanisms of uptake, and they propose a "normalized" Weibull function to account for difficulties in geometry, thickness, final water content, etc. Wang and Flanagan (2002) performed reconstitution experiments (using a confusing apparatus) with guar gum (a hydrocolloid; § 6.1) and measured samples with a capillary viscometer, and plotted viscosity vs. time and fitted the results to a first-order, Weibull, and (vertically shifted) logarithmic model. They reported poor fitting for first-order, but good fitting for Weibull and logarithmic models. Parvathy et al. (2007) reported very similar results for the same powder type. A number of modifications to the models previously mentioned can also be found in the literature (e.g. a *double* exponential model (Kravtchenko et al., 1999), zero$^{\text{th}}$-order kinetics for "sink" conditions (§ 1.4), etc.) It should also be noted that the models reported in the literature focus on the evolution of the *dissolved* concentration. However, no models have been found that describe dispersing and dissolving phenomena *separately*, which would be interesting in the context of the current project. Such a novel model is presented in Ch. 9.

As discussed by Siepmann and Siepmann (2008), while such empirical models are useful to describe experiments that have already been performed, more useful models would be those that are mechanistically/theoretically based, as they could be used to *predict* powder behavior. According to Hörmann et al. (2011), such *in silico* predictions are extremely useful to the industry as, if they are accurate, one could simulate experiments on a computer without wasting valuable materials, as well as time and money. As reviewed by Jeantet et al. (2010) and Richard et al. (2013), such models do exist for powders (based on diffusion, swelling, and erosion mechanisms), but as there are so many factors to consider, the results from such models can seriously deviate from empirical results. According to Forny et al. (2011), such

models applied to food powders would need to incorporate complex wetting/capillarity, and dissolving phenomena, which are still not completely understood. According to Siepmann and Siepmann (2008), models are by their nature always simplifications of real systems, and the more complex (and computer-intensive) the model, the more accurate it is expected to be.

In the current author's opinion, too much attention has been paid in the relevant literature to *which* model best fits the already-obtained raw data, and there has not been enough of a critical discussion on the setups used to obtain the data itself, for instance: questioning the validity of techniques, asking if the setup geometries are comparable to other studies, considering how liquid flow and feeding affect results, or if some useful information can be obtained using a simple visual observation rather than always trying to extract numbers from a rehydration profile. In general the phenomena most interesting from a problem-solving point of view cannot be adequately described with such models. In Chapters 10 and 11, a novel mapping approach to studying powder reconstitution is presented to circumvent such problems.

§5.12 Comments on Mixing Setups

In the previous sections in this chapter, different measurement devices used for studying powder reconstitution were presented, along with their advantages and disadvantages. However, such devices are only a part of the overall picture; the mixing vessel setup overall is also extremely important to consider, yet in the literature reviewed, it is rarely, if ever, explicitly discussed.

The first consideration is the mixing vessel itself. While most studies to use **impellers**, which are relatively easy to control and induce quite well-defined flow patterns, some studies unfortunately use magnetic stir bars. These can easily become stuck or behave erratically, and the flow is not well defined in comparison to impeller-mixing. As for the vessel **geometry**, the vast majority of studies use quite arbitrary (or unspecified) configurations, which may limit reproducibility and result comparison between different research groups. However, a handful of studies did adhere to the standards in Fig. 3.4, e.g. Freudig et al. (1999) and Lefebvre (2010); this is the only standard configuration mentioned in the literature.

Another consideration is the **baffling** of liquid flow. Some studies added **baffles** on purpose (e.g. Richard et al. (2013) added one baffle; Freudig et al. (1999) added four), and some flows were unintentionally baffled simply due to the presence of their measurement device (see Fig. 5.9). However very few studies directly investigate the effect of baffling (Ch. 13) on powder dispersion – Freudig et al. (1999) only superficially studies these effects. Several different types of impellers have also been used for such studies, which makes it difficult to compare studies; in addition no studies comparing impeller types could be found for food powder reconstitution studies in the literature search.

As mentioned in § 3.4, the **feed rate** can also have a major impact on heap formation, and reconstitution overall. Unfortunately, however, the method of powder addition is almost never specified. Some studies use a sort of mechanism (Fig. 5.2) where a trap-door-like trigger is quickly pulled by hand to add the powder all at once. However, this does not allow for a study on feed rate. Freudig et al. (1999) used a vibratory feeder to control the feed rate, but the height and position from which the powder is dropped is not specified. As discussed in § 1.2, the impact when particles hit the liquid surface may play a role in sinking.

The next consideration is the **conditions** applied during studies. In general, articles in the literature employ quite a limited range of conditions, and these are mostly studied unidimensionally (only changing one variable, e.g. stir rate N, while maintaining all other variables constant, without considering the interplay of variables such as temperature T and stir rate N). Moreover, many different powders have been studied, which makes it challenging for those not well versed in food science to understand, and comparing results between studies can be tricky due to the vast number of factors that can affect rehydration properties (e.g. manufacture and storage conditions; see Ch. 2). The amount of powder added during reconstitution also varies quite considerably, further complicating matters. As so many factors of reconstitution can influence the process, choosing which variables to alter, and which to keep constant, was one of the challenging aspects of the current project.

Finally, as discussed, there are clear advantages of *in situ* probe-based techniques, due to the many issues with *ex situ* approaches (requiring tubes/pumps or sampling); in particular FBRM is attractive as it can both enumerate and size the suspended particles. However, as discussed in Ch. 1, reconstitution involves many complex physical processes, but such probes can only measure particles that flow into the measurement zone, but ignore processes

such as sinking and sedimentation behavior. While Schober and Fitzpatrick (2005) did use a stopwatch to determine the sinking time, a more sophisticated approach would, for instance, count the number of frames in a video recording to accurately and objectively determine sinking behavior. In terms of sedimentation and other phenomena, in some cases these processes could easily be studied if one uses a transparent mixing vessel; however, most studies use opaque stainless steel. The group of L. Galet at the Ecole Mines d'Albi (France) used the setup shown in Fig. 5.2, and the group of C. Gaiani at the Université de Lorraine used the setup in Fig. 5.12.

Figure 5.12: Setup used by Gaiani (2006) in a stainless steel (opaque) vessel.

In Ch. 7, for the current PhD, all of the above-mentioned aspects were taken into account when constructing the rig for analysis, in the hopes of obtaining data of highest possible quality. A summary of the key advantages and disadvantages of the main analytical techniques is given in Fig. 5.1.

Table 5.1: Comparison of main analytical techniques for reconstitution studies.

Technique	Advantages	Disadvantages
Instant Properties	Cheap, easy, Quality Control	Off-line, poor reproducbility, single value, no kinetic info
Turbidity	*In situ*, monitors conc., cheap	Cannot distinguish sinking/dispersing, no sizing
Conductivity	*In situ*, cheap	Misleading results, no info on sinking/dispersing, size
Laser Diffraction	Sizing	Off-line, no info on sinking/conc., dilution, expensive
Rheology	Change in viscosity	Unrealistic mixing, no info on sinking, size
NMR Relaxometry	*In situ*	Expensive, special vessel needed, no info on sinking or size
Ultrasonic Spectroscopy	*In situ*, concentration and size	Probes baffle flow, no sinking info
Electrical Tomography	*In situ*, 3-D info	Resolution weak, conducting materials only, no sinking info
FBRM	*In situ* conc. & size, no dilution	Expensive, no sinking info

Chapter 6

Previous Studies on Food Powder Rehydration

Many of the food powder reconstitution studies in the literature focus on the effects of process and storage conditions on the particle properties (especially surface characteristics; Ch. 2), and the "stability" of each powder is determined at defined conditions for comparison purposes. **However the current project is more heavily focused on the mechanisms of reconstitution itself**, under a wider range of dissolution conditions. The three most commonly studied types of food powder for such studies are hydrocolloids, dairy powders (especially those high in protein), and cocoa-based beverage powders. As these powders have been referenced in previous chapters, they will be reviewed briefly in the following sections, along with a discussion of studies that have investigated their reconstitution behavior. In § 6.4, other food and non-food powders will also be briefly mentioned.

Contents

§6.1 Hydrocolloids

Hydrocolloids are a common ingredient in food (and pharmaceutical (Wang et al., 2008b)) formulations, and are added to impart a range of functional properties to the final product (Laaman, 2011). According to Wang et al. (2008b), many of these can be labelled as "soluble fiber" on an ingredient label as well. The group consists primarily of carbohydrate polysaccharides; however, there are some notable exceptions (e.g. gelatin). The term also incorporates food gums, which are highly-branched water-soluble polymers from a variety of sources. According to Vaclavik and Christian (2008), the majority are plant-derived, e.g. pectin, guar gum, starch (and starch derivatives, such as maltodextrins), alginates, and carrageenans (seaweed-derived), but some are synthetic, or microbial extrudates (xanthan gum). Some hydrocolloids are polyelectrolytic, i.e. possess charged groups (negative) in solution, which are more water-soluble than neutral hydrocolloids, and can behave in a complex and ion-specific behavior in the presence of cations (§ 4.5).

6.1.1 Functional properties

According to Laaman (2011), such functions resulting from the water-holding capacity due to many hydrogen-bonding sites include beverage emulsion stability, or preventing ice

crystal growth, foam collapse or particle settling. Saha and Bhattacharya (2010) reviews the thickening and gelling properties of hydrocolloids, and state that these have a number of usages, e.g. replacing fat, to attenuate a rise in postprandial blood glucose levels for diabetics, and can be used to produce restructured foods, and products such as jams, gravies, soups, sauces, etc.

According to Saha and Bhattacharya (2010), the thickening ability (**viscosity increase in solution**) of a particular hydrocolloid will be a function of the concentration, the temperature, and (possibly) the shear strain rate applied. According to Dogan and Kokini (2007), the **temperature** dependence usually follows an Arrhenius-like behavior:

$$\mu = \mu_0 \, \mathrm{e}^{-E_a/(RT)} \tag{6.1}$$

where μ_0 is the viscosity at a reference temperature, E_a is the "activation energy," R is the ideal gas constant, and T is the absolute temperature. As with any Arrhenius plot, a linear plot of $\ln(k)$ vs. $1/T$ would yield a plot with a slope from which E_a can be determined.

Saha and Bhattacharya (2010) explains that the rise in μ with **concentration** depends on properties such as the molecular weight and the hydrodynamic radius (influenced by charge density, degree of branching, etc.). At lower concentrations, there will be a slower rise in μ with concentration; however, above a certain critical concentration (the overlap concentration $C^\star$), there will be a sharper rise in μ with concentration due to the entanglement of dispersed polymers with one another. It is also above this $C^\star$ that such solutions exhibit non-Newtonian behavior, due to structure formation, and $C^\star$ decreases as the molecular weight increases, according to a function.

The same authors discuss the mechanisms for **gelation** of some hydrocolloids, and explain that these form due to the creation of cross-linked "junction zones" between dispersed polymers in a three-dimensional network, in which the liquid solvent becomes immobilized in the interstices. As a result, the gel itself will exhibit a viscoelastic behavior. Different types of gel formation mechanisms are discussed further in Saha and Bhattacharya (2010). Loret et al. (2004), for instance, demonstrated the interrelation of concentration, gelation temperature, and gel time for maltodextrin DE3 solutions (§ 8.1). As discussed earlier (§ 4.5), divalent cations may also induce gel formation for some hydrocolloids. As discussed in § 1.1 and § 1.4, according to Parker et al. (2000) and Forny et al. (2011), phenomena such as thickening and

gelation can play a significant role on mechanisms responsible for poor rehydration and lump formation.

According to Parker et al. (2000), hydrocolloid powders are generally produced by drying and milling, and in order to take advantage of their functional properties they must be completely dissolved; however, this is challenging (somewhat ironically) due to their gelling and thickening effects when they first contact water, sometimes resulting in lump formation (§ 1.4). As such, there have been a number of studies focused on investigating their rehydration, mostly using a rheological approach (§ 5.5).

6.1.2 Studies on Hydrocolloid Dissolution

Klein Larsen et al. (2003) studied powdered alginate rehydration using a rheological approach (measuring torque from the impeller), and investigated the effect of particle size distributions (by sieving the powder into different fractions), water temperature, and "viscosity" (actually, the molecular weight of the polymer rather than the liquid viscosity itself). They fitted the results to a first-order (exponential) model (Eq. 5.2) to extract the "dissolution rate" (k) and reported an Arrhenius-like increase in k with temperature (analogous to Eq. 6.1), as well as a faster k with decreasing particle sizes, as one might expect from Eq. 1.50. However it is important to note that their experiments were performed under "dispersing conditions" (Ch. 2), i.e. dry mixed with 5× more sucrose than alginate. These authors also reported no significant effect of molecular weight on k, although the range they tested was rather narrow.

Bonacucina et al. (2009) used an ultrasonic spectroscopy-based rheological approach (§ 5.7) to study the rehydration of three types of food polysaccharides: λ-carrageenan, gellan gum, and xanthan gum. They reported an "initial swelling rate" from the initial slope of G' vs. t (see § 5.7), and also reported an improvement at higher temperature (45 °C vs. 25 °C) and at smaller sieved fractions; although, these powders were also rehydrated under "dispersing conditions" by mixing with glycerine.

Kravtchenko et al. (1999) draws a bigger distinction between results obtained using *dispersing* and *non-dispersing* conditions, and even uses two different models to fit the data, depending on which condition is applied. For *dispersing* conditions, a simple exponential

model (Eq. 5.2) is used (mass dissolved, derived from the torque on the paddle), but for *non-dissolving* conditions, a sum of two exponentials is used:

$$m = A\left(1 - \mathrm{e}^{-k_a\, t}\right) + B\left(1 - \mathrm{e}^{-k_b\, t}\right) \tag{6.2}$$

where m is the mass dissolved, A is the mass that dissolves "normally," and B corresponds to the amount that forms lumps, with $A+B$ equal to the total amount of powder added, the fitted parameters k_a and k_b are the corresponding rates, and t is time. This model allows them to not only describe the rates of the process but also the "index of dispersibility," corresponding to A at the end of the measurement. They reported for pectin powder under non-dispersing conditions, with decreasing sieved size fractions, the dissolution rate improved up to a point, but decreased at very small fractions ($< 45\,\mu\mathrm{m}$). As for the index of dispersibility (A), this value continually decreases with smaller sieve fractions, which is an indication of greater number of fish eyes. Although they do not directly study the effect of temperature, they explain that it is often better to dissolve such powders in colder water, as higher water temperatures can induce greater lump formation (§ 1.4). **Parker et al. (2000)** continued this work using the same setup for a larger range of powders: pectin, carrageenan, xanthan and guar gum, at different size fractions as well, and reported similar results – they proposed that an **optimum size** may exist for ideal reconstitution, for non-dispersing conditions, but that this size would be material-specific. They argue that having a size larger than this optimum is better than a size that is too small, as when lumps do form, they are very difficult to disperse.

Wang et al. (2003) used a rheological approach to characterize the influence of molecular weight (MW) and concentration of guar gum under non-dispersing conditions, and used a logarithmic model to extract the "rehydration rate" (k). Unlike Klein Larsen et al. (2003), they report an inverse relationship between MW and k; the range in MW tested was much larger than that used by Klein Larsen et al. (2003). For the effect of concentration, they reported an increase in k with concentration up to about 1.2 % w/v; however at higher concentrations they observed slower kinetics. They related both observations to the interplay between the concentration C and the overlap concentration $C^\star$. As MW increases, $C^\star$ decreases (as mentioned previously); thus, both an increase in MW and C increase the value of $C/C^\star$; thus polymer chains interact more strongly with each other as $C/C^\star$ increases above unity. They even report the possible presence of a "swollen **gel layer**" that inhibits reconstitution.

§6.2 Dairy Powders

As mentioned in Ch. 2, one of the most heavily studied types of food powders for reconstitution purposes is dairy powders. In that chapter, it was revealed that a number of factors affect the "solubility" of such powders including composition, as well as manufacturing and storage conditions, which are particularly relevant to surface properties. In § 4.5, the complex effects of salts were reviewed as well; particularly for powders high in casein content. The current section will focus mainly on the effects of the conditions of reconstitution, and how the powder behavior is affected.

Compared to hydrocolloids, dairy powders are much more complex in structure (while the *variety* of hydrocolloids is quite vast, each hydrocolloid powder itself is rather homogeneous in composition). This is because dairy powders may have significant quantities of carbohydrates, proteins, and lipids, which along with water are the major components of foods (Forny et al., 2011). The most commonly studied dairy powders in the literature are: **skim milk powder (SMP)** and **whole milk powder (WMP)**, as well as higher-protein content powders: **milk protein concentrate (MPC), native micellar casein (NMC), sodium caseinate (NaCas)**, and **native whey protein isolate (NWPI)**. While some other dairy-derived powders have also been investigated (e.g. butterfat cream powder (Kim et al., 2005b) and lactose powders, especially for the pharmaceutical industry), the current section will focus on the above-mentioned powders.

6.2.1 Uses in food formulations

According to Chávez Montes et al. (2011b), dairy powders are extremely important for the food industry; many dry formulations involve high amounts of dairy ingredients, e.g. instant cappuccino or infant formula powders. In particular, the dairy powders high in protein are relatively new to the industry (Richard et al., 2013), and exert a number of important functionalities. For instance, like hydrocolloids, they can be added for purposes such as hydration, swelling, viscosity modification, gelation and texturization, and they can also be added for nutritional reasons, as well as purposes related to their surface activity (emulsification, foam stabilization, etc.) (Damodaran et al., 2008). They can also be used to encapsulate bioactive

heath-promoting food ingredients (Tavares et al., 2014), for instance. However, according to Richard et al. (2013), such powders are difficult to rehydrate, making them often difficult to utilize, hence the growing number of studies to understand their behavior (Gaiani et al., 2007).

6.2.2 Structure of liquid milk

As milk is a complex system, it is worth mentioning its structure and composition before discussing the separation processes needed to produce different types of dairy powders. Liquid (bovine) milk is a colloid produced in the mammary gland of lactating cows in order to provide complete nutrition for their calves; for details see Walstra et al. (2006). According to their chapter, the composition of milk can vary quite considerably due to factors such as cow breed, lactation stage, feed composition, and illness (e.g. mastitis); however, they report **approximate compositions** for raw milk (expressed in % w/w): water (ca. 87.1 %), lactose (ca. 4.6 %), protein (ca. 3.3 %), lipids (ca. 4.0 %), minerals (ca. 0.7 %), as well as small amounts of organic acids, enzymes, and vitamins. The protein fraction can be divided into casein (2.6 % of the total milk), and serum ("whey") proteins (0.7 %). Milk is in fact a double-colloid, with both fat globules (2 – 6 µm) as well as casein micelles (30 – 300 nm) both suspended in a continuous aqueous medium called the serum (serum + casein = "plasma"). Dissolved in the serum are the lactose (ca. 0.5 nm), whey proteins (4 – 6 nm), minerals, etc. (Swaisgood, 2007).

Lactose

As mentioned in Ch. 2, the state of lactose in milk powders plays a role in the stability of the powder, and that amorphous lactose dissolves more quickly than its crystalline counterpart. Lactose (IUPAC[1] name β-D-galactopyranosyl-(1 $\rightarrow$ 4)-D-glucose) is a disaccharide consisting of repeating residues of galactose and glucose (Fig. 6.1).

According to Fitzpatrick et al. (2010), two lactose anomers (α and β) both exist in

[1] International Union of Pure and Applied Chemistry

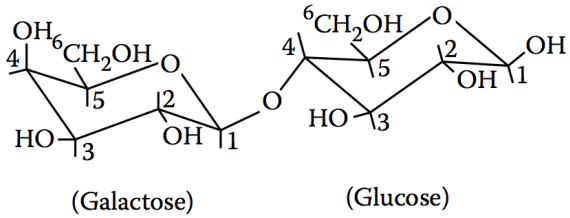

Figure 6.1: β-Lactose (Walstra et al., 2006)

equilibrium in solution. As discussed by Palzer et al. (2012), the supramolecular state of lactose during the drying of milk powders depends on drying kinetics; lactose is small enough of a carbohydrate that it can crystallize when water is removed, if it has enough time to do so. However, if drying is very fast, more of the lactose will be "frozen" in a glassy, amorphous state. According to Smith (2008), the two main types of crystals that form during the drying of lactose are α-lactose monohydrate and β-lactose crystals. For milk powders with amorphous lactose, the depression of the glass transition temperature (T_g) as a function of water activity (a_w) can be estimated using a state diagram (Vuataz, 2002). According to Bhandari and Roos (2012), the solids content of milk powders are generally a continuous matrix of amorphous lactose with embedded fat/proteins, thus lactose is very important to the particle properties (see Ch. 2).

Protein

The proteins in milk are generally classified into two major fractions: caseins and serum proteins (Damodaran et al., 2008). Caseins are defined as the proteins that coagulate when milk is brought down from its original pH of ≈ 6.7 to 4.6 at 20 °C, which is the isoelectric pH of casein micelles. At this pH the zeta potential (ζ) of the micelles is reduced from ca. -25 mV to ca. 0 mV, thereby reducing the electrostatic repulsion, and allowing for a coagulation (see § 4.2). The serum proteins are the proteins that do not precipitate and remain dissolved.

According to Swaisgood (2007), there are four types of **casein proteins** α_{s1}, α_{s2}, β, and κ, in the ratio of 3:1:3:1, with the first three being sensitive to interactions with calcium, and κ being calcium-insensitive. According to the same authors, casein proteins have very little tertiary structure (due to a high proline content in the amino acid sequence), and as a result, **caseins are more stable against denaturation** than serum proteins, e.g. at

higher temperatures. These proteins are also amphiphilic, and therefore surface active, due to different domains within the structure, with the polar domains consisting largely of phosphoryl residues, which at the pH of milk are negative in charge. Out of the casein proteins, α_{s1} and α_{s2} are the most hydrophilic (sensitive to ionic strength; § 4.2), and β are the most hydrophobic (also particularly sensitive to temperature due to effects on hydrophobic interactions; § 4.3).

According to Swaisgood (2007), as caseins do not crystallize their structure is not known, but several models exist to describe their structure. Most models agree that caseins are arranged as a spherical so-called **"micelle,"** which, in the current author's opinion, is a confusing term because compared to micelles of surfactants (§ 12.2), casein micelles have a more complex structure and are porous to water. Different models exist to describe the make-up of these micelles (e.g. submicelle and nanocluster models), but these are still the subject of debate (Baldwin, 2010; Dalgleish, 2011). However, most models agree that α and β caseins are mostly located in the *inside* of the micelle, held together by hydrophobic interactions as well as calcium phosphate bridges (as discussed in Ch. 2). The κ caseins are located on the *surface* of the micelle and the polar domain consists of a large glycomacropeptide, and it extends into the serum as a sort of "hairy layer" that helps to stabilize casein micelles due to steric repulsion (§ 4.4). By cleaving κ-casein by use of a proteolytic enzyme (chymosin, which is present in rennet), this hairy layer can be largely removed, helping to destabilize milk as a colloid. Both rennet and acid coagulation are involved in cheese production, where the caseins are destabilized and form coagulates with fat globules forming a curd, which can be further processed into cheese. The liquid left over containing dissolved lactose and serum protein is called the "whey," which is very similar, but not identical, to the original serum. (The whey could also contain dissolved fragments broken off from the κ-casein, as well as bacterial starter cultures used to acidify the original milk). This is why serum proteins are often called "whey proteins," even if the proteins are separated from the *serum*, which is usually the case, and not from whey. If the "whey proteins" are isolated from milk via membrane filtration, then this confusion is sometimes compensated for by calling serum proteins **"native whey proteins."**

According to Damodaran et al. (2008), unlike casein proteins, **serum proteins** contain more evenly distributed polar and non-polar amino acids, and have a more globular structure. These globular proteins fold such that its native structure preferably contains more hydrophobic

residues shielded from the aqueous medium on the inside of the globule, with more hydrophilic side chains on the outside. Compared to caseins, these proteins are more susceptible to denaturation (at approximately 70 °C), which affects solubility (Singh and Flanagan, 2006) – see Ch. 2. According to Singh and Flanagan (2006) serum proteins are more heterogeneous in structure than caseins and include β-lactoglobulin (ca. 50 % of all serum proteins), α-lactalbumin (ca. 20 %), serum albumin (ca. 5 %), immunoglobulins, and some other minor serum proteins. Within these types, there are many varieties as well (Hui, 2006).

Fat

The fat in milk consists primarily of triacylglycerols[2], with many different possibilities for compositions based on the esterified fatty acids. The fats exist primarily in fat globules – when the globules form and grow in the mammary secretory cell, and when they are released into the lumen, the globules become surrounded in material from the apical cell membrane (a merocrine secretion (Walstra et al., 2006)). This becomes the **"native fat globule membrane"** (NFGM), which helps prevent coalescence of globules. It contains cholesterol and enzymes, and as it is derived from a cell membrane, it contains polar lipids, particularly phospholipids (see Ch. 2 for why this is important). **Some of the most heat-sensitive proteins are located in the NFGM** and when denatured these can affect interactions with other milk components (cf. Ch. 2 on coffee stability).

6.2.3 Processing of liquid milk

Once raw milk is received it is generally cooled during transport and storage to delay degradation reactions (e.g. lipolysis). When the milk arrives at the processing facility it undergoes a number of processes, such as *cream separation* using a flow-through centrifuge (by exerting a large centrifugal acceleration, thus the fat quickly creams to the surface, according to Eq. 1.31), *heat treatment* to kill off harmful bacteria and inactivate degradative enzyme (time-temperature profile varies between countries and product types, depending on consumer preference), **homogenization** of the fat by forcing it through small gaps under high pressure

[2]Formerly called triglycerides, which was a confusing term in the current author's opinion – it is still used by some authors, though.

to rip apart the fat globules to produce much smaller fat droplets ($< 2\,\mu m$, which would have a greater stability against creaming, again, governed by Eq. 1.31), as well as *standardization* of fat back into the skim milk (which at that point typically has a low fat concentration ca. 0.5 %), to obtain different fat grades. As discussed in Ch. 2, the degree of homogenization on the milk prior to drying can significantly affect the functional properties of some dairy products. As the NFGM is destroyed during homogenization, the newly-formed small droplets adsorb solids (especially casein), which stabilize it as a sort of Pickering emulsion (Damodaran et al., 2008).

6.2.4 Manufacture of spray dried dairy powders

As discussed in Ch. 2, there are many possibilities for producing food powders, but by far the most common method is spray drying. Following drying, depending on the powder type it may be "instantized" by lecithination and/or agglomeration as well. Prior to spray drying, the materials need to prepared into a concentrate (e.g. via evaporation). To prepare whole milk powder (WMP), and skim milk powder (SMP), the process is quite straightforward. As for the production of MPC (milk protein concentrate), NMC (native micellar casein), NaCas (sodium caseinate), and NWPI (native whey protein isolate), the processes are a bit more complicated, as they require additional separation procedures, typically membrane separation – see Fig. 6.2.

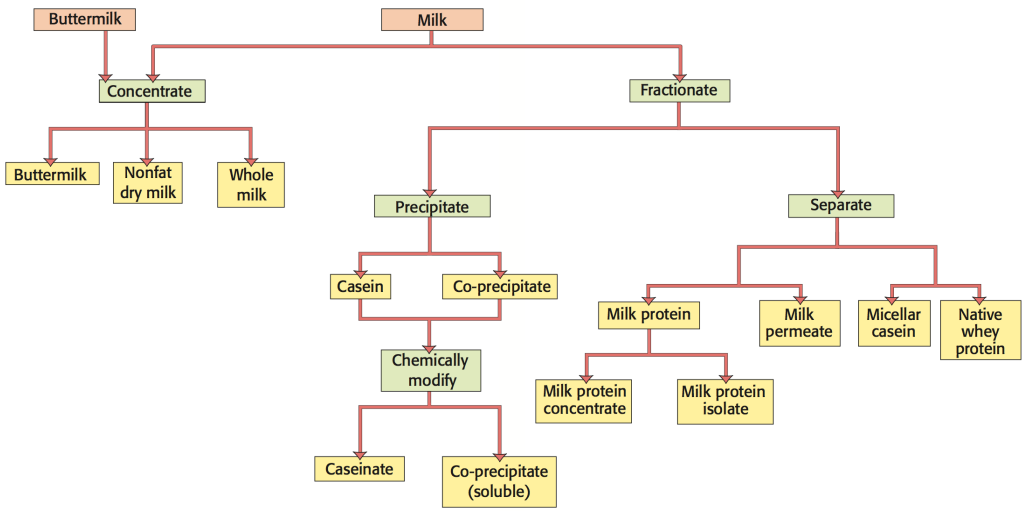

Figure 6.2: Separation processes of milk prior to drying (Smith, 2008)

Milk protein concentrate

According to Walstra et al. (2006), MPC can be obtained from skim milk using **ultrafiltration**, where a pressure difference is applied across a semi-permeable membrane with a relatively small pore size distribution (10^{-2} – 10^{-1} µm) at rather high pressures (1 – 10 Bar). This technique takes advantage of the fact that milk components have different molecular weights, and this sort of membrane has a molecular weight cut-off (MWCO) that would allow lactose to pass into the permeate, while keeping casein and serum proteins in the retentate, which can be dried into a powder. **MPC thus contains the same ratio of casein to whey proteins as in raw milk.** The percent of protein is generally specified in the name; e.g. MPC85 means 85 % protein in the powder. According to Smith (2008), generally MPC has a protein concentration of ca. 42 – 85 %, and above 90 % it would be called "milk protein isolate" (further processing steps, e.g. diafiltration, would be required to obtain very high protein contents.)

Casein and whey powders

Another membrane separation technique relevant for dairy powder production is **microfiltration.** It operates under the same principle, but with a larger pore size distribution (10^{-1} – 10^{1} µm), and thus has a larger MWCO and operates at lower pressure ($<$ 1 Bar). This technique can be used on skim milk to separate the casein (retentate) from serum proteins (along with lactose, etc.) in the permeate. As **the casein structure remains mostly intact**, the concentrate is called "*native* micellar casein" (NMC) or native phoshocasein (Smith, 2008), which can then be dried.

If ultrafiltration is applied to the permeate from skim milk microfiltration, one can obtain an isolate high in serum proteins called "native whey protein isolate" (NWPI), or "concentrate" at lower protein contents. Unfortunately some studies in literature use the confusing term "whey proteins," without specifying that they are "native," which could imply that the isolate is obtained from *actual whey*, even if it is really obtained via membrane processing of milk.

Another powder that has occasionally been studied (Zhou and Labuza, 2007), and that

is sometimes used in formulations for nutritional purposes is **whey hydrolysate powders**, which are pre-digested either enzymatically or by acid treatment (Gerhardt and Tasker, 2009), and is more easily digested and absorbed in the body, and has modified allergenic properties. In addition, **individual serum proteins** have also been isolated and produced as powders for reconstitution studies, e.g. β-lactoglobulin in Gianfrancesco et al. (2011). This isolation can be performed via chromatography or ion exchange (Smith, 2008).

Sodium caseinate

A casein powder can also be produced from acid-precipitated casein. In order to make this casein "soluble" it is treated (neutralized) with a dilute alkali, e.g. NaOH or KOH prior to drying to yield a "caseinate," e.g. sodium caseinate (NaCas), or potassium caseinate, respectively (Smith, 2008). According to Walstra et al. (2006) NaCas is the most common type of caseinate, and each type is used in different situations. As discussed at length in Ch. 2, **the fact that casein molecules in caseinates are no longer in their native micellar structure plays a significant role in their reconstitution behavior**.

Confusing terminology

In the current author's opinion, one term often appearing in the literature – "native phosphocaseinate" is rather confusing, as it actually refers to membrane-filtered native micellar casein (NMC), but the "-ate" suffix almost suggests that it is more related to caseinates. For instance the term has unfortunately been used by Gaiani et al.'s group in Nancy, France, e.g. Gaiani et al. (2006) and (Gaiani et al., 2009), but it appears that since 2010 the same group now uses the more widely understood "micellar casein" (Gaiani et al., 2010). However some studies (e.g. those from the group at the INRA[3] in Rennes, France) continue to use this term (Richard et al., 2013), possibly confusing readers.

[3]Institut National de la Recherche Agronomique

6.2.5 Studies on dairy powder rehydration

Dairy powders are the most commonly studied food powders in terms of reconstitution properties. In Ch. 2 a number of studies on dairy powders were already discussed, in terms of how manufacturing conditions (e.g. spray dry conditions, pre-treatments to disrupt the micellar structure, effects of additives, agglomeration, lecithination, ...) all affect rehydration behavior. However relatively few studies focused on the actual conditions during reconstitution (e.g. temperature, impeller type, agitation speed, amount of powder added, ...) on rehydration; this is the focus of the current section.

The current section will be organized by research group, as each group appears to have their own focus in terms of powder tested, apparatus used, and result analysis. The person indicated alongside the group is not necessarily the principal investigator for each study, but does appear on each paper from the corresponding group.

Karlsruher Institut für Technologie (KIT), Germany (H. Schubert)

Freudig et al. (1999) used a turbidity setup (§ 5.2) in an agitated vessel with a six-45°-pitched blade turbine to investigate the effect of baffling and particle size distribution (by sieving) on the reconstitution behavior of skim milk powder (SMP). They reported an optimum size for good reconstitution (similar to Parker et al. (2000) for hydrocolloids under "non-dispersing conditions.") As discussed in § 3.4, they observed better reconstitution in an *un*baffled vessel due to less heap formation on the liquid surface. The effects of lecithination of SMP were also discussed in § 2.3.

University College Cork (UCC), Ireland (J. Fitzpatrick)

This group at UCC mostly investigated the reconstitution of SMP and WMP in an unbaffled tank with a 6-flat-blade turbine (similar to the Lightnin R100 – Fig. 3.1). Fitzpatrick et al. (2000) modified the IDF standards for "dispersibility" and "solubility" (§ 5.1), mixing WMP to high solids content, and they reported better sinking and dispersion at higher impeller speeds.

Fitzpatrick et al. (2001) used a similar approach to study the behavior of SMP and WMP, as well as whey powders.[4] They observed better "wettability" (§ 5.1) and "dispersibility" at lower powder amounts, and higher temperatures, which they attributed to a lower viscosity, for high solids contents up to about 50–60 % w/w, depending on the temperature (20 °C, 50 °C, or 70 °C) – this improvement was especially marked for SMP. Fitzpatrick et al. (2004) investigated the influence of temperature on the behavior of SMP at high solids content and reported that a higher temperature not only improved sinking but also delayed age thickening. Schober and Fitzpatrick (2005) observed similar trends on sinking time for SMP and WMP at different concentrations. These authors also investigated the effect of impeller position (§ 3.4) – they also mistakenly assumed that the vortex depth determined sinking, as discussed in the Mixing Chapter earlier. The majority of studies on dairy powders in the same group at UCC since 2005 have been on flowability and caking of dairy powders (§ 2.2).

Université de Lorraine, Nancy, France (C. Gaiani)

While the group at UCC focused mainly on milk powders (SMP and WMP), the group at Nancy focused particularly on dairy protein powders, especially **native micellar casein (NMC)**, and to some extent native whey protein isolate (NWPI). They generally used techniques such as rheology or an agitated vessel with a turbidity meter (Ch. 5) to characterize the behavior. It is not specified if the agitated vessel includes baffles, so it is assumed that it was unbaffled, although the probes they used most likely unintentionally baffled the flow (see Fig. 5.12). As for the type of impeller used, this is a bit unclear as well. Gaiani et al. (2007) does not specify the impeller type, and Gaiani et al. (2009) and Hussain et al. (2011) both claim that they used a "45° pitched blade impeller ... the Lightnin R100," however, the Lightnin R100 impeller is not pitched-blade; it is a Rushton turbine (Fig. 3.1). It is assumed that they meant the Lightnin A200, although no picture was provided for verification. Gaiani (2006) used a rheological approach (paddle geometry; see Fig. 5.5) to investigate the rehydration of NMC (native micellar casein) powder as a function of concentration and temperature. Consistent with previous results for milk powders, they observed faster reconstitution at lower amounts and higher temperatures, relating this to the **swelling behavior of the casein micelles**. Gaiani et al. (2007) used a turbidity approach (§ 5.2) to compare the behaviors of NMC, NWPI (native whey protein isolate), as well as mixes of NMC/lactose, and NMC/NWPI (see

[4] Not whey protein, but *actual whey*, the by-product of cheese making.

Ch. 2). Gaiani et al. (2009) performed a similar study and also compared the behavior of NMC to NaCas (sodium caseinate, a non-micellar casein) – see Ch. 2. Hussain et al. (2011) and Hussain et al. (2012) used the same approach to study the effect of ionic strength of the liquid (§ 4.5). Murrieta-Pazos et al. (2012a) performed a comprehensive literature review on food powder structure and highlighted how particle morphology, as well as surface chemistry, influence powder functional properties.

INRA, Rennes, France (P. Schuck)

The group at the INRA (Institut National de la Recherche Agronomique) focused on the same powders as the group at Nancy, and as such, the groups have often published jointly in the past ten years (e.g. Gaiani et al. (2009)). However the techniques used to describe the rehydration behavior are quite different. Davenel et al. (1997) used NMR relaxometry (§ 5.6) to investigate the behavior of NMC. They report faster rehydration at higher stir speed, but report no significant effect of powder amount. They also report faster rehydration when additives are incorporated into NMC before drying (see Ch. 2). Davenel et al. (2002) used the same technique and looked at the effect of more co-ingredients (Ch. 2). They also compared NMC obtained from milks of different animals; rehydration was fastest for goat, followed by ewe, and bovine being the slowest. Schuck et al. (2002) and Schuck et al. (2007) used the same material and setup, with a greater focus on salt additions (Ch. 2).

More recent studies have been performed in an impeller-agitated vessel, mostly with a 6-blade 45° pitched-blade impeller. The studies used one baffle in order to limit the formation of a vortex.[5] Jeantet et al. (2010) used a laser diffraction technique (§ 5.4) to study NMC rehydration where samples were taken via syringe at regular intervals for size analysis, and obtained a sort of "t_{90}" value[6] by normalizing the median particle size against the final size (see § 5.4). They investigated the effect of agitation speed ($N = 400$ – 1000 rpm), temperature ($T = 26$ – $30\,°C$), and concentration (4.8 – 12 % w/w) as well as combinations of T and N. They reported a significant increase in rehydration rate with even a small change in

[5] According to Roustan et al. (1999), a vortex can still form if one baffle is used, but the center of the vortex will be shifted away from the impeller shaft, which could be beneficial for powders that might stick to stainless steel – see Ch. 3.

[6] Actually, a "t_{70}" value, but the concept is the same.

T, but a relatively large change in N was required to bring about the same improvement. A *combination* of an increase in N with T resulted in a much greater effect as well. The dimensional analysis approach they used was described in § 3.6; for a given concentration and T, the number of impeller revolutions (Θ_{90}) was independent of N.

Richard et al. (2013) studied NMC, NWPI, NMC/lactose, and NMC/NWPI (see Ch. 2) and also used laser diffraction, but with an automated dilution loop with hoses and a pump for sampling. They investigated the influence of water T, N, as well as impeller type: "type 1" impeller was the same as that in Jeantet et al. (2010) (6-blade, 45° pitch), and "type 2" was an unusual propeller with four blades total, but instead of having all four blades at the same submergence, two 2-blade propellers are placed at 90° to one another, separated vertically by 50 mm on the shaft. They reported a similar effect on impeller speed: reconstitution was faster at higher N, and $\Theta_{90} \neq f(N)$, everything else being constant. For an increase in T, in general an increase in kinetics was seen, however above 35 °C, the *extent* of dispersing was worse, which they explain as being due to aggregation effects (presumably due to stronger hydrophobic interactions at higher temperature; cf. § 4.3). As for the impeller design, they performed experiments at the same N and, in general, observed "better rehydration" (i.e. it was faster to achieve a defined size reduction) with impeller "type 1" compared to "type 2". They explain that type 1 had a greater local energy dissipation (greater shear effects), whereas type 2 favored circulation of particles in the vessel, but less particle-breakup. However they noted that type 2 was better at sinking the powder.

The current author finds two aspects of this study (Richard et al. (2013)) particularly troubling. The first is that their methodology involves applying a very fast N in order to force the powder to sink, before then reducing N once the powder has sunk. This can introduce quite some error, as well as misleading results – **wetting/sinking are *part of* the reconstitution process and should not be ignored** simply because the technique at one's disposal has no way to characterize the phenomena.[7] Secondly, the impellers used, to the author's best knowledge, are not very common and it is unclear if any characteristic curves exist, and Richard et al. (2013) did not report the power supplied by each impeller for an efficiency analysis. One would expect (based on the relative similarity of impeller type 1 to the Lightnin R100, and impeller 2 to the A100), that for a given N, type 1 would draw more power (Ch. 3).

[7] In the current study, the impeller speed is not changed during the course of a single experiment – Ch. 7.

Groups in Brisbane and Melbourne, Australia

While the groups in France have focused mainly on NMC (and NWPI), groups in Australia have focused more heavily on **milk protein concentrate** (MPC), which contains casein and whey in the same ratio as in milk (ca. 80/20, respectively), the rest being mostly ash and lactose.

At the University of Queensland in Brisbane, Mimouni et al. (2009) used laser diffraction (aliquots over time) in an unbaffled stirred vessel with a 45° pitched blade impeller to investigate the reconstitution of MPC85 as a function of T (at 24, 30, or 35 °C). They report faster kinetics at higher T, related to a better disruption of agglomerates and material (casein micelles) from primary particles. However, it is unclear if they would have observed similar aggregation at higher temperatures, like Richard et al. (2013) did for NMC.

At Monash University in Melbourne, Fang et al. (2011) also investigated MPC85 in an unbaffled vessel (except for the unintentional baffling effect from the probes – see Fig. 5.9). Unfortunately the impeller type was not specified; they cite their setup from Fang et al. (2010) that mentions a "four blade impeller" but not what type. In any case, the group used an FBRM approach where the reconstitution kinetics are also based on the mean particle size (cf. Eq 5.13). As mentioned in § 2.2, these authors investigated the "solubility" loss during storage at different combinations of temperature and time, and they also tested the effect of water T during rehydration. They reported faster kinetics (higher k from Eq 5.13) from 20 °C up to 50 °C (in 10 °C intervals), but from 50 °C to 60 °C, they report a *decrease* in k, and an increase in d_∞ (Eq. 5.13) – an indication of worse dispersing of primary particles. They explain that at higher T, the "solubility" deteriorated, but offer no mechanistic explanation. They also noted a greater effect of water T on *fresh* powders compared to those that had been subjected to different aging studies.

§6.3 Cocoa & Chocolate Beverage Powders

Another class of food powder that has received considerable attention with regard to reconstitution behavior is those containing cocoa powder. Cocoa powder is of particular interest to Nestlé, as it is an important ingredient in several of its popular brands, e.g. Nesquik, Milo, hot cocoa mixes, TollHouse products, Nescau, etc. It is especially worth studying upon rehydration as the cocoa powder contains fat on its surface that can hinder wetting/sinking, and possibly also dispersing (see § 11.2). According to Codex[8] standards 105–1981, "cocoa powder" is defined as having a minimum of 20 % cocoa butter, "fat-reduced cocoa powder" contains a minimum of 10 % and a maximum of 20 %, and "highly-reduced cocoa powder" contains < 10 %. However, for the purposes of the current report, the term "cocoa powder" will be used even if the fat content is < 20 %, but the fat content will be specified in the materials chapter (§ 8.3).

6.3.1 Production of cocoa powder

The production of cocoa powder is very different from the processes of dairy powders, which involve the removal of *water* from a milk-derived concentrate; in the case of cocoa powder production, liquid *oil* is actually removed from a fat-continuous cocoa liquor via hydraulic pressing. As explained by Kamphuis (2009), cocoa products originate from cocoa trees *Theobroma cacao*, which bears fruits (pods), each of which contain approximately 40 fatty seeds, known as cocoa "beans." These are harvested, allowed to ferment, and dried before being sent to a manufacturer for processing, where they may be stored and/or blended with different types of cocoa beans, depending on the application. As described in more detail in Meursing (2009), they are then broken/winnowed, to remove the undesired husk surrounding the beans to obtain deshelled kernals (nibs) and are sterilized, usually with a steam treatment. At this point they may or may not be **alkalized** ("Dutched"); during this process an alkaline solution (usually K_2CO_3 or Na_2CO_3) is applied (usually to the nibs). According to Abdelaziz et al. (2014), this was originally done to improve the "solubility" of cocoa powders, but it also modifies the color and taste. Kamphuis (2009) reports that for beverages, alkalized cocoa

[8] Codex Alimentarius is a commission founded by the United Nations to establish harmonized international food standards.

powders are generally preferred over non-alkalized powders.

The next step is roasting during which much of the flavor development occurs (see Martins et al. (2000) for a discussion on the complicated Maillard reactions). The nibs are then finely ground in a multistage process; during the grinding the cellular structure of the nibs is broken, thereby releasing cocoa butter (about $\frac{1}{2}$ of the nib). As a result, this hot mass becomes fat (oil)-continuous liquid called cocoa liquor. This liquor can then either be further processed to create chocolate, or to be pressed. During pressing, a hydraulic press partially removes the cocoa butter from the nibs, leaving behind a cake.[9] Depending on pressing conditions, as little as $\approx$ 10 % cocoa butter can remain; further reduction of fat can be performed with additional extractions, e.g. using CO_2. According to Meursing (2009), at this point, flavors or lecithin (§ 2.3) may be added to the cake, which is then transformed into cocoa powder via pulverizing – usually with a pin or hammer mill.

The cocoa powder is then cooled; but according to Kamphuis (2009), **ideally the cocoa powder should be tempered to obtain the most stable crystals of cocoa butter**, as is typically done for chocolate. As explained by Windhab (2009), cocoa butter is monotropically polymorphic, which means that it can crystallize in several different ways (see § 11.3), but they will eventually all convert to the most stable crystal if enough time is allowed. As is well known to food scientists, the desired crystal configuration for cocoa butter is the β-V crystal, which has a melting temperature (T_m) of about 34 °C. According to Meursing (2009), compared to less stable crystals, the β-V crystal has the triacylglycerols packed more tightly together, and as a result has a higher T_m (most others have a T_m of about 18–27 °C, depending on the type – see Meursing (2009) for specifics). The β-V are also preferred due to their appearance, hardness, and stability against undesirable process, e.g. **fat bloom**, oil migration, etc.

According to Meursing (2009), for an 11 % (w/w) fat cocoa powder, about 23 % is protein, ca. 12 % starch (of which $\approx$ 36 % amylose), and ca. 32 % dietary fiber. Of the fat, the majority (60 %) is saturated: 26 % of fatty acids are palmitic acid (C16:0), 34.5 % stearic (C18:0), and 34.5 % is oleic (C18:1, i.e. monounsaturated), with $<$ 5% of all other types of fatty acids. Although not discussed in the literature (to the author's best knowledge), the

[9] This removed cocoa butter can be added to the cocoa liquor along with sugar (and milk powder, depending on the product) to eventually produce chocolate.

fact that much of the cocoa powder consists of starch, fiber, and protein may play a role during rehydration due to swelling phenomena (§ 11.2).

When cocoa powder is dispersed in water, **it does not completely dissolve**, and many particles will become suspended, producing a turbid, brown liquid. As suspended particles may eventually settle out (i.e. sediment; Eq. 1.2), a stabilizer (§ 6.1) may be added (Meursing, 2009). The fact that the beverage becomes turbid upon rehydration has important consequences for reconstitution analysis (Ch. 11). As explained in further detail by Meursing (2009), the brown color is mostly developed during fermentation, during which enzymes oxidize precursors (mostly flavanoids) into reactive quinones that can form covalent complexes with amino acids and polymerize into high-molecular weight condensed tannins with a number of chromophoric groups. These brown tannins are insoluble in water. Other processing steps (especially alkalization) play a role in determining the final color.

6.3.2 Composition of chocolate beverage powders

In the case of chocolate beverage powders (CBPs), cocoa powder is usually combined with crystal sugar (for a "2-component" CBP) or possibly also milk powder (for a "3-component" CBP). This is both to improve the taste as well as to improve the wetting/sinking behavior of cocoa powder, as the fat on the surface may make this step challenging (Schubert, 1993). According to Kyaw Hla and Hogekamp (1999), the cocoa used for this application is generally fat-reduced (< 15 % fat) to improve reconstitution. According to Abdelaziz et al. (2014), generally only about 20 % w/w of CBP consists of cocoa powder, with the rest mostly consisting of other ingredients, especially sucrose, which may be a health concern. According to Shittu and Lawal (2007), the compositions can vary quite considerably (from as little as ≈ 50 % sugar to possibly even as high as ca. 91 %). According to Meursing (2009), the ingredients should not simply be dry-mixed, as they can separate upon reconstitution; instead they should be agglomerated together into composite granules. This can be done by fluid bed agglomeration (Benković and Bauman, 2011) or steam jet agglomeration (Vissotto et al., 2010), for example.

6.3.3 Studies on cocoa powder reconstitution

Given the competitive nature of the food industry regarding cocoa-containing powders (cf. the discussion of patents in § 2.3), relatively little literature on the subject is available.

In the group of L. Galet at the Ecole des Mines d'Albi-Carmaux in France, a couple of studies have been performed investigating the dispersion of cocoa powder (10 – 12 % fat) in an unbaffled, agitated vessel, using an "optical fiber technique" (§ 5.2).[10] They claim that the impeller position plays no significant role in the rehydration, so they did not specify the geometry of their setup, unfortunately (in § 13.2 it is demonstrated why impeller position *should* be reported). **Vu et al. (2003)** used a "turbine agitator" (unspecified type) to study the effect of particle size, agitation speed, and powder amount. They granulated cocoa powder in a high shear mixer, using water as the binder, and dried the granules at 45 °C for 5 h, and they obtained different size fractions by sieving. Agitation was performed at 470 rpm and 1000 rpm, and they also reported the corresponding specific power draws (P/V), which is rare for reconstitution studies; these were 90 W m^{-3} and 870 W m^{-3}, respectively. The amount added ranged from 10 g to 60 g in 2 L of water at 22 °C. Data were normalized to obtain a "dispersion time" (similar to a "t_{90}" value), and fitted to the rising exponential decay model (Eq. 5.2). They found that granules rehydrated more readily than non-agglomerated powder, but smaller *granules* were faster to rehydrate than larger *granules*, suggesting that an optimal size exists. Rehydration was also faster at higher agitation speed (N), and decreasing powder amounts, but there was less of an influence of powder amount at higher N.

Galet et al. (2004) continued this work using the same setup, but with a "dispersion disk" agitator (again, the type was not specified). They tested greater amounts of N values, as well as powder amounts, and also water temperatures T (20, 25, 30, 35 °C). They reported that at lower N, at lower T, and at higher powder amounts, the kinetics (k from Eq. 5.2) was slower; in addition reconstitution was less "complete" (A from Eq. 5.2) at lower T and N values. For some reason they explain that the increased temperature improved the "dispersion rate" k due to a decreased work of cohesion (Eq. 1.1). However, they did not discuss the possible role of fat melting – as discussed for whole milk powder in Ch. 2, may play a significant role in the sinking behavior of powders. In fact **the current author believes that the**

[10] This same setup is also used for talcum powders (§ 6.4) in the same group.

term "dispersion rate" itself is confusing, as it incorporates two different physical processes: sinking and agglomerate dispersing, both of which would lead to a rise in turbidity signal (§ 5.2). Thus a more controlled experiment in this field would ideally be able to monitor *both* sinking *and* dispersing, as simultaneously occuring, separate phenomena (Ch. 7).

6.3.4 Reconstitution studies on chocolate beverage powders

A number of studies have also investigated the rehydration of CBPs. In C. Gaiani's group in Nancy, Abdelaziz et al. (2014) investigated the behavior of CBP in an agitated vessel, using an image analysis technique (QicPic with pumps and hoses; see § 5.10), and monitored the decrease in the median particle size (d_{50}; EQPC – see § 5.10) over time, and they also used (modified) IDF *dairy* standards (§ 5.1) to determine the "wettability," "dispersibility," and "solubility," even though CBP is not always a dairy-containing powder. Unfortunately they did not specify the configuration of their agitated vessel – it is assumed it was unbaffled, but the impeller type was not specified. They tested the effect of sugar type, sugar size, and sugar concentration on the rehydration behavior. The sugar type was either sucrose or lactose, the sugar size (d_{50} EQPC) was about 30 or 480 µm for each sugar, and the ratio of sugar-to-cocoa was 70:30, 80:20, 90:10 or 0:100 (only cocoa powder) – they do not specify the % fat in the cocoa. These ratios with sugar were done for all four combinations of size and sugar type. Even though dry-mixing is discouraged for CBP in favor of agglomerating, for an unspecified reason the ingredients were simply dry-mixed in their study. Measurements were performed at constant agitation rate N and temperature T (25 °C). They mostly reported better "wettability" and "dispersibility" with lactose than sucrose, and saw a slight improvement in "wettability" with increasing sugar size. They also reported better "wettability," "dispersibility," and "solubility" at higher sugar amounts, although the degree of improvement did depend on other factors as well (sugar size and type).

There are some other studies in the literature that also investigated rehydration properties of CBPs; however, they were **not performed in stirred vessels, and focused mainly on the sinking times on a static volume of water.** The current author would like to caution the reader that if one reads each article below, it becomes clear that the papers contain many mistakes when it comes to explaining the results (and materials) of *other* papers

in relation to their own studies, thus it may be better to read each paper separately to avoid confusion.

In Malaysia, Selamat et al. (1998) mixed the ingredients together, added water and then spray dried the mixture to obtain composite granules. They tested the influence of the amount of alkalized cocoa powder (10 – 30 %) and soy lecithin (0 – 4 %), with the other ingredients being milk powder, sugar, etc. They reported faster sinking for lower amounts of cocoa and/or higher amounts of lecithin.

Kyaw Hla and Hogekamp (1999) from Myanmar (in collaboration with KIT in Germany), went to the supermarket and purchased different types of CBPs, and used sieving to obtain different size classes. They also created their own CBP using steam jet agglomeration, and used the "slider method" for "wettability" (§ 5.1). They reported a wide variability in results from different manufacturers, and reported particularly good sinking behavior when particles smaller than 200 µm were removed by sieving.

In Nigeria, Omobuwajo et al. (2000) proposed a very low-budget method to agglomerate powders into (nutritionally fortified) CBPs, which they claim could be used to compete with companies that have access to more sophisticated agglomeration process technology. They call their approach "thermal aggregation," and essentially powders are added to a hot sheet of metal and are agitated to agglomerate powders. Although the adhesive mechanisms are not discussed, it is possible that the agglomeration effects may be due to the stickiness of the cocoa powder when the cocoa butter is (at least partially) melted. They investigated the influence of cocoa-to-sucrose ratio (1:4, 1:3, 1:2, 1:1) and sugar particle size, and reported faster rehydration (using the stopwatch method (§ 5.10) at 30 °C using a magnetic stirrer) at higher amounts of sugar and smaller sugar particle sizes. While these results appear to contradict Abdelaziz et al. (2014), it is important to remember that CBP was *dry mixed* in that study.

Also in Nigeria, Shittu and Lawal (2007) purchased several local CBPs and tested them for different properties such as "wettability." They performed a multivariate statistical analysis and concluded that sucrose amount was the most important factor for good sinking, with higher amounts resulting in faster sinking.

In Poland, Kowalska and Lenart (2005) created CBPs in a fluidized bed and tested the influence of coating cocoa particles with a sucrose solution (0 – 80 %), milk[11] (0 – 80 %), and maltodextrin[12] (0 – 80 %). The coated cocoa powder[13] amount was 20 %. They reported faster sinking with increased amount of sucrose coating, as well as larger granule size after agglomeration.

Vissotto et al. (2010) in Brazil used steam jet agglomeration to create CBPs and tested the "wettability" and "insolubility" (§ 5.1). They reported better sinking for larger granule size, and also that the "insolubility" was worse at higher dryer temperature, and explain that this was due to the formation of stronger solid bridges that resist dispersing.

§6.4 Other Powders

While the majority of studies on dispersion of food powders have focused on hydrocolloid, dairy and cocoa-based powders, there have occasionally been studies on other food powders. In addition, studies with non-food powders may also yield interesting information on dispersion mechanisms.

The group of L. Galet in Albi, France, whose setup was described in § 5.2 and uses an impeller-agitated vessel with an 'optical fiber sensor,' also studied the dispersion behavior of **talcum powder** ($Mg_3Si_4O_{10}(OH)_2$), which is a powder of irregularly-shaped particles often used in the paper, pharmaceutical, and cosmetic industries, to name a few. As this powder does not dissolve, it has the benefit over food powders that the dissolving/swelling aspects do not apply, and thus the first three steps of reconstitution (wetting, sinking, and dispersing) can be studied more directly without interfering phenomena. Goalard et al. (2006) performed experiments in a baffled agitated tank, but did not specify the number of baffles or impeller type. The authors produced granules either in a high shear granulator ("type 1 powders") or they prepared a suspension of talc that was electro-spray & freeze-dried ("type 2 powders"). For "type 2 powders," droplets are produced in the presence of an electric field and droplets are frozen in liquid nitrogen and dried under vacuum to produce highly-porous

[11] Unspecified if the milk was whole, skim, etc.
[12] The dextrose equivalents (DE) was not specified.
[13] Fat content not specified.

(but non-hollow) spherical particles. They observed superior dispersion properties (higher k and A values from curve fitting with Eq. 5.2) for "type 2" powders, and noted that an optimum size of particles exists.

Galet et al. (2009) also used **talcum powder** in a vessel with four baffles, although the baffle size, vessel configuration, and impeller type are unspecified. They investigated the effect of power draw (P) for the impeller at 20 °C and observed that k and A improved with increasing P, but above a certain optimum P_{opt}, the values leveled off. They also investigated the effect of amount of powder added, and observed that k and A were improved at lower powder amounts. They also measured the "dynamic contact angle" (θ) using the Washburn technique for powders (§ 1.1) and obtained a value of 88°, from which they could calculate the "work of dispersion" ($W_{\text{dis}} = -\gamma \cos(\theta)$), where γ is the water surface tension ($\gamma \approx 72\,\text{mN}\,\text{m}^{-1}$ at 20 °C), with $W_{\text{dis}} = -2.5\,\text{mJ}\,\text{m}^{-2}$. Thus they propose that as the powder amount increases, W_{dis} becomes more negative (more surface area) and this is supposedly what causes the slower dispersion. However, **they did not consider the possibility that a larger powder *heap* could develop with greater powder amounts**, which could lead to problems related to capillarity, water-logging, and sinking (§ 1.2), which as discussed previously, is very much a possibility for baffled tanks (§ 3.2). Perhaps if they could have *seen* the liquid surface they would have come to a different conclusion (the tank they used did not allow for analysis of the liquid surface – see Fig. 5.2).

Lefebvre et al. (2011b) from the same group used the same technique, but used three baffles instead of four; the reasoning for this is unclear. The impeller type is also not specified. These authors investigated the effect of **dry particle coating** of talcum powder (host particles) with different amounts of hydrophobized silica nano-particles (guest particles) using a high shear mixer. They measured the contact angle θ of the resulting powder by compressing the powders into tablets and using the sessile drop method (§ 1.1) with water droplets. As expected, θ increased (more hydrophobic) with greater amounts of silica coating. Not surprisingly, they also reported worse dispersion in water with increasing particle hydrophobicity. They related to the work of adhesion ($W_{\text{adh}} = \gamma\,(1 + \cos(\theta))$, and explained that this decrease in W_{adh} with increasing θ was responsible for slower and less complete dispersing (lower k and A, respectively; cf. Eq. 5.2). They report essentially the same results in Lefebvre et al. (2011a), but with more of a focus on the time in the high shear mixer during coating. **Once again, wetting/capillarity effects are not considered, and it is unclear how the *sinking***

behavior would have changed; thus the results interpretation is questionable.

In South Korea, Park et al. (2001) investigated the effect of "microparticulating" powders of **green tea extract** and coating onto sucrose particles. Compared to normal green tea powders, they observed faster sinking and better stability against sedimentation.

In the Peoples' Republic of China, Ren et al. (2003) investigated the stability against sedimentation of **calcium carbonate and talcum powders** in different liquids (water, ethanol, and kerosene). Not surprisingly, they observed better stability when the polarities of the powder and liquid were more similar.

At Nestlé in Switzerland, Chávez Montes et al. (2011b) investigated the effect of composition and process conditions on the reconstitution of **multi-component milk-based powders**. A carbohydrate (either pre-gelatinized starch or maltodextrin DE2)[14] was incorporated into the powder base either by dry mixing or by fluid bed agglomeration. Reconstitution was performed at 40 °C using a conductivity-based approach (§ 5.3), where normalized results were used to obtain a "t_{90}" value. In general the incorporation of either carbohydrate resulted in worse reconstitution, which they explained as being due to the development of a **swollen viscous layer preventing mass transfer of water**. They performed viscosity measurements using a cone-and-plate setup (§ 5.5), and reported shear-thinning behavior; but the apparent viscosity increased with increasing amount of carbohydrate. Starch resulted in a higher viscosity increase (by about two decimal orders of magnitude) compared to maltodextrin, and as a result was more difficult to reconstitute. They investigated the effect of spray drying conditions to produce the base dairy powder (prior to the addition of carbohydrate); they altered the inlet and atomization pressures and exhaust air temperature. For powder base produced at high pressure and temperature, they observed a greater amount of free fat[15] in the powder, which they note may be due to the disruption of emulsified fat, and that they note correlated with slower rehydration. Although the current author would be surprised if this played a significant role, as at 40 °C, one would expect most of the dairy fat to have melted (Ch. 2 and § 11.1). They also note that an optimum particle size range appeared to exist. Comparing the powders that were dry mixed with polysaccharide to those

[14] For an explanation on DE value, see § 8.1.

[15] As explained in Ch. 2, this is the amount of unencapsulated fat on the particle surface that can be extracted using hexane.

combined by fluid bed (FB) agglomeration, they reported much better behavior in the FB granules. In fact, using a FB, polysaccharides up to 15 % could be incorporated without a significant change to t_{90}.

Ishwarya and Anandharamakrishnan (2015) in India investigated the effect of processing type on the solubility and aroma profiles[16] of **instant coffee**. In addition to spray dried and freeze dried coffee powders, they also applied a "spray-freeze-dry" process on coffee extract; in this process the feed solution is atomized and the resulting droplets are immediately frozen, then dried under vacuum. They explain that due to the faster mass transfer from *droplets* compared to a sheet of frozen coffee extract concentrate (as in conventional freeze drying), the process is less expensive and intense. They report better aroma and solubility than spray- or freeze-dried coffee powders, as the process is less harsh and the powder contains high porosity. (Solubility measurements were determined by dissolving the powder in freshly boiled water and is deemed to be "good" if it dissolves in under 30 s.)

In addition to these studies, there is a wealth of information in the **patent** literature regarding producing powders for "instant" beverages with different desired properties upon dissolution. For instance Kraft Foods/Mondelēz, which owns coffee brands Maxwell House and Gevalia, and up until recently had an (albeit troubled) partnership with Starbucks, has filed a number of patents related to the reconstitution of **coffee beverages**. To name only a few of many examples, Imison et al. (2012) patented an "instant espresso" that upon reconstitution produces a foam on the surface (resembling a crema) by fusing insoluble finely ground (micronized) roasted coffee material to the surface of *soluble* coffee powders. This is done either by compression or by making the soluble coffee sticky by heating it above its glass transition temperature (T_g). Pressurized gas is incorporated into the soluble particles to produce the foam, and the insoluble coffee oils help to stabilize the foam. Fountain and Gundle (2014) reviewed the difficulties of producing micronized insoluble ground roast coffee, such as issues like clumping and fouling when the coffee oil is released, and also mixed this with a soluble coffee particles (70 – 95 %), which gave a similar barista-style appearance (dark color) of the espresso. They patented an approach that involves forming and foaming concentrated coffee extract before freezing and milling it. Massey and Massey (2013) patented an approach to produce coffee-based powders that produce multiple layers upon reconstitution, with a foamed layer of coffee creamer on the top, whitened coffee beverage on the bottom,

[16] Using gas chromatography-mass spectrometry.

and a weak gel layer separating the two. This approach involves the use of a foaming agent, a protein source, and carrageenan (§ 6.1).

While the patent literature does demonstrate just how competitive this industry is, it is not particularly relevant to the current project, as mixing conditions and revealing mechanisms responsible for reconstitution are not the focus of the publications.

§6.5 Comments on previous studies

In the author's opinion, there are a number of frustrating aspects about reviewing the literature for food powder reconstitution, besides the fact that different techniques, powders and conditions were applied, and that even for the same powder type, significant differences can exist depending on factors such as production and storage. In particular, it appeared that most of the focus has been given to the powders themselves, and the mixing during reconstitution is treated almost as an afterthought. Very often the vessel configuration, impeller type, and feeding conditions are left unspecified, making reproducibility and direct result comparison problematic. Moreover, no studies on scale-up considerations have been found, and during measurements, the techniques used for analysis often interfere with liquid flow by unintentionally baffling the flow, or even interfere with the particles, due to sampling, diluting, or pumping through a tube, all of which is alarming. Thus, it would appear that there is vast room for improvement with regards to methods development and results analysis, and there are many possibilities for testing wide ranges of conditions for different food powders.

Part II

Methodology and Materials

Chapter 7

Reconstitution Apparatus

The most dangerous phrase in the language is, 'we've always done it this way.'

U.S. Rear Admiral Grace Hopper

As discussed in Ch. 5, there are a number of concerns with the setups used to analyze powder reconstitution described in the literature. In the current report, one major objective was to develop a technique to analyze powder reconstitution that:

1. Can analyze *all* types of food powders,
2. Adheres to the standard ratios defined by Rushton et al. (1950) (Fig. 3.4),
3. Does not contain probes entering from the top (liquid free surface) that could inadvertently disturb liquid flow,
4. Uses controlled feeding conditions,
5. Is able to characterize wetting/sinking, dispersing, and dissolving as **separate phenomena** in order to relate observations to corresponding physical equations (Ch. 1).

Contents

§7.1 Features of Novel Rig

A cartoon of the custom-built reconstitution rig is depicted in Fig. 7.1.

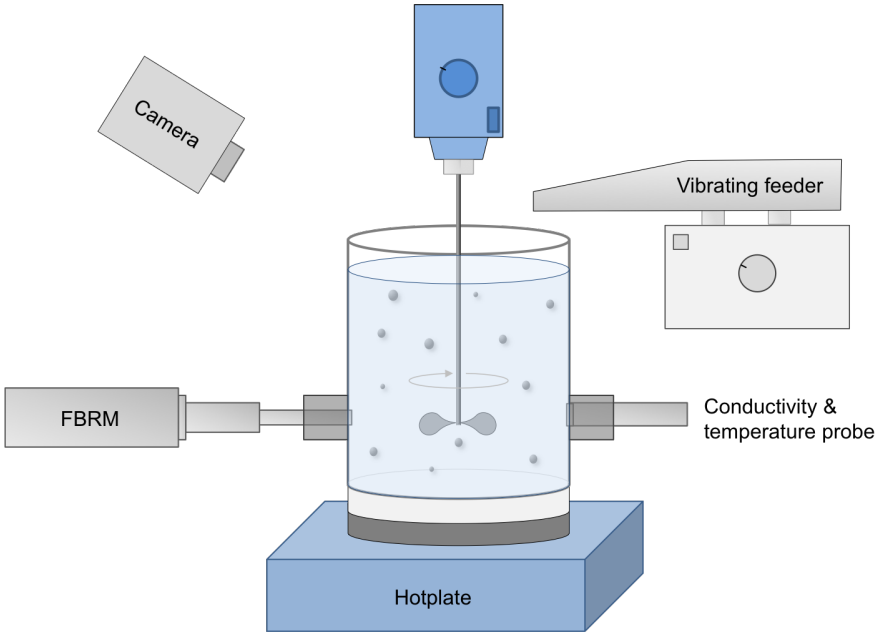

Figure 7.1: Cartoon of custom-built vessel for current study.

It consists of (A) a transparent vessel that adheres to the dimensions in Fig. 3.4, (B) an impeller, (C) a vibratory feeding device, (D) a video camera, (E) and FBRM probe (see § 5.9), and (F) a conductivity probe (see § 5.3):

7.1.1 Vessel

The transparent vessel was custom-built by the University of Sheffield technical staff, and it is produced out of a *transparent* PVC (polyvinyl chloride) so that one can view reconstitution from the side. It is cylindrical with a flat bottom, and two fittings are designed specifically for the FBRM and conductivity probes so that they can enter the *side* of the vessel, with the probe tips being flush with the vessel wall in order for these not to disrupt liquid flow. The fittings are secured in place using o-rings and screw fittings to prevent any leakage, and are positioned to be in-line with the impeller blades. By default the vessel is unbaffled, but insertable baffles were also constructed with the vessel (see § 13.1). This default vessel was designed around a 33 mm-diameter impeller to adhere to Rushton et al. (1950)'s standards; in § 13.3, a similar scaled-up vessel is shown, designed around a larger impeller.

7.1.2 Impeller

By default an axial 3-blade propeller with a pitch p ca. 18° (Lightnin A100, Rochester, NY, USA) was used, which enters the liquid from the top with a 0° angle, centrally positioned, and an off-bottom clearance h equal to the diameter d. The impeller is rotated for downward-pumping, and mixing of the liquid is started several minutes before the powder is added to achieve steady-state. Impeller rotation is controlled with an agitator (Eurostar control-visc, IKA Labortechnik, Germany), with an in-built tachometer to control the agitation speed N.

7.1.3 Vibratory feeder

As discussed in § 1.2 and § 3.4, even though the conditions of powder addition may be important to the reconstitution behavior, feeding conditions are rarely ever specified in the literature, and some require manual manipulation, which can introduce bias. In the current study, a vibratory feeder (Retsch DR1000, Germany) is used from a defined and fixed position to add the powder. The feeder is positioned such that particles are dropped from a height of 60 mm above the still liquid surface, and the feeder is positioned tangentially such that particles contact the water halfway between the impeller shaft and the vessel wall (the exiting

powder stream has a thickness of 15 mm, and the center of this stream is positioned at the half-way point). When the feeder is turned on, particles are thrown upwards and forwards, and the amplitude of these oscillations, along with the powder flowability, determine the mass flow rate ($\dot{m}$). As discussed in Ch. 2, processes such as agglomeration can improve flowability; thus, to maintain a constant $\dot{m}$ of $3.8\,\mathrm{g\,s^{-1}}$, the feeder setting was calibrated for each powder – this was done using a video camera to determine the flow rate at each setting, then performing a regression.

7.1.4 Video camera

For all experiments, videos are systematically taken using a camera (Canon Powershot SD1100 IS, Japan, at 30 frames per second in a macro setting) in order to capture both the side (exploiting the transparency of the vessel) and the free surface of the liquid.[1] Particularly for powders that sink gradually (Ch. 11), videos are used to determine the powder sinking time (t_{sink}) by counting the number of frames from when the last particle hits the surface until all particles have sunk. Black construction paper is placed around the vessel to reduce glare and deliver high-quality images for time-lapse purposes.

7.1.5 FBRM

The FBRM model[2] was the G400 series, released by Mettler Toledo (Columbus, OH, USA) in September 2011, shortly before the start of the current PhD project. When the laser is emitted into the liquid, the beam is focused at the sapphire window, and the penetration depth for measurement depends on a number of factors such as the chord selection method (in the current study a *primary* setting was used), as well as the particle concentration, optics, etc.; according to the manufacturer (personal communication), the effective penetration depth will be ca. 200 µm for the conditions used. The focused laser rotates in a circular path of radius 5.2 mm at a speed of $2\,\mathrm{m\,s^{-1}}$ (i.e. $>$ 60 revolutions per second). The software iC FBRM 4.2.234 SPI was used to interpret data, with the acquisition rate set to its fastest setting (one measurement every 2 s). According to the manufacturer, the detection range of

[1] The exact position of the camera depends on the powder type – compare Ch. 10 and 11.

[2] For the theory on how FBRM operates, see § 5.9.

the probe is from 500 nm to 2000 µm.

7.1.6 Conductivity

A conductivity probe (Jenway Geneflow 4510, UK, cell constant $k = 0.97\,\mathrm{cm}^{-1}$ at 25 °C) was used to measure the electrical conductivity of the liquid during reconstitution, along with FBRM measurements and video recordings for all trials. The reason this measurement technique was chosen is because it is a sort of "gold standard" for Nestlé.[3] The conductivity probe also records the water temperature to ensure that the temperature remains constant at a desired value.

§7.2 Default Conditions

For the experimental study, a number of default conditions are defined, and these defaults are assumed to be used unless otherwise specified. These are defined in Table 7.1.

The reason that 2.0 % w/w was chosen is because it is the amount used in the Nestlé SOP (standard operating procedure) for dissolution study (as the amount is low, one can assume negligible change to the rheology of the liquid medium).

§7.3 Vessel Characterization

The mixing characteristics (Ch. 3) are determined for the default vessel for the range of agitation rates (N) used ($N = 200, 400, \ldots, 1000\,\mathrm{rpm}$). These characteristics are particularly important for the discussion in Ch. 13, and characteristics for other vessel configurations can be found in Ch. 13 as well. For power (P) calculation (Eq. 3.9), the power number N_p is needed, where $N_p = f(\mathrm{Re})$ as well as the vessel configuration – characteristic curves, provided

[3] For a discussion about why the current author believes conductivity should be abandoned as a gold standard, see Ch. 14.1.

Table 7.1: Default conditions for the current study.

Condition	Default Setting
Impeller type	Lightnin A100 (axial)
Impeller diameter (d)	33 mm
Submergence (H')	$2d$
Tilt of impeller shaft	0°
Impeller position	Center of vessel
Impeller entrance	From above
Impeller rotation	Down-pumping
Number of baffles	None
Feed rate	3.8 g/s
Feeding height	60 mm (undisturbed liquid)
Powder amount	2.0 % w/w
Water type	Deionized

that one adheres to Rushton et al. (1950)'s ratios (Fig. 3.4), can be used (Fig. 7.2).

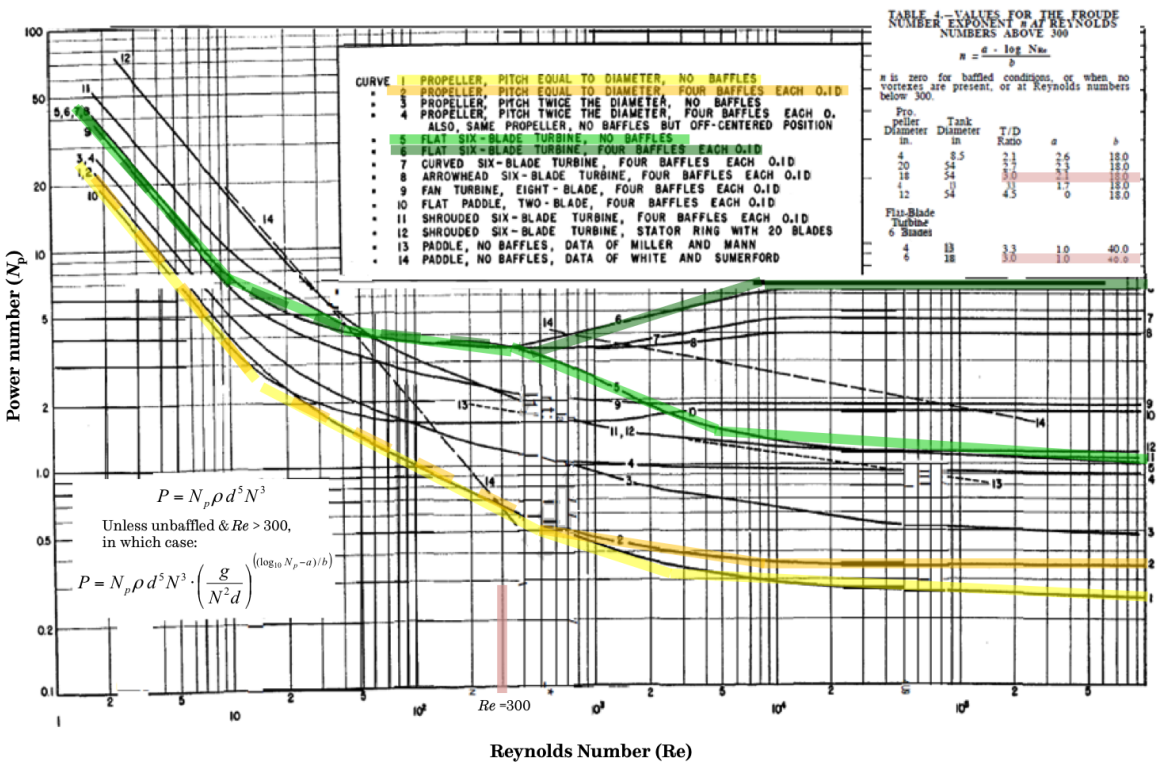

Figure 7.2: Characteristics curves adapted from Rushton et al. (1950) used for the current report.

In Fig. 7.2, the curve number 1 is applicable for the default configuration.[4] Curves 2, 5, and 6 are needed for alternative configurations in Ch. 13.

Note in Fig. 7.2 that low Re (laminar flow), there is a quite linear decrease in N_p with increasing Re, but for high Re, it levels off. The reasons for why the R100-type impeller has a higher N_p for each Re compared to A100, and for why there is a bifurcation between unbaffled and baffled conditions at higher Re, are discussed in Ch. 3.

In addition to calculating characteristics such as the power P (Eq. 3.9), Re (Eq. 3.5), Fr (Eq. 3.6), shear rate $\dot{\gamma}$ (Eq. 3.12), tip speed v_p (Eq. 3.14), Kolmogorov length scale λ (Eq. 1.42), predicted vortex depth h' (Eq. 3.15), We (Eq. 3.8), and pumping capacity (Eq. 3.10), a few characteristics were also measured, e.g. the vortex depth h' (Fig. 3.4), exploiting the fact that the vessel is transparent.

[4] The pitch $p = \pi\, d\, \tan(\alpha)$, where α is the angle of blade inclination. As $\alpha = 18° \therefore p/d = \pi\, \tan(18°) \approx 1$. Thus curve 1 (and not 3) is needed.

In addition it was realized that the **liquid surface speed** around the impeller shaft increased with increasing agitation. In order to characterize this effect, tiny negatively buoyant tracer particles (hollow glass beads, Q-cell, effective density $0.27\,\mathrm{g\,cm^{-3}}$, size 5 – 115 µm, Potters, UK) were placed at the liquid surface, and the camera was placed overhead to record particle rotation around the impeller shaft. Particles were selected that made a full rotation half-way between the shaft and vessel wall, i.e. where food particles are dropped during reconstitution trials, and the revolution time is used to approximate the instantaneous surface velocity (v_{surf}).

Mixing characteristics are shown in Tab. 7.2.

Note that for all values of N in Tab. 7.2, $10^1 < \mathrm{Re} < 10^4$, (i.e. transitional flow), $\mathrm{Fr} < 1$, and $\mathrm{We} \gg 1$. The predicted and measured values for vortex depth (h') are not very close; better agreement was seen with the alternative (unbaffled) configurations in Ch. 13.

Note that since power draw P is particularly interesting in order to study energy efficiency of mixing, and since P depends on the liquid properties, which can change with temperature T, if one applies the same agitation speed N for all values of T, P will not remain constant. However, this effect was rather negligible – for instance at $N = 1000$ rpm, $P_{5\,^\circ\mathrm{C}} = 55\,\mathrm{mW}$ and $P_{65\,^\circ\mathrm{C}} = 50\,\mathrm{mW}$. Thus, **the same N was used for all values of T** (Ch. 10 and 11).

Table 7.2: Mixing characteristics for the default vessel (Lightnin A100, unbaffled) for water at 25 °C.

N	N	Re	Fr	v_p	N_p	P	P/V	v_{surf}	h'_{pred}	h'_{meas}	We	$\dot{\gamma}_{\text{av,imp}}$	$\dot{\gamma}_{\text{av,tank}}$	Q	λ_{imp}	λ_{tank}
[rpm]	[s^{-1}]	[-]	[-]	[$m\,s^{-1}$]	[-]	[mW]	[$W\,m^{-3}$]	[$m\,s^{-1}$]	[mm]	[mm]	[-]	[s^{-1}]	[s^{-1}]	[$\times 10^5\,m^3\,s^{-1}$]	[µm]	[µm]
200	3.33	4066	0.04	0.35	0.38	0.72	0.95	0.03	1.6	0.0	5.7	116.7	33.9	6.6	165	77
400	6.67	8133	0.15	0.70	0.35	4.90	6.43	0.05	6.3	0.0	22.9	223.3	67.8	13.2	102	48
600	10.0	12199	0.37	1.04	0.33	14.52	19.05	0.15	14.0	3.0	50.3	350.0	100.5	19.5	75	36
800	13.3	16266	0.60	1.38	0.32	31.44	41.25	0.19	24.4	10.0	88.0	466.7	132.9	25.8	64	30
1000	16.7	20332	0.93	1.68	0.30	54.64	71.71	0.26	36.5	21.0	131.3	583.3	162.4	31.5	56	26

Chapter 8

Materials

By default, the water used for reconstitution experiments is ultrapurified by reverse osmosis (Purelab Option S/R 7/15, ELGA Vedia, UK). Three main types of powders are used for experiments: (1) maltodextrin, a water-soluble hydrocolloid, (2) milk powders, and (C) cocoa powders.[1] As discussed in Ch. 6, these three powders are common ingredients for beverages powders, and have unique biochemical compositions. All experiments were performed using the same lot of powders received in early 2012; powders were stored hermetically at room temperature; however, even under the best storage conditions, aging effects, which could affect reconstitution properties, are still possible (§ 2.2), thus experiments that are directly compared are performed within a few days of each other.

Contents

[1] It was decided to use *real* food powders rather than "model powders" (e.g. ceramic or glass beads), as the behavior was very different and the inert particles did *not* capture the complex mechanisms of dispersion relevant for food materials.

§8.1 Maltodextrin

8.1.1 Theory

Maltodextrin ($C_{6n}H_{(10n+2)}O_{(5n+1)}$) is a common food additive in the food industry. Derived from plant starch, it is an amorphous[2] water-soluble oligo– or polysaccharide with a number of functionalities. For instance it can be used as a drying aid to increase the glass transition temperature (T_g) of a product to reduce stickiness (Caliskan and Dirim, 2013), as a binder for wet granulation (Ghosal et al., 2010), to inhibit crystallization (Potes et al., 2012), as a bulking agent (Ash and Ash, 2007), as a fat replacement via gelation (Hadnadev et al., 2014), or for the encapsulation of sensitive materials (Quintanilla-Carvajal et al., 2014).

Within the Nestlé Research community, it has particularly been used as a model amorphous material, for instance to study fluid bed agglomeration (Palzer, 2005; Fries et al., 2013), pressure agglomeration (Haider et al., 2012; Osborne et al., 2013), spray drying (Gianfrancesco et al., 2010), caking (Hartmann and Palzer, 2011; Haider et al., 2014), thermal aging (Descamps et al., 2013), or thermal degradation (Claude and Ubbink, 2006), among others.

According to Loret et al. (2004), maltodextrins are typically produced via enzyme hydrolysis using α-amylase at the gelatinization temperature of the starch. Of course a more extensive hydrolysis will lead to maltodextrins with a shorter chain length and thus a lower molecular weight. This is typically denoted using the "dextrose equivalents" (DE) of the maltodextrin, which is an indication of its reducing power. Like its parent starch molecule, maltodextrin consists of repeating monomeric residues of anhydro-D-glucose, joined together mostly via $\alpha(1 \rightarrow 4)$-glycosidic bonds, with occasional $\alpha(1 \rightarrow 6)$ branch points for amylopectin

[2]DSC (differential scanning calorimetry) experiments under a range of conditions revealed no crystallization or melting, consistent with many other studies. It is believed that the polymer chains are too long to form significant crystalline structures on timescales of interest, and thus the maltodextrins used are assumed to be purely amorphous for the current study (no solid-phase crystallization upon plasticization).

(Damodaran et al., 2008). A molecule of glucose (dextrose) is shown in Fig. 8.1.

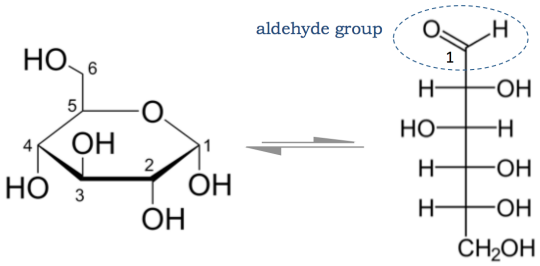

Figure 8.1: Haworth projection (left) of α-D-glucopyranose in equilibrium with its open chain configuration (right) – D-glucose, Fisher projection.

In the open chain configuration, the aldehyde group can be oxidized into a carboxylic acid group, thereby reducing the functional group of another molecule. Now if one considers the repeating *di*mer of maltodextrin (maltose residues), one notices less reducing power on a mass basis, as the anomeric carbon (C_1) is involved in a glycosidic linkage and can no longer open up to its chain configuration (Fig. 8.2).

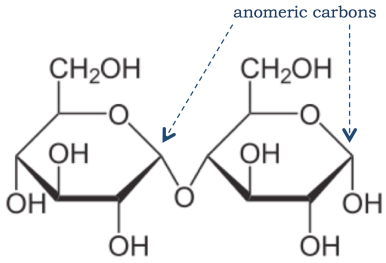

Figure 8.2: Maltose, the repeating dimer of maltodextrin (and starch).

This maltose has $\approx \frac{1}{2}$ the reducing power of glucose. A molecule with three glucose monomers would have ca. $\frac{1}{3}$, etc., with starch having ca. 0 % the reducing power of glucose. Thus the DE value is assigned to 100 (%) for glucose, maltose would have a DE of 50, etc. **The higher the DE value, the lower the molecular weight** (MW). According to Marchal et al. (1999), suppliers do not produce specific chains of defined length, but report and *average* value of mixtures of different MWs. Avaltroni et al. (2004) investigated the influence of DE vs. properties like T_g and viscosity, and they suggest that reporting the effective average molecular weight (via size exclusion chromatography) would actually be a more useful indication of the material properties; nevertheless, DE values are still generally reported by suppliers in the industry. For information on how to measure the DE value, the reader is referred to Rong et al. (2009).

Table 8.1: Properties of DE6 (& IT6) and DE21 (& IT21) powders, according to Roquette.

	DE/IT6	DE/IT21
Average DE value	5 – 8	20 – 23
% Glucose	0.5	3
% Maltose	1.0	7
% Oligo– /polysaccharides	98.5	90
Source	Waxy maize	Potato
No. glucose residues	≈ 17	≈ 5
Molecular mass ($g\,mol^{-1}$)	≈ 2720	≈ 790
True density ($g\,cm^{-3}$)	1.44	1.53

Unfortunately for those familiar with carbohydrate chemistry, for some reason the European Union[3] legally defines maltodextrins with a DE value above 20 as "glucose syrups" or "dextrose syrups." However as already mentioned, glucose has a DE value of 100, and a DE value of 20 corresponds to an oligomer with ca. 5 glucose residues as monomers. Similar confusing definitions were also adopted by the USA.[4] For the sake of scientific logic, in the current report the term "maltodextrin" is used even for DE > 20.

8.1.2 Maltodextrins used

The maltodextrins used in the current report were supplied by Roquette (Lestrem, France) under the brand name Glucidex® DE21, DE6, IT21, and IT6. The "DE" powders are fine, white spray-dried powder, where DE6 has a higher molecular weight than DE21 (Tab. 8.1).

According to Roquette, the "IT" ("instant") powders are chemically identical to the corresponding "DE" powder – to produce them, the smaller DE particles are agglomerated in

[3] EU directive 73/437/CEE of 1973-12-11

[4] Code of Federal Regulations (CFR) Title 21.

a fluidized bed, with water as the only binding material, to produce larger granules (Tab. 8.3) for improved handling, etc. Note that Roquette specifies a *range* of DE values rather than an exact value. DE21, which is a "glucose syrup", only contains ca. 3 % actual glucose monosaccharides. According to the manufacturer, waxy maize is ca. > 95% amylopectin, and potato starch is ca. 75 % amylopectin (branched via $\alpha(1 \rightarrow 6)$ linkages), with the rest of course being amylose. The true density (ρ_t) of each material was measured using a helium pycnometer (Accupyc, 1330, Micrometrics, Norcross, GA, USA). Note the much higher molecular weight (mass) of the DE6/IT6 compared to DE21/IT21.

§8.2 Dairy

A discussion about the theory of milk powders can be found in § 6.2. In the current study, skim milk powder (SMP) and whole milk powder (WMP) – both spray dried, non-lecithinated, non-agglomerated – were supplied by Emmi (Lucerne, Switzerland). The approximate compositions (according to the supplier) are shown in Tab. 8.2.

Table 8.2: Approximate compositions of SMP and WMP, according to the manufacturer.

Composition (approx.)	SMP	WMP
Lactose	50 %	37 %
Protein	35 %	25 %
Minerals	8.5 %	6 %
Moisture	3.5 %	3.5 %
Fat	< 1 %	26 %

§8.3 Cocoa

Cocoa powders are discussed in detail in § 6.2. Cocoa powders were supplied by ADM (Decatur, IL, USA). Two powders were used; they are identical except that one is sprayed with 5 % lecithin on the surface of the powders after pulverization. The fat content is 10 – 12 %, and the lecithinated cocoa (LC) is sold under the brand name "Sol." Nonlecithinated cocoa will be abbreviated NC where appropriate.

§8.4 Particle Size Distribution

Due to the tendency of water-soluble components of food powders to dissolve in water, and fat-soluble materials to dissolve in oil, particle size distributions were measured using an air dispersion unit that feeds powders into the analysis zone of a laser diffraction unit (Malvern Mastersizer S, Malvern Instruments, UK). Measurements were performed in triplicate, at an obscuration of 10 – 15 %, with a 60 s scan with 3×10^4 sweeps per measurement. The Mie theory (§ 5.4) was used to convert diffraction data to sizes, assuming spherical particles. Results were unimodal; the d_{10}, d_{50} (median), and d_{90} sizes (volume-based) are shown in Tab 8.3.

Note that the IT maltodextrins are larger in size and narrower in span than the corresponding DE powders, and the cocoa primary particles are smallest of all powders tested.

§8.5 Scanning Electron Microscopy

Scanning Electron Microscopy (SEM) images were taken of each powder at the University of Sheffield SORBY Center, using a Camscan Mk II at 20 kV. In this technique, particle surfaces are analyzed by emitting an electron beam and detecting how these interact with the sample. In order to improve conductivity (and thus image quality), all samples were sputter-coated with nanogold using an Emscope SC 500 (under vacuum at 0.5 Torr). Results

Table 8.3: Mastersizer sizing results for the powders used in the current study.

Powder	$d_{10,3}$ [µm]	$d_{50,3}$ [µm]	$d_{90,3}$ [µm]
DE21	27	149	308
DE6	30	125	283
IT21	131	301	601
IT6	152	374	638
SMP	23	62	130
WMP	42	108	231
NC	5	11	28
LC	6	12	31

are shown in Figures 8.3 and 8.4 at $10^3\times$ magnification.

Note that the maltodextrins are very jagged and irregular. The SMP particles are hollow (spherical or partially deflated), and WMP also appear to be hollow – this is consistent with the discussion in Ch. 2 for spray dried dairy powders. At the same scale, one can see primary cocoa particles together in clumps.

§8.6 Water Activity

As discussed in Palzer (2007), the water activity (a_w) of a sample at a defined temperature is equal to the vapor pressure in the headspace above a sample (p), compared to the vapor pressure above pure water (p_0), and this is equal to the equilibrium relative humidity (ERH):

$$a_w = \frac{p}{p_0} = \text{ERH} \tag{8.1}$$

In the current study, a_w is measured at 25 °C using calibrated Rotoronic HygroLab HW4 cells (Bassersdorf, Switzerland); essentially it measures the relative humidity (RH) in the headspace above the sample, and the RH once equilibrium is reached is reported as the a_w.

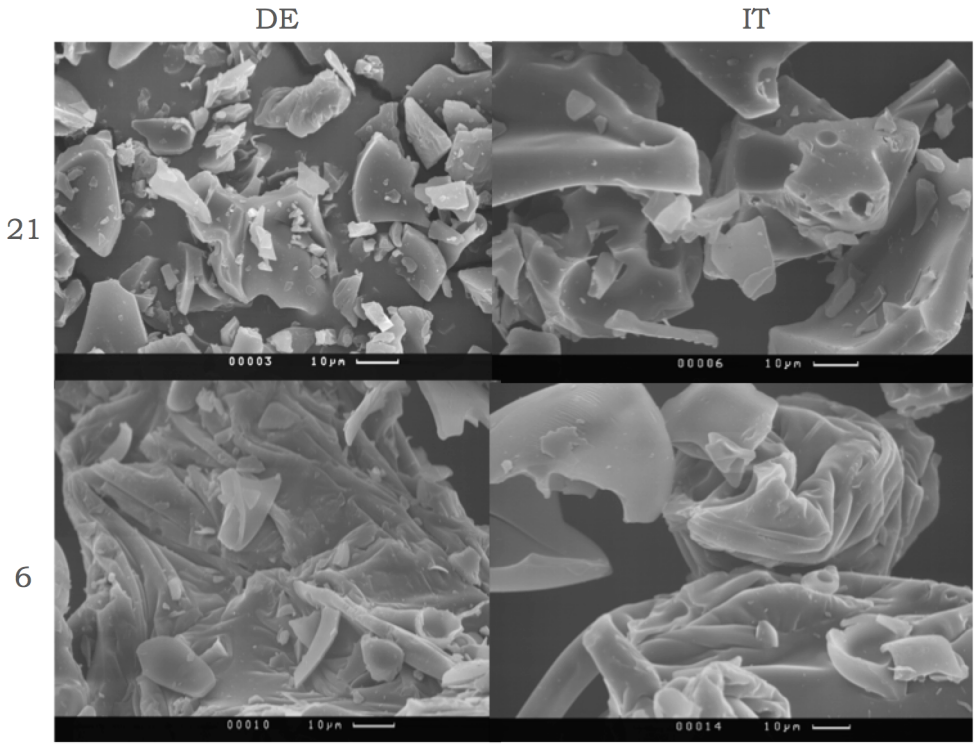

Figure 8.3: SEM images of maltodextrins DE21, IT21, DE6, and IT6.

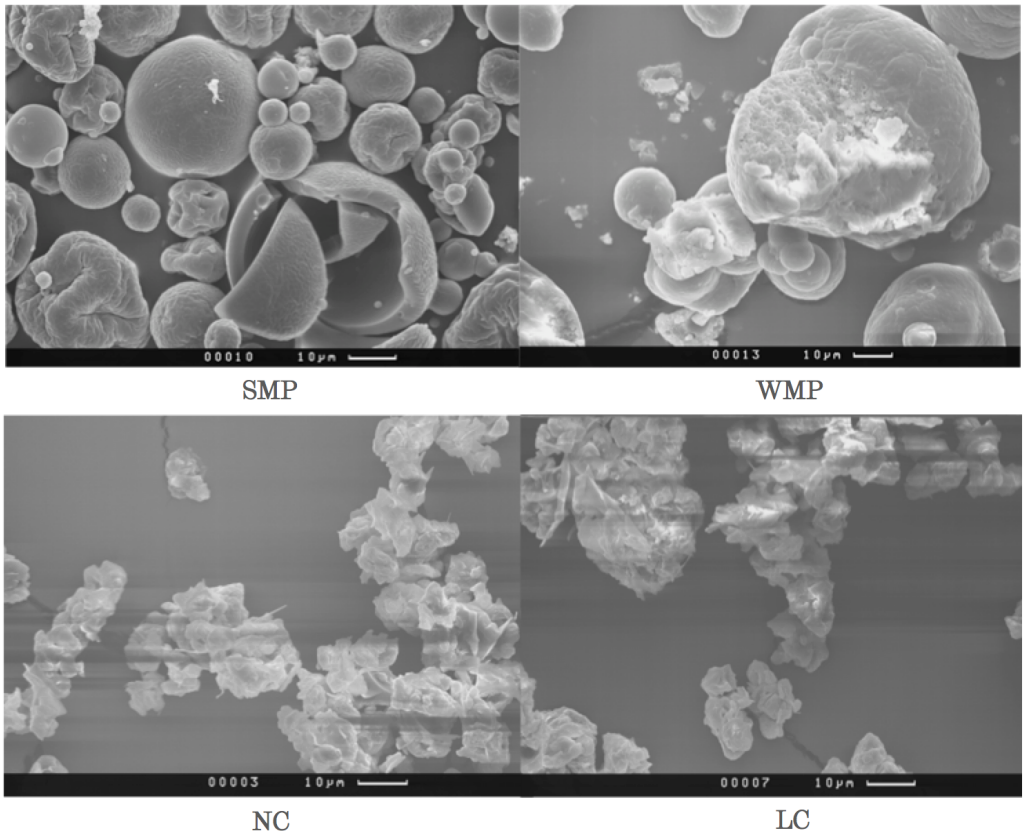

Figure 8.4: SEM images of skim milk powder (SMP), whole milk powder (WMP), non-lecithinated cocoa powder (NC), and lecithinated cocoa powder (LC).

Results are reported where appropriate in the experimental chapters.

§8.7 Differential Scanning Calorimetry

DSC measurements were performed using the DSC1 Star^e System (Mettler Toledo, Switzerland). The DSC was calibrated with an indium sample, nitrogen (N_2) was used as the purge gas, and ca. 10 mg of sample was sealed into a small aluminum crucible for analysis. Measurements were performed to study phenomena such as glass transition, melting, crystallization, etc. (see Palzer (2007)). For glass transition temperature (T_g) analysis, a double heat scan was performed in order to eliminate thermal aging effects, and a temperature range of $\gtrless \pm$ 20 °C of the expected T_g was used for measurement. The heat ramp was set to 10 °C min^{-1}, and the T_g is taken at the *onset* of glass transition (following Haider et al. (2014)). Results are reported where appropriate.

Part III

Experimental Study

Chapter 9

Modeling the Dispersing and Dissolving of Water-soluble Powders

Remember that all models are wrong; the practical question is: 'How wrong do they have to be not to be useful?'

George E. P. Box

In the present chapter, we consider powders that are completely water-soluble – that is, those that do not contain components that become *suspended*, as is the case for milk and cocoa powders (Ch. 11). In particular, the current chapter focuses on such soluble powders that can be reconstituted under "good dispersing conditions," i.e. wetting/sinking is instantaneous, and the submerged powder does not sediment to the vessel floor – these "bad" behaviors will be considered in Ch. 10.

Contents

§9.1 Preliminary Trials

For the present study, maltodextrin DE21 (§ 8.1) was chosen as a model water-soluble powder (a_w 0.22 at 25 °C). Preliminary trials were performed at 25 °C using default conditions (§ 7.2) at different agitation speeds ($N = 200, 400, \ldots, 1000$ rpm). For the default setup, at $N < 600$ rpm, the powder wetted and sank quickly ($t_{\text{sink}} \approx 500$ ms), but the powder sedimented to the vessel floor. However at $N \geq 600$ rpm, there was good dispersing and dissolving. Although FBRM does have sizing capabilities (§ 5.9), for water-soluble powders, the size results were very noisy and uninterpretable.[1] However, the total counts of particles (per meter scanned) was an interesting parameter to study.

A very similar profile was obtained to what Hussain et al. (2011) reported for whey protein isolate using their turbidity approach (Fig. 5.3), where there is a relatively linear rise in signal as particles disperse, followed by a more gradual decay in response as dissolving takes place. In their analysis of the results Hussain et al. (2011) extract very simple **gross characteristics**, such as the "wetting time" (time between powder addition and the peak of the turbidity response), and "total rehydration time" (from beginning to when the signal is finished decaying). However, in the current report, such gross characteristics are defined differently. Fig. 9.1 shows a cartoon example of a typical result for maltodextrin DE21.

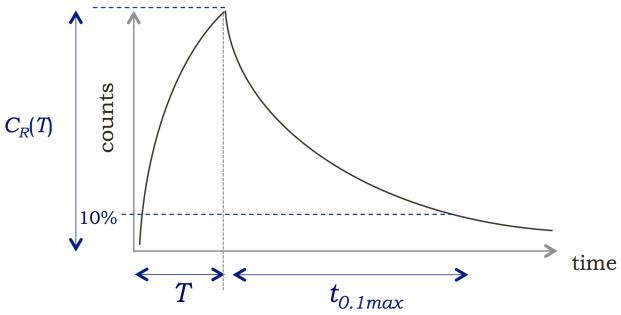

Figure 9.1: Gross characteristics of FBRM curve for current chapter.

[1] The same is *not* true for other powders – see Ch. 11.

One could theoretically easily extract the time from powder addition to the peak (T in Fig. 9.1), which Hussain et al. (2011) call the "wetting time." However, a direct comparison to the videos demonstrated that the powder typically wets and sinks at a time $t \ll T$, thus perhaps the term "wetting time" would be misleading. The rise in signal is therefore likely to be due also to *dispersing* of particles and agglomerates throughout the vessel, leading to an increase in total counts. Other extractable values are, for instance, the time to go from $t = T$ to the time where counts $= \frac{1}{10}$ the maximum counts, or the maximum number of counts itself.

However, instead of only reporting these gross characteristics, in the current chapter, the question was posed **whether FBRM results could be used to quantify the dispersing and dissolving behavior** of the materials. The initial linear increase in counts followed by a more gradual decay (Fig. 9.1) is resemblant of a 0^{th}-order chemical reaction followed by a 1^{st}-order reaction (a "(0,1)" model) in shape (Levenspiel, 1999); thus an analogy was proposed for the data analysis. (For other models of powder dissolution derived from analogies with chemical reaction kinetics, see Ch. 5). In Fig. 9.2, the square-weighted[2] counts are plotted on a linear axis (a) and on a logarithmic axis (b) vs. time. The fact that the initial rise is linear on a linear scale is indicative of 0^{th}-order-like behavior, and the fact that the second part of the curve is linear on a logarithmic axis is indicative of 1^{st}-order-like behavior.

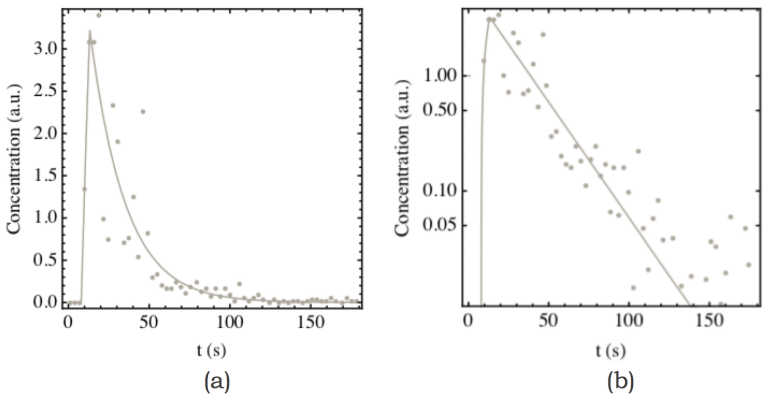

Figure 9.2: Square weighted counts (arbitrary units) on (a) linear and (b) logarithmic axes (maltodextrin DE21, 25 °C, 600 rpm).

[2]For a discussion about why *square-weighted* counts are used, see § 9.4 later in the current chapter.

§9.2 Kinetic Hypothesis and Model Development

Thus, based on these observations, a kinetic hypothesis of powder dispersing and dissolving was proposed (Fig. 9.3): the food material can exist in one of three states – a dry heap of powder (A), a suspended dispersion (R), which is what would be detected by the FBRM probe, or in a dissolved solution (S).

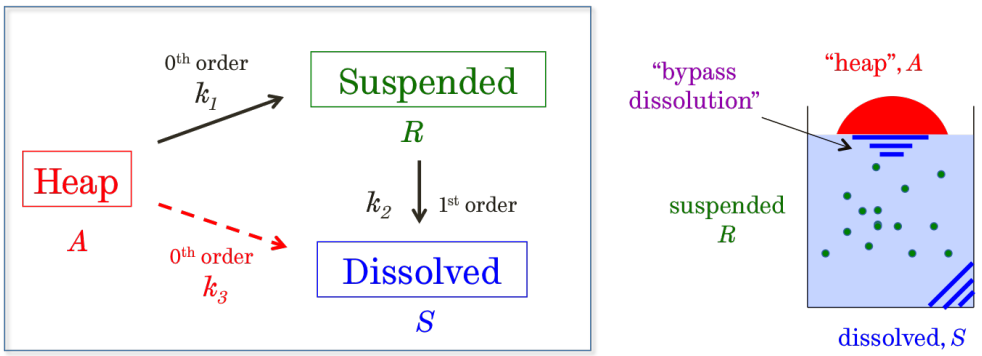

Figure 9.3: Cartoon to describe the kinetic hypothesis.

Three different non-reversible rates are defined: k_1 is the so-called "dispersing rate" (from A $\rightarrow$ R), which is 0^{th}-order (i.e. independent of the amount in the heap), and k_2 (R $\rightarrow$ S) is the "dissolving rate *via* suspension," which is 1^{st}-order. The (0,1) description from earlier was modified to allow for a so-called "bypass dissolution" to account for the fact that powder may dissolve before it can be detected by the FBRM probe.[3] A rate k_3 (A $\rightarrow$ S) is thus defined as the "dissolving rate *bypassing* suspension." From this hypotheiss, a semi-empirical model was developed, where the concentration of suspended particles C_R could be fitted to the FBRM results (square–weighted counts). If C is the concentration, t is time, and the subscripts $_A$, $_R$, and $_S$ correspond to Fig. 9.3 (i.e. heap, suspended, dissolved, respectively) then the three rates of change for concentrations C_A, C_R, and C_S will be:

$$\frac{\mathrm{d}C_A}{\mathrm{d}t} = -k_1 - k_3 \qquad \frac{\mathrm{d}C_R}{\mathrm{d}t} = k_1 - k_2\,C_R(t) \qquad \frac{\mathrm{d}C_S}{\mathrm{d}t} = k_2\,C_R(t) + k_3 \tag{9.1}$$

The ordinary differential equations were solved for analytically; the equations are discontinuous at $t = T$ (Fig. 9.1).

$$C_A(t) = \begin{cases} C_{A,0} - (k_1 + k_3)\,t & \text{if } t < T \\ 0 & \text{if } t \geq T \end{cases} \tag{9.2}$$

[3] Discussed further in § 9.4.

$$C_R(t) = \begin{cases} k_1 \dfrac{1 - \mathrm{e}^{-k_2\, t}}{k_2} & \text{if } t < T \\ \dfrac{k_1}{k_2}\left(1 - \mathrm{e}^{-\frac{k_2\, C_{A,0}}{k_1 + k_3}}\right) & \text{if } t = T \\ \mathrm{e}^{-k_2\,(t-T)} C_R(T) & \text{if } t > T \end{cases} \tag{9.3}$$

$$C_S(t) = \begin{cases} k_1 \dfrac{\mathrm{e}^{-k_2\, t} - 1}{k_2} + (k_1 + k_3)\, t & \text{if } t < T \\ C_{A,0} - \dfrac{k_1}{k_2}\left(1 - \mathrm{e}^{-\frac{k_2\, C_{A,0}}{k_1 + k_3}}\right) & \text{if } t = T \\ C_{A,0} - \mathrm{e}^{-k_2 (t-T)}\, C_R(T) & \text{if } t > T \end{cases} \tag{9.4}$$

where $C_{A,0}$ is the initial amount of powder added, and the time at $C_R = C_{R,\max}$ i.e. T, is:

$$T = \frac{C_{A,0}}{k_1 + k_3} \tag{9.5}$$

Fig. 9.4 demonstrates how the plots of $C_A(t)$, $C_R(t)$, and $C_S(t)$ evolve over time.

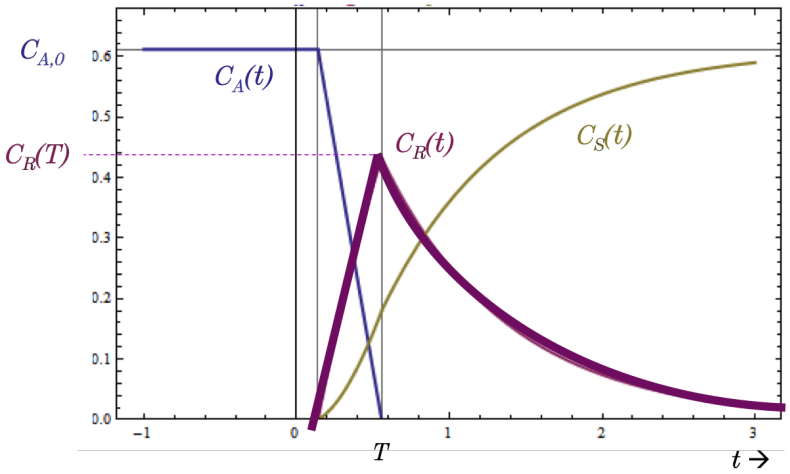

Figure 9.4: Example of how the model represents the evolution of the three concentrations (A, R, and S).

Note that $C_A(T) = 0$, and $C_R(T) = C_{R,\max}$, indicating that the peak is obtained once the "heap" of powder (A) is completely dispersed and no longer exists. $C_S(t)$ rises more gradually and reaches a maximum as $C_R(t) \to 0$. It is $C_R(t)$ that is fitted to the FBRM raw

data in order to extract the rates k_1, k_2, and k_3; this modeling is done in Mathematica (see Appendix). A "piecewise" function is used to account for the discontinuities at $t = T$, and as the model is nonlinear, initial guesses are used for convergence: $\mathrm{k}_{1,\mathrm{guess}}$ is based on the slope of the initial linear rise ($0 \leq t \leq T$) and $k_{2,\mathrm{guess}}$ is obtained by fitting an exponential decay for ($T \leq t \leq t_{\max}$) where $C_R(t_{\max}) = 0$, and $k_{3,\mathrm{guess}} = k_2\, C_R(t)$.

§9.3 Effect of Powder Amount and Agitation

A number of trials were performed with maltodextrin DE21 at 25 °C with different powder amounts (M_0), where M_0 = 5, 10, 20, and 40 kg m^{-3}, and agitation speeds (N), with N = 600, 800, and 1000 rpm. Ten replicates of each trial was performed[4] and the ten replicates from each trial were plotted together prior to data fitting to obtain a combined fit. Based on the raw results, it was decided to fit the values of k_1, k_2, and k_3 for all values of M_0 for each N (i.e. for each N, the k values are the same for all values of M_0), where the $C_{A,0}$ is adjusted for each M_0 (see Appendix). Results from each fit are shown in Fig. 9.5.

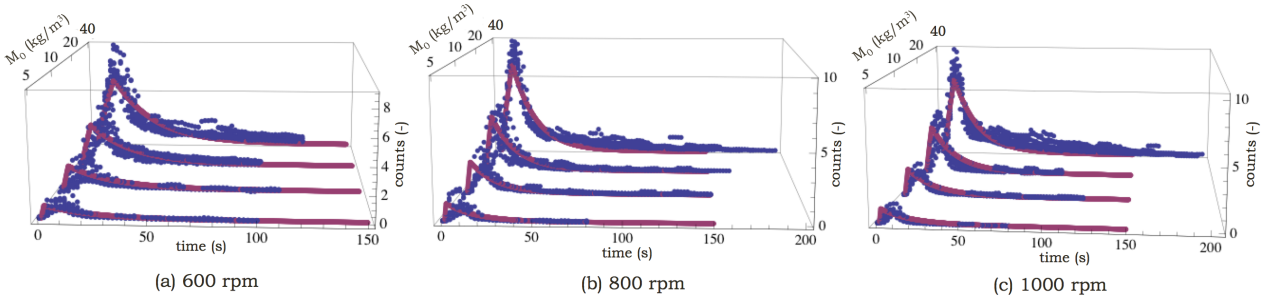

Figure 9.5: Model fitting results: (a) 600 rpm, (b) 800 rpm, (c) 1000 rpm.

The results show that good fitting is obtained for all M_0 values using the same k fits. However, the fits do appear to be better for higher M_0 values – for $M_0 = 5\,\mathrm{kg\,m^{-3}}$, the model fit is showing a rise faster than the experimental data. This may be due to the fact that at lower M_0 values, less of the powder will succeed in presenting itself in front of the FBRM window, compared to at higher M_0, thereby delaying the signal rise.

Extracted values for k_1, k_2 and k_3 are plotted in Fig. 9.6.

[4] 4 M_0 values × 3 N values × 10 reps = 120 dissolution trials.

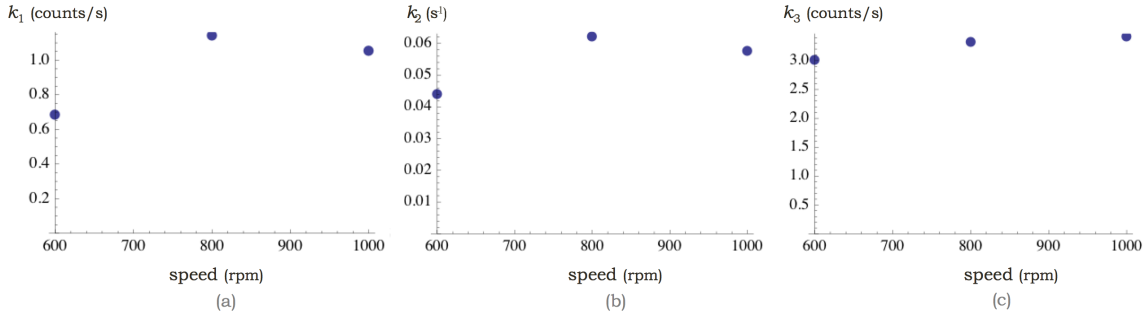

Figure 9.6: Extracted values for (a) k_1, (b) k_2, and (c) k_3 following model fitting.

Results do not indicate a major influence of N for the range tested for the current powder under the given conditions.[5]

The *repeatability* is also affected by the amount of powder added (M_0); reconstitution experiments performed at higher M_0 values were repeatable, and thus had a higher coefficient of determination (r^2). Three examples are shown in Fig. 9.7 for $M_0 = 10$, 20, and 40 kg m^{-3} with $N = 600$ rpm.

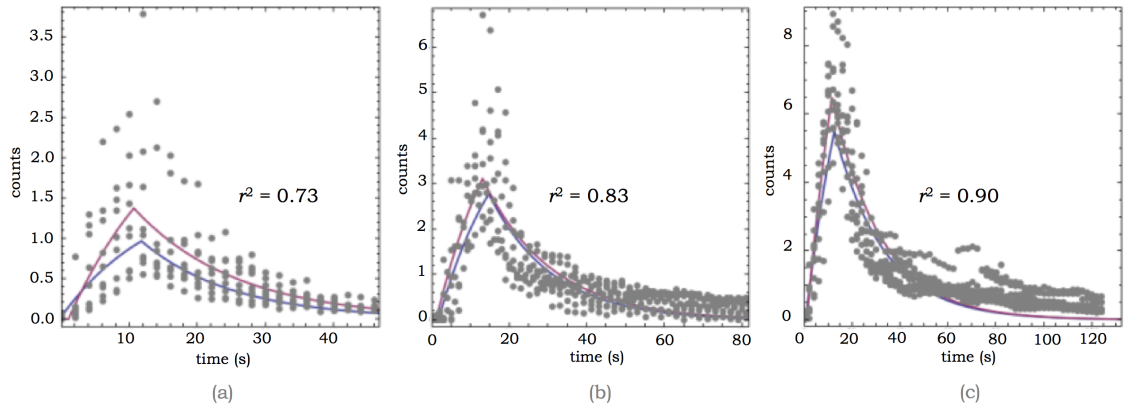

Figure 9.7: Repeatability of experiments improves with increasing M_0: (a) $M_0 = 10\,\mathrm{kg\,m^{-3}}$, (b) $M_0 = 20\,\mathrm{kg\,m^{-3}}$, (c) $M_0 = 40\,\mathrm{kg\,m^{-3}}$. Experiments performed with maltodextrin DE21 at 25 °C and N=600 rpm. The blue line shows the initial fit following guessing, and the pink line shows the final fit.

The water temperature (T) and agitation speed (N) also play a role in repeatability (results not shown). If T is too high then the reconstitution may be too fast for the resolution of the FBRM measurements.[6] A similar problem is observed for high N; with more repeatable

[5] The effect of N for a wider range of conditions and powders are tested in Chapters 10 and 11.

[6] The fastest acquisition rate in the iC FBRM version used is one measurement every 2 s; however, the author sees no reason why the resolution could not be improved by Mettler Toledo, as more than 100 measurements

results at a *lower* N value. However, an optimum appears to exist, and if N is too low then powder will sediment; $N = 600\,\text{rpm}$ yielded the best results for the conditions tested.

The **particle size** and **molecular weight** also appear to have an effect on the FBRM results, which would affect the fitted k values. In Fig. 9.8a, maltodextrins DE21 (fine powder – in green), and IT21 (granules – in pink) are compared, and one observes slightly greater dispersing for the granules; however the results are very similar. However in Fig. 9.8b, where the behaviors of granules[7] of maltodextrin IT21 and IT6 are compared, it is clear that there is much more dispersing for the IT6 powder, but much faster dissolving for the IT21 powder; the fact that the values of $C_R(T)$ are different for the two powders, despite the same mass being added, is an indication that allowing for bypass dissolution (including k_3) into the model was justified, as IT21 would exhibit a stronger bypass dissolution than IT6.

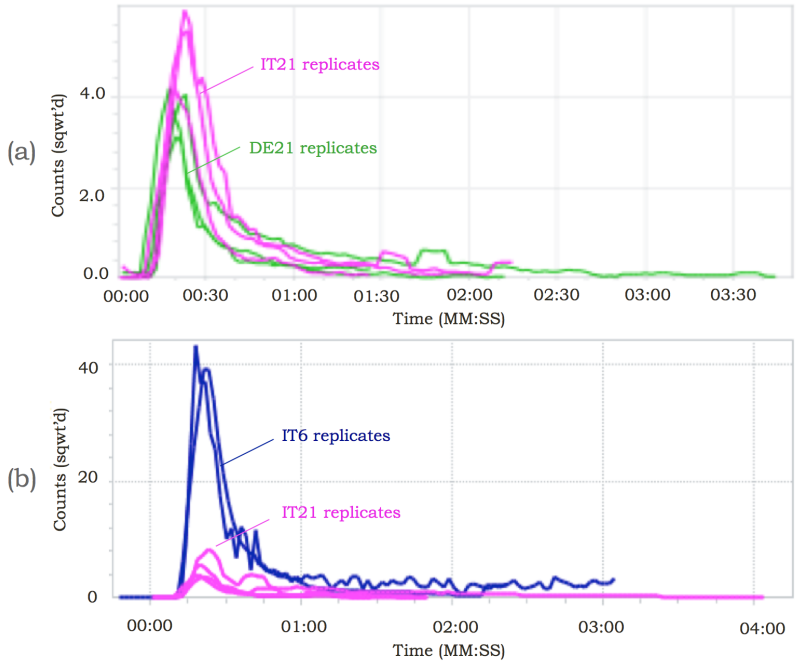

Figure 9.8: Profiles of reconstitution of other maltodextrins under default conditions, $M_0 = 20\,\text{kg}\,\text{m}^{-3}$: (a) DE21 vs. IT21 at 600 rpm, (b) IT21 vs. IT6 at 800 rpm

A more comprehensive discussion on the effects of particle size and molecular weight is given in Ch. 10.

are taken each second.

[7]Both powders are large granules, with IT6 having a higher molecular weight.

§9.4 FBRM Calibration Study

One of the major challenges for quantitatively describing the dispersing and dissolving of powders with FBRM (e.g. to express the values of k_1 and k_3 in terms of a concentration rather than counts), is the calibration of the FBRM instrument. One major question was whether or not the FBRM counts vs. concentration is *linear* in nature, and another is if a calibration can be performed. Of course, such a calibration for maltodextrin in water is not possible, since the powder dissolves. Another question is *which statistic* could be used from the FBRM measurements to express the concentration (mass of suspended particles) *independently of size*. This is because the particles will, of course, shrink as dissolving occurs.

According to Wynn (2003), for a chord length (C), from an FBRM measurement, with f being the frequency distribution of C, and μ_j being the j^{th} moment of f, μ_j is defined as:

$$\mu_j \equiv \int_0^\infty f(C)\, C^j \,\mathrm{d}C \tag{9.6}$$

whereas for a particle size distribution, with D as the particle size (diameter of a volume-equivalent sphere), and n being the density distribution, and m_j being the j^{th} moment of n:

$$m_j \equiv \int_0^\infty n(D)\, D^j \,\mathrm{d}D \tag{9.7}$$

For a number of assumptions (see Wynn (2003)):

$$\mu_j \propto m_{j+1} \tag{9.8}$$

Therefore, if one wishes to use an FBRM statistic dependent on particle mass (or volume), but *independent of size*, similar to the third moment of particle size (i.e. m_3) one should use μ_2 $(3-1=2)$ from the chord length. As mentioned earlier in the current chapter, square-weighted counts were used for modeling purposes. As explained in the iC FBRM manual, weighted channels (y_i) are obtained by multiplying a channel-specific weighting factor (w_i) to the raw counts (n_i), via:

$$y_i = w_i\, n_i \tag{9.9}$$

where w_i is determined based on the *midpoint* of the i^{th} channel (M_i) via:

$$w_i = \frac{M_i^\gamma}{\sum_{j=1}^{N} M_j^\gamma} \cdot N \tag{9.10}$$

which is essentially multiplying the i^{th} channel, raised to a certain power γ, divided by the average (where the total number is N), of the weighted midpoints. The exponent γ determines the *type* of weighting.[8] Using a different weighting type for FBRM, measurements can be used to **emphasize either the fines fraction (usually by leaving counts unweighted), or the coarse fraction (usually by square-weighting, or even cube-weighting for studying very large particles)** – similar to the difference between number vs. volume-based distributions for particle sizing (see Figura and Teixeira (2007, Ch.3)) – this ability to focus either on fine or coarse particles is extensively used in Ch. 11. One will note a close relationship between moments (Eq. 9.6) and weighting (Eq. 9.10), as both involve raising a length to a defined exponent (hence why square-weighting was chosen for counts at the beginning of the current chapter). A key difference is that due to the averaging aspect of weighting factors, **weighted counts remain dimensionless, unlike moments.** Another important use of weighting in FBRM statistics is the mean chord length ($\bar{C}$), which is obtained from the counts per channel and the channel midpoints via:

$$\bar{C} = \frac{\sum_{i=a}^{b} y_i \, M_i}{\sum_{i=a}^{b} y_i} \tag{9.11}$$

where a and b denote the limits of a subrange. This $\bar{C}$ can also be expressed in terms of the unweighted counts (as well as moments) via:[9]

$$\bar{C} = \frac{\sum_{i=a}^{b} n_i \, M_i^{\gamma+1}}{\sum_{i=a}^{b} n_i \, M_i^{\gamma}} = \underbrace{\frac{\mu_{\gamma+1}}{\mu_{\gamma}}}_{\text{moments}} \tag{9.12}$$

Since maltodextrin calibrations cannot be performed in an aqueous medium, trials were performed in a lipophilic medium (high oleic sunflower oil, type F, Sofinol Speciality Oils SA, Switzerland), under high agitation ($N \approx 2000\,\text{rpm}$) for the default configuration. Three different sieve fractions were tested at increasing concentrations of powders (63 – 106 µm, 106 – 150 µm, and 150 – 212 µm). For each concentration, moments μ_{0-4} were calculated and plotted as a function of concentration (Fig. 9.9).

The results reveal firstly that **linearity is very good** for the range tested (which is greater than the range tested for reconstitution measurements). With regards to which statistic

[8] $\gamma = 0$ implies unweighted counts ($w_i = 1 \therefore y_i = n_i$), $\gamma = 1$ is length-weighting, $\gamma = 2$ is square-weighting, and $\gamma = 3$ is cube-weighting.

[9] See iC FBRM user manual for the derivation.

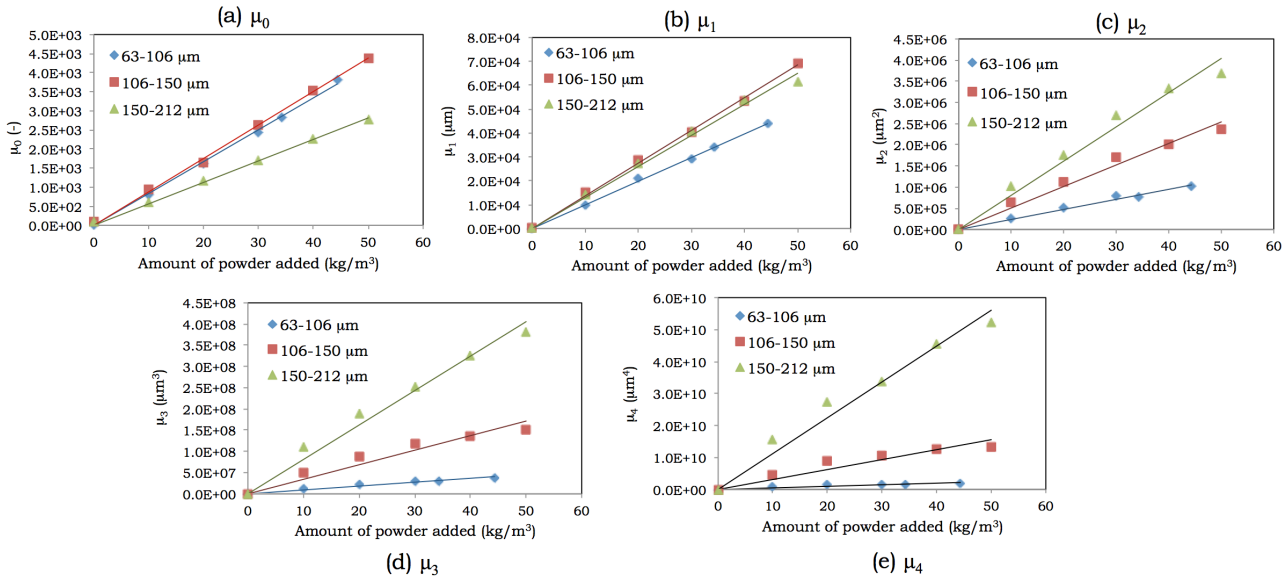

Figure 9.9: Moments calculated for increasing concentrations of maltodextrin DE21 in oil: (a) μ_0, (b) μ_1, (c) μ_2, (d) μ_3, and (e) μ_4.

would be best for size-independent signal, μ_0 and μ_1 both, unfortunately, appear to be better than μ_2. Similar experiments were performed with sand (SiO_2, Sigma-Aldrich, St. Louis, MO, USA), sieved into three different size fractions (90 – 125 µm, 125 – 212 µm, and 212 – 300 µm), in two different media: oil (the same as before) and deionized water, for comparison purposes. Results are shown in Figs. 9.10 and 9.11.

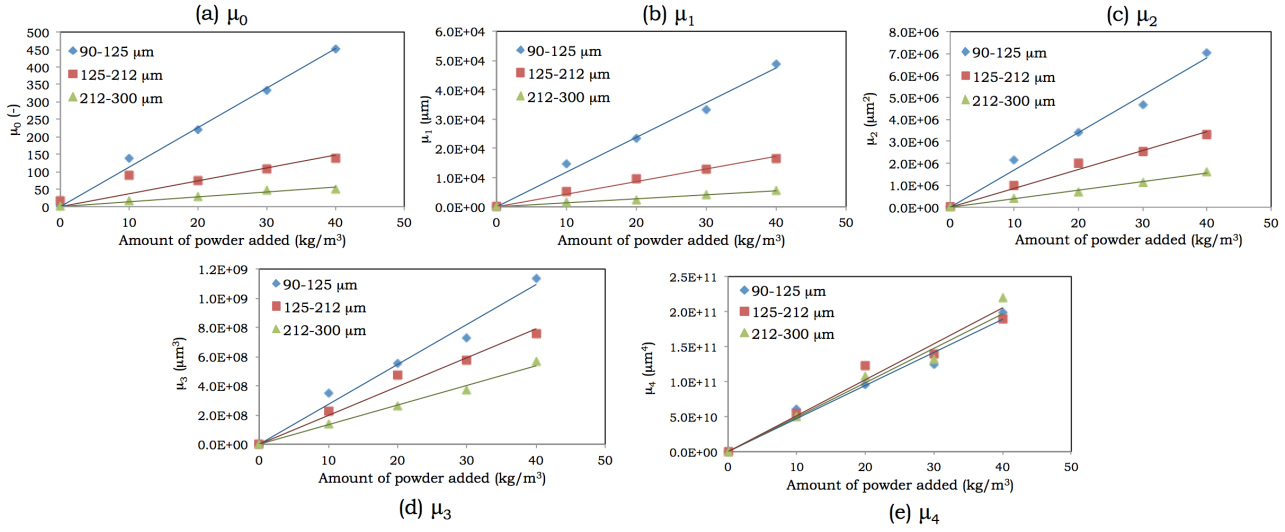

Figure 9.10: Moments calculated for increasing concentrations of sand in oil: (a) μ_0, (b) μ_1, (c) μ_2, (d) μ_3, and (e) μ_4.

Comparing Figs. 9.10 and 9.11, it is clear that the response is much higher in water than in oil, likely due to the faster movement of the sand particles in water than in oil, even at a

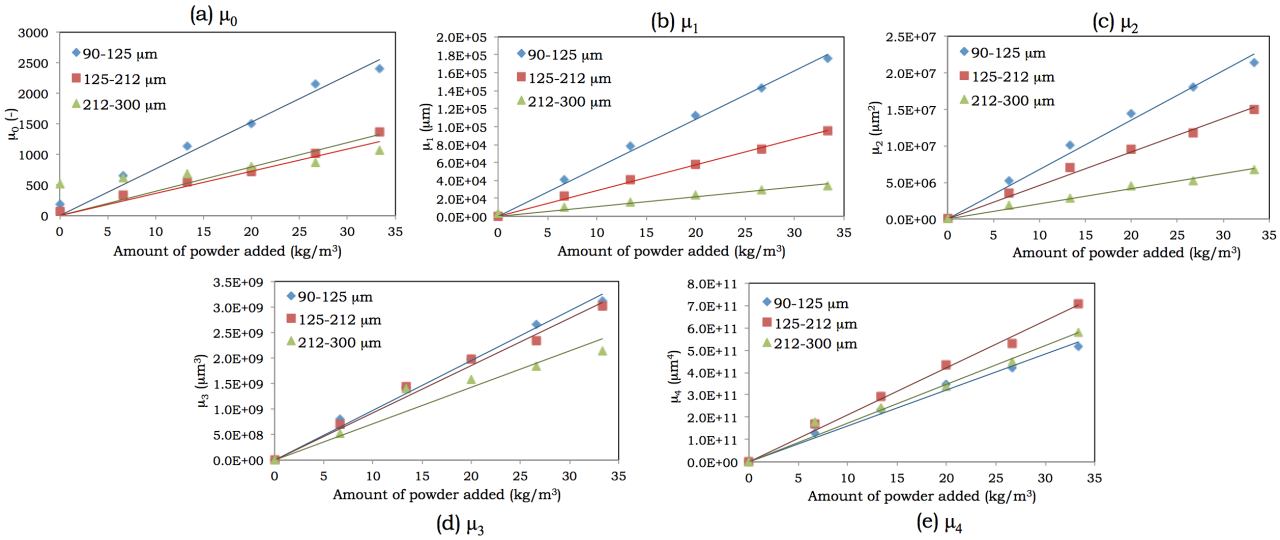

Figure 9.11: Moments calculated for increasing concentrations of sand in H_2O: (a) μ_0, (b) μ_1, (c) μ_2, (d) μ_3, and (e) μ_4.

lower N. In any case, what is interesting is that the statistic least dependent on size is now μ_4; this is true for both media. These results indicate that the best statistic may depend on the optics of the powder, and this is non-universal. For the current powders, the fact that μ_2 was not size-independent is a possible indication that Wynn (2003)'s assumptions were not completely valid. For instance, he states in his assumptions that particles would have the same shape, and that the "two-dimensional chord" model is assumed. However in reality, particles do not have the same shape, and also FBRM software employs a chord selection model (see § 5.9) to determine which chords to keep and which to ignore; this is based on the intensity profile of the backscattered laser light – a profile that is not sharp enough is ignored. Further work should be performed in this area to determine how statistics are affected by different variables.

One approach that was attempted for calibration purposes was to **use the conductivity measurements**, which were also performed for every DE21 dissolution trial, and were (originally) assumed to be representative of the amount of *dissolved material*, i.e. $C_S(t)$, and to then use the fitted results of $C_S(t)$ from the conductivity measurements to extract the k values, and thereby calibrate $C_R(t)$. However it was quickly realized that **conductivity measurements are *not* necessarily an indication of dissolved material.** Consider for instance Fig. 9.12.

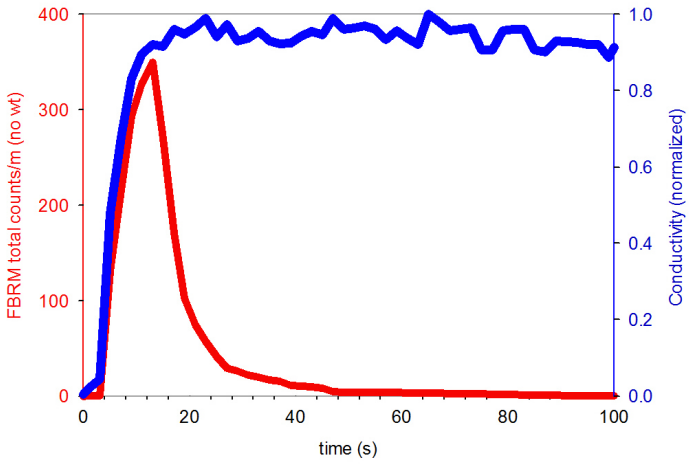

Figure 9.12: Simultaneous FBRM and conductivity measurements for maltodextrin DE21 ($N = 800\,\text{rpm}$, $T = 25\,°\text{C}$, default conditions (§ 7.2)).

The conductivity measurement rises much too quickly to a maximum value (cf. the expected profile in Fig. 9.4). It is believed that the rise in conductivity values is due to impurities on the surface of the powder rather than the dissolution of the carbohydrate molecules, as these would not be expected to conduct electricity. Additional problems regarding conductivity measurements for powder reconstitution trials are discussed in Ch. 14. Possibilities for future work on calibration are discussed in Ch. 14.

§9.5 Benefits and Limitations of Model

To the author's best knowledge, the model presented in the current chapter is the first of its kind, and is a promising tool to analyze the reconstitution behavior of many water-soluble powders, such as hydrocolloid materials or whey proteins (Fig. 5.3) for instance, once issues regarding calibration are sorted. The model is capable of describing both the dispersing and dissolving behaviors separately, yet simultaneously, and gives a more complete picture of these overlapping phenomena than have previous models.

However, even after the model has been improved, there are a number of limitation to consider. The model is *only* applicable for a relatively narrow range of conditions: the powder must be completely water-soluble, and it must sink quickly and disperse well to be detected by the probe. However, often the behaviors most interesting to food technologists from a

problem-solving point of view are more complex; for instance, poor sinking, lump formation, and sedimentation, which cannot be adequately described using the proposed model (see Ch. 10 for an alternative approach). In addition, most food powders are not completely soluble, and contain components that *disperse* in the medium – as a result the FBRM profile obtained will be completely different. Nevertheless, the current setup can also be used to analyze such powders as well (Ch. 11).

Chapter 10

Mapping the Reconstitution of Water-soluble Powders

If a picture is worth a thousand words, what's a video worth?

Scott MacFarland

As discussed in Ch. 9, the model proposed in the previous chapter is only applicable to a relatively narrow range of conditions. However, experiments with different powders have revealed that a number of diverse behaviors can exist for powders; for instance powders may sink slowly or float indefinitely, some might sediment, and others may form lumps that are hard to disperse. Such behaviors are not only dependent on the powder itself, but also conditions of reconstitution, especially the water temperature T and impeller stir rate N. Although these behaviors cannot be adequately described using the FBRM (or conductivity) measurements, understanding these behaviors is quite important to product developers. In particular, it is important to understand *under which combinations of conditions* such behaviors might arise, in order to find and implement appropriate solutions.

Contents

§10.1 Maltodextrin Maps

10.1.1 Novel mapping strategy

In the current chapter, a novel "mapping approach" is proposed for characterizing the *limiting regime* behaviors of food powders, at different conditions. The inspiration for producing such maps arises from regime maps commonly used in the granulation research community, to describe how combinations of conditions (usually expressed with dimensionless groups) affect a process. For instance Iveson and Litster (1998) and Iveson et al. (2001) studied the growth regimes for granules in the presence of a liquid binder in a fluidized bed, high shear mixer, and tumbling drum. Dhenge et al. (2013) constructed similar maps in a twin screw granulator. Cavinato (2010) also proposed a "formulation map" for high shear wet granulation.

For the present study, regime behaviors are described qualitatively as a function of combinations of agitation speed (N) and water temperature (T); an illustration is given in Fig. 10.1.

The so-called "rate-limiting regimes" are as follows: sinking-limited, sedimentation, lump forming, and "normal," for which all four steps of reconstitution take place with ease. Regime behaviors are determined by reviewing video recordings of each trial, taking advantage of the fact that a transparent vessel is utilized. One map is constructed for each powder, allowing

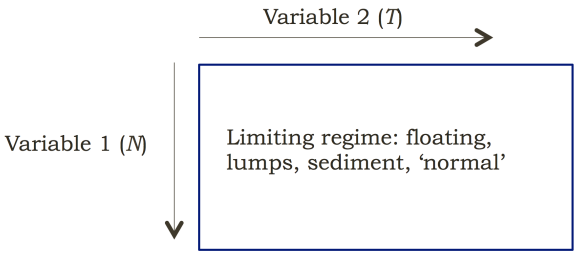

Figure 10.1: Cartoon of regime maps.

the operator to understand the effects of N and T, and by creating maps for different powders, one can have a better understanding of particle properties under a range of conditions (e.g. cold-water vs. hot-water applications).

10.1.2 Maltodextrin regime maps

Regime maps were constructed for four types of maltodextrins: Glucidex DE21, DE6, IT21, and IT6. As explained in § 8.1, the "DE" powders are spray dried and very fine, whereas the "IT" powders are formed by agglomerating the "DE" powders in a fluid bed with water as the only binder. The DE21 and IT21 powders are thus chemically identical, as are the DE6 and IT6 powders. The number (21 or 6) refers to the dextrose equivalents: a value of 6 indicates a much higher molecular weight than 21, as explained in § 8.1. Thus by testing these four powders, one investigates the effect of molecular weight and particle size, as well as N and T. The N and T values were chosen to cover a wide range of conditions, from cold to hot (T = 0, 25, 45, and 65 °C), and from gentle stirring to vigorous agitation (N = 200, 400, ..., 1000 rpm). All other conditions were kept to adhere to default conditions previously defined (§ 7.2), and the water activity (a_w) of the powders was 0.2 ± 0.03 at 25 °C prior to dissolution.

All experiments were performed at least in triplicate[1] to ensure consistent results.

[1] 5 values of N × 4 values of T × 3 reps = 60 expts.

Maltodextrin DE21 results

Under all conditions, wetting and sinking of the maltodextrin DE21 powder occurred instantly, within 500 ms of the particles contacting the liquid surface. However as shown in Fig. 10.2, reconstitution was not always 'normal'. At lower agitation speeds (200 and 400 rpm), particles sedimented to the bottom of the vessel, and under some conditions, lumps of particles broke off from the sedimented layer and then rose to the liquid surface, floating just beneath the interface for longer periods of time (Fig. 10.3). This is an indication that the lumps that form contain dry powder (and air) on the inside, and as a result buoyant forces are responsible for the floating of the lump once it has broken off from the sedimented layer.

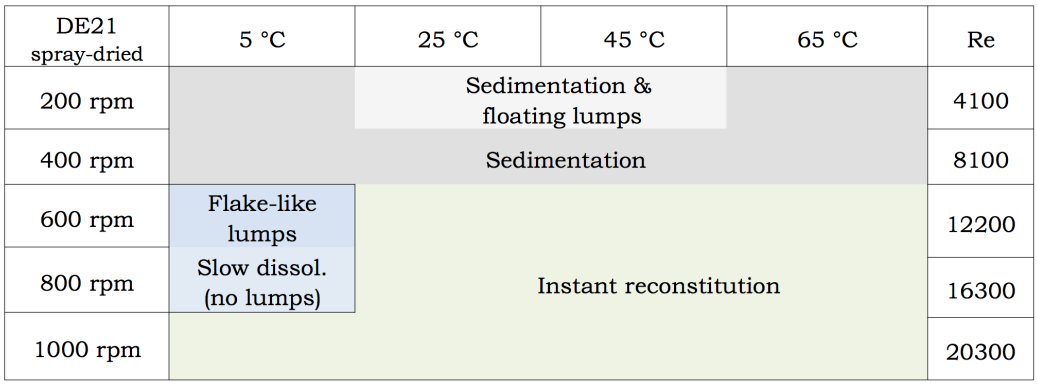

Figure 10.2: Maltodextrin DE21 regime map.

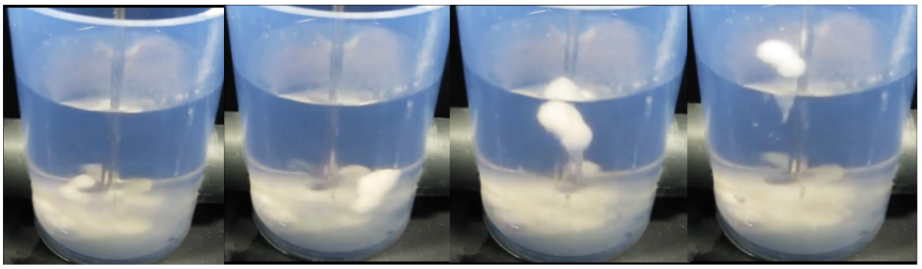

Figure 10.3: Lump of maltodextrin DE21 forming from sedimented layer at [200 rpm, 25 °C]. Similar lumps formed at [200 rpm, 45 °C] for the same powder.

At $N = 600$ rpm and higher, no sedimentation takes place; however, at $T = 5$ °C the dissolution of the individual particles takes place slowly. A different kind of lump is observed at [600 rpm, 5 °C] as well; rather than floating near the liquid surface, these remain closer to the vessel bottom as flake-like aggregates (Fig. 10.4).

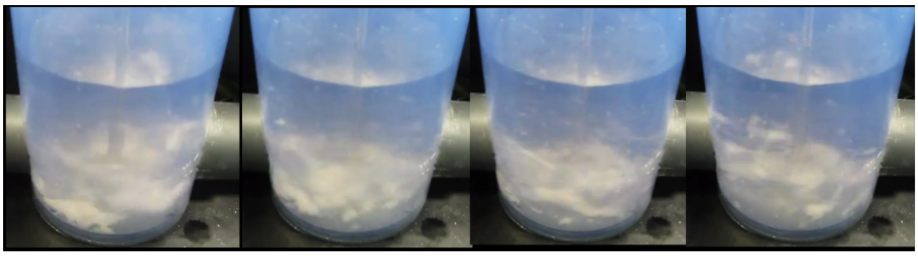

(a) t = 10 s (b) t = 20 s (c) t = 30 s (d) t = 40 s

Figure 10.4: Flakes of maltodextrin DE21 at [600 rpm, 5 °C].

Maltodextrin IT21 results

Similar to the results for maltodextrin DE21, the larger maltodextrin IT21 particles sank instantly and settled to the vessel bottom at lower N. The limiting regime map is shown in Fig. 10.5. Above 600 rpm, reconstitution took place normally, and at 5 °C no flake-like lumps were observed, as had been observed for maltodextrin DE21 at 5 °C (Fig. 10.2).

IT21 agglomerated	5 °C	25 °C	45 °C	65 °C	Re
200 rpm	Sedimentation				4100
400 rpm			Light sedimentation		8100
600 rpm	Instant reconstitution				12200
800 rpm					16300
1000 rpm					20300

Figure 10.5: Maltodextrin IT21 regime map.

Maltodextrin DE6 results

Maltodextrin DE6, which is spray-dried and has a larger molecular weight than maltodextrin DE21, was rehydrated under the same conditions; the map of the limiting regimes is shown in Fig. 10.6.

Wetting and sinking do not take place readily at lower N – much of the powder remains at the liquid surface for an extended period of time (Fig. 10.7).

<table>
<tr><th>DE6
spray-dried</th><th>5 °C</th><th>25 °C</th><th>45 °C</th><th>65 °C</th><th>Re</th></tr>
<tr><td>200 rpm</td><td colspan="3" rowspan="3">Large floating layer develops</td><td rowspan="2"></td><td>4100</td></tr>
<tr><td>400 rpm</td><td>8100</td></tr>
<tr><td>600 rpm</td><td colspan="2">Improved, but incomplete,
sinking</td><td>12200</td></tr>
<tr><td>800 rpm</td><td>Lumps form</td><td colspan="3" rowspan="2">Instant reconstitution</td><td>16300</td></tr>
<tr><td>1000 rpm</td><td>Slow dissolving
(no lumps)</td><td>20300</td></tr>
</table>

Figure 10.6: Maltodextrin DE6 regime map.

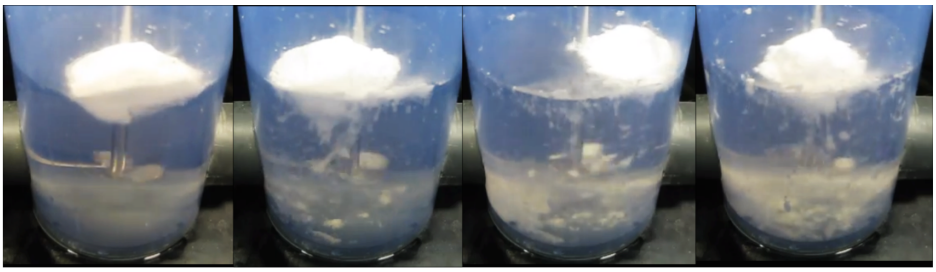

(a) t = 5 s (b) t = 15 s (c) t = 25 s (d) t = 35 s

Figure 10.7: Floating layer of maltodextrin DE6 at [200 rpm, 25 °C].

Increasing T helps improve sinking as well (Fig. 10.8), although it is not until higher value of N (800 and 1000 rpm) that the powder sinks completely.

(a) t = 10 s (b) t = 20 s (c) t = 30 s (d) t = 40 s

Figure 10.8: Improved sinking of maltodextrin DE6 at higher temperatures [600 rpm, 45 °C].

At [800 rpm, 5 °C], lumps of powder form (Fig. 10.9) and remain after the rest of the powder has dissolved, floating near the liquid surface. These lumps are not observed at higher T or at 1000 rpm.

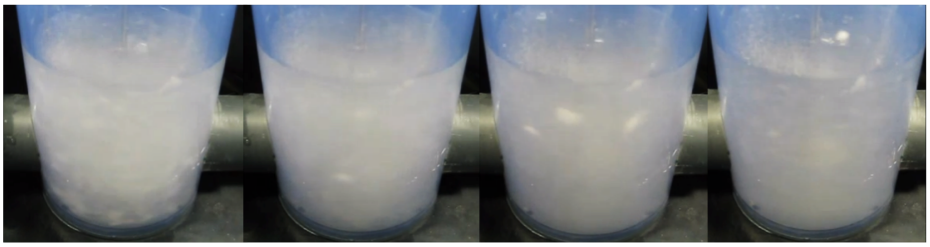

(a) t = 15 s (b) t = 30 s (c) t = 45 s (d) t = 60 s

Figure 10.9: Lumps of maltodextrin DE6 [800 rpm, 5 °C].

Maltodextrin IT6 results

This powder (Fig. 10.10) sank instantly when it contacted the liquid, and at lower agitation speeds it sedimented to the vessel bottom. At [200 rpm, 25 °C] and [200 rpm, 45 °C], floating lumps formed from the sediment, similar to what had been observed for DE21 (Fig. 10.3). Above $N = 600$ rpm reconstitution was normal; however, at $T = 5$ °C the dissolution of individual particles was rather slow, but no lumps formed as they did for the DE6 powder.

<table>
<tr><th>IT6
agglomerated</th><th>5 °C</th><th>25 °C</th><th>45 °C</th><th>65 °C</th><th>Re</th></tr>
<tr><td>200 rpm</td><td colspan="4" rowspan="2">Sedimentation &
floating lumps</td><td>4100</td></tr>
<tr><td>400 rpm</td><td>8100</td></tr>
<tr><td>600 rpm</td><td rowspan="2">Slow
dissolving
(no lumps)</td><td colspan="3" rowspan="3">Instant reconstitution</td><td>12200</td></tr>
<tr><td>800 rpm</td><td>16300</td></tr>
<tr><td>1000 rpm</td><td>20300</td></tr>
</table>

Figure 10.10: Maltodextrin IT6 regime map.

10.1.3 Discussion

Four major types of limiting regimes have been observed for maltodextrin; reconstitution can be “normal”, or it can be limited by undesirable floating, sedimentation or by slow dissolving. By observing a single map, conclusions about the influence of T and N on powder behavior can be drawn. In general, an increase in both T and N improved reconstitution, but depending on the other conditions, the way in which these two variables influence the reconstitution process changes. Both improve sinking if sinking is a problem (e.g. for maltodextrin DE6), and help

reduce sedimentation, prevent lump formation, and facilitate the dissolving of individual particles. By comparing maps for different powders, one can understand the influence of size enlargement (by comparing maltodextrin DE vs. IT powders), and molecular weight (by comparing powders of different DE values) on the rehydration process.

Size enlargement helped improve the wetting/sinking of powders, especially for maltodextrin DE6 which tends to float at the liquid surface at lower agitation speeds. This is due to the improved capillary rise into the porous granules that help submerge the solids below the liquid surface. Secondly, the agglomerated powders were less likely to form lumps; the proposed mechanism responsible is that the granules have better permeability to water, thus when water penetrates the granules it helps disperse them more easily; this also may allow for faster dissolving of individual primary particles due to an increase in contact area between individual particles and water.

The **molecular weight** plays a defining role in determining the type of limiting regime for reconstitution. The longer-chained spray dried powder, maltodextrin DE6, did not wet and sink readily, whereas maltodextrin DE21, which has a similar particle size, sank instantly. In order to better understand the differences in capillarity between the two materials, penetration experiments were performed using tablets of compacted DE21 and DE6 using a tabletting simulator (MedelPharm StylOne Model 105ML, France). The two tablets have equal porosity (36 %)[2] and are placed into a thin layer of deionized water (25 °C) dyed with methylene blue. It is clear from the penetration time-lapse (Fig. 10.11) that capillarity effects are at least partially responsible for the poor sinking of DE6 powders.

To specifically test the difference in *wetting* behavior, the sessile droplet method (§ 1.1) was used to measure the contact angle θ formed between the liquid and the solid surface. A glass slide was dip-coated in 15 % w/v maltodextrin solutions and dried at 80 °C in a convection oven for 15 h to obtain smooth surfaces of maltodextrins DE6 and DE21. Droplets of deionized water were then deposited onto the surfaces at 25 °C and the contact angle formed between the droplet and the material was determined using image analysis (programmed using Fiji, an open-source software); essentially the boundary formed by the droplet is recognized and the contour is approximated to obtain the contact angle from the slope of this curve where it

[2]These two materials needed to be compacted to different pressures to obtain the same porosity – see Mitchell et al. (2011).

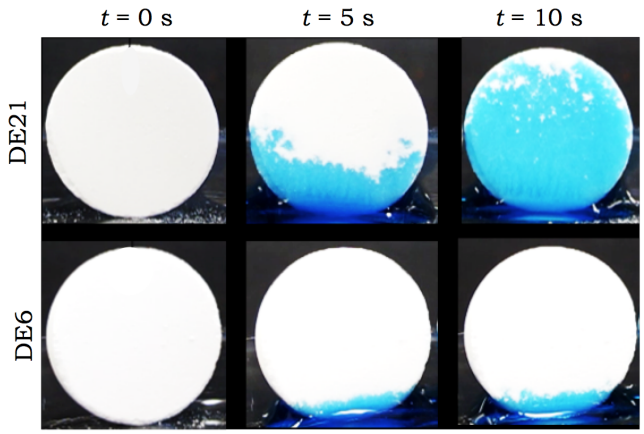

Figure 10.11: Imbibition of (dyed) water into tablets of maltodextrin DE21 and DE6.

intersects the baseline (Fig. 10.12 insert). As discussed in § 1.1, generally a $\theta < 90°$ is said to indicate "wetting behavior" and a $\theta > 90°$ indicates "non-wetting behavior". Results from the measurements are shown in Fig. 10.12.

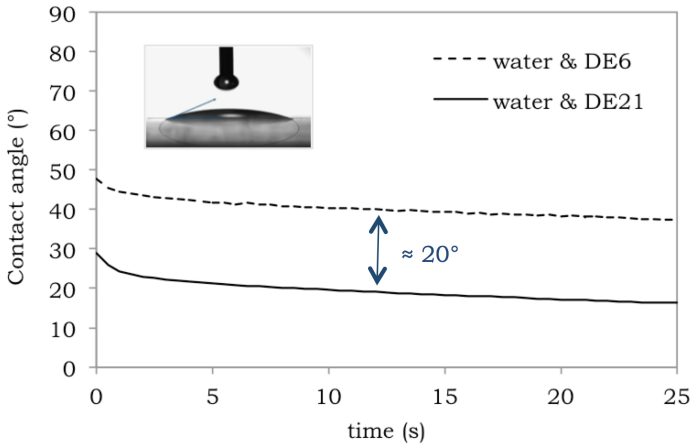

Figure 10.12: Contact angle of water with dip-coated maltodextrin slides.

When the water droplet contacts the maltodextrin-coated surface it spreads, and due to the hydrosoluble nature of the polymer, instead of reaching an equilibrium state the droplet continues to spread due to mechanisms discussed in § 1.1. However the respective contact angles for the first 30 s of spreading were $\theta_{DE6} \approx 40°$ and $\theta_{DE21} \approx 20°$. If one assumes that capillary rise behaves according to Washburn's law (Eq. 1.14)[3], one can use this equation to compare how the change in θ might be expected to affect capillary rise. The ratio of the

[3] As discussed in § 1.1, complex geometric considerations may complicate matters with regards to capillary rise, and thus possibly an even lower θ is needed for good capillarity than Washburn's equation could predict.

penetration distances l for any time t would be:

$$\frac{l_{\text{DE6}}}{l_{\text{DE21}}} = \sqrt{\frac{\cos 40^\circ}{\cos 20^\circ}} \approx 0.9 \tag{10.1}$$

If Washburn's equation for this system is applicable, then it appears that such a smaller difference in θ for the two materials might not be the only cause for the worse sinking for the higher-MW powder.

Another interesting observation is that when DE6 is placed in a static volume of water, a very conspicuous gel-like layer forms at the solid-liquid interface, and a sort of raft-like structure forms. In Fig. 10.13a, the water interface actually curves downward closer to the heap, and the floating appears to be due to a buoyant effect, as a result of the clogged pores due to the viscous layer. A bottom-view of this layer (Fig. 10.13b) also shows air bubbles escaping out of the bottom, presumably due to pore collapsing.

(a) (b)

Figure 10.13: Maltodextrin DE6 on a static volume of deionized water at 25 °C.

Fig. 10.14 is a picture taken from one of the [600 rpm, 25 °C] trials for maltodextrin DE6. A bubble-like lump forms at the liquid surface (a), which "pops" spontaneously (b). A viscous layer of solution can be clearly seen that encapsulates dry powder on the inside – the layer forms a boundary between the dry particles and the liquid medium.

Figures 10.3, 10.13 and 10.14 support the description of "lumps" by Parker et al. (2000) (see § 1.4). From these results, it is evident that a viscosity-related mechanism may be involved in the poor reconstitution of high-MW powders. For a further discussion about viscosity effects, see § 12.3.

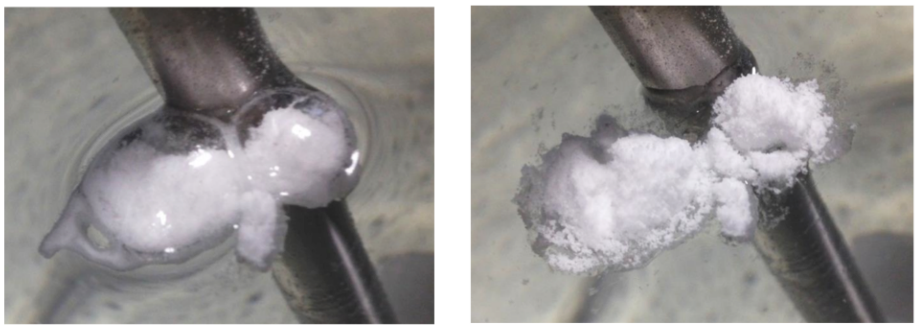

(a) (b)

Figure 10.14: Bubble-like lump forming for maltodextrin DE6 at liquid surface.

§10.2 Water Activity

As mentioned in previous chapters, the water activity a_w of amorphous materials can significantly affect the powder's behavior, for instance with regards to caking, or in some cases, solid-phase crystallization, both of which may result in poor reconstitution properties (Ch. 2). However, with regards to how a_w itself affects the reconstitution of a powder, the literature appears to be conflicting. Dupas et al. (2013) demonstrated how an increase in the a_w (and moisture content) improves wetting (see § 1.1). However Marabi et al. (2007) noticed that an increase in a_w leads to a less exothermic dissolving, which they claim would result in delayed reconstitution; however, as mentioned in § 1.4, they *only* tested this with skim milk powder, a powder containing lactose that can crystallize. Dupas (2012) describes mechanisms explaining why the crystalline form of sugars such as lactose have worse wetting properties than their amorphous forms (§ 1.1). In the current section, the *overall* reconstitution of an amorphous material, maltodextrin (§ 8.1), is studied at different a_w values.

10.2.1 Powder equilibration to desired a_w

According to Eq. 8.1, the a_w of a material at a specified temperature will be equal to the relative humidity (RH) of the surrounding air once equilibrium has been reached. Accordingly, powders were subjected to air of different RH values – Marabi et al. (2007), Syll et al. (2012), and Osborne et al. (2013) did this by placing powder in desiccators containing saturated salt solutions. In an earlier project (Mitchell et al., 2011) the current author equilibrated powders

in an environmental chamber by spreading out powders into thin layers on trays, and a fan is used to circulate the air about the chamber, and the air is adjusted to the corresponding RH. In the same project, it was demonstrated using a dynamic sorption device (DVS) (SPS-11, Mercer Instruments, Switzerland) that equilibrium could be attained much more quickly if the temperature T is also increased during equilibration, such that $|T - T_g|$ is relatively low, for increased molecular mobility and thus moisture diffusivity.

In the current project, a similar technique was used on a larger scale inside the environmental chamber: the amorphous powder was placed in a chamber for two days (in thin layers) at the RH corresponding to the desired moisture content, measuring the T_g (§ 8.4) at regular intervals. Once reached, the powders were placed in hermetically sealed aluminum bags, and the T was increased to ca. 5 °C below the T_g – this heat shock was applied for 2 h before cooling.

In order to understand how the a_w will affect the T_g of the two materials (DE21 / DE6) used, (simplified) state diagrams were supplied by the Nestlé Water Management Team (Fig. 10.15), fitted using the Gordon & Taylor equation (Eq. 10.3) and the GAB equation (Eq. 10.4), which are described later in the current section.

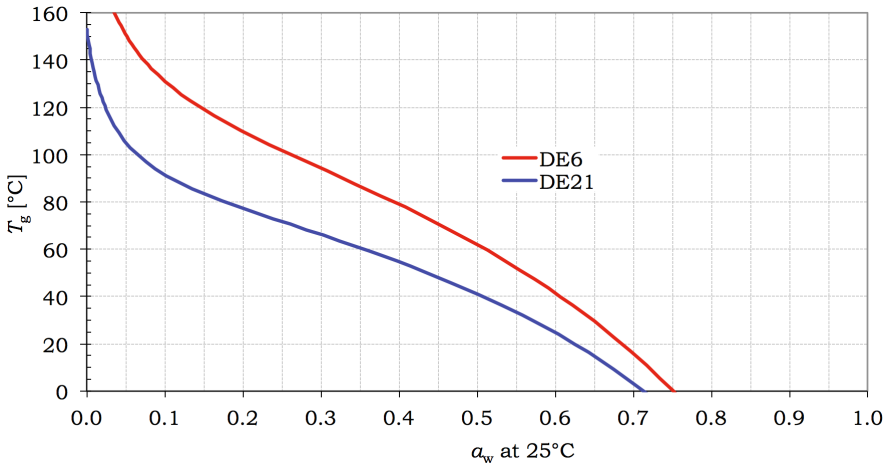

Figure 10.15: State diagrams for maltodextrins DE21 and DE6.

For both powders, increasing the moisture content (and a_w) plasticizes the molecules, allowing for glass transition at a lower T, as discussed in Ch. 2. For each a_w value, the higher-MW (molecular weight) material, DE6, has a higher T_g; this is because of clusters of the larger polymer chains needing more movement before they can "slip past one another" (see Palzer (2007)). This higher T_g as a function of MW is described by the (simplistic)

Fox-Flory equation (Eq. 10.2) (Fox and Flory, 1950):

$$T_g = T_{g,\infty} - \frac{A}{M_w} \tag{10.2}$$

where $T_{g,\infty}$ is the theoretical T_g of a polymer with a chain of infinite length, M_w is the molecular weight (mass), and A is a fitting parameter. According to Okos et al. (2007), its practical use is rather limited for real applications.

For equilibration purposes it is also important to keep the T_g in mind to avoid caking, as this could reduce dispersibility and introduce complications – thus the experiments are limited to a a_w range for which $T_g \gtrapprox 25\,°\mathrm{C}$. This range is of course larger for DE6 ($a_w \lessapprox 0.65$) than for DE21 ($a_w \lessapprox 0.55$). Moreover, Tam (2013), an MEng student supervised by the current author, investigated the effect of a_w on the reconstitution properties of maltodextrin DE21 (using default conditions (§ 7.2), 25 °C, etc.), and observed no difference for DE21 (for $0.1 \leq a_w \leq 0.5$), since reconstitution for this powder was very quick under all conditions. Thus for the current project only the higher-MW material (DE/IT6) was chosen for a_w experiments.

10.2.2 T_g depression during plasticization

In order to describe how T_g is depressed as a function of moisture content, the Gordon & Taylor equation (Eq. 10.3) (Gordon and Taylor, 1952) is used:

$$T_g = \frac{\overbrace{(1 - w_{\mathrm{wb}})\, T_{\mathrm{g,s}}}^{\text{material}} + \overbrace{k\, w_{\mathrm{wb}}\, T_{\mathrm{g,w}}}^{\text{water}}}{(1 - w_{\mathrm{wb}}) + k\, w_{\mathrm{wb}}} \tag{10.3}$$

where k is an empirical fitting parameter, $T_{\mathrm{g,s}}$ is the T_g of the dry solid material, w_{wb} is the water content (on a wet basis), where the material content $= 1 - w_{\mathrm{wb}}$. $T_{\mathrm{g,w}}$ is the T_g of water (amorphous ice), where $T_{\mathrm{g,w}} \approx 136\,\mathrm{K} = -137\,°\mathrm{C}$ (Capaccioli and Ngai, 2011). To describe the relationship between a_w as a function of moisture content, a sorption isotherm can be constructed, and the data can be fitted empirically using the GAB (Guggenheim, Anderson,

deBoer) equation Guggenheim (1966):

$$w_{\mathrm{db}} = w_{\mathrm{m,db}} \cdot \frac{C\,k\,a_w}{(1 - k\,a_w)(1 - k\,a_w + C\,k\,a_w)} \tag{10.4}$$

where w_{db} is the moisture content (on a *dry* basis), $w_{\mathrm{m,db}}$ is the moisture content of a monomolecular layer of water forming on the solid surface, and C and k are empirical fitting parameters.[4] Since Eq. 10.3 uses moisture content on a wet basis (w_{wb}) and Eq. 10.4 on a dry basis (w_{db}), it is useful to understand how the convert between the two:

$$w_{\mathrm{wb}} = \frac{w_{\mathrm{db}}}{w_{\mathrm{db}} + 1} \tag{10.5}$$

$$w_{\mathrm{db}} = \frac{w_{\mathrm{wb}}}{1 - w_{\mathrm{wb}}} \tag{10.6}$$

10.2.3 Experimental conditions

For the a_w experiments, both maltodextrins DE6 and IT6 were equilibrated to a_w values of 0.22 ($T_g \approx 105\,^{\circ}\mathrm{C}$) and 0.56 ($T_g \approx 50\,^{\circ}\mathrm{C}$) at 25 °C. The DE6 powder was reconstituted at $T = 25\,^{\circ}\mathrm{C}$ and $N = 900\,\mathrm{rpm}$ (sinking-limited conditions), and the IT6 was reconstituted at $T = 25\,^{\circ}\mathrm{C}$ and $N = 600\,\mathrm{rpm}$ (dispersing-limited) – see § 10.1. These conditions were chosen to focus both on the wetting/sinking and dispersing/dissolving effects of a_w, respectively.

The *amount* of powder added was slightly different for low-a_w and high-a_w conditions. For low-a_w powder, the default amount of powder was added (§ 7.2). However, a slightly higher mass of high-a_w powder was added (and slightly less water was added to the vessel prior to powder addition), in order to maintain the total amount of maltodextrin material in the final solution constant. This was done using the GAB data (Eq. 10.4) (fitting parameters not reported due to confidentiality concerns), and it worked out to be about 1 g extra high-a_w powder to be added. Each trial was performed in triplicate to ensure consistent behavior.

[4] For $k = 1$, the GAB equation reduces to the BET (Brunauer, Emmett and Teller) equation.

10.2.4 Results of the a_w study

The FBRM data (Fig. 10.16) demonstrate that the IT6 powder dispersed more rapidly throughout the vessel prior to dissolving than did DE6, even though IT6 was reconstituted at a lower N.

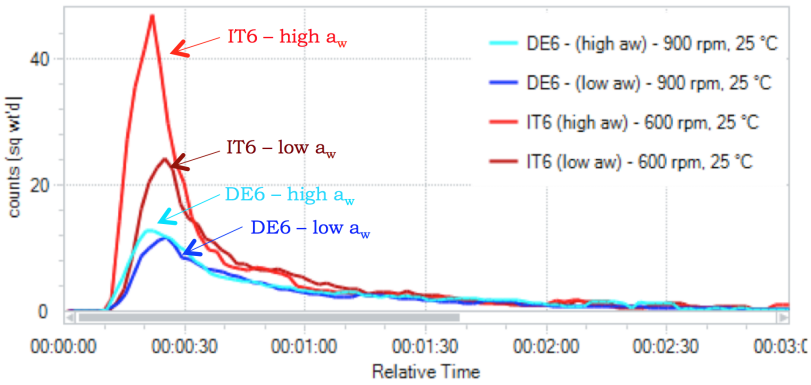

Figure 10.16: FBRM results for maltodextrins DE6 and IT6 at low- and high-a_w.

It is also apparent that the high-a_w powder appears to disperse slightly more rapidly than the low-a_w material for both IT6 and DE6, although dissolving appears to be similar between high– and low-a_w conditions. However, the videos reveal that wetting/sinking is slower, and often less complete, for low-a_w conditions (compare Figures 10.17 and 10.18).

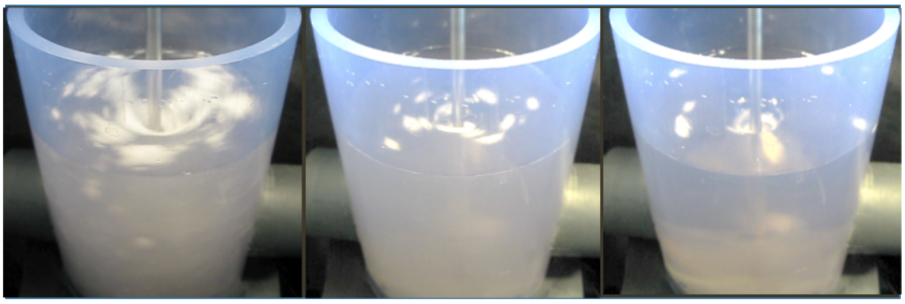

(a) t = 0 min (b) t = 1 min (c) t = 2 min

Figure 10.17: Video time-lapse for maltodextrin DE6 at low-a_w. Fish eyes remain at the surface for several minutes.

Another interesting observation is that if one looks at the stainless steel vibratory feeder surface after powder addition, the low-a_w powder left a dusty residue on the surface, whereas the feeder was relatively clean following addition of the high-a_w powder, indicating better flowability (Fig. 10.19).

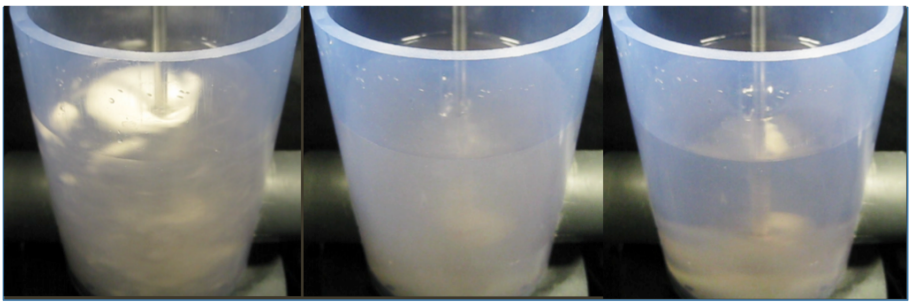

Figure 10.18: Video time-lapse for maltodextrin DE6 at high-a_w. No lumps form.

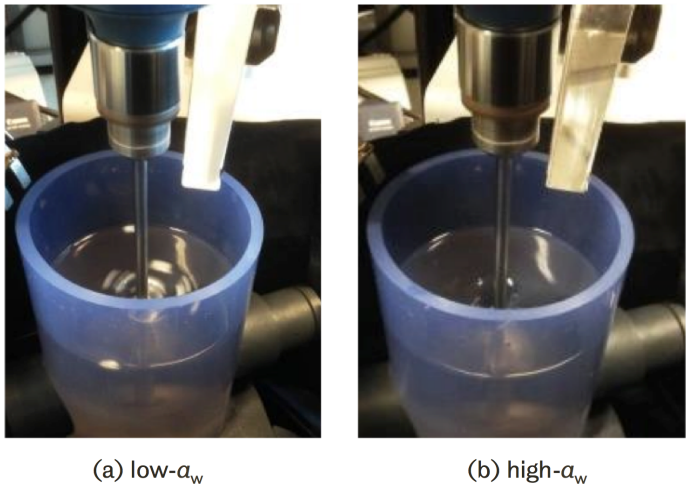

Figure 10.19: Video frame at $t = 2\,\text{min}$ for (a) low-a_w and (b) high-a_w maltodextrin DE6. Note the difference in vibratory feeder powder coverage.

When looking at the IT6 results, there are no fish eyes left after the powder is added, presumably due to good capillarity and water-logging (§ 1.1), however if one considers the first 4 s of reconstitution for low– vs. high-a_w (Figs. 10.20 and 10.21), one observes faster capillary penetration (and better overall dispersion) for the *high*-a_w IT6.

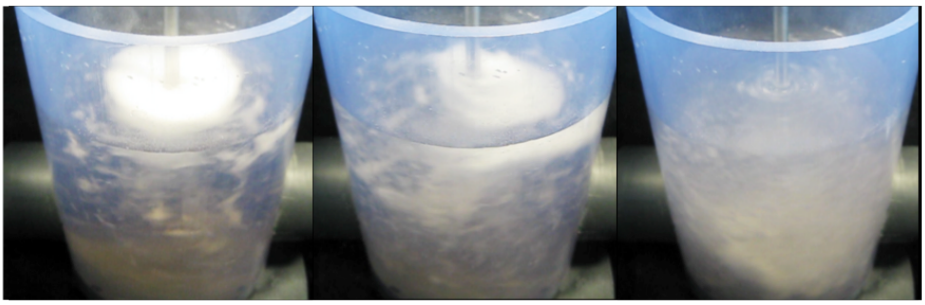

(a) t = 0 s (b) t = 2 s (c) t = 4 s

Figure 10.20: First 4 s of reconstitution of maltodextrin IT6 at low-a_w.

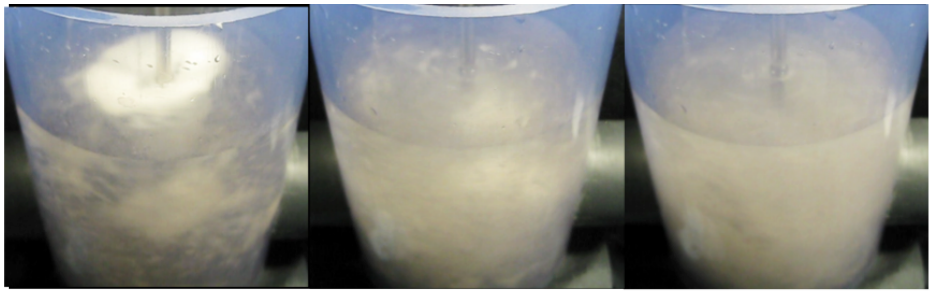

(a) t = 0 s (b) t = 2 s (c) t = 4 s

Figure 10.21: First 4 s of reconstitution of maltodextrin IT6 at high-a_w.

10.2.5 Discussion of a_w results

It has been demonstrated in the current section that an increase in a_w of an amorphous powder *improved* the wetting/sinking behavior of the powder, and thus reconstitution overall. It is important to note that for the powder and conditions used, solid-phase crystallization and caking/glass transition effects were *not* a concern (§ 8.1). The results from the current section are *not* in agreement with Marabi et al.'s hypothesis that a more exothermic dissolution results in faster rehydration – for more information about what phenomena might have actually been responsible for their observations, see § 1.4. The results *were* very much in agreement with Dupas et al. (2013), who explained that an increase in a_w can improve a material's wetting properties (§ 1.1), which may have improved the capillarity of water into the material. Another consideration is that at a higher a_w, molecules will have more mobility, and thus may be easier to untangle. As explained in § 1.4, a phenomenon can occur for

polymers (that is essentially a glass transition) during polymer dissolution, and thus if the material can more easily achieve glass transition, dissolving may be faster – Dupas et al. (2014) also demonstrated that glass transition to a rubbery state from a glassy state further improves the wetting properties of amorphous materials (see § 1.1).

Moreover, flowability appeared to improve as well at higher a_w values. However, before recommending increasing the a_w of all food powders, there are a number of other concerns to be considered, discussed in § 15.6.

Chapter 11

Mapping the Reconstitution of Colloid-forming Powders

Not everything that can be counted counts, and not everything that counts can be counted.

Albert Einstein

In the two previous experimental chapters, the powders used (maltodextrins) were relatively simple in composition, and the material completely dissolved. However, in most food applications, powders are much more complex, containing ingredients (like dairy or cocoa powders) that do not completely dissolve and thus become turbid upon reconstitution; this turbidity plays a very important role in data analysis. Moreover, such powders may behave very differently from powders like maltodextrin; therefore, it is worth studying some of these more complex materials to better understand what mechanisms may be responsible for powder dispersion behavior.

Contents

§11.1 Milk Maps

11.1.1 Experimental conditions

The experimental conditions chosen were very similar to those used in § 10.1 for maltodextrin powders; a wide range of N (600, 800, and 1000 rpm) and T (5, 25, 45, and 65 °C) were used, at different combinations in order to produce "maps." At least two replicates were performed for each trial to ensure that the behavior was consistent.[1] The skim milk powder (SMP) and

[1] $3N \times 4T \times 2$ reps $= 24$ trials per map.

whole milk powder (WMP) used was described in § 8.2; the a_w (at 25 °C) was 0.2 ± 0.03. All other experimental conditions were default (§ 7.2).

11.1.2 Use of novel rig to analyze complex colloid-forming powders

Unlike in Chapters 9 and 10, where the FBRM sizing information was too noisy to interpret, for milk powders this information *was* very interesting to describe not only the kinetics of reconstitution, but also the *extent* of dispersing. For FBRM sizes (chord length, § 5.9), there are several options for the operator. For instance, in the current chapter, the (unweighted) counts were extracted above and below a certain user-defined size threshold (150 µm) in order to track the *lumps* (in green color in the curent thesis), and fines (red color), respectively.[2] Another option for showing sizing data is to observe a three-dimensional surface plot, where the size distribution is plotted as a function of time. Plotting the mean size over time is also a possibility. As mentioned in § 9.4, different weighting functions can also be applied to sizing data in order to emphasize either fine particles (unweighted counts, i.e. $\gamma = 0$, cf. Eq. 9.10) or larger particles (usually square-weighted, i.e. $\gamma = 2$); in the current section, it was found via trial-and-error that unweighted sizes were more interesting to consider for SMP, whereas square-weighting was often more interesting for WMP.

With regards to the *videos*, unlike in Ch. 10, where a clear solution was formed upon dissolution, for milk the turbidity of the beverage rendered observations of the *side* of the vessel rather uninteresting. However, with regards to the *sinking* behavior, in Ch. 10, if floating layers did form, they often remained present for hours, due to the mechanisms involved in their formation, discussed earlier. However for milk, sinking tended to be more *gradual*; thus the sinking time t_{sink} was particularly interesting to study as a function of temperature T, agitation speed N, and fat content. Thus the camera was positioned from *above* the vessel, in order to obtain more accurate t_{sink} data. The value of t_{sink} is defined in the current report from the time when the last particle contacts the liquid surface to the time that the last particle disappears beneath the surface. This is done by counting the number of frames and dividing by the frame rate (30 fps).

[2] Choosing 150 µm as a cut-off was somewhat arbitrary. It was chosen based on the fact that in the IDF "dispersibility" technique (§ 5.1), a 150 µm mesh sieve is used. As discussed in Ch. 14, it is possible that a different cut-off may be more appropriate for different contexts.

Once again, conductivity measurements were not particularly useful. Whereas for maltodextrin, the conductivity probe most likely detected mineral impurities (§ 14.1); in the case of milk, it is detecting the mineral content of the powder, which is ca. 8 % of the powder mass (§ 8.2). However, it is important to realize that minerals are *not* expected to significantly contribute to the dispersing behavior of powders; if lumps form, minerals may simply wash off the lump surface, resulting in misleading results. It was discovered that the conductivity measurements ("t_{90} value") correponded very well to the t_{sink} for all conditions, simliar to in Ch. 9 for maltodextrin. For instance in Fig. 11.1, SMP and WMP results are shown at $T = 25\,°\text{C}$ and $N = 1000\,\text{rpm}$.

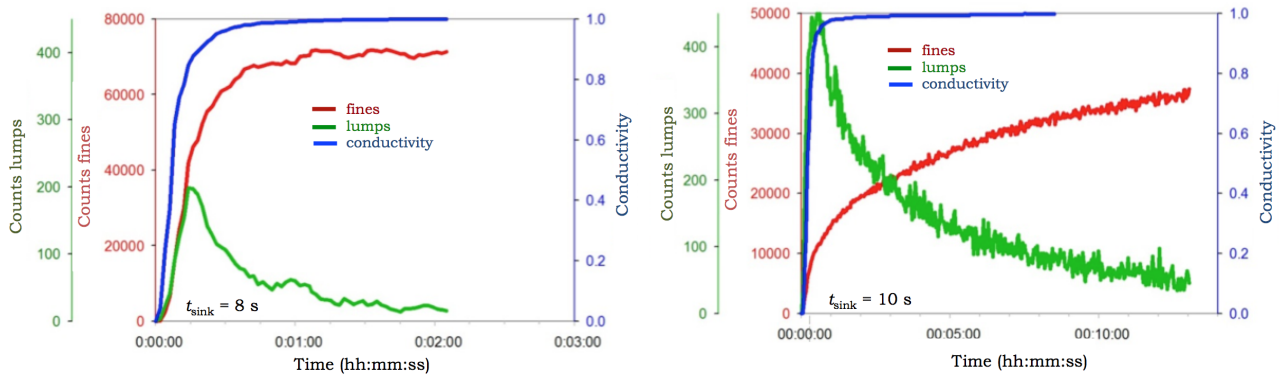

(a) SMP (b) WMP

Figure 11.1: Direct comparison of FBRM and conductivity measurements for SMP and WMP.

For SMP, the conductivity measurements are not too different from the counts of fine particles. However for WMP there is a huge difference between the FBRM counts and conductivity measurements – this can be explained due to the fact that sinking was very quick ($t_{\text{sink}} = 10\,\text{s}$) but dispersing took more time. Whereas for SMP, once the powder sank, dispersing occurred relatively quickly. Therefore is it once again recommended to abandon a conductivity approach for reconstitution analysis (§ 14.1).

11.1.3 Sinking & regime maps

The results for the sinking times (averages) are shown in Tab. 11.1.

The boxes shaded in blue indicate that SMP sank faster than WMP, boxes shaded in green

Table 11.1: Average t_{sink} values for SMP (top) and WMP (bottom).

SMP WMP	5 °C	25 °C	45 °C	65 °C
600 rpm	41 min > 1 h	7 min 47 min	40 s 30 s	18 s 15s
800 rpm	5.5 min > 1 h	2 min 5 min	10 s 5 s	2 s 2 s
1000 rpm	50 s 1 min	8 s 10 s	1 s 1 s	< 1 s < 1 s

indicate that WMP sank faster than SMP, and gray shading indicates that t_{sink} values for SMP and WMP were very similar. One interesting realization is that at lower T (5 and 25 °C), SMP sank more quickly than WMP, as one would expect due to the hydrophobicity of the fat, inhibiting wetting and capillarity effects. However at $T = 45$ and 65 °C (at least for low N), WMP sank more quickly than SMP – this could be explained due to the fact that at 45 °C, one would expect all of the solid fat on the particle surface to melt off of the particles, allowing for good liquid penetration into the rest of the particle. For SMP, on the other hand, which contains < 1 % fat on average, an increase in T may lead to significant swelling of other dairy components (particularly casein; § 6.2), which is present in much greater quantity than fat (§ 8.2), and thus would inhibit the capillarity needed for water-logging/sinking (§ 1.2).

For both powders, increasing the T improved the t_{sink} for all values of N; for SMP, this can be explained due to the fact that even for a small overall amount of fat in the particles, the residual fat content can be over-exaggerated on the particle surface, as discussed in Ch. 2. Increasing the N for all values of T also improved the sinking of both powders; this can be explained due to the greater downdraw at increasing N (§ 3.4). By studying both the sinking behaviors as well as the FBRM results for all trials, "limiting-regime maps" (Figures 11.2 and 11.3) were constructed (similar to in Ch. 10) to describe the reconstitution behaviors.

SMP	5°C	25°C	45°C	65°C	Re
600 rpm	Very slow sinking	Gradual sinking, gradual dispersing	Fast sinking, gradual dispersing	Fast sinking, quick and complete dispersing	12200
800 rpm	Gradual sinking, lumps do not disperse readily				16300
1000 rpm	Sinks readily, lumps do not disperse readily	Fast sinking, gradual dispersing			20300

Figure 11.2: Limiting regime map for skim milk powder.

<table>
<tr><th>WMP</th><th>5°C</th><th>25°C</th><th>45°C</th><th>65°C</th><th>Re</th></tr>
<tr><td>600 rpm</td><td colspan="2" rowspan="2">Static when hits liquid – extremely slow sinking</td><td rowspan="3" colspan="2">Fast sinking, fast & complete dispersing</td><td>12200</td></tr>
<tr><td>800 rpm</td><td>Gradual sinking, gradual dispersing</td><td>16300</td></tr>
<tr><td>1000 rpm</td><td>Gradual sinking, lumps do not disperse easily</td><td>Fast sinking, gradual disper-sing of lumps</td><td>20300</td></tr>
</table>

Figure 11.3: Limiting regime map for whole milk powder.

The maps indicate that both powders, in general, improved with both sinking and dispersing as the T and N were increased; best overall behavior was at high T and N (together). However at 5 °C (where $\approx$ 80 % of the fat would be expected to be solid (Kim et al., 2005b)), lumps were very difficult to disperse, even when sinking was very fast (i.e. at 1000 rpm), but dispersing (and sinking) was improved as the T increased, which was most likely related to fat melting. One notable exception is at the "top-right corner" of the WMP map, where at 600 rpm, dispersing did not appear to be improved at 65 °C (explained in the following discussion).

11.1.4 A closer look at SMP results

Not all of the FBRM results are shown in the current report, due to the large amount of space it would require; however, some results were selected based on the mapping results for further discussion. The FBRM results (lumps vs. fines) for SMP at 25 °C demonstrate that dispersing was faster as the N increased; it is also interesting to note that the maximum number of lumps detected by the probe was higher as the N increased (Fig. 11.4). This can be explained by the faster sinking of the powder, as well as the greater downdraw, which would bring more lumps closer to the probe window – these lumps dispersed quickly at high N as well – the final number of fines was slightly lower at 600 rpm compared to 800 or 1000 rpm, indicating less complete dispersing.

However at 45 °C (Fig. 11.5), one does not see a strong influence of N on the kinetics or on the *extent* of dispersing – the only major difference is that the maximum number of counts of lumps obtained was greater at higher N, as more powder was quickly incorporated into the liquid. Very similar results were obtained at 65 °C (not shown).

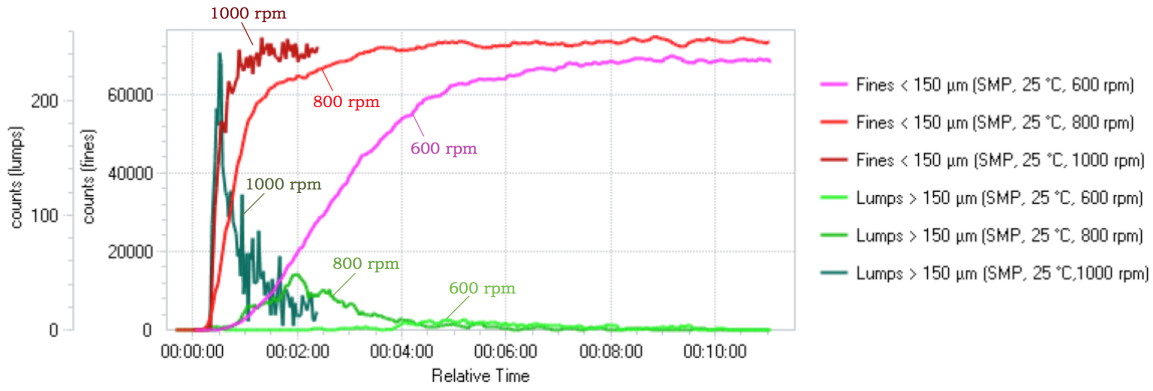

Figure 11.4: FBRM results for SMP at 25 °C.

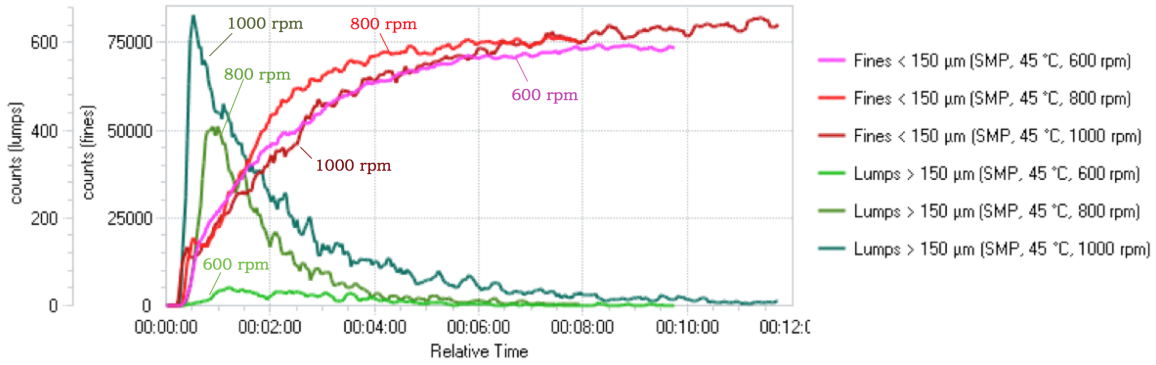

Figure 11.5: FBRM results for SMP at 45 °C.

11.1.5 A closer look at WMP results

For WMP at 25 °C, many more lumps were seen compared to SMP at the same T (Fig. 11.6). It is very clear that increasing N improves both the kinetics and the extent of dispersing, but also the improved sinking behavior should be kept in mind.

For the 600 rpm result in Fig. 11.6, the number of lumps increases gradually to a plateau, then at around 42 min[3] the powder suddenly becomes entrained (Fig. 11.7).

The videos show that around the time when there is an increase in the lumps (Fig. 11.6) at about 45 min, more of the floating layer sinks into the vessel, but much of the powder still floats near the liquid surface (an indication of entrapped air in the lump; § 10.1). Another interesting observation is that the *evolution* of lump population also depends on N at 25 °C; see the surface plots in Fig. 11.8.

[3]Entrainment did not always occur at 42 min, but always at $t > 30$ min.

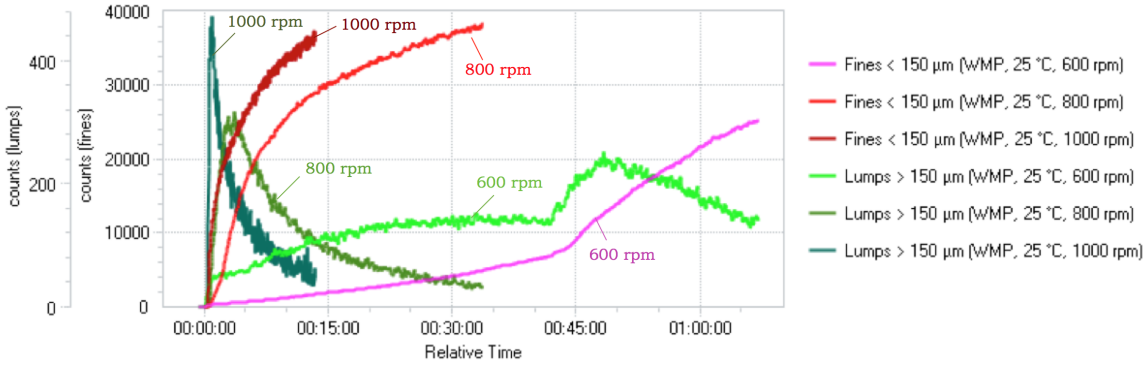

Figure 11.6: FBRM results for WMP at 25 °C.

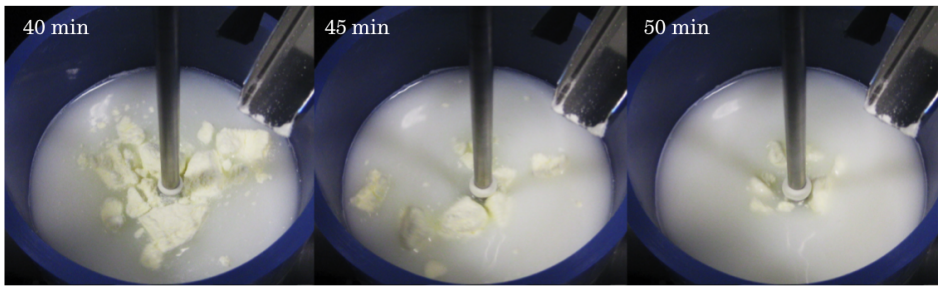

Figure 11.7: Time-lapse of slow WMP sinking at [25 °C, 600 rpm].

At 600 rpm, there is a very gradual increase in lumps (corresponding to slow sinking), where the number of lumps levels off, indicating that the energy supplied by the impeller is not great enough to adequately disperse lumps. However, the behavior is very different at 800 and 1000 rpm; there is a *quick* rise in lumps at the beginning of reconstitution (corresponding to faster sinking), followed by gradual dispersing of lumps. What is also interesting to note is that the maximum number of (square-weighted) counts of lumps increases at higher N, but this does not correspond to worse dispersing by any means, but shows that there is an important link between sinking and lump formation.

At 45 °C (Fig. 11.9), the behavior was similar for all values of N, but unlike for SMP, there *was* a clear influence of N on dispersing.

As pointed out earlier, there is an odd behavior in the top-right corner (high T and low N) for the WMP regime map (Fig. 11.3). The results surrounding the [600 rpm, 65 °C] results i.e. the [600 rpm, 45 °C] and the [800 rpm, 65 °C], are plotted alongside this result in Fig. 11.10.

What is particularly striking is that, looking at the number of fines, the initial rise in

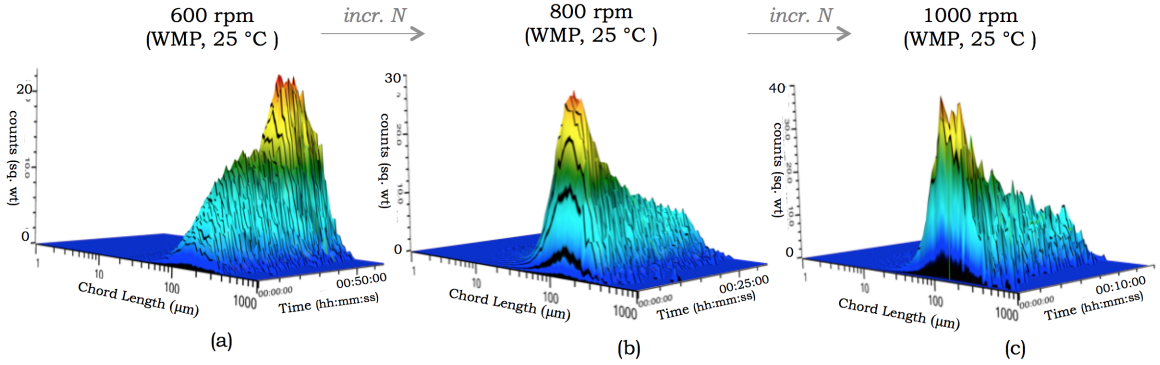

Figure 11.8: Surface plots (square-weighted) for WMP at 25 °C: (a) 600 rpm, (b) 800 rpm, (c) 1000 rpm.

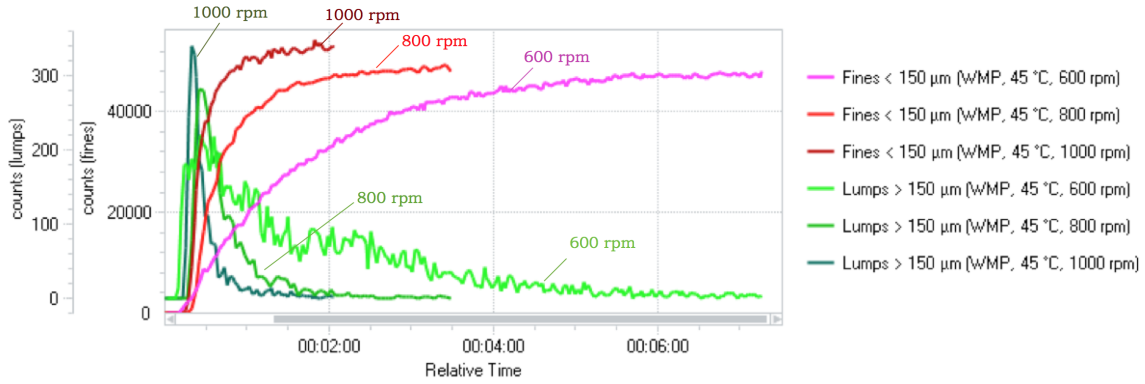

Figure 11.9: FBRM results for WMP at 45 °C.

counts is faster for [600 rpm, 65 °C] compared to [600 rpm, 45 °C] (also corresponding to faster sinking); however, the *extent* of dispersing is greater at the lower T. This is also true looking at the lumps – at [600 rpm, 65 °C], lumps form that resist breakage and remain suspended, whereas dispersing was better at a lower T. This formation of "strong lumps" was not observed at [800 rpm, 65 °C], however. Similar trends were also seen looking at the surface plots (Fig. 11.11).

Video time-lapses (Fig. 11.12) of the liquid surface demonstrate that lumps are initially visible at $t = 30$ s for [600 rpm, 45 °C] and [600 rpm, 65 °C], but at 2 min, lumps were only seen for the [600 rpm, 65 °C] trials.

In addition, following one of the WMP [600 rpm, 65 °C] trials, at $t = 15$ min, the reconstituted whole milk was poured through a 63 µm-mesh sieve, and many "specs" (Fig. 11.13) were observed; these were not observed for the other conditions.

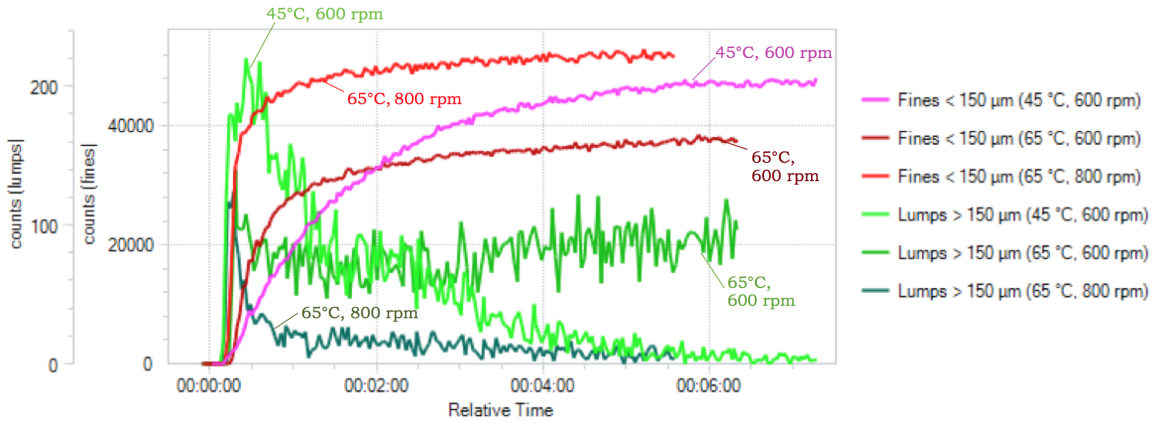

Figure 11.10: FBRM results corresponding to the "top right corner" of Fig. 11.3.

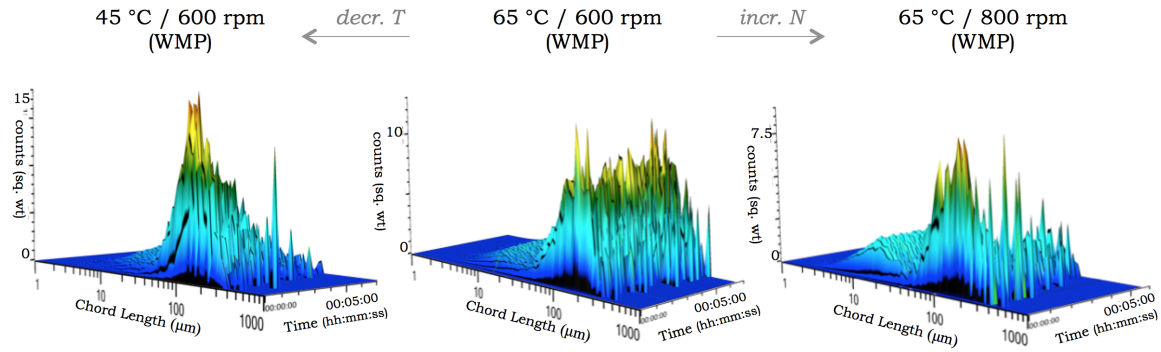

Figure 11.11: FBRM surface plots (square-weighted) corresponding to the "top right corner" of Fig. 11.3.

Thus based on these results, two possible mechanisms are proposed for "lump" formation for WMP at [600 rpm, 65 °C]: the first is related to the discussion of whole milk mentioned in Ch. 2 (cf. coffee instability, where proteins originally associated with the native fat globule membrane denature and form complexes with other components in the milk). The second is related to the swelling of micellar casein and/or increased hydrophobic interactions (§ 4.3) at higher T. However it does not appear that the description of "lumps" given by Parker et al. (2000) (see § 1.4 and § 6.1), related to gelation, is necessarily applicable to the current results.

11.1.6 Discussion

For SMP trials, increasing the T always improved reconstitution for the range tested; under sinking-limited conditions it improved sinking, and for dispersing-limited conditions, it

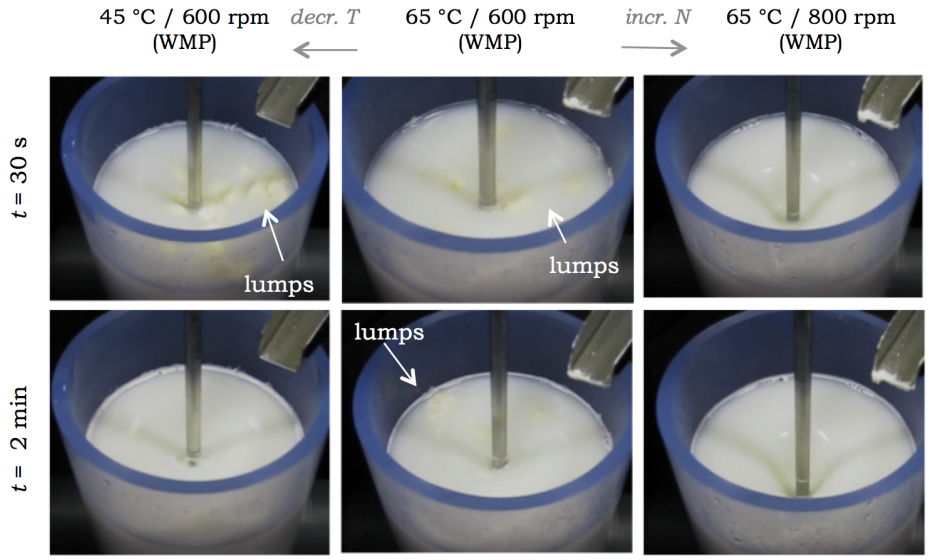

Figure 11.12: Video time-lapses corresponding to the "top right corner" of Fig. 11.3.

Figure 11.13: Specs after pouring a [600 rpm, 65 °C]-reconstituted WMP through a 63 µm-mesh sieve at $t = 15$ min.

improved dispersing. At high T, however, results did not heavily depend on N. For WMP, the story is not quite as straightforward. Increasing the T to 45 °C (where *all* butterfat would expect to melt (Kim et al., 2005b)), vastly improved the sinking of the powder, very much in agreement with Kim et al. (2005b). However, at higher T, lumps were likely to form, unless enough agitation was applied to prevent their formation.

One possible explanation for why t_{sink} was better for WMP than SMP at $T \geq 45$ °C was that for WMP, since so much of the powder (ca. 26 %) consists of fat, most of it could easily melt off, allowing the water to quickly wet the remaining components. Meanwhile SMP, which contains only $\lessapprox 1$ % fat, most likely contains a greater amount of fat on the surface

compared to the bulk (Ch. 2), thus why the increase in T also greatly improves its sinking. However at lower T, this surface fat may only pose a barrier to *initial* wetting/capillarity, but once past this barrier, waterlogging can take place – this is not true for WMP which would contain much more encapsulated fat inside the particle. At $T \geq 45\,°C$, however (where fat is no longer a major barrier to wetting effects), sinking might be slower for SMP than WMP because more solid material (non-melting) is present, and thus the water needs to make its way through the particle structure for water-logging to occur. At higher T as well, liquid penetration may also be hampered by swelling and/or hydrophobic effects – particularly from the high amount of micellar casein (§ 6.2).

Thus it is important to note the effect of T vs. the melting properties of the fat on sinking behavior, and how this relates to overall reconstitution. Marabi et al. (2008b) reported slower "t_{90}" results using a conductivity approach for increasing fat content of a dairy powder at $T = 30\,°C$ and reported slower reconstitution at increasing fat contents (and attributed this to a less exothermic "dissolution"). However, the technique they used (conductivity) is more representative of the *sinking behavior* than dissolution, and butterfat does not dissolve in water from a thermodynamic point of view. The faster reconstitution of WMP than SMP at 45 °C is another observation that contradicts Marabi et al. WMP would *still* be expected to have a less exothermic response than SMP if calorimetric experiments were to be performed. This is an indication that capillarity effects, melting characteristics of fat, and sinking are more likely to be responsible for determining the powder behavior than a "heat mechanism."

§11.2 Cocoa Maps

Similar to milk powders, cocoa powders also do not completely dissolve in water, but instead form a turbid[4] suspension; sizing data from FBRM measurements thus are also interesting to consider. In the current section the effects of temperature T and agitation speed N on the behavior of such powders are considered. While for milk we also considered the effect of fat content, here we look at the effect of lecithination of the particle surface.

[4]For a discussion on the reasons for the turbidity of cocoa suspensions, see § 6.3.

11.2.1 Experimental conditions

Similar conditions were used as for milk powders in the previous section to produce regime maps; i.e. $N = 600, 800, 1000$ rpm and $T = 5, 25, 45, 65$ °C, two replicates per map, default conditions (§ 7.2), etc. To test lecithination effects, the effects of "normal" (unlecithinated) cocoa powder (10 – 12 % fat) (NC) as well as the same powder but lecithinated with 5 % w/w lecithin by spraying on the powder surface (LC), were compared at each condition. For more information about the powders, see § 8.3. As discussed in Ch. 2, lecithin is a mixture of different (zwitterionic) phosphatides that can improve the wettability of hydrophobic surface by water. As mentioned in § 4.2, Freudig et al. (1999) also claims that the negative charge of the lecithin in water can bring about greater electrostatic repulsion (studied further in § 12.1).

11.2.2 Sinking & regime maps

The average sinking time t_{sink} is reported for each condition in Tab. 11.14; t_{sink} is black for non-lecithinated (NC) and brown for lecithinated (LC) cocoa powders.

NC LC	5° C	25° C	45° C	65° C
600 rpm	> 2 h 22 min	8 min 7 min	5 min 7.5 min	2.5 min 9 min
800 rpm	20.5 min 9.5 min	2 min 2 min	30 s 30 s	21 s 30 s
1000 rpm	5.25 min 2.25 min	1 min 5 s	2 s 2 s	1 s < 1s

Figure 11.14: Sinking times for non-lecithinated cocoa (NC) and lecithinated cocoa (LC).

The results show that t_{sink} improved with increasing N, and (in general) with increasing T. Tab. 11.14 is also shaded to show regions where LC sinks faster than NC (no shading), regions where t_{sink} is about the same for NC and LC (blue shading), and regions where NC sinks faster than LC (gray shading). It is clear that at lower T, lecithination helps with poor sinking, however this does not appear to be true at higher T (at least under the conditions tested). Looking at the videos it become clear that a possible mechanism for the worse

swelling at higher T (and low N) might be related to (a) swelling mechanism(s). For instance Fig. 11.15 shows a time-lapse comparison for NC vs. LC at [65 °C, 600 rpm].

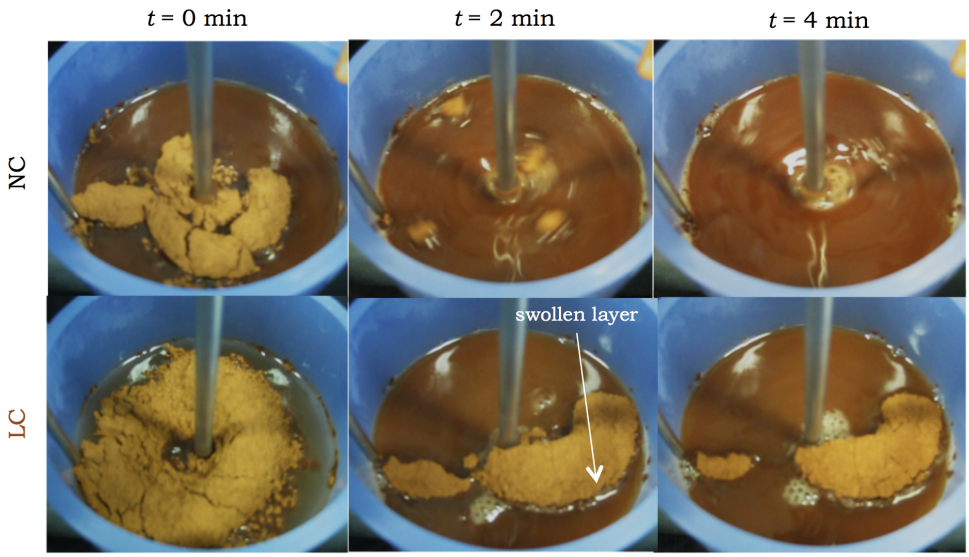

Figure 11.15: Time lapse for non-lecithinated (NC) and lecithinated (LC) cococa at [65 °C, 600 rpm].

For LC, a swollen layer appears between the dry powder heap and the liquid – this does not occur for NC. The mechanism responsible may be similar to that described in Ch. 2 – cf. Westergaard (2004), who stated that if penetration of water into swellable materials is too fast, then swelling may occur faster than particle dispersing can occur. The increase in T may promote the swelling of certain materials in the cocoa powder (e.g. starch; cf. § 6.3) – and the lecithin presence helps the liquid penetrate (too quickly). However at lower T, swelling is less of an issue, thus the lecithin presence may promote good capillarity and water-logging (§ 1.2).

Another observation is that for NC when increasing the T from 25 °C to 45 °C (at 600 rpm), there is not quite the same *dramatic* improvement in sinking for cocoa as there was for milk powder, even though the melting T of the fat crystals would be expected to be below 45 °C (§ 6.3), as was also the case for milk fat. This less dramatic improvement in t_{sink} may be due to the different particle structures of milk vs. cocoa. Firstly the cocoa particles are smaller in size, which may pose an additional barrier to capillarity and downdraw – and higher values of N may be needed. Moreover the morphology of the particles is very different (Fig. 8.4). Milk particles (formed by spray drying; § 2.1), are more spherical and hollow, whereas cocoa powders (formed by pulverizing a pressed cocoa cake; § 6.3), are more irregular and dense. The fact that milk particles are hollow may aid in capillary/water-logging for $T \geq 45$ °C when

the fat is melted.

The rate-limiting regime maps, formed after considering the videos and FBRM results, are shown in Fig. 11.16 for NC and Fig. 11.17 for LC. Maps indicate that in general the degree of dispersing was improved by lecithination, for most conditions.

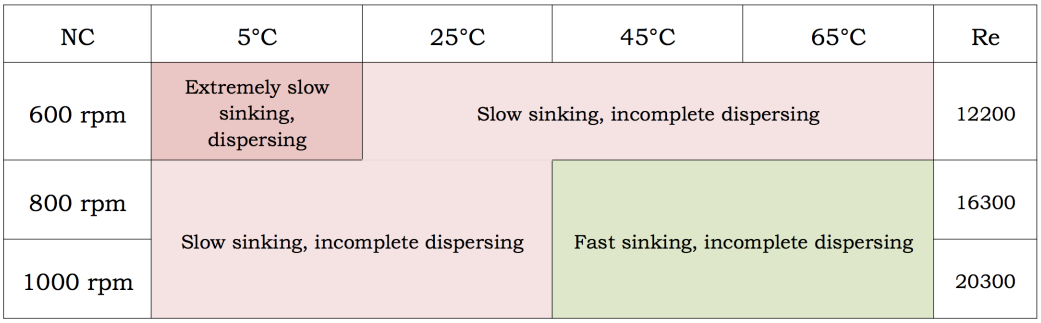

Figure 11.16: Limiting regime map for non-lecithinated cocoa powder (NC).

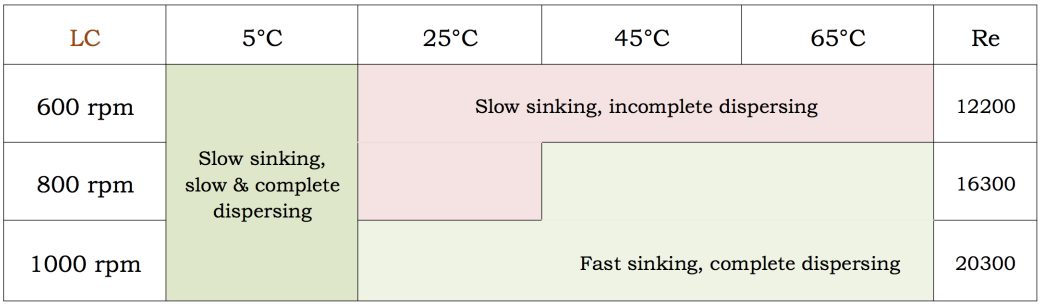

Figure 11.17: Limiting regime map for lecithinated cocoa powder (LC).

11.2.3 FBRM results

Fig. 11.18 shows the evolution of the total (unweighted) counts (a) and the evolution of (unweighted) mean size (b) for NC and LC at $T = 5\,°C$.

Different colors are used for each N applied; the ligher hue (e.g. pink) is for LC; darker colors (e.g. red) are for NC. Looking at the results at 600 rpm (blue), it is clear that the kinetics of dispersion (left) is faster for LC than NC, corresponding to the slower sinking of NC. However observing the *extent* of dispersing (b), there is not a very strong difference in size for NC vs. LC, although LC does have a slightly smaller mean size. At 1000 rpm however, the counts evolution appear quite similar at the beginning, but while the counts for NC increases to a maximum, the counts for LC decreases once all the particles have sunk. It

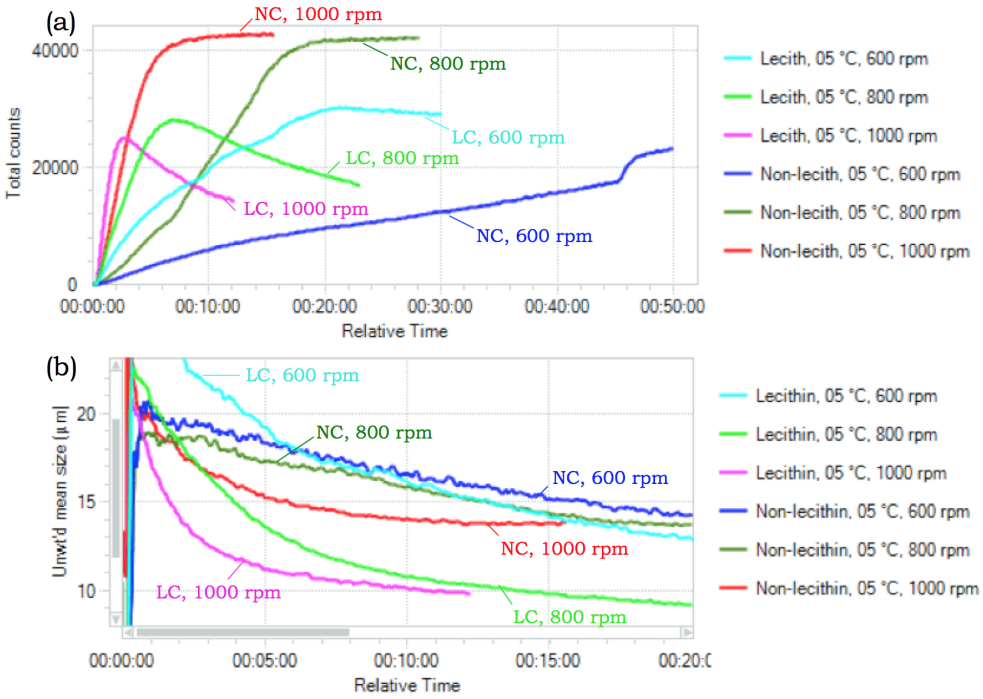

Figure 11.18: FBRM results for NC and LC at 5 °C: (a) total counts (unweighted), (b) mean chord length (unweighted) [µm].

is not entirely clear why this occurs, but one possibility might be that the particles disperse more easily to a small size below the detection limit of the FBRM ($\approx 0.5\,\mu m$). The difference in mean size between the NC and LC for 1000 rpm (and 800 rpm) is apparent in Fig. 11.18. For 800 rpm both the kinetics (sinking) and extent of dispersing are better for LC than NC.

At $T = 25\,°C$ (Fig. 11.19), it is clear that at lower N (600 rpm), both the kinetics (sinking) and the extent of dispersing are improved with lecithination. At higher N, however, the kinetics are very similar, but the extent of dispersing is better for LC than NC.

Unlike at a lower T where LC saw a decrease in total counts, LC counts increase to a maximum value – if the hypothesis about particles dispersing to below the detection limit are true (for 5 °C results), then possibly the particles do not disperse to the same degree at 25 °C, possibly related to greater swelling before dispersing can take place.

Results at $T = 45\,°C$ (Fig. 11.20) indicate no significant difference in kinetics or dispersing for NC vs. LC – only the N determines kinetics and dispersing extent.

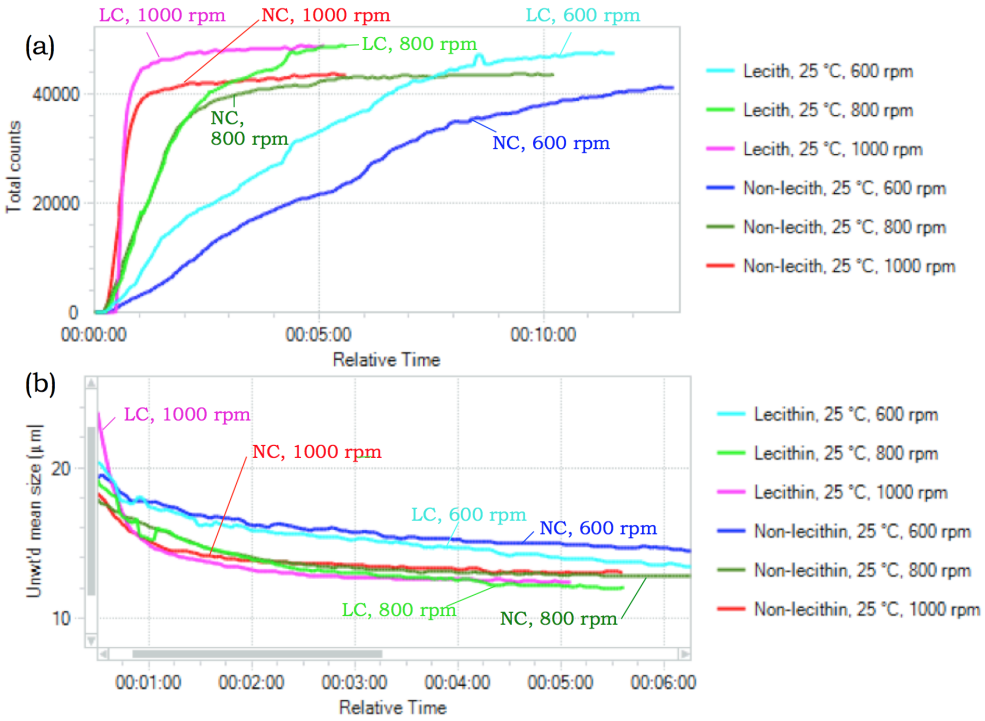

Figure 11.19: FBRM results for NC and LC at 25 °C: (a) total counts (unweighted), (b) mean chord length (unweighted) [µm].

For $T = 65\,°C$ (Fig. 11.21), the opposite behavior is observed with regards to NC vs. LC, particularly at $N = 600\,\text{rpm}$ and 800 rpm. Not only are kinetics slower (slower sinking) for LC but also the extent of dispersing is worse; this may also be related to the swelling mechanism discussed earlier – leading to a greater formation of lumps.

11.2.4 Discussion

The question regarding whether or not adding lecithin to the surface of powders will improve reconstitution does not appear to be as straightforward as one might expect. Similar to the discussion for SMP vs. WMP in § 11.1, the answer seems to be T-dependent, thus the results suggest that one should consider the application (e.g. hot– or cold-beverage) before deciding to modify the surface of a cocoa powder.

Lecithination appears to improve the wetting, sinking and dispersing of powder at low T, but at higher T it may bring about undesired swelling effects, or possibly faster capillary contraction (where the capillary force brings particles together (Walstra, 2003)), and lump

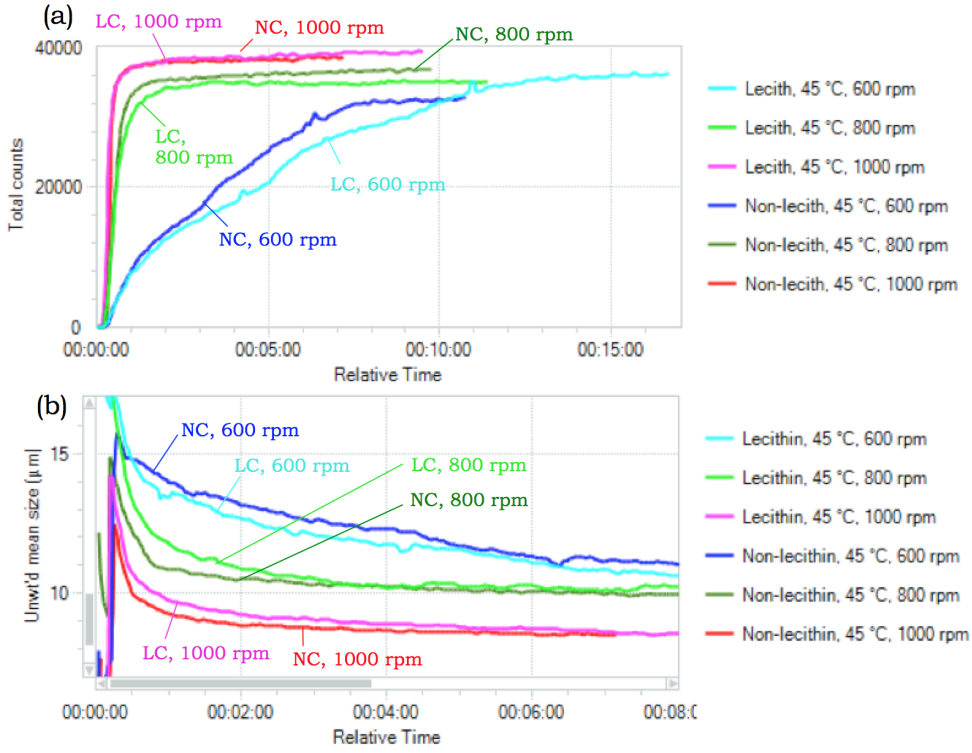

Figure 11.20: FBRM results for NC and LC at 45 °C: (a) total counts (unweighted), (b) mean chord length (unweighted) [µm].

formation. As for whether lecithin improves dispersing due to electrostatic repulsive forces (cf. Freudig et al. (1999)), this is explored further in § 12.1. The addition of surfactant to the *liquid* (rather than particle surface) prior to reconstitution is discussed in § 12.2.

§11.3 Heat Treatment

In § 11.1 and § 11.2 of the current chapter, it was clear that a relationship exists between the state of fat (solid vs. liquid), and the sinking behavior (and overall reconstitution) for milk and cocoa powders. In addition, in Ch. 2, it was discussed how for spray-dried milk powders, fat with a lower melting temperature (T_m) is more likely to be encapsulated in an amorphous lactose matrix, whereas higher–T_m fat is more likely to be located on the particle surface (cf. Kim et al. (2002)); and this encapsulated fat can be expelled to the surface if a heat treatment is applied. In § 6.3, it was discussed how the cocoa butter on the particles is polymorphic, thus powder is typically tempered during production to achieve optimal stability of the crystals, which have a high T_m. In § 6.2, it was mentioned how milk fat is

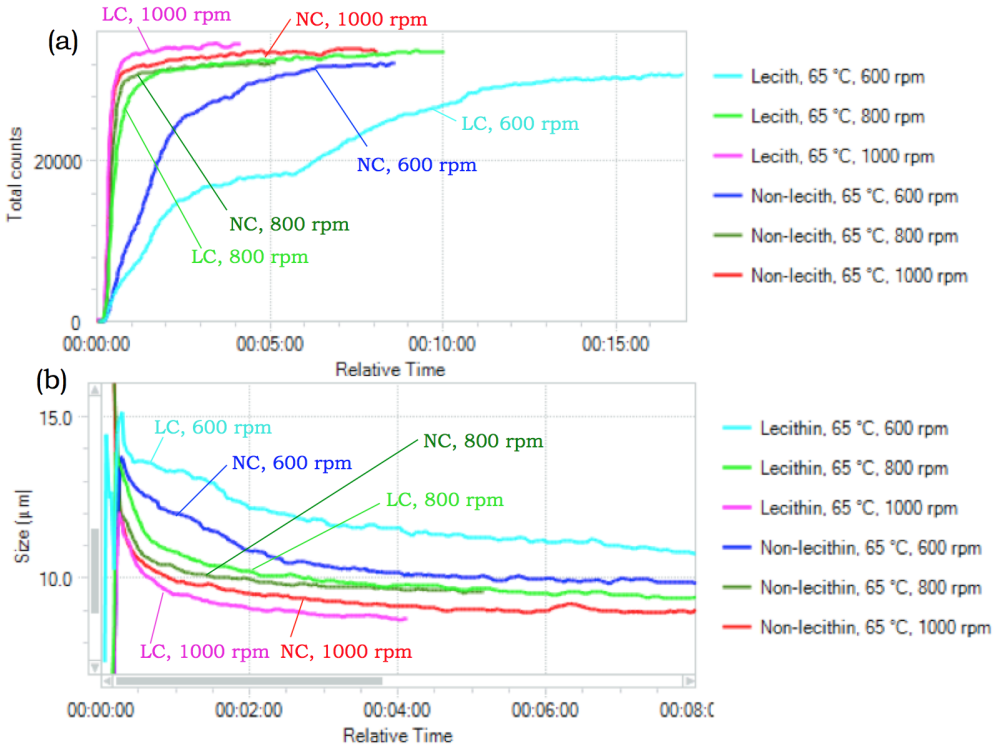

Figure 11.21: FBRM results for NC and LC at 65 °C: (a) total counts (unweighted), (b) mean chord length (unweighted) [µm].

also polymorphic. Due to these realizations, cocoa and milk powders were subjected to a heat treatment at a temperature where all fat crystals would melt, then allowed to cool slowly at room temperature. The idea is that the fat would recrystallize to form less stable (lower–T_m) crystals, thus less *solid* fat may be present upon reconstitution, aiding with sinking.

11.3.1 Experimental conditions

The heat treatment was performed by placing the powders into hermetically sealed pouches, and placing them in thin layers in an oven at 50 °C for 24 hours to melt all of the fat (see Kim et al. (2005b)). The powder was then allowed to cool at room temperature ($\approx$ 24 °C) for more than 24 h. Reconstitution was performed under default conditions (§ 7.2) at $T = 25$ °C; this T was chosen not only because it is an easy T to maintain during experiments, but also because (as will be seen in Fig. 11.28), the T_m of the cocoa butter may decrease from $T_m \approx 35$ °C to $T_m \approx 20$ °C following heat treatment, and for milk fat, Kim et al. (2005b) show that at $T = 25$ °C, ca. 20 % of milk fat would be expected to be solid, whereas at 45 °C,

ca. 0 % would be solid, thus one might expect no influence of a heat treatment on the powder sinking at 45 °C, since all the fat may melt anyway.

11.3.2 WMP results

Following the heat treatment of whole milk powder (WMP), there was significant caking of the powder (Fig. 11.22). This can be explained by the formation of fat bridges between particles, as discussed in § 2.2.

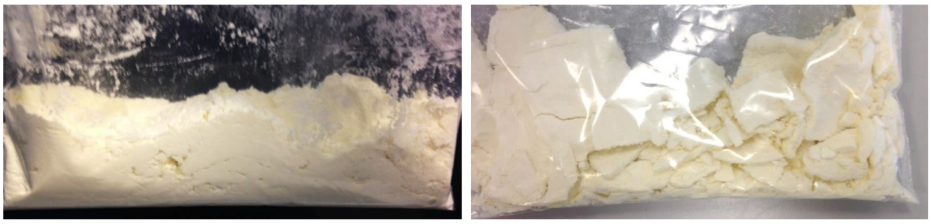

Figure 11.22: Caking of WMP during heat treatment: (a) before, and (b) after.

Prior to reconstitution, caked powder was lightly broken up to primary particles – the powder also had a softer texture post-treatment, most likely due to a greater amount of liquid fat at room temperature.[5]

Reconstitution experiments were performed at $N = 600$, 800, and 1000 rpm – sinking times (t_{sink}) are plotted in Fig. 11.23.

There is a clear improvement in sinking at $N = 600$ rpm; however at higher N, where downdraw is already quick, there was no clear difference. FBRM results were also very similar at $N = 800$ rpm and 1000 rpm for the "before" and "after" powders. At $N = 600$ rpm, however, FBRM results indicated superior kinetics (related to sinking) as well as the extent of dispersing, following the heat treatment (Fig. 11.24).

[5] DSC results (§ 8.4) were performed, but due to the overlap of fat melting and lactose glass transition effects, results were too noisy to interpret.

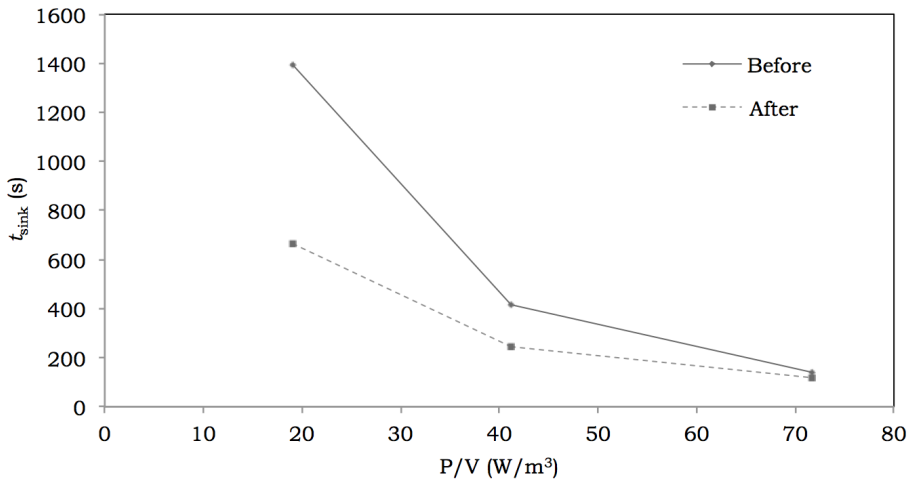

Figure 11.23: Sinking times for WMP pre– and post-heat treatment ($T = 25\,°C$).

11.3.3 SMP results

Experiments were also performed with skim milk powder (SMP) at reconstitution temperatures $T = 25\,°C$, $N = 600\,\text{rpm}$, before and after the heat treatment. Unlike for WMP, there was no significant caking of the particles for SMP (Fig. 11.25), indicating that fat bridges were indeed the mechanism responsible for caking in Fig. 11.22. (The T_g of SMP was $\approx 55\,°C$, explaining the lack of caking via a glass transition-related mechanism; cf. § 2.2).

The t_{sink} for the "before" SMP was 14 min, and for the "after" SMP $t_{\text{sink}} = 11.75\,\text{min}$; thus, sinking was also improved following a heat treatment, despite there being little fat in the powder overall. As mentioned in § 2.1, a higher percentage of fat is likely to be on the surface than the bulk. Although, the improvement in t_{sink} is not as strong as it was for WMP. FBRM results (Fig. 11.26) show that the overall extent of dispersing was about the same for "before" and "after" powders – the faster kinetics can be explained by the faster sinking of the "after" powder.

11.3.4 Cocoa results

Cocoa powder (20 – 22 % fat), alkalized (§ 8.3) was subjected to the heat treatment as well. In Fig. 11.27, it is clear that at room temperature, the "before" cocoa powder is grainy and a lighter color, but the "after" powder is softer and darker in color.

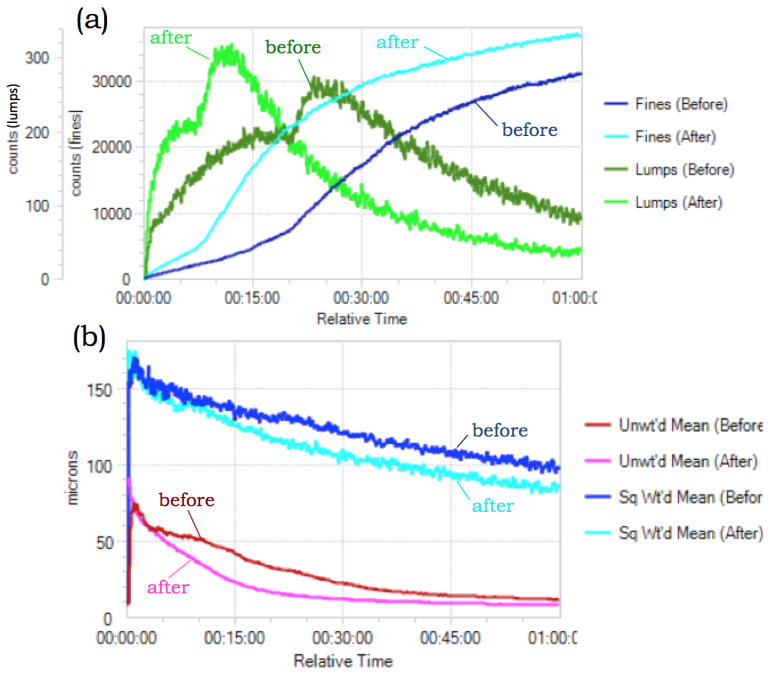

Figure 11.24: FBRM results for WMP pre- and post-heat treatment ($T = 25\,°C$, $N = 600\,\text{rpm}$): (a) counts of lumps and fines, (b) unweighted and square weighted mean chord lengths. The average $t_{\text{sink,before}} = 23\,\text{min} : 25\,\text{s}$ & $t_{\text{sink,after}} = 11\,\text{min} : 45\,\text{s}$.

DSC trials (§ 8.4) of the powder (Fig. 11.28), (which, due to the absence of lactose was easier to interpret than for milk powders), show that at 25 °C, more of the fat is solid in the "before" powder, because as the T increases during the scan, there is a stronger melting curve than for the "after" powder. Moreover, a second scan is performed for both the "before" and "after" powders at a cooling rate of $-10\,°C/\text{min}$ to allow for (untempered) crystallization to occur; the second heat scan shows that the T_m of the cocoa butter had decreased from $\approx$ 35 °C in the first scan to ca. 20 °C in the second scan.

Reconstitution was performed at $T = 25\,°C$, $N = 600\,\text{rpm}$ – clumps of powder were broken up before addition to the water. The average t_{sink} for the "before" powder was 16 min:45 s, t_{sink} for the "after" powder was 7 min:15 s, indicating a significant improvement in the wetting/sinking properties, due to the lesser amount of solid fat. A closer look at the sizing data from FBRM measurements (Fig. 11.29) also demonstrate that dispersing was improved with the heat treatment.

Another observation (Fig. 11.30) was that the color of the beverage after the powder was added was different; a lighter brown color was obtained with the "before" powder, but a more

Figure 11.25: No caking observed after heat treatment for SMP: (a) before, and (b) after.

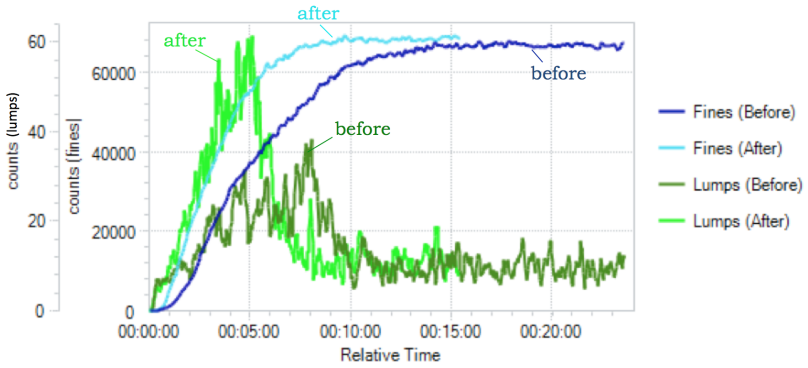

Figure 11.26: FBRM results for SMP pre- and post-heat treatment [25 °C, 600 rpm].

reddish brown was observed for the "after" powder; it is possible that the fact that the fat is melted for the "after" powder may affect how light is diffracted. Observing the stainless steel vibratory feeder also reveals that some dust is left on the feeder for the "before" powder, whereas the feeder for the "after" powder is largely clean; this is an indication that flowability may also be improved with the heat treatment.

11.3.5 Discussion

It appears that for fat-containing powders, both sinking and dispersing can be improved if, upon reconstitution, the water T is greater than the T_m of the fat crystals, and this T_m can be modified with a heat treatment. However, there may be concerns for having less stable fat crystals or a greater amount of liquid oil in powders, particularly for retail applications. For instance, as discussed in § 6.3, unstable cocoa butter crystals can lead to fat bloom. To demonstrate this, some of the "after" cocoa powder was stored at room temperature for six months in a hermetically sealed bag (Fig. 11.31). The pictures reveal a significant amount of

Figure 11.27: Cocoa powder (a) before and (b) after heat treatment.

bloom on the surface, and the inside of the bag also had a greasier texture after storage.

Moreover, liquid oil may be more susceptible to other degradative processes (e.g. lipolysis or oxidation) if not stored properly. Thus, it is unclear if such a heat process should be recommended for retail purposes. However, it may find uses in industrial or vending applications, particularly for colder–water applications, as well as in capsules (tightly sealed and flushed with N_2 gas), for instance for latte–type or mocha–type beverage applications (using milk and cocoa powders).

§11.4 Surface Dispersing

As discussed in § 1.2, small particles may disperse at the liquid-air interface upon contact due to the action of capillary suction forces, and resulting oscillatory waves that drive dispersing, and clumps of floating particles can be broken apart due to similar mechanisms. As mentioned in § 6.1, Parker et al. (2000) noticed better dispersing at the surface of water after dry-mixing pectin with a surfactant, and attributed the better dispersing due to Marangoni effects (related to surface tension γ gradients, where mass transfer takes place from regions of lower to higher γ due to its contractile nature). In the current section, the surface dispersion behavior of skim milk powder (SMP) vs. whole milk powder (WMP) and non-lecithinated cocoa (NC) vs. lecithinated cocoa (LC) are compared by sprinkling a small amount of powder (a few mg) to the surface of static deionized water at $T = 25\,°C$. Videos are taken using a camera positioned from above a petri dish containing the water.

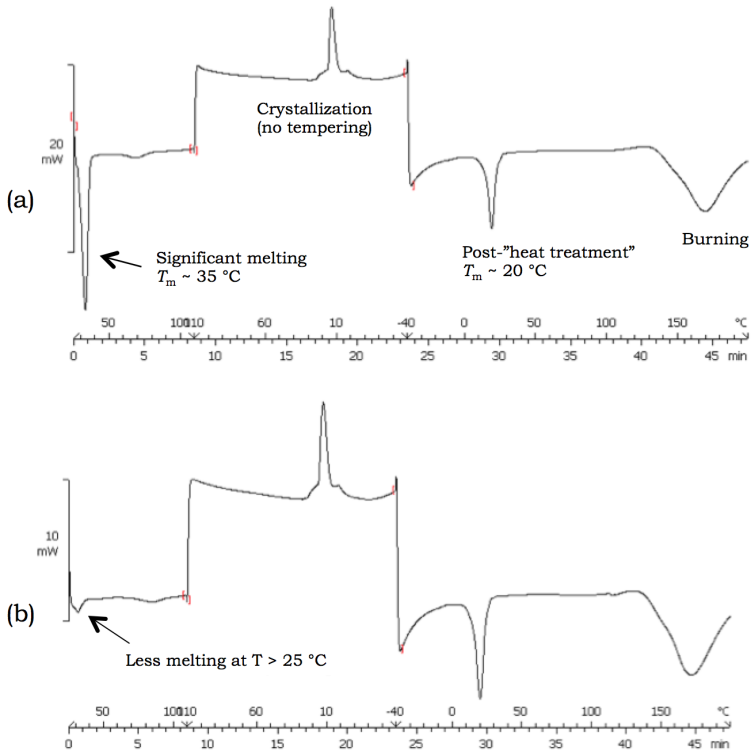

Figure 11.28: DSC measurements for cocoa powder (a) before and (b) after heat treatment.

11.4.1 Milk results

The milk results (Fig. 11.32) indicate that SMP experienced a violent initial dispersion upon liquid contact, and clumps of powder broke apart very easily. However WMP took much longer to disperse across the surface, and clumps of particles dispersed much more slowly.

11.4.2 Cocoa results

The cocoa results (Fig. 11.33) reveal a fast initial dispersing for LC, followed by an explosive breakup of floating clumps of particles. However, NC disperses more slowly across the liquid surface, and powder clumps take longer to break up.

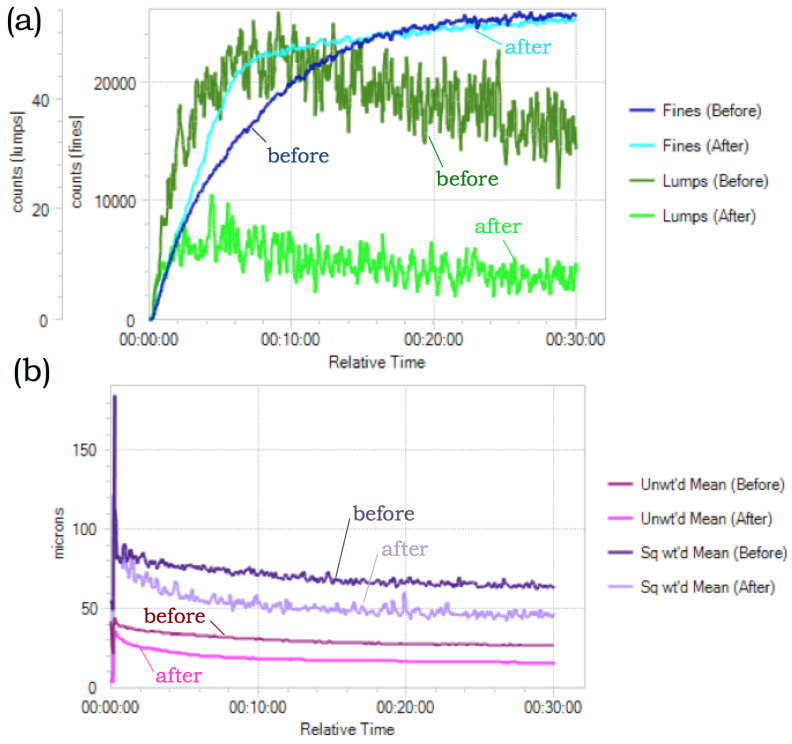

Figure 11.29: FBRM data for cocoa powder before and after heat treatment [600 rpm, 25 °C]: (a) counts of lumps and fines, (b) unweighted and square–weighted mean chord length.

11.4.3 Discussion

The Marangoni-related mechanism discussed earlier may be (partially) responsible for the better dispersing of LC compared to NC, as it is possible that the lecithin molecules at the particle surface, when in contact with water, detach from the particle to lower the γ of the water in the vicinity of the powder, and thus the tension pulls the water (and particles) towards regions of higher γ. However this hypothesis does not seem to be able to explain the results for SMP vs. WMP. However, the capillary suction mechanism may be able to explain the improved dispersing and clump breakup of SMP compared to WMP, as the suction would be expected to be greater (see § 1.2) for a less hydrophobic surface, resulting in a greater initial downward pull into the surface, creating more repulsive waves. However, one should also consider that the fat on the surface of WMP particles may result in a greater cohesivity of the WMP, resisting particle breakup as well.

It is possible that the surface dispersion described above may play a role in preventing

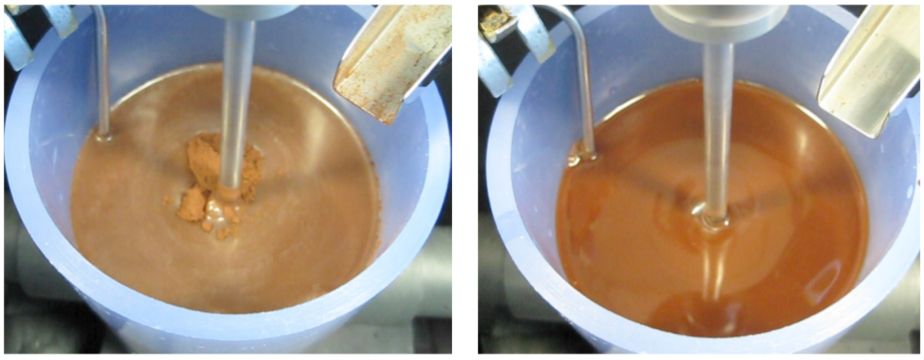

(a) (b)

Figure 11.30: Cocoa powders after 15 min of reconstitution for the (a) "before" and (b) "after" cocoa powders [600 rpm, 25 °C].

(a) (b)

Figure 11.31: Cocoa powders after heat treatment (a) with and (b) without six months of storage.

lump formation. Particularly for retail applications, where a consumer might add powder to a stationary liquid surface *prior to* mixing, this initial explosion may physically separate grains before processes like swelling can take place; narrowly escaping lump formation. However, it may be worth studying the effect of powder *amount* vs. free liquid surface area for dispersing effects.

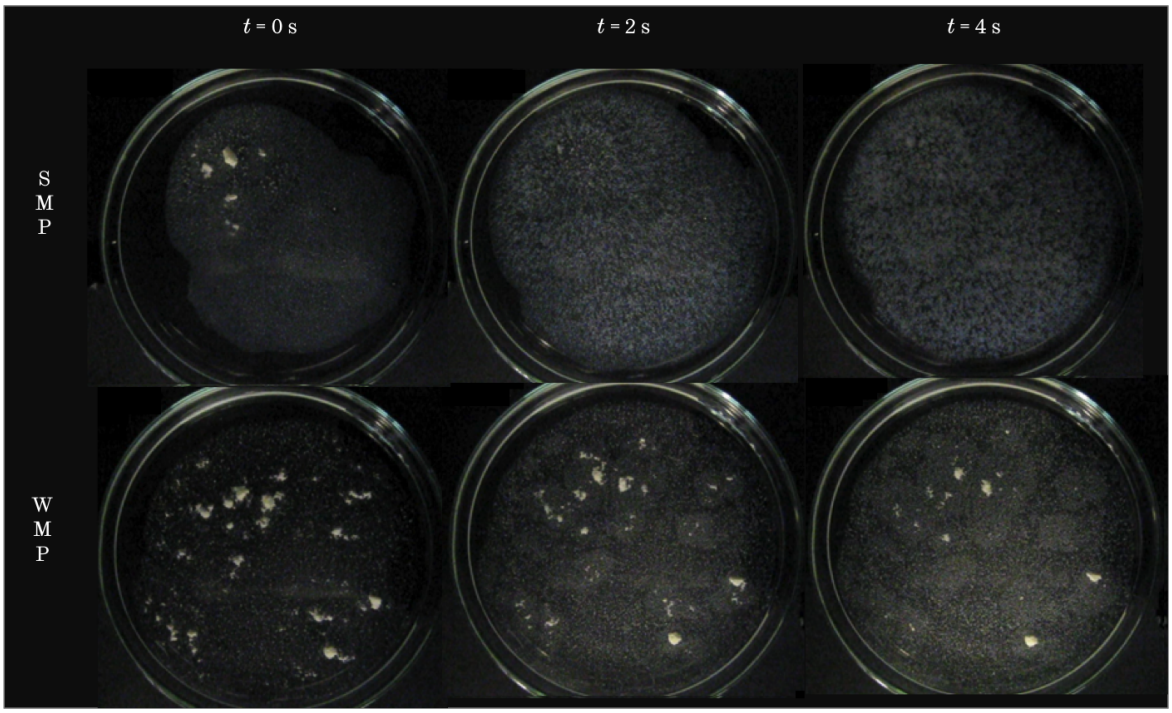

Figure 11.32: Surface dispersion of SMP and WMP.

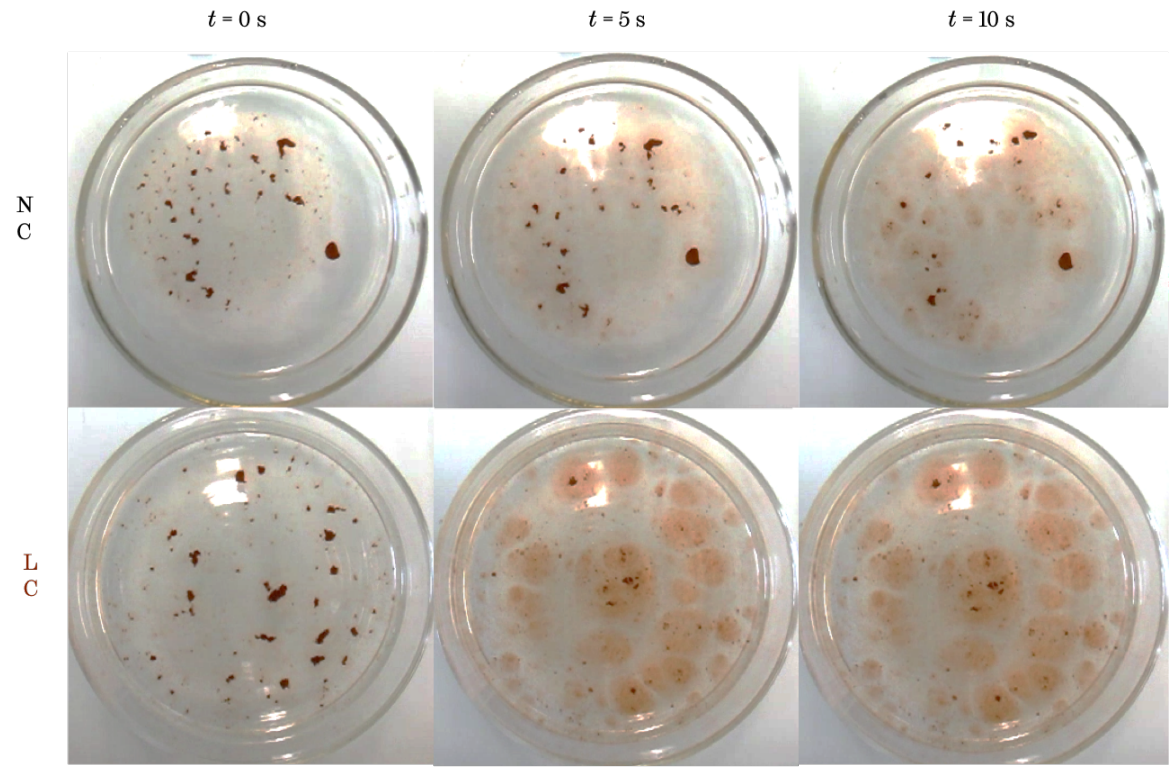

Figure 11.33: Surface dispersion of NC and LC.

Chapter 12

Other Liquid Properties

In addition to water temperature T, there are other properties of a reconstitution medium that could affect the behavior of food powders. As discussed in Ch. 2 and § 4.5, salt presence may affect the dispersing and/or dissolving of powders such as hydrocolloids or those containing micellar casein. In § 2.3 and § 11.2, it was demonstrated that the presence of surfactant on the particle surface may influence wetting/sinking and dispersing. In Ch. 10.1, the influence of molecular weight (MW), which affects viscosity when particles dissolve, was studied. In the current chapter, a stronger focus on how the ionic strength (§ 12.1), surface tension (§ 12.2), and viscosity (§ 12.3) of the liquid (prior to powder addition) influence reconstitution, keeping in mind, as discussed in the literature review, how particle interactions (Ch. 4) and transport processes (Ch. 1) may be affected. The conditions chosen for each experiment were chosen based on the rate-limiting regime maps constructed in Chapters 10 and 11, depending on whether studying the effects of wetting/sinking *or* dispersing/dissolving was desired.

Contents

§12.1 Ionic Strength

As mentioned previously, studying the influence of ionic strength on powder reconstitution is not only interesting because of the possible variability in drinking water around the world (WHO, 2003), but also because it may allow for further insight into the mechanisms behind dispersing phenomena. In the current section, to alter the ionic strength we only consider NaCl, which is a common component in many foods, and contains a monovalent cation (Na^+); as discussed in § 4.5, divalent cations (e.g. Ca^{2+}) may interact in a more complex manner with food materials.

In Ch. 2, it was mentioned that several studies reportedly observed improved dispersing of micellar casein powders with higher concentrations of NaCl ([NaCl]) in the reconstitution medium, possibly due to the solubilization of Ca^{2+} from the $CaPO_4$ bridges at high [NaCl], allowing for better release of micelles from primary particles. However the author did not find studies on the effect of [NaCl] on the reconstitution of *non*-micellar casein powders (e.g. sodium caseinate (NaCas)), for which an improvement in dispersing might not be expected at higher [NaCl]. In addition, as made evident in § 6.2, skim milk powder (SMP), which contains mostly lactose ($\approx$ 50 %), but also $\approx$ 28 % casein by mass embedded in the amorphous lactose matrix (§ 8.2), would contain large amounts of *micellar* casein; however, it is not clear if an improvement in dispersing at higher [NaCl] would still be expected. In addition whole milk powder (WMP) would contain ca. 20 % (micellar) casein, however it

also contains ≈ 26 % fat; as mentioned in § 4.3, hydrophobic attractions increase in strength at higher ionic strengths, which may have some effect on dispersing.

As discussed in Chapters 2 and 11, the addition of lecithin to the surface of powders, like cocoa powder, may (at least under some conditions) improve both the wetting/sinking *and* dispersing of the powders. Freudig et al. (1999) attributed the better wetting to a reduction in the contact angle with water (§ 1.1), and the better dispersing to a greater electrostatic double layer (EDL) repulsion (§ 4.2); however they did not actually test these mechanisms. If the EDL mechanism is relevant, one might expect a stronger effect of [NaCl] on lecithinated cocoa (LC) compared to normal cocoa (NC) due to screening of the EDL repulsion (§ 4.5).

As discussed in § 4.5, Klein Larsen et al. (2003) claims that the slower dissolution of hydrocolloid powders in the presence of NaCl was due to slower mass transfer during dissolving, but did not consider possible EDL effects – since they used a rheological approach (§ 5.5) to study rehydration, they would have no way to look at the dispersing and dissolving as separate phenomena; however, using a technique like FBRM, one *can* consider them separately (Ch. 9).

12.1.1 Experimental conditions

For all experiments in the current section, the NaCl was obtained from Sigma Aldrich (St. Louis, MO, USA). Experiments were performed in saline solutions ranging from 0 M to 2 M, which is about the same range used by Hussain et al. (2011) (see § 4.5). For each experiment where the [NaCl] of the liquid is altered, the same agitation speed N is used; it is important to note that the liquid properties such as surface tension γ, viscosity μ, and density ρ will change as a $f([\text{NaCl}])$ – see Tab. 12.1.

Data for γ is obtained from Pegram and Record (2007) (note the "antisurfactant" effect of NaCl), and data for μ and ρ is from Kestin et al. (1981). Even though the liquid properties change, the effect on power draw P is very low. For instance at constant $N = 600$ rpm, P would only be expected to change from 14.5 mW at 0 M to 15.4 mW at 2 M (cf. Eq. 3.9).

Note that for calculating the ionic strength for NaCl (cf. Eq. 4.8), where for Na^+, $z_+ = 1$

Table 12.1: Water properties (25 °C) at increasing [NaCl].

Conc. NaCl [M]	% NaCl	γ [mN m^{-1}]	μ [µPa s]	ρ [kg m^{-3}]
0.0	0.00	71.99	890.0	996.9
0.5	2.92	72.79	928.6	1016.9
1.0	5.84	73.59	972.0	1036.2
1.5	8.76	74.49	1020.5	1054.8
2.0	11.68	75.29	1075.5	1072.7

and for Cl^- $z_- = -1$, since $(\pm 1)^2 = 1$ and $\frac{1}{2}(1x + 1x) = x$, the ionic strength of NaCl solutions is the same as its concentration. All experiments are performed at least in duplicate to ensure repeatability. Conductivity measurements were too noisy to interpret when [NaCl] $\neq 0$.

12.1.2 Sodium caseinate

Sodium caseinate ($a_w = 0.39$ at 25 °C) was obtained from Emmi (Lucerne, Switzerland) – compared to the other powders used in the current report, it was much finer and fluffier, and had a very strong tendency to swell when in contact with water (Fig. 12.1).

Figure 12.1: Sodium caseinate swells when in contact with water.

The powder was very difficult to make wet and sink, and finding appropriate conditions for reconstitution took some trial and error; in the end the conditions chosen were: powder amount: 1 % w/v, $N = 1100$ rpm, $T = 55$ °C, all other conditions being default (§ 7.2). The FBRM results (Fig. 12.2) and videos revealed that at 0 M there was (relatively) good sinking ($t_{\text{sink}} = 15$ min), and the mean size was relatively low – an indication of good dispersing.

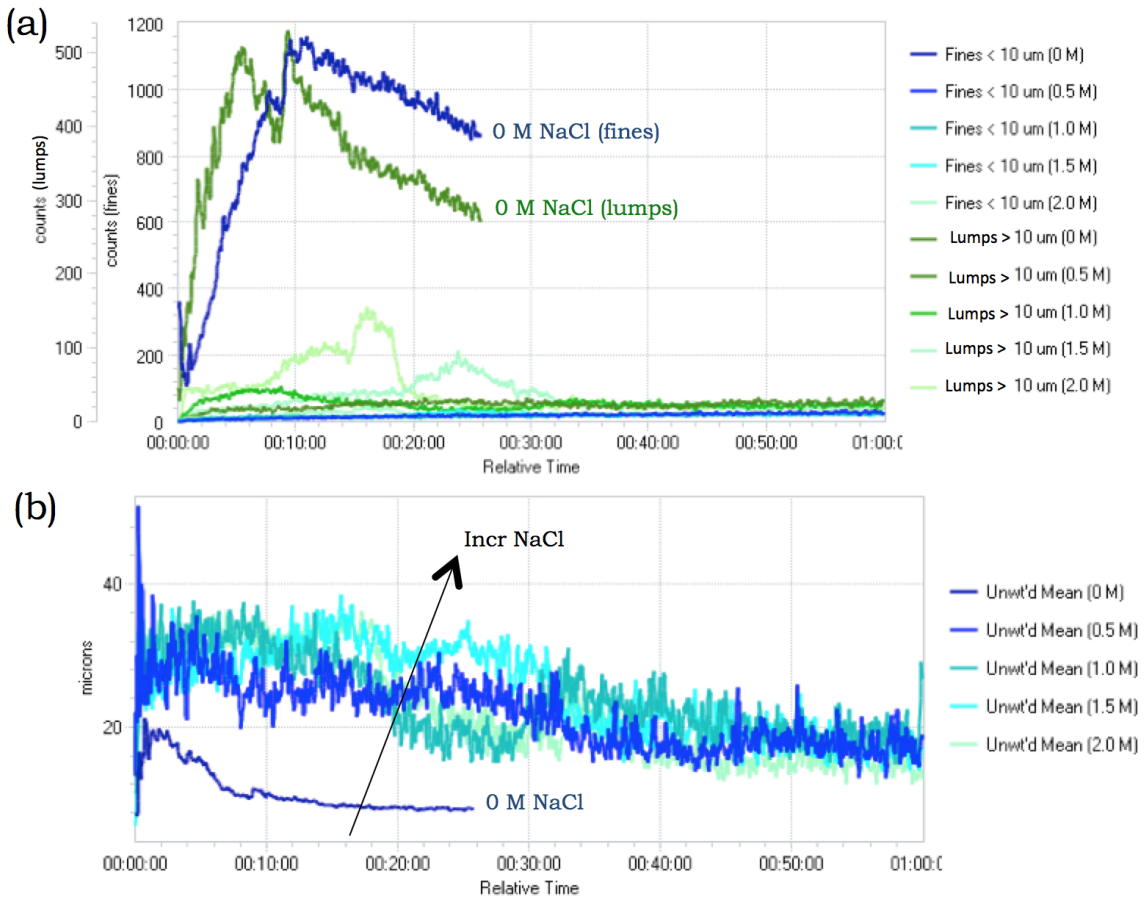

Figure 12.2: FBRM results for sodium caseinate at increasing [NaCl]: (a) counts of lumps and fines, (b) mean chord length (unweighted and weighted).

However already at 0.5 M NaCl, the sinking becomes extremely poor, and the mean size is much greater – thus both sinking and dispersing became worse. For 0.5 – 2.0 M NaCl experiments, a larger stiff lump of solid material formed at the liquid surface that was very difficult to break up (Fig. 12.3).

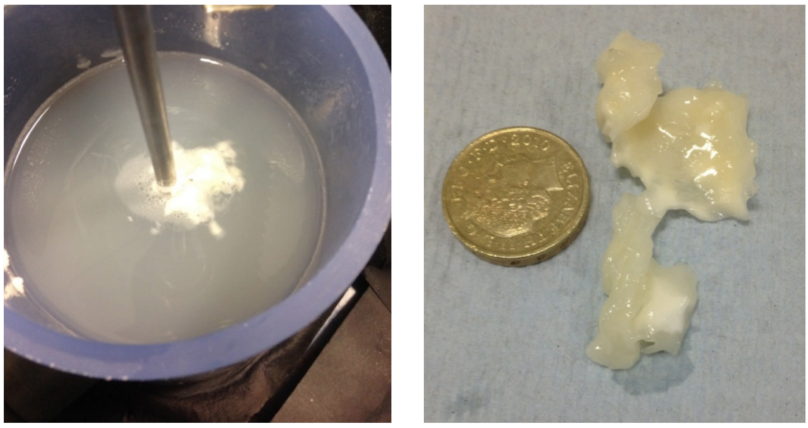

Figure 12.3: Lumps of sodium caseinate in the presence of NaCl: (a) [NaCl] = 0.5 M at $t = 1$ h, and (b) [NaCl] = 1.0 M at $t = 1$ h.

One possible mechanism for the poor reconstitution is the increasingly strong hydrophobic attractions at increasing [NaCl] – these may cause a stronger association of the caseins, resisting dispersion and thus water transfer. The lump formation does *not* appear to be due to a gel layer forming around a sack of dry particles, as was described in § 1.4.

12.1.3 Milk powders

Experiments were performed with skim (SMP) and whole (WMP) milk powders (§ 8.2, $a_w = 0.3 \pm 0.02$ at 25 °C), under the same range of [NaCl]. Based on the mapping results from Ch. 11 it was decided to perform experiments at $N = 600$ rpm, $T = 45$ °C, since both sinking and dispersing occur readily (but not instantly) for both powders. The a_w was 0.3 ± 0.03 at 25 °C. All other conditions were kept as default (§ 7.2) i.e. 2.0 % w/v added, etc. The average sinking time (t_{sink}) for both powders is plotted as a f([NaCl]) in Fig. 12.4.

As discussed in § 11.1, at 45 °C WMP sinks faster than SMP due to fat melting effects. The [NaCl] does not appear to influence t_{sink} for WMP, but for SMP between 1.0 M and 1.5 M there is a sudden jump in t_{sink}.

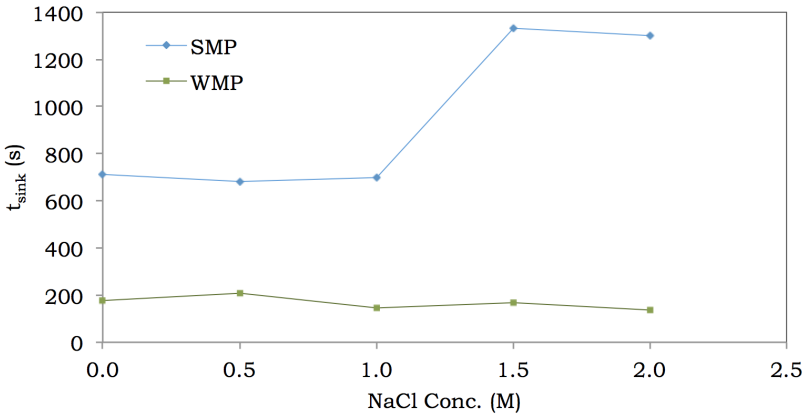

Figure 12.4: Sinking times for SMP and WMP at increasing [NaCl].

SMP

At 1.5 M for SMP there was also a large lump that floated at the liquid surface, with a clear swollen layer at the lump/liquid interface (Fig. 12.5).

Figure 12.5: Lump of SMP at [NaCl] = 1.5 M, t = 10 min.

FBRM results (Fig. 12.6) demonstrate that the extent of dispersing decreases with increasing [NaCl] for SMP; a greater amount of lumps form as [NaCl] increases as well.

Looking at the evolution of mean sizes for SMP (Fig. 12.7), particularly for the square-weighted mean (which would emphasize the lump fraction), a greater mean is seen at 1.5 M and 2.0 M compared to at lower concentrations.

However, a slightly more complex relationship is seen for the unweighted mean (which

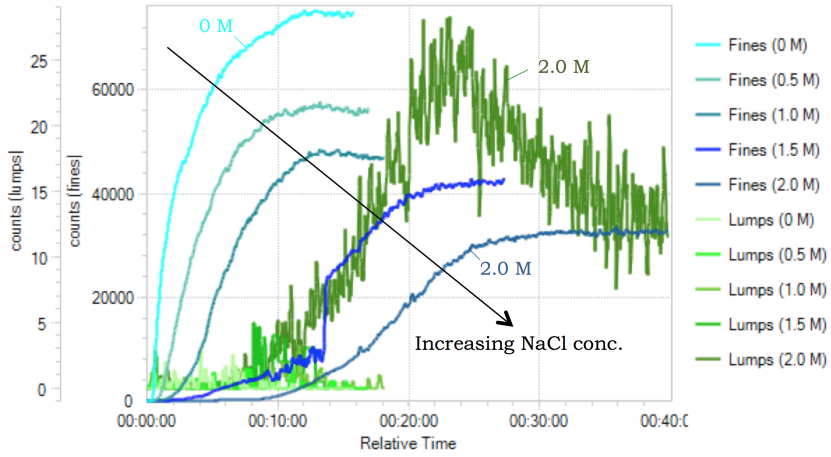

Figure 12.6: FBRM results for SMP at increasing [NaCl].

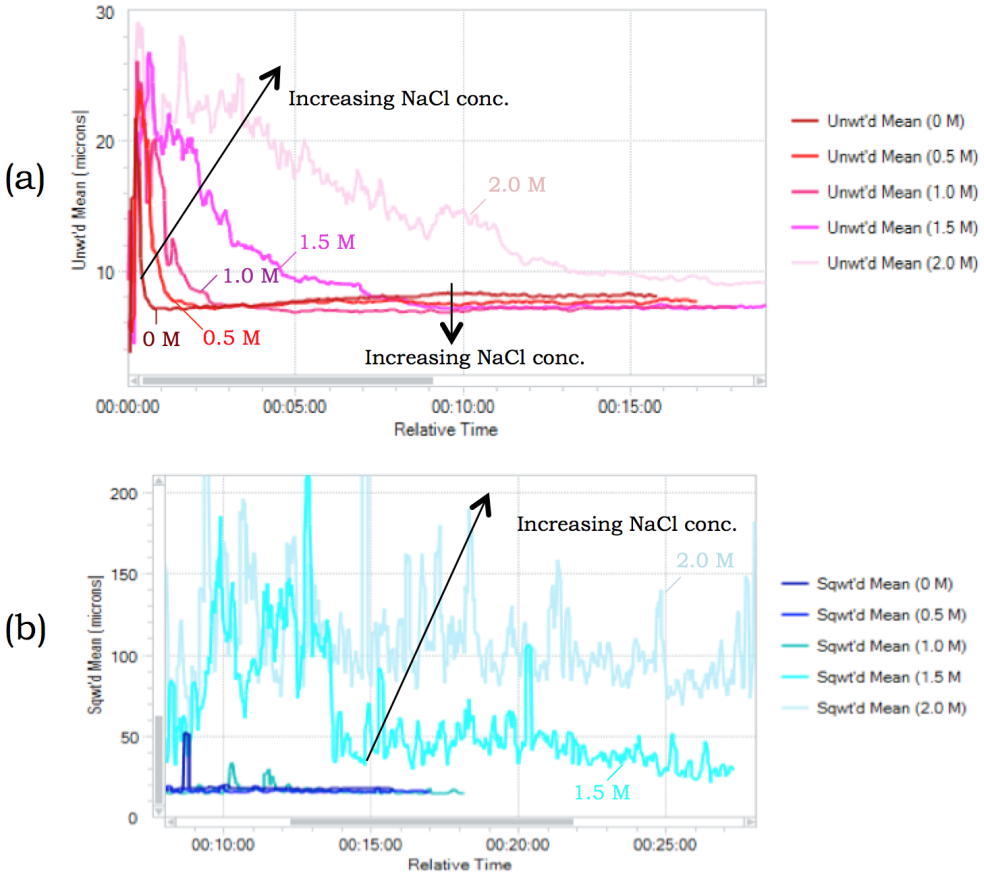

Figure 12.7: FBRM mean size results for SMP at increasing [NaCl]: (a) unweighted, and (b) square weighted.

focus more on the behavior of fine particles). For the first 3 min, the mean size is greater with increasing [NaCl] for each point in time. However, between about $t = 3 - 9$ min, there is a cross-over, where the mean size is actually *lower* for higher [NaCl] (up to 1.5 M). This may be due to the mechanism related to solubilization of Ca^{2+} in micellar casein (discussed in Ch. 2), as at these points in time the lactose would be expected to have mostly dissolved, and thus SMP may behave similarly to micellar casein powders. These results for unweighted mean appear to be in agreement with the studies that reported improved dispersing with increasing NaCl concentration for higher micellar casein powders, where they used techniques like laser diffraction (§ 5.4). However, it is important to note that these studies require off-line sampling (unlike FBRM), and since they did not use video recordings, it is possible that those studies may have *missed out on lump formation mechanisms, which are more important for powder reconstitution than the final size of the fines fraction.* Therefore, it may be that their conclusions are misleading.

WMP

For WMP, there is a more gradual impact of [NaCl] on the dispersing ability (Figures 12.8 and 12.9).

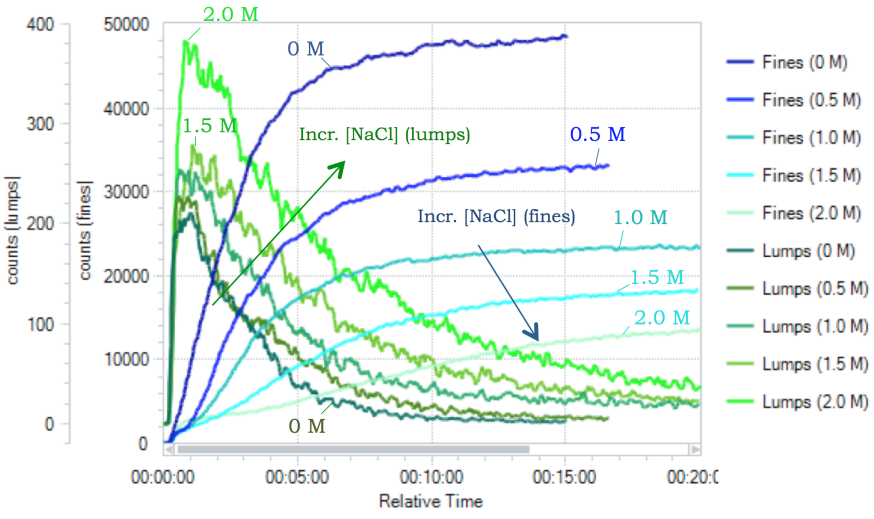

Figure 12.8: FBRM results for WMP at increasing [NaCl].

As was shown in Fig. 12.4, the sinking times t_{sink} were the same for all [NaCl], thus the slower rise in the counts of fines at increased concentrations is due to the slower dispersing of lumps. The trends are more straightforward, and there is no reversal in sizes at high [NaCl]

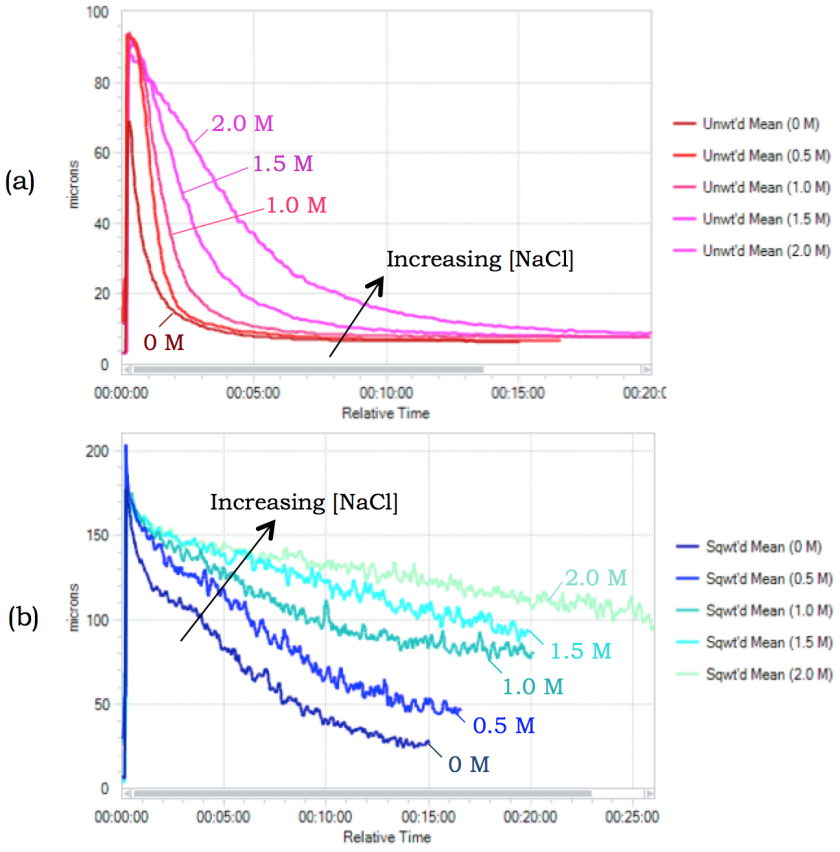

Figure 12.9: FBRM mean sizes for WMP at increasing [NaCl]: (a) unweighted mean size, (b) square weighted mean size.

as was seen for SMP.

Comparing the square-weighted mean values (taken at $t = 15\,\text{min}$) for SMP and WMP reveals an interesting trend (Fig. 12.10): for WMP the size increase with NaCl is more gradual; for SMP the increase between 1.0 and 1.5 M is very sudden, mirroring in the influence of [NaCl] on t_{sink} (Fig. 12.4).

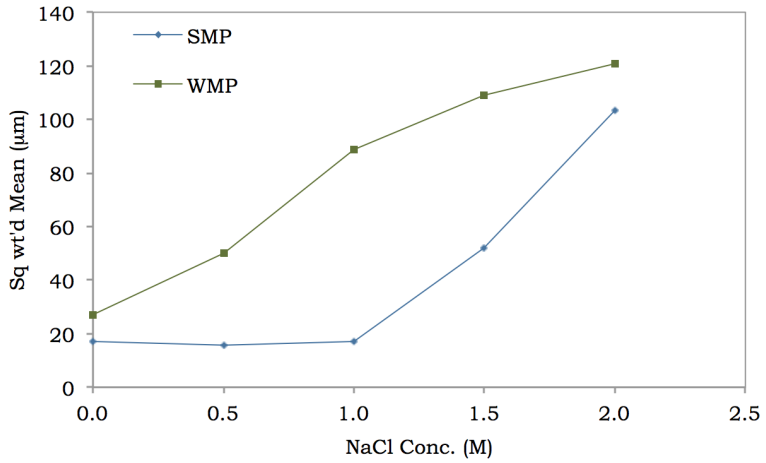

Figure 12.10: FBRM square-weighted mean sizes at $t = 15\,\text{min}$ SMP and WMP at increasing [NaCl].

There appears to be a critical [NaCl] for lump formation for SMP – the mechanism for lump formation may be related to poorer dispersing from screening effects, combined with increasing hydrophobic association with micellar casein. For WMP, the gradual increase in size may be explained rather due to hydrophobic interactions due to the high amount of fat closer to the particle surface, rather than due to casein effects.

12.1.4 Cocoa powders

Similar experiments were performed for non-lecithinated cocoa (NC) and lecithinated cocoa (LC) – see § 8.3 – with $N = 800\,\text{rpm}$ and $T = 45\,^{\circ}\text{C}$, with all other conditions being default (§ 7.2). These conditions were chosen based on the regime maps in Ch. 11 (at 0 M NaCl) – at these conditions, sinking was gradual, but not instant, with $t_{\text{sink}} \approx 30\,\text{s}$ for *both* NC and LC, and dispersing was also gradual. The average t_{sink} results are shown in Fig. 12.11. While t_{sink} at 0 M is very similar for NC and LC, at increasing [NaCl] the t_{sink} for NC remains relatively constant, whereas sinking becomes worse for LC.

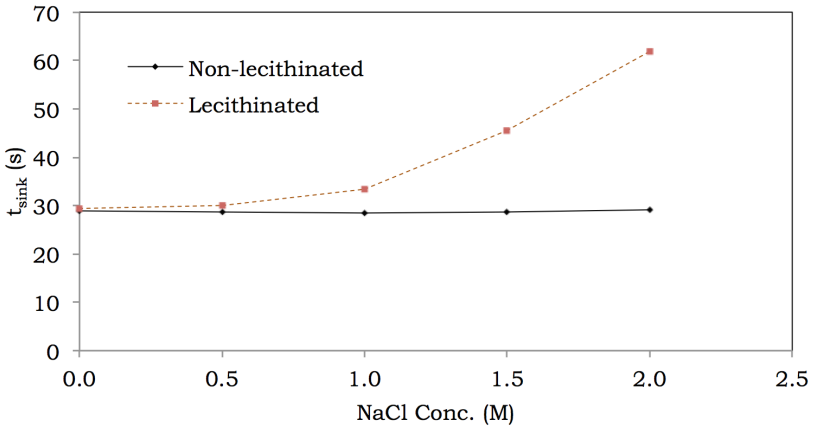

Figure 12.11: Sinking times for NC and LC at increasing [NaCl].

FBRM results (Fig. 12.12) reveal that while dispersing is worse at increasing [NaCl] for NC, the effect is more dramatic for LC.

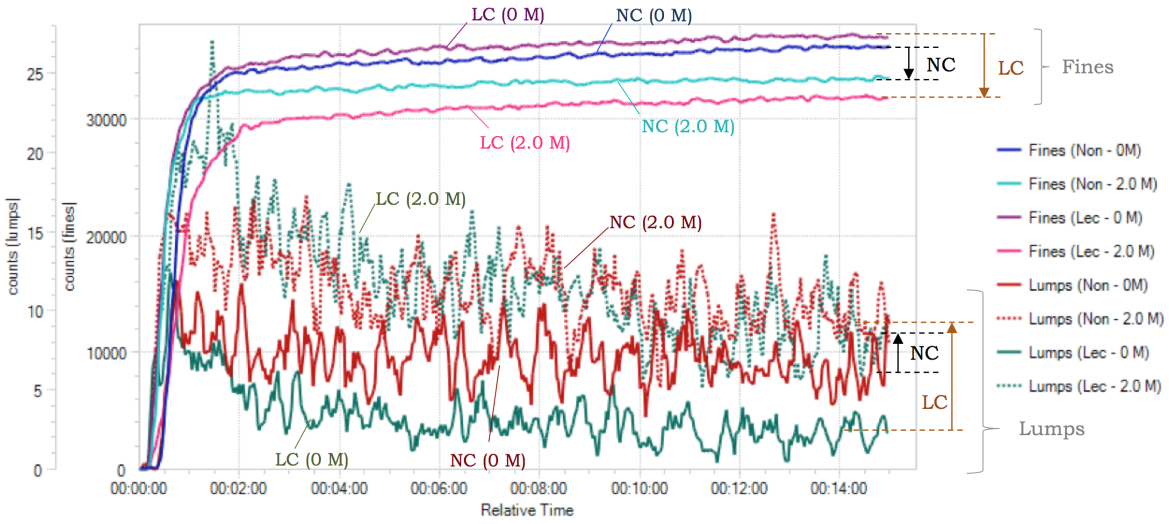

Figure 12.12: FBRM for NC and LC at increasing [NaCl]. Similar trends exist for 0.5 – 1.5 M, but they are not shown for better visualization.

The final square–weighted mean results (Figure 12.13) show that the final particle size was larger for NC than LC, but that LC was more sensitive to changes in NaCl concentration.

The worse dispersing for NC may be explained due to stronger hydrophobic interactions between particles. Originally (at 0 M) one sees better dispersing for LC than NC; however, as [NaCl] increases, dispersing becomes worse for LC – and the effect is greater than the effect for NC. The results appear to be in agreement with Freudig et al. (1999)'s claim that an EDL (§ 4.2) mechanism, due to lecithin presence, would help promote dispersing – as [NaCl]

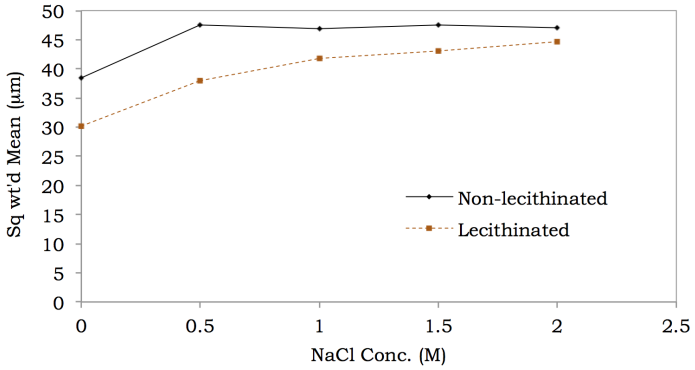

Figure 12.13: Final square weighted mean values (average) for NC and LC as a function of NaCl concentration.

increases, EDL effects would thus be screened. As for why the t_{sink} increases for LC but not NC, and why at higher [NaCl] the extent of dispersing is worse for LC than NC, this may be due partially to the higher hydrophilicity of the lecithinated surfaces, which could lead to swelling effects (discussed in § 11.2) that, since dispersing is inhibited by NaCl presence, could lead to worse dispersing.

12.1.5 Maltodextrin

Experiments were performed with maltodextrin DE21 at several different combinations of conditions, but no significant difference was observed, as reconstitution was so fast anyway (results not shown). However, similar experiments were performed with maltodextrin DE6 at $T = 25\,^{\circ}\text{C}$ and $N = 1000\,\text{rpm}$, as the regime maps in § 10.1 reveal fast sinking but more gradual dispersing and dissolving. As discussed in the introduction to the current section, the main reason for these experiments is to see if *dispersing* or *dissolving* effects are inhibited by an increase in ionic strength.

FBRM results (Fig. 12.14) reveal that dispersing appears to be similar for all three conditions (and sinking was instant), but *dissolving* was slower at higher [NaCl]. The higher peak at 2 M is believed to be due to less "by-pass dissolution" (cf. k_3 in Ch. 9) rather than greater dispersion.

This trend is also apparent in Fig. 12.15, where at $t = 1\,\text{min:}30\,\text{s}$, particles are still dissolving

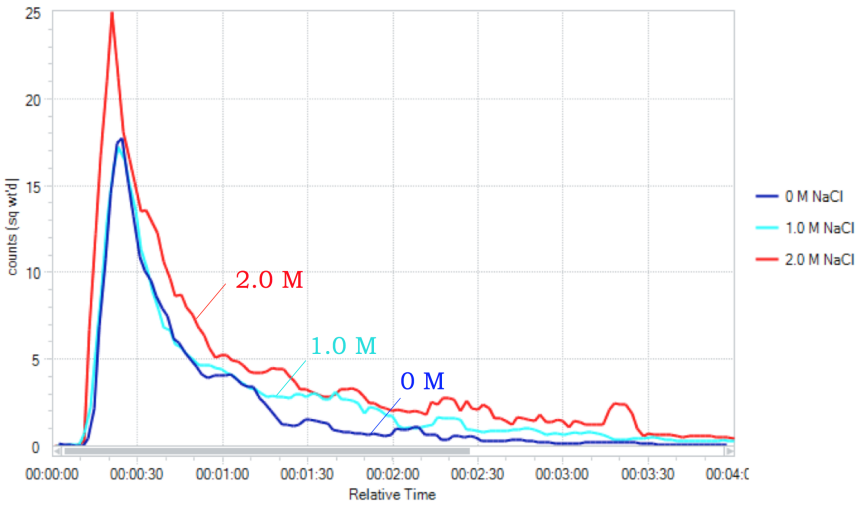

Figure 12.14: FBRM results for maltodextrin DE6 at increasing [NaCl].

at 2 M but are mostly dissolved at 0 M NaCl.

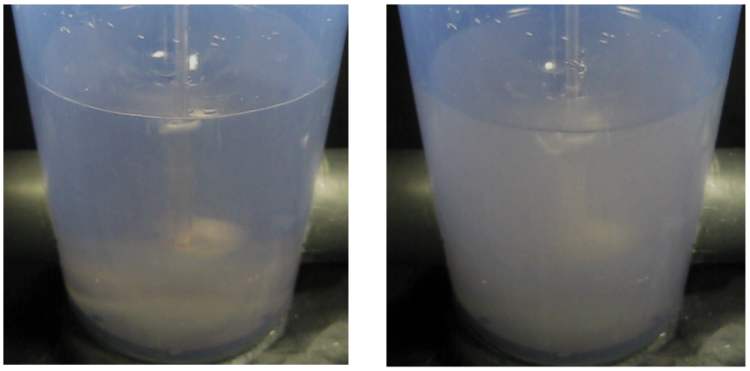

Figure 12.15: Picture of maltodextrin DE6 at (a) 0 M and (b) 2 M NaCl ($t = 1$ min:30 s).

Thus the results appear to support the claim by Klein Larsen et al. (2003) that mass transfer may be reduced during *dissolving* (§ 4.5) of hydrocolloids, when in the presence of NaCl.

§12.2 Surface Tension

In § 11.2, it was demonstrated that the addition of a surfactant to the surface of a food powder can (depending on the conditions) improve both sinking and dispersing, and in § 12.1, the theory that improved dispersing may be related to an improved EDL repulsion (§ 4.2)

was supported. In the current section, the effect of *liquid* surface tension is investigated.

As mentioned in § 2.3, Freudig et al. (1999) tested the influence of dry-mixing powdered lecithin with skim milk powder (SMP), as well as adding lecithin to the water *before* adding SMP, and observed better reconstitution with both systems compared to SMP being added without any lecithin, although dry-mixing was better. However, using their turbidity technique (§ 5.2) they were not able to characterize the sinking or dispersing of powder directly. Schubert (1993) (the supervisor of B. Freudig at KIT in Germany) claims that the reason that food powders often sink poorly is the fact that the surface tension (γ) of water is so high – thus, if this is true, one would expect better sinking of a small particle upon surfactant addition, which of course lowers γ. This is a well-known phenomenon, and can be explained mathematically according to the equations in § 1.2. *However, Schubert (1993) does not consider capillarity effects in his statement.*

As discussed in Forny et al. (2011), when food powders are added to an aqueous liquid, they generally are added as a bulk solid, and *not* as individual particles, and this resultant "bed of powder" may be considered as a capillary network. Thus, according to Forny et al. (2011), principles related to capillarity (cf. Washburn equation (Eq. 1.14), etc. in § 1.1) may help to understand how factors, such as γ, may influence capillary penetration (and water-logging; § 1.2). As discussed in § 1.1, a decrease in γ would *inhibit* capillary action ($\frac{l^2}{t} \propto \gamma$; Eq. 1.14). Thus, in the current section, these conflicting phenomena will be kept in mind.

12.2.1 Lowering the surface tension

There are a number of ways to lower the surface tension (γ) of water. For instance one possibility would be to mix the water with ethanol (EtOH). However, this approach was not chosen for a number of reasons: not only would an increase in EtOH change γ, but other liquid properties would also change, such as density ρ, viscosity μ, dielectric constant ε, polarity, etc. Moreover, according to Swaisgood (2007), EtOH can affect the stability of casein micelles.

In the current section, a surfactant was used to lower the surface tension of water. A common food-grade emulsifier – polysorbate 20 (polyoxyethylene sorbitan monolaurate,

assigned the E-number E432 by the European Union), also known as Tween 20 – was used to lower γ prior to powder addition. The surfactant was supplied by Sigma Aldrich (St. Louis, MO, USA). The molecule is depicted in Fig. 12.16. The HLB value (Hydrophile-Lipophile Balance) is 16.7; an indication that it is very soluble in water and appropriate for oil-in-water emulsification purposes (Walstra, 2003, Ch.10).

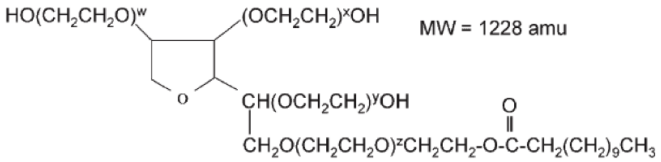

Figure 12.16: Polysorbate 20. $w + x + y + z = 20$ (Kerwin, 2008).

According to Kerwin (2008), the critical micellization concentration (CMC) of polysorbate 20 at 25 °C is ca. 60 µM, with the corresponding surface tension $\gamma \approx 32\,\mathrm{mN\,m^{-1}}$, whereas the γ of pure water at the same T is ca. $72\,\mathrm{mN\,m^{-1}}$. As explained by Walstra (2003), above the CMC the surface becomes saturated and excess surfactant will form micelles[1], which would not affect γ. In the current study, experiments were performed at 0 M and at the CMC of polysorbate 20 – prior to powder addition to the liquid, several minutes were allowed for diffusion of the surfactant to ensure even distribution at the surface (cf. Walstra (2003, Ch.10)).

12.2.2 Maltodextrin experiments

Experiments were performed with maltodextrin DE21 under a range of conditions; like in the ionic strength experiments (§ 12.1), no difference in behavior was seen for this powder, as reconstitution was very quick (results not shown). However, experiments with maltodextrin DE6 ($a_w = 0.22$ at 25 °C) were more interesting – reconstitution was performed at $N = 800$ rpm and $T = 25$ °C, since regimes maps in § 10.1 indicated that the powder would sink completely, but not instantly, under these conditions. Video time-lapses are shown in Fig. 12.17.

In the CMC video, at the surface a clear ring of foam can be seen along the vessel wall,

[1] *Actual* micelles, not like casein "micelles" – § 6.2.

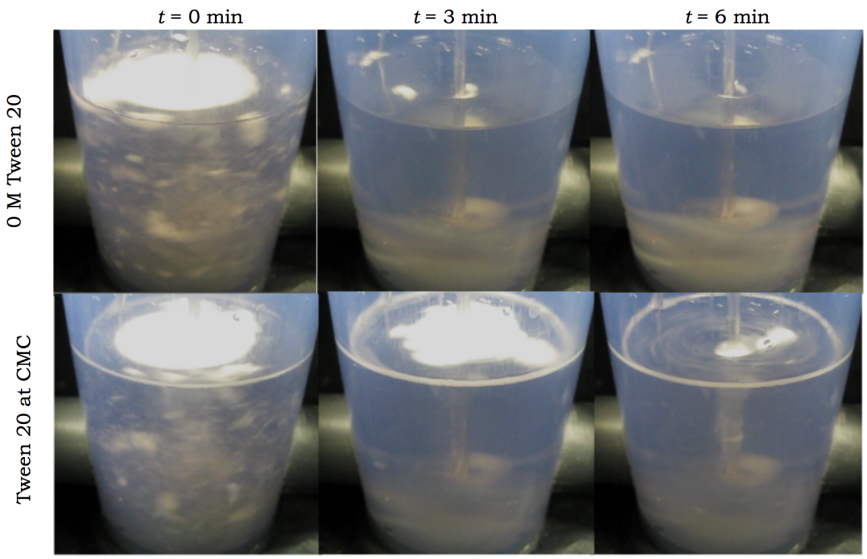

Figure 12.17: Maltodextrin DE6 reconstitution at 0 M and at the CMC of polysorbate 20.

indicating that a surface excess is present, due to the detergent-like properties of polysorbate 20. What is particularly striking from the videos is that better sinking (and overall reconstitution) was seen at *higher* γ. FBRM results (Fig. 12.18) show a similar trend: at 0 % tween 20, all of the powder sinks at the beginning, disperses, and dissolves. However, at the CMC, most of the powder sinks and disperses, but some remains floating before being entrained several minutes later.

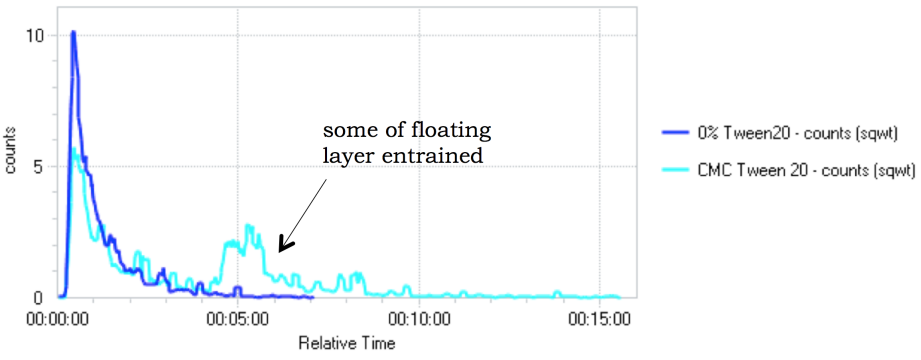

Figure 12.18: FBRM results of maltodextrin DE6 reconstitution at 0 M and at the CMC of polysorbate 20.

12.2.3 Milk experiments

Whole milk powder (WMP, $a_w = 0.32$ at 25 °C) experiments were also performed at 0 % and at the CMC of polysorbate 20. The conditions chosen were $N = 600$ rpm and $T = 45$ °C, since sinking would be gradual but complete (see regime maps in § 11.1). FBRM results (Fig. 12.19) suggest very similar behavior under both conditions, with a slight improvement in dispersing at the CMC of polysorbate 20 – one possible explanation is that as particles contact the surface (where surfactant molecules would preferentially orientate their lipophilic moieties into the air) some surfactant may adsorb to the surface of the lipophilic particle surface, and these newly "partially coated" particles would disperse better once submerged, possibly due to improved EDL dispersion (§ 12.1).

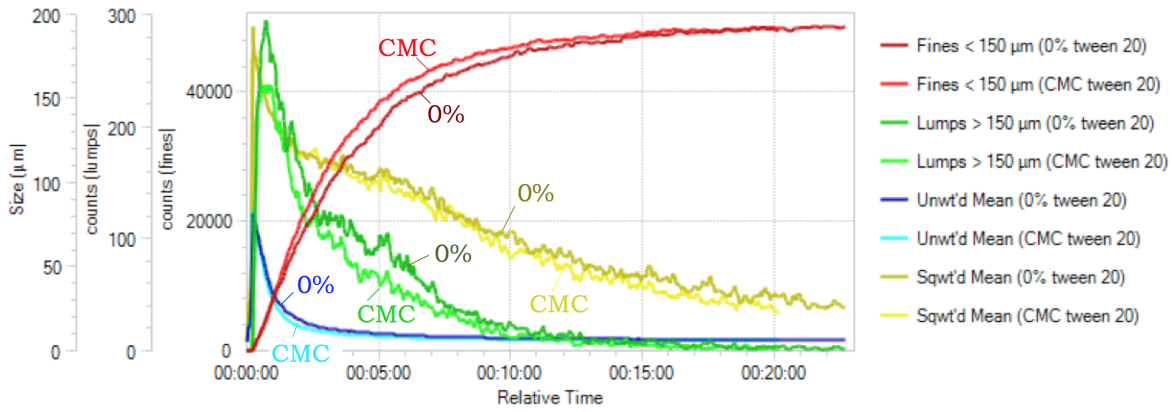

Figure 12.19: FBRM results of WMP reconstitution at 0 M and at the CMC of polysorbate 20.

However, if one observes the videos (Fig. 12.20) a different trend becomes apparent. Lumps at the surface are less likely to disperse at the CMC – and as these lumps are floating just below the liquid surface (likely because they contain dry particles and air – § 10.1), they would not be detected by the FBRM probe. This is an indication that *large lump* dispersing was worse as a result of the lowered γ. Thus perhaps the slower capillary penetration into the powder bed was *too slow* compared to the pore-collapse phenomena, and as a result lumps were more difficult to disperse.

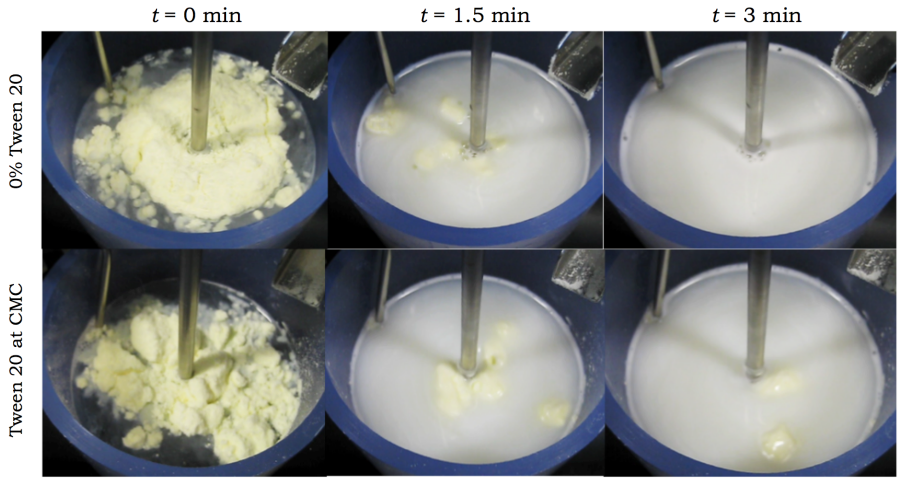

Figure 12.20: Videos of WMP reconstitution at 0 M and at the CMC of polysorbate 20.

12.2.4 Discussion

It appears that a reduced γ by adding surfactant is *not* an effective way to improve sinking and lump formation of bulk food powders, contrary to the claims of Schubert (1993). Thus, one should consider the bulk solids as a capillary network rather than thinking of them as single particles. The effect of surfactant addition on the capillary rise of water into a porous network (tablet) is demonstrated in Fig. 12.21. Maltodextrin DE21 was compressed in a tabletting simulator to obtain a porosity of 32 % (see Mitchell et al. (2011) for more specific details). The tablets were then placed into a thin layer of water at 25 °C, colored with methlyene blue for easier visualization. It is apparent from the time-lapses that penetration is faster when γ is higher, in agreement with the Washburn Equation (§ 1.1).

§12.3 Viscosity

As discussed in § 10.1, maltodextrin DE6 was much more difficult to sink than DE21, due to the high molecular weight (MW). It was also shown (Fig. 10.11) that capillary penetration into tablets of equal porosity was better for the lower–MW material (i.e. DE21). However, as the contact angles θ were not extremely different, it is possible that a difference in wettability may not be the only mechanism for the slower capillary rise (and water–logging) associated

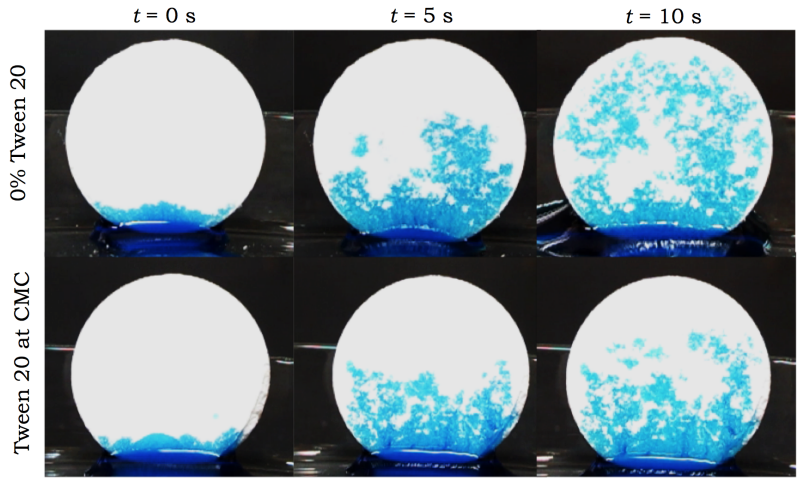

Figure 12.21: Capillary penetration of water into tablets of maltodextrin DE21, at 0 M and at the CMC of polysorbate 20.

with sinking, but that the *viscosity* (μ) of the resultant solution upon dissolving may also play a role[2], as explained in Chávez Montes et al. (2011b). To test the effects of μ on powder wetting/sinking, dispersing, and dissolving, maltodextrins IT21 and IT6 (a_w 0.22 at 25 °C) were reconstituted into aqueous solutions of the same respective materials. (Both powders sink into water instantly, as demonstrated in § 10.1.)

12.3.1 Experimental conditions

All experiments were performed at $N = 600$ rpm and $T = 25$ °C, as regime maps in § 10.1 demonstrated that under these conditions, both powders exhibit good dispersing, but dissolving is not extremely fast. All other conditions were kept at the default values (§ 7.2), i.e. 2.0 % powder added, etc. Conductivity measurements, once again, are ignored due to uninterpretable results at concentrations $\neq 0$; see, for instance, Fig. 12.22.

12.3.2 Results

The sinking times (t_{sink}) are shown in Tab. 12.2. For IT21, sinking was instant up until about 12 %, above which it only took a few seconds. However, for IT6, t_{sink} at 0 % already requires

[2] cf. Eq. 1.14; $\frac{l^2}{t} \propto \mu^{-1}$.

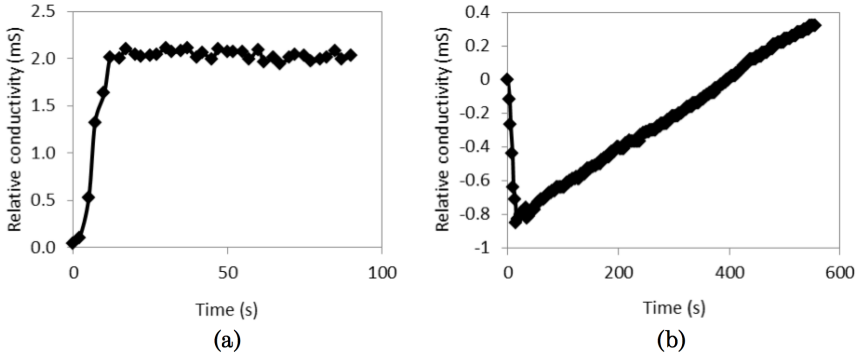

Figure 12.22: Conductivity measurements of maltodextrin IT21 added to (a) deionized water, (b) 18 % solution of the same material.

a few seconds, and always increases with higher concentrations. Between 6 and 8 %, there is a huge jump in t_{sink}, from $\approx 10\,\text{s}$ to $\approx 10\,\text{min}$. At 14 % the powder did not sink within 30 min, thus higher concentrations were not tested.

The IT21 FBRM results (Fig. 12.23) reveal that with increasing concentration, the peak of the curve increases, and dissolving is slower – referring to the discussion from Ch. 9, it is believed that the bypass dissolving (k_3) is slower, as well as the "dissolving rate via suspension" (k_2).

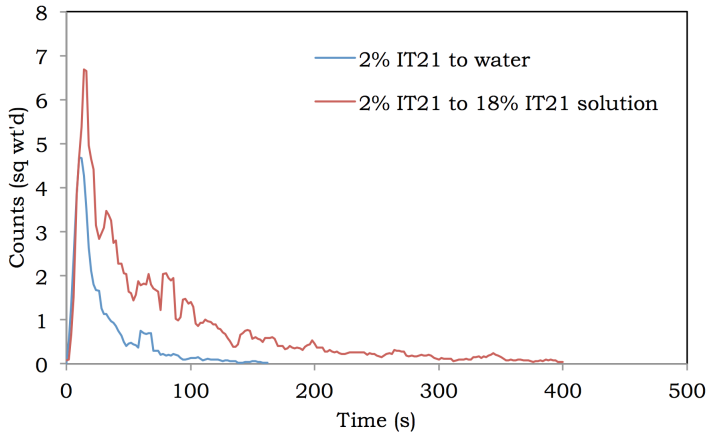

Figure 12.23: FBRM results of maltodextrin IT21 being added either to deionized water or an 18 % IT21 solution.

Video time-lapses for the first few seconds (Fig. 12.24) also revealed that at 0 %, the powder sinks and disperses immediately as it hits the water. However at 18 %, the particles collect at the surface as a powder bed, then sink together as one entity, that gets broken up by the spinning impeller.

Table 12.2: Sinking times for maltodextrins IT21 and IT6 into solutions of increasing concentrations of the same material, respectively.

Conc. (before 2 % powder addition)	IT21	IT6
0 %	Instant	2.5 s
2 %	Instant	3.5 s
4 %	Instant	6.5 s
6 %	Instant	10.5 s
8 %	Instant	10 min 30 s
10 %	Instant	10 min 50 s
12 %	1 s	15 min 20 s
14 %	2 s	> 30 min
16 %	2 s	N/A
18 %	2 s	N/A

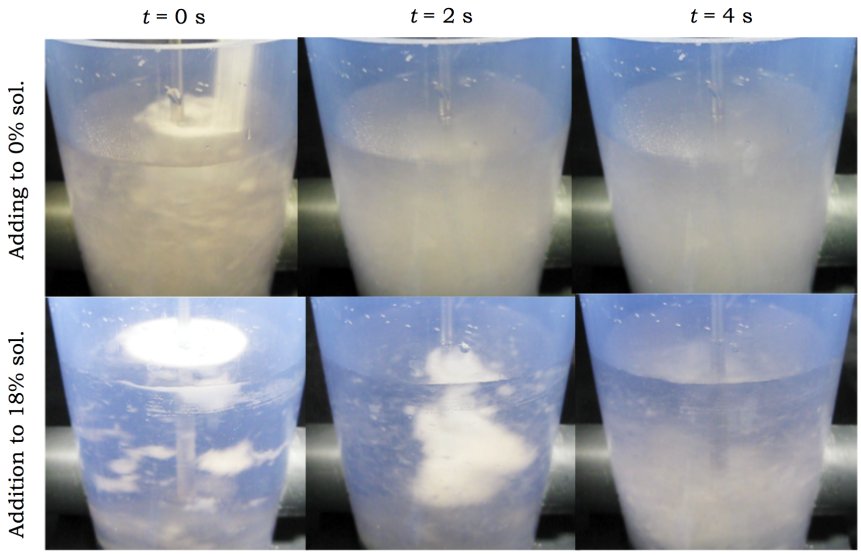

Figure 12.24: First few seconds of the video of maltodextrin IT21 being added either to deionized water or a 18 % IT21 solution.

For IT6, the FBRM results (Fig. 12.25) are not quite as useful due to poor sinking. At 0 % sinking was quick, and a peak in counts is quickly reached, followed by quick dissolving. However for 10 %, a lower peak is obtained, and dissolving was slower – the lower peak can be explained by the slower sinking of the powder (*not* related to bypass dissolving) – see Fig. 12.26.

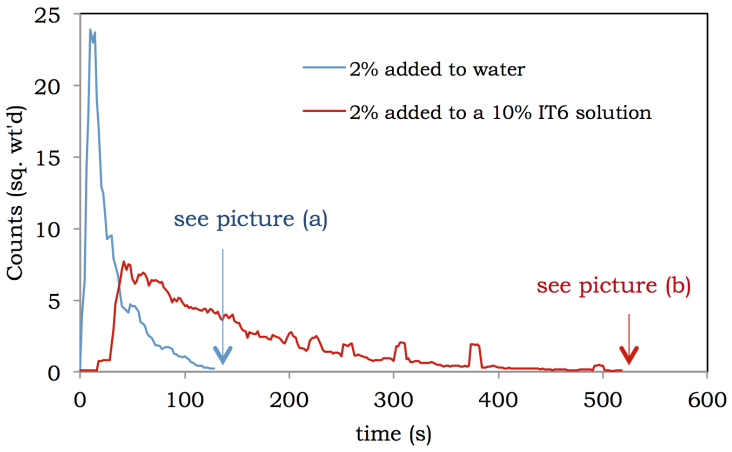

Figure 12.25: FBRM results of maltodextrin IT6 being added either to water or a 10 % IT6 solution.

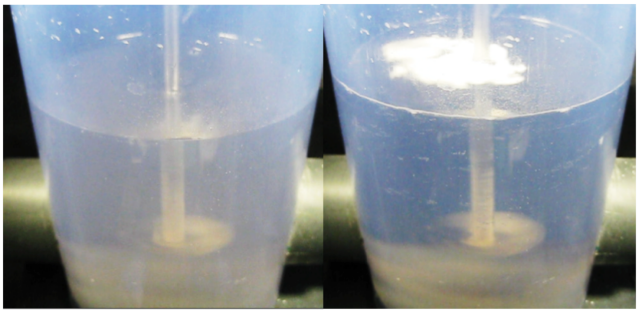

Figure 12.26: Videos of maltodextrin IT6 being added either to (a) water ($t = 2\,\text{min}$) or (b) a 10 % IT6 solution ($t = 9\,\text{min}$). These two figures correspond to Fig. 12.25.

Looking closer into the initial few seconds of reconstitution for IT6 at 0 % (Fig. 12.27), a similar result is obtained as for IT21 at 18 % (Fig. 12.24), where powder collects at the surface before falling as a single bed.

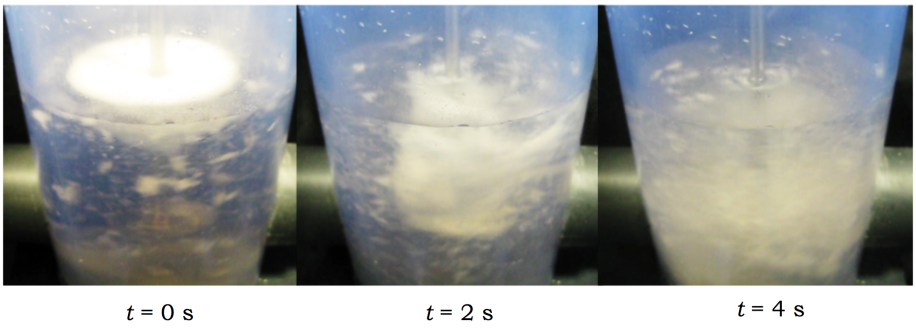

Figure 12.27: First 4 s of maltodextrin IT6 being added to water.

12.3.3 Viscosity of maltodextrin solutions

Viscosity measurements of solutions of maltodextrins IT21 and IT6 were performed using a Malvern Kinexus Pro (Malvern, UK) using a cone-and-plate setup (see § 5.5), with a cone angle of 1° and a plate of diameter 50 mm. Measurements were performed at 25 °C with a solvent cover used to prevent evaporation. Viscosity (μ) measurements were taken at a range of shear rates ($\dot{\gamma}$) from 10^{-1} to $10^{3}\,s^{-1}$, with 10 measurements per decimal order. This range more than spans the $\dot{\gamma}$ values of interest for mixing applications in the current study (Tab. 7.2). Plots of μ vs. $\dot{\gamma}$ reveal Newtonian behavior, i.e. $\mu \neq f(\dot{\gamma})$ (not shown), in agreement with Dokic et al. (1998). Results of μ vs. concentration for IT21 and IT6 are shown in Fig. 12.28.

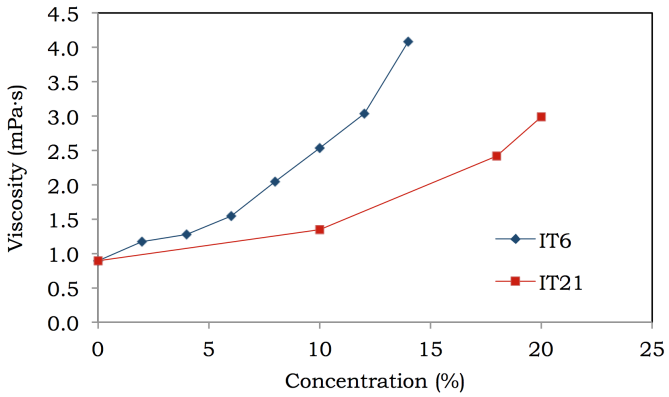

Figure 12.28: Viscosity measurements for increasing concentrations of maltodextrins IT21 and IT6.

As expected, μ increases with concentration for both materials, and a lower DE value (§ 8.1) resulted in a higher μ, also in agreement with Dokic et al. (1998), and as explained in § 6.1, the relationship between μ and concentration is not linear. One important observation

is that the μ at 18 % IT21 is higher than the μ for 10 or 12 % IT6; however, as shown in Tab. 12.2, at 18 %, IT21 still sank after a few seconds but at concentrations $\geq$ 10 % for IT6, sinking took several minutes. Therefore it appears that μ alone cannot explain the observed difference in behavior of maltodextrins DE21 and DE6 (§ 10.1) – it may be that a combination of wetting and viscosity effects are responsible for the results, as well as (possibly) the fact that less entropy is to be gained from the dissolving of higher-MW materials.

In addition, rheological experiments were performed at different temperatures T, and a decrease in μ was observed at increasing T (following an Arrhenius-like pattern, similar to Abbès et al. (2015)); results are not shown. This lower μ at higher T may have helped with capillary penetration, thus partially explaining why increasing the T helped improve the sinking of DE6 at $N = 600\,\mathrm{rpm}$ (§ 10.1).

Chapter 13

Vessel Configuration

Large-scale problems do not require large-scale solutions; they require small-scale solutions within a large-scale framework.

David Fleming

In all of the previous experimental chapters, a default vessel configuration (§ 7.1) was used; the vessel was unbaffled and an axial (Lightnin A100) impeller was used. As discussed in § 3.2, a more radial impeller (e.g. Lightnin R100) and baffles will change the mixing patterns (§ 13.1). As discussed in § 3.4, some studies have reported better drawdown if the impeller is positioned closer to the vortex bottom (§ 13.2). In § 3.5, it was explained that upon geometrically-similar scale-up, different scale-up criteria are possible to attempt to preserve dispersion behavior on a larger scale, such as the impeller tip speed (v_p) or specific power draw (P/V) (§ 13.3).

Contents

§13.1 Impellers and Baffling

In the current section, two impeller types are compared: the Lightnin A100 and the Lightnin R100 (for comparison purposes, see Fig. 3.1) – the diameter d of the two impellers is the same. As discussed in § 3.2, the axial impellers would convert more energy into swirling rather than shearing effects compared to the radial impellers. For baffling, the same vessel is used as in the default configuration, but a baffle insert (with four baffles, placed at 90° from each other), which was custom-made along with the vessel, is added; the baffle width adheres to Rushton et al. (1950)'s standards (Fig. 3.4), i.e. $\frac{1}{10}$ the vessel diameter D, and the thickness is $\frac{1}{2}$ its width. There is no offset of the baffles from the vessel wall. As discussed in § 3.4, there are conflicting reports in the literature about whether unbaffled or baffled vessels are better for powder downdraw, and overall mixing.

In total, four vessel configurations were tested in the current section: (1) A100, unbaffled (default configuration), (2) A100, baffled, (3) R100, unbaffled, and (4) R100, baffled. Since energy efficiency is a major concern for mixing applications (Ch. 3), the same power draw (P) – or specific power draw (P/V) as the volume V is constant – is used to compare different configurations. As discussed in Ch. 3, each configuration will have a different relationship between P and agitation speed N: R100 will draw more power than A100 at the same N, as will a baffled configuration compared to unbaffled.

13.1.1 Characterization of alternative configurations

The characterizations for configuration 1 was already shown in Tab. 7.2; the five P/V values from this characterization were also used for configurations 2 – 4. Regression equations (not shown) were used to determine the N necessary to obtain those five P/V values. Based on the N needed, other vessel characteristics (for water at 25 °C) are then also determined (see Tables 13.1–13.3).

Table 13.1: Vessel configuration for *baffled* vessel with Lightnin *A100* impeller with water at 25 °C.

P/V	P	N	N	Re	Fr	v_p	v_{surf}	h'_{meas}	We	$\dot{\gamma}_{\text{av,imp}}$	$\dot{\gamma}_{\text{av,tank}}$
$[\text{W m}^{-3}]$	[mW]	[rpm]	$[\text{s}^{-1}]$	[-]	[-]	$[\text{m s}^{-1}]$	$[\text{m s}^{-1}]$	[mm]	[-]	$[\text{s}^{-1}]$	$[\text{s}^{-1}]$
0.95	0.72	219	3.65	4454	0.04	0.38	N/A	0	6.6	127.8	36.5
6.43	4.90	420	7.00	8529	0.16	0.72	N/A	0	24.3	245.0	69.9
19.05	14.52	607	10.11	12336	0.34	1.05	N/A	0	50.9	354.1	101.1
41.25	31.44	789	13.14	16036	0.58	1.36	N/A	0	86.0	460.3	131.4
71.71	54.64	952	15.86	19347	0.85	1.64	N/A	0	125.1	555.3	158.6

Table 13.2: Vessel configuration for *unbaffled* vessel with Lightnin *R100* impeller with water at 25 °C.

P/V	P	N	N	Re	Fr	v_p	v_{surf}	h'_{pred}	h'_{meas}	We	$\dot{\gamma}_{\text{av,imp}}$	$\dot{\gamma}_{\text{av,tank}}$	Q
$[\text{W m}^{-3}]$	[mW]	[rpm]	$[\text{s}^{-1}]$	[-]	[-]	$[\text{m s}^{-1}]$	$[\text{m s}^{-1}]$	[mm]	[mm]	[-]	$[\text{s}^{-1}]$	$[\text{s}^{-1}]$	$[\times\ 10^5\ \text{m}^3\ \text{s}^{-1}]$
0.95	0.72	118	1.97	2404	0.01	0.20	0.06	1.7	0	1.9	118	25.6	5.7
6.43	4.90	237	3.94	4814	0.05	0.41	0.13	6.9	4.0	7.8	237	51.3	11.3
19.05	14.52	351	5.85	7141	0.12	0.61	0.17	15.2	13.0	17.1	351	76.1	16.8
41.25	31.44	465	7.74	9452	0.20	0.80	0.23	26.7	24.0	29.9	465	100.7	22.3
71.71	54.64	568	9.47	11552	0.30	0.98	0.47	39.9	39.0	44.6	568	123.1	27.2

Table 13.3: Vessel configuration for *baffled* vessel with Lightnin *R100* impeller with water at 25 °C.

P/V	P	N	N	Re	Fr	v_p	v_{surf}	h'_{meas}	We	$\dot{\gamma}_{\text{av,imp}}$	$\dot{\gamma}_{\text{av,tank}}$
[W m^{-3}]	[mW]	[rpm]	[s^{-1}]	[-]	[-]	[m s^{-1}]	[m s^{-1}]	[mm]	[-]	[s^{-1}]	[s^{-1}]
0.95	0.72	91	1.51	1840	0.01	0.16	N/A	0	1.1	91	19.1
6.43	4.90	169	2.81	3431	0.03	0.29	N/A	0	3.9	169	36.6
19.05	14.52	240	4.01	4888	0.05	0.42	N/A	0	8.0	240	52.1
41.25	31.44	309	5.15	6286	0.09	0.53	N/A	0	13.2	309	67.0
71.71	54.64	370	6.17	7527	0.13	0.64	N/A	0	18.9	370	80.2

Comparing A100 and R100, unbaffled

Comparing the characterization of the unbaffled A100 (Tab. 7.2) vs. R100 (Tab. 13.2) impellers, as expected the stir rate N to obtain the same P/V is lower for R100, thus the tip speed v_p (Eq. 3.14) is also lower. While Re (Eq. 3.5) is higher for A100, the cut-off between transitional and turbulent flows is lower for R100 for A100 (10^4 vs. 10^5 – see § 3.3), and thus for $P/V = 71.71\,\mathrm{W\,m^{-3}}$, the flow is transitional for A100 but turbulent for R100; otherwise all flows are transitional. The vortex depth h' predicted (Eq. 3.15) was about the same for A100 and R100; however, the measured depth was much greater for R100 than A100, and the predicted value was close to the measured value, but the same was not true for the A100 vessel (Tab. 7.2). The speed at the vessel surface v_{surf} (§ 7.3) was also faster for R100. The average shear rate in the impeller region $\dot{\gamma}_{\mathrm{av,imp}}$ was about the same for A100 and R100, but the $\dot{\gamma}$ for the whole tank would be higher for A100. The pumping capacity Q (Eq. 3.10) is also greater for A100, as expected. For estimating N_{js} (Eq. 3.17) at 25 °C, the D_p was assumed to be the $d_{50,3}$, and ρ_p was assumed to be the ρ_t of maltodextrin DE21 (§ 8.4): the N_{js} would be higher for A100 compared to R100 (ca. 682 rpm vs. 435 rpm, respectively), but the corresponding "$(P/V)_{\mathrm{js}}$" is lower for A100 ($26.8\,\mathrm{W\,m^{-3}}$) than R100 ($34.8\,\mathrm{W\,m^{-3}}$).

Comparing unbaffled and baffled configurations

For A100, as the power number N_p does not change significantly with baffling (Fig. 7.2), the agitation speed N does not change very much and thus characteristics such as v_p are very similar. However the baffles prevent vortex formation and the circular surface movement seen with unbaffled vessels; this is also true for R100 (un– vs. baffled). However, for R100 N_p dramatically increases with baffling (Fig. 7.2), thus a much lower N is needed to obtain the same P/V. As a result, characteristics such as v_p, etc. are much lower.

13.1.2 Results

Maltodextrins DE21 and DE6 (§ 8.1; $a_w = 0.23 \pm 0.02$ at 25 °C) were reconstituted at $71.71\,\mathrm{W\,m^{-3}}$ (equivalent to $N = 1000$ rpm for the default vessel) at 25 °C, with all other

conditions adhering to the defaults (§ 7.2). Experiments are performed in triplicate to ensure repeatable behavior. FBRM results for all configurations for DE21 are shown in Fig. 13.1.

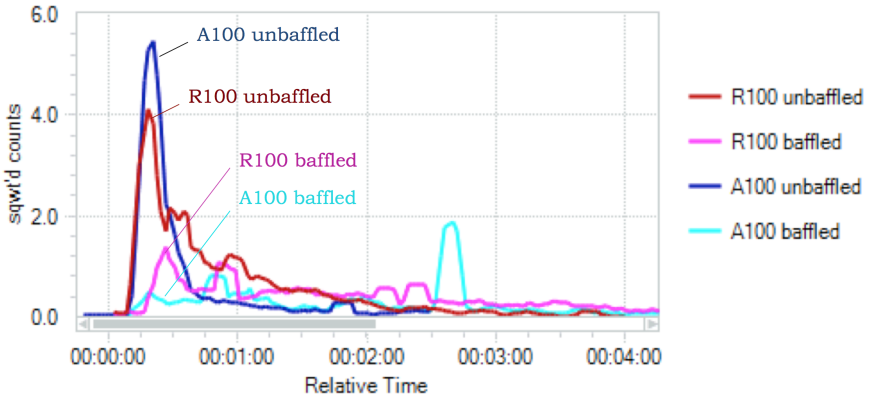

Figure 13.1: FBRM results for maltodextrin DE21 for all four configurations.

The results for R100 and A100 (unbaffled) are very similar – dispersing is quick, as is dissolving. However, there is a much lower rise in signal for both impellers under baffled conditions. Videos reveal that this is due to heavy sedimentation for this fast-sinking powder (Fig. 13.2).

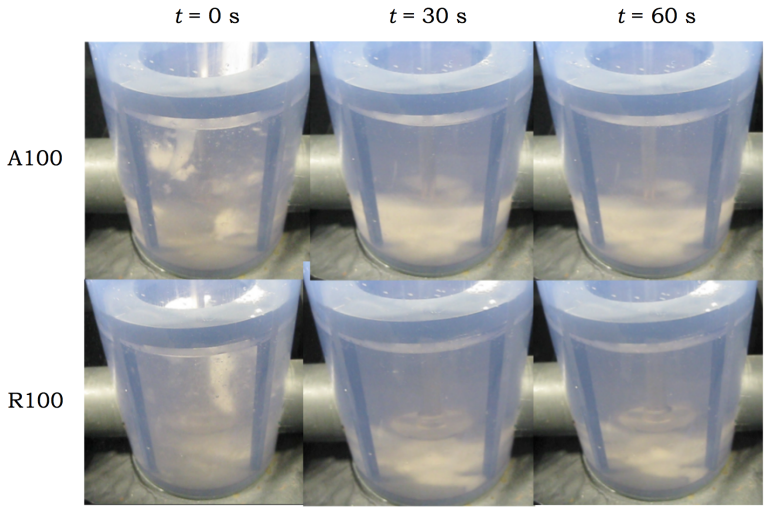

Figure 13.2: Time-lapses from the baffled configurations of maltodextrin DE21 reconstitution.

For maltodextrin DE6, FBRM measurements also appear similar (Fig. 13.3) – A100 and R100 results for unbaffled conditions show good dispersing and dissolving, but not for baffled conditions.

However, the cause for the poor dispersion for baffled conditions is not due primarily to

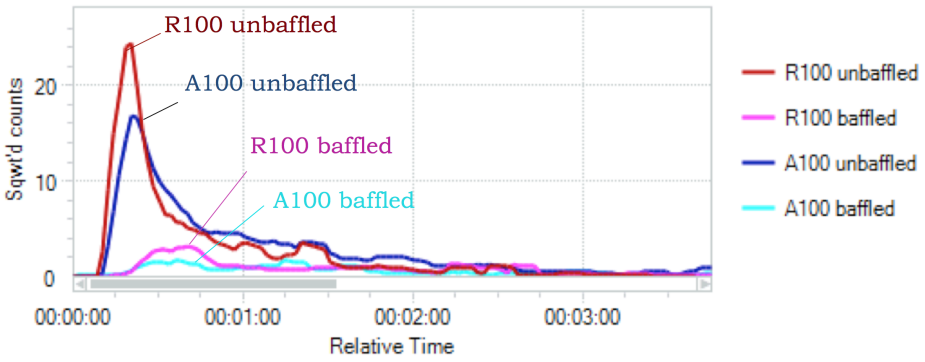

Figure 13.3: FBRM results for maltodextrin DE6 for all four configurations.

sedimentation, but rather to poor sinking (Fig. 13.4).

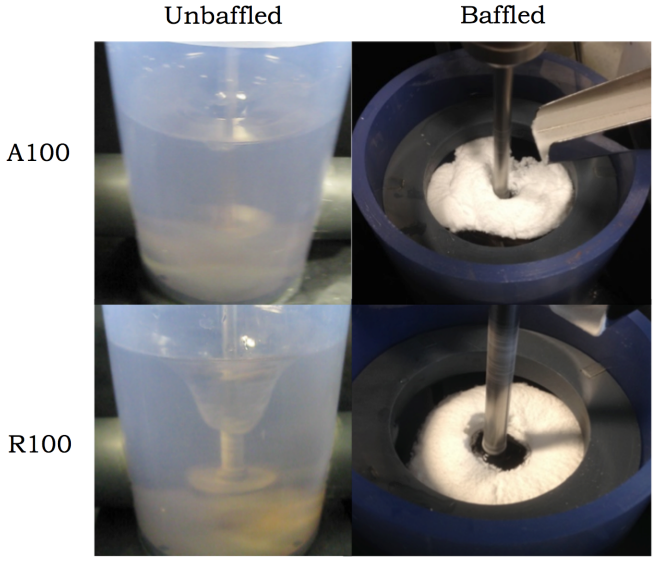

Figure 13.4: Video capture at $t = 2\,\text{min}$ of maltodextrin DE6 for all four configurations.

SMP

Skim and whole milk powders (SMP and WMP, $a_w = 0.3 \pm 0.02$) were reconstituted at $P/V = 71.71\,\text{W m}^{-3}$ at $T = 45\,°\text{C}$, with all other conditions being default (§ 7.2). FBRM results SMP are shown in Fig. 13.5.

Results suggest that for the unbaffled vessel, results obtained with the A100 and R100 impellers are very similar. For both impellers, dispersion was worse with baffling, with A100 (baffled) being worse than R100 (baffled). A closer look at the videos of the liquid surface (Fig. 13.6) reveal that due to poor downdraw into the vessel, baffled conditions led to the

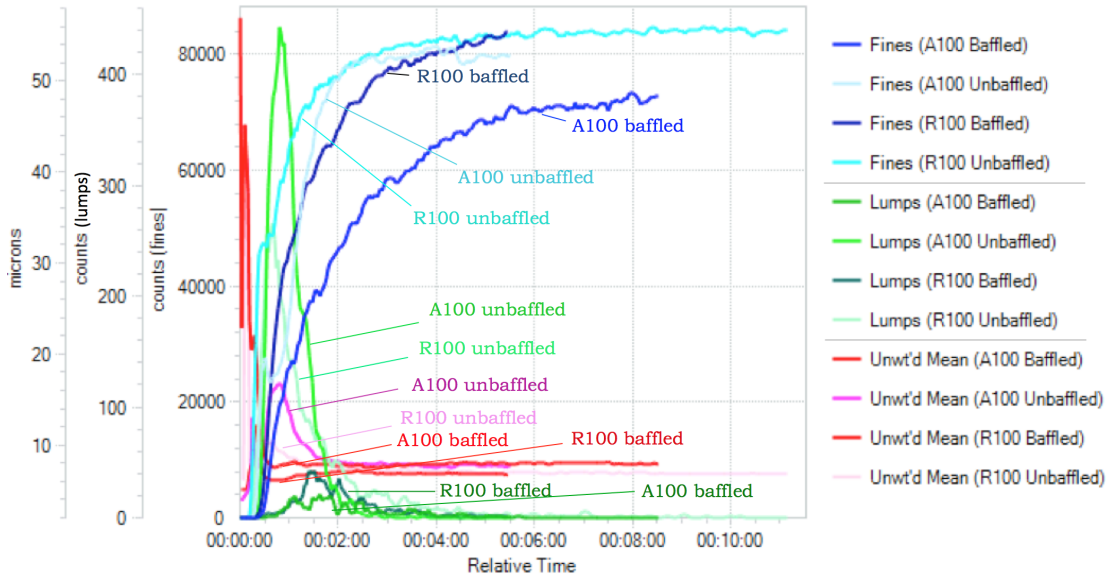

Figure 13.5: FBRM results for SMP for all four configurations.

formation of a heap of powder, that could evolve into a floating lump with encapsulated dry grains (and air), if the heap periphery becomes wetted. The floating heap/lump may remain for even longer than one hour.

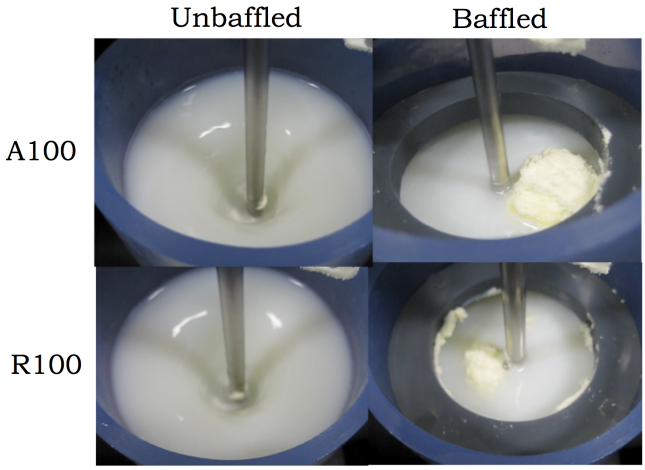

Figure 13.6: Video captures of SMP ($t = 2\,\text{min}$) for all four configurations.

WMP

The FBRM results for WMP are shown in Fig. 13.7. Results indicate better dispersing for unbaffled than baffled conditions. Moreover, it appears that the R100 impeller was slightly better than the A100 impeller at drawing the powder down and dispersing it.

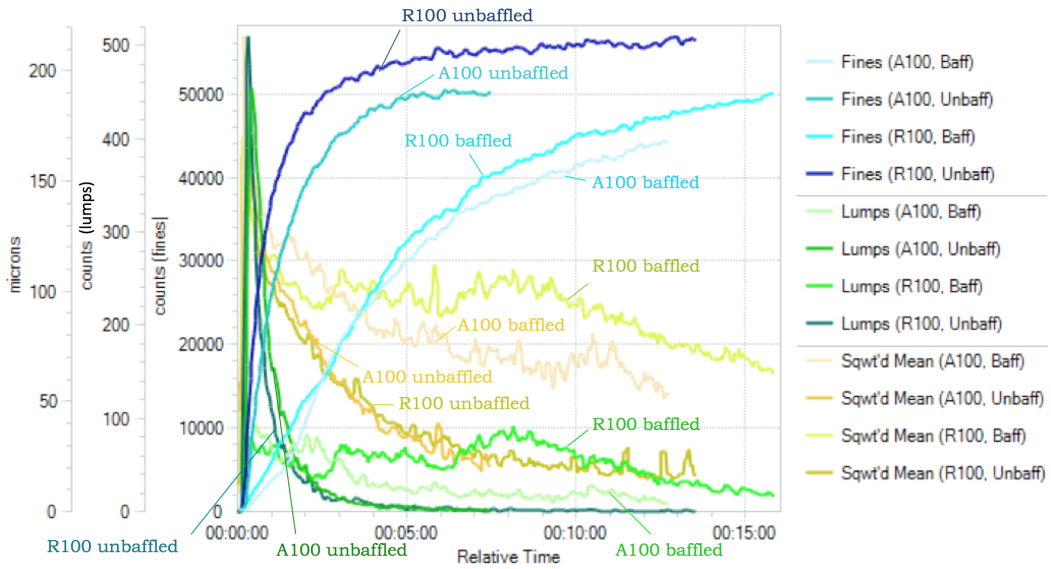

Figure 13.7: FBRM results for WMP for all four configurations.

Videos (Fig. 13.8) reveal, similar for SMP, that a heap/lump is likely to form at the liquid surface, limiting overall reconstitution.

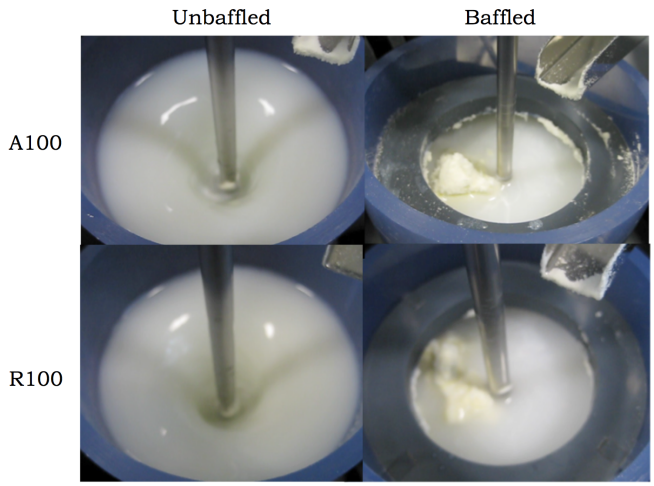

Figure 13.8: Video results for WMP ($t = 2\,\text{min}$) for all four configurations.

13.1.3 Discussion

For all powders tested, unbaffled configurations were preferable to baffled conditions – this is likely due to the fact that, for baffled conditions, there is little liquid motion at the water surface as the powder is being added, thus powder will fall on top of other particles forming an undesirable heap. The vortex formed for unbaffled conditions may also help

incorporate powder into the liquid bulk (§ 3.4). For fast-sinking powders (maltodextrin DE21), sedimentation appears to be a problem for baffled configurations, and for slow-sinking powders, heap or floating layer formation may become a problem. Thus *unbaffled conditions are preferable to baffled when reconstituting food powders.* For the Lightnin A100 and R100 impellers, results appear to be similar for equivalent power draw P, but there is some evidence to suggest that the R100 impeller was more effective at drawing powder down, possibly due to faster liquid surface speed v_{surf} and a deeper vortex h'. The importance of vessel configuration was demonstrated in the current section; as discussed in § 5.12, it is frustrating to review the literature on food powder reconstitution in stirred tanks, as the vessel configuration is very often left unspecified.

§13.2 Impeller Submergence

As discussed in § 3.4, there is evidence to suggest that a lower submergence (H' in Fig. 3.4) can aid in drawing down hard-to-sink food powders, and thus can improve reconstitution overall. This was tested using the default vessel configuration (§ 7.2), by testing the t_{sink} and dispersion characteristics at $H' = 2\,d$ (default), where d is the impeller diameter, and $H' = d$ (high impeller position). Experiments were performed (in duplicate) using skim milk powder (SMP) ($a_w = 0.27$) at $T = 25\,°\text{C}$ and $N = 800\,\text{rpm}$, where according to the limiting regime maps in § 11.1, sinking would be expected to be gradual. FBRM results are shown in Fig. 13.9; the $t_{\text{sink}} = 9\,\text{min}45\,\text{s}$ for default submergence, and $5\,\text{min}30\,\text{s}$ for high impeller position.

Results suggest better sinking, as well as better dispersing, when the impeller is closer to the liquid surface.

§13.3 Scale-Up

As discussed in Ch. 3, scaling-up mixing processes is challenging due to the complex relationship between different mixing characteristics and the characteristic length. Geometric

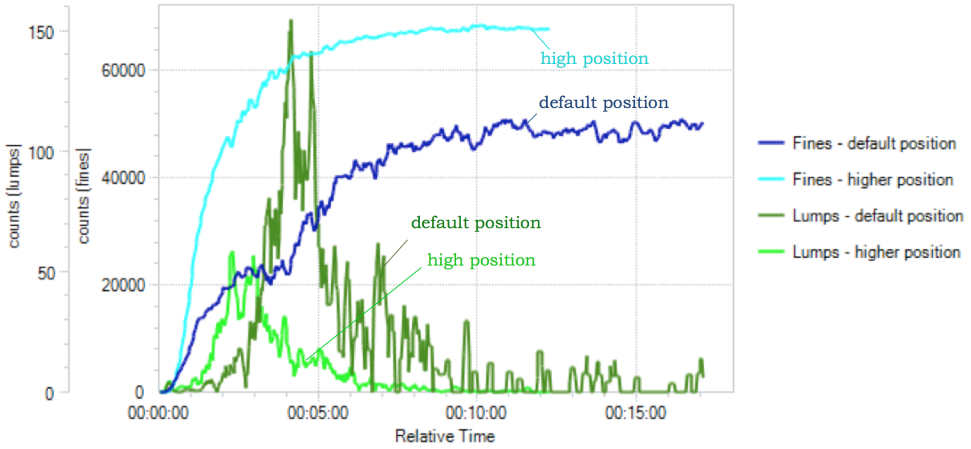

Figure 13.9: FBRM results for SMP for low and high impeller submergence H'.

similarity between the small and large vessel can simplify scale-up with, in general, the only parameter to be adjusted being the stir speed N. Upon scale-up, N is reduced, and two common scale-up criteria to determine N_2 (Eq. 3.18) are the specific power draw (P/V) and the tip speed (v_p), depending on the *aim* of scale-up (§ 3.5). In the current study, experiments are performed with different powders: maltodextrin DE6 and whole milk powder (WMP), in the smaller vessel (default vessel; § 7.1) and a larger vessel (Fig. 13.10), with a linear scale-up factor (d_2/d_1; Eq. 3.18) of 2.22. The larger vessel was also custom-built out of PVC at the University of Sheffield workshop, and also adheres to Rushton et al. (1950)'s standards (Fig. 3.4). The impeller is a larger Lightnin A100 propeller with the same pitch-to-diameter ratio ($p/d = 1$; cf. Fig. 7.2) as the smaller impeller. Therefore the vessel is geometrically similar, simplifying scale-up.

Figure 13.10: Smaller and larger vessels for scale-up study.

For each trial performed in the smaller vessel, two experiments are performed in the larger vessel: with an N_2 corresponding either to constant P/V or v_p (see § 3.5).

13.3.1 Characterization of scaled-up vessel at constant P/V and v_p

N_2 values for P/V– and v_p–scale up correspond to those used for the default vessel in (Tab. 7.2), i.e. $N_1 = 200, 400, \ldots, 1000\,\text{rpm}$. They are determined for water at 25 °C. P/V–scale-up N_2 values, and corresponding mixing characteristics, are shown in Tab. 13.4. Results for constant v_p are shown in Tab. 13.5.

Table 13.4: Mixing characteristics of larger vessel, maintaining constant P/V (cf. Tab. 7.2). For the highest setting, the hollow glass beads were sucked into a very strong vortex (Fig. 13.11), and thus no value of v_{surf} is specified.

P/V	P	N	N	Re	Fr	v_p	v_{surf}	h'_{pred}	h'_{meas}	We	$\dot{\gamma}_{\text{av,imp}}$	$\dot{\gamma}_{\text{av,tank}}$
$[\text{W m}^{-3}]$	[mW]	[rpm]	$[\text{s}^{-1}]$	[-]	[-]	$[\text{m s}^{-1}]$	$[\text{m s}^{-1}]$	[mm]	[mm]	[-]	$[\text{s}^{-1}]$	$[\text{s}^{-1}]$
0.95	130503	119	1.98	10873	0.03	0.44	0.06	4.2	0	19	69.3	19.8
6.43	883729	238	3.96	21743	0.12	0.87	0.15	16.7	15	75	138.6	39.6
19.05	2619685	352	5.87	32233	0.25	1.29	0.22	36.7	44	164	205.5	58.7
41.25	5671222	466	7.77	42642	0.43	1.71	0.34	64.3	72	287	272.0	77.7
71.71	9858319	569	9.49	52099	0.64	2.09	N/A*	95.9	105	428	332.2	94.9

Table 13.5: Mixing characteristics of larger vessel, maintaining constant v_p (cf. Tab. 7.2).

v_p	N	N	P/V	P	Re	Fr	v_{surf}	h'_{pred}	h'_{meas}	We	$\dot{\gamma}_{\text{av,imp}}$	$\dot{\gamma}_{\text{av,tank}}$
$[\text{m s}^{-1}]$	[rpm]	$[\text{s}^{-1}]$	$[\text{W m}^{-3}]$	[mW]	[-]	[-]	$[\text{m s}^{-1}]$	[mm]	[mm]	[-]	$[\text{s}^{-1}]$	$[\text{s}^{-1}]$
0.35	94	1.57	0.56	77437	8626	0.02	0.04	2.63	0	12	55.0	15.7
0.70	189	3.14	3.82	524593	17252	0.07	0.09	10.5	0	47	109.9	31.4
1.04	283	4.71	11.68	1606396	25877	0.16	0.14	23.7	22	106	164.9	47.1
1.38	377	6.29	25.85	3553826	34503	0.28	0.18	42.1	45	188	220.2	62.8
1.68	471	7.86	47.85	6579266	43129	0.44	0.23	65.7	73	293	275.1	78.6

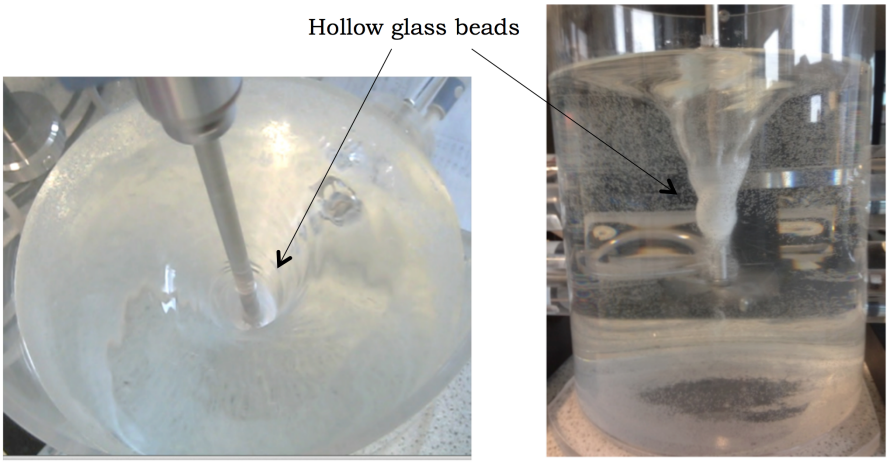

Figure 13.11: Hollow glass beads at $P/V = 71.71\,\mathrm{W\,m^{-3}}$ in large vessel.

Of course, as was made evident in § 3.5, the N_2 values for constant P/V are higher than for constant v_p, thus the power draw P, tip speed v_p, vortex depth h', shear rates $\dot{\gamma}$, surface speed v_{surf}, pumping capacity Q, etc. are all greater for constant P/V than for constant v_p.

With regards to how these mixing characteristics compare with those of the default vessel (Tab. 7.2), some are more similar for v_p-based, and others more similar for P/V-based scale up (S.U.). For instance the surface speed (v_{surf}) is closer between the default and v_p-based S.U., with v_{surf} being "too fast" for P/V-based S.U. The vortex depth h' (relative to the characteristic length) is also closer for v_p-based S.U., with h' being very deep for P/V-based S.U. *Both v_{surf} and h', which are better preserved for v_p-based S.U., are believed to be particularly important for powder* ***sinking*** *effects* (§ 1.2).

The average shear rate $\dot{\gamma}_{\mathrm{av}}$ for the impeller region and the whole tank, on the other hand, are more similar for P/V-based S.U., although $\dot{\gamma}_{\mathrm{av}}$ are much higher for the small vessel. *It is believed that shear effects, which are better preserved for P/V-based S.U., are especially relevant for* ***dispersing*** *(and dissolving when applicable)* – see § 1.3. With regards to Re, the flow regimes remains transitional for all values of N. For all conditions, $\mathrm{Fr} < 1$ and $\mathrm{We} \gg 1$, as expected. It is also worth noting that the predicted vortex depths h' (Eq. 3.15) were quite accurate, especially for stronger agitation speeds; much more accurate than for the default vessel (Tab. 7.2).

13.3.2 Experimental conditions

Since a much greater volume of water and mass of powder are required for experiments in the larger vessel (preserving chemical similitude – see § 3.5), and due to limited resources (powders were of the same respective lots for the materials used in the previous sections, deionized water was difficult to obtain in large quantities, and a large-enough vibratory feeder was not available), a number of conditions were modified from the defaults (defined in § 7.2) for experiments with both the small and large vessels:

- Instead of adding 2.0 % w/v powder, 1.0 % was added.
- Tap water (electrolytical conductivity $< 5\,\mu S\,cm^{-3}$) was used instead of deionized water.
- Instead of adding powder under highly controlled conditions, powder was added manually, all at once.

As the water temperature T was difficult to control for the large vessel, experiments were only performed at 25 °C. The agitation rates N_1 for the default vessel were 600 rpm and 1000 rpm. These were chosen because, as discussed in § 10.1 for maltodextrin DE6 and § 11.1 for WMP, reconstitution is *sinking*-limited at 600 rpm and *dispersing*- (and, in the case of maltodextrin, *dissolving*-limited) at 1000 rpm. Experiments are performed in duplicate to ensure repeatable behavior.

13.3.3 Results – maltodextrin DE6

The FBRM results for maltodextrin DE6 (a_w 0.22 at 25 °C) for $N_1 = 600$ rpm are shown in Fig. 13.12.

Video time-lapses are shown in Fig. 13.13. Results reveal that under these *sinking*-limited conditions, reconstitution behavior was better preserved with v_p as the scale-up criterion – "too much" powder was initially incorporated into the vessel at constant P/V.

For $N_1 = 1000$ rpm, FBRM results are shown in Fig. 13.14. Video time-lapses are shown in Fig. 13.15. Videos reveal that for all conditions, sinking was instant, thus reconstitution is

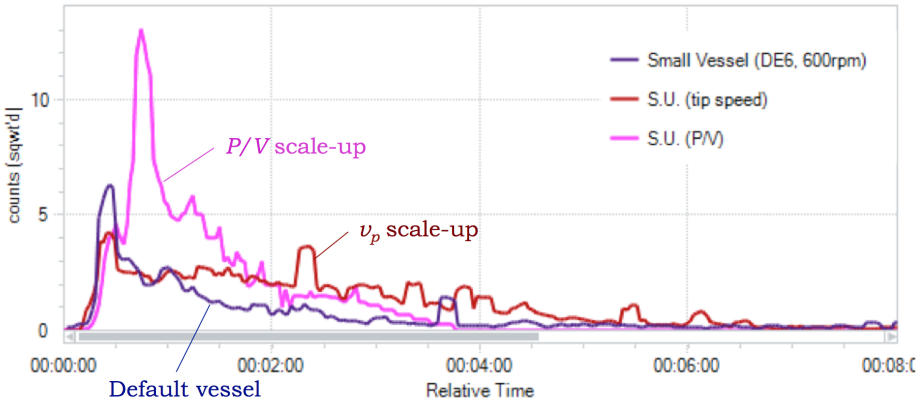

Figure 13.12: FBRM results for maltodextrin DE6 in small and large vessels (N_1 = 600 rpm).

dispersing/dissolving-limited (§ 10.1). FBRM results indicate faster dissolving (decay of the counts from the maximum peak; see Ch. 9) for the default vessel than the scaled-up vessel; as discussed earlier, the $\dot{\gamma}_{av}$ is higher for the smaller vessel, which would explain this observation. However, as the $\dot{\gamma}_{av}$ for P/V-based scale-up is slightly closer to the $\dot{\gamma}_{av}$ values for the default vessel, dissolving for the P/V-based S.U. is slightly closer to the FBRM plot of the default vessel than for v_p-based S.U.

13.3.4 Results – whole milk powder

FBRM results for WMP at N_1 = 600 rpm are shown in Fig. 13.16. Video time-lapses are shown in Fig. 13.17.

For the (mostly) *sinking-limited* conditions, the initial rise in the total counts (i.e. the kinetics) are closer between the default and the v_p-constant S.U. results; this can be explained by similar liquid surface-related characteristics (v_{surf} and h'). However, the overall *extent* of dispersing (the final counts and the mean size), are closer between the default and the P/V-based S.U. conditions, since the $\dot{\gamma}$ is more similar between the two. The fact that the total counts for the P/V results are slightly higher than for the small vessel may be explained by the fact that some of the powder remains at the liquid surface.

Experiments performed at N_1 = 1000 rpm, however, were dispersing-limited, as the powder sank instantly for all conditions. FBRM results (Fig. 13.18) show similar "kinetics" between

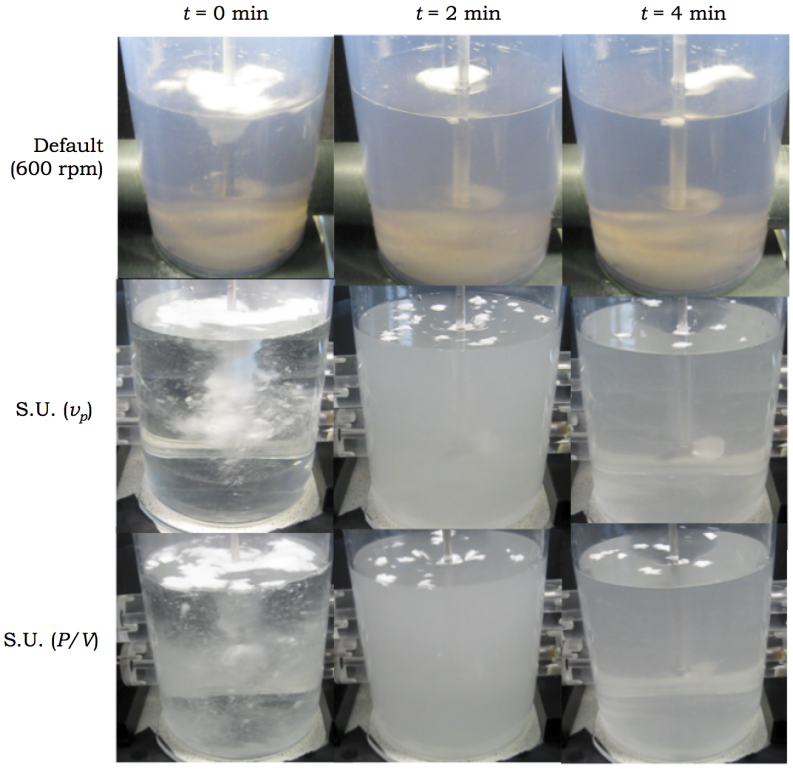

Figure 13.13: Time-lapse results for maltodextrin DE6 in small and large vessels (N_1 = 600 rpm).

the default and P/V-based S.U. results (related to the fact that sinking was similar – see Fig. 13.19). However, dispersing was best (see total counts and mean size) for the default conditions, with P/V-based S.U. being more similar to the default, due to the closer $\dot{\gamma}$, as discussed before.

13.3.5 Discussion

Results from the current section indicate that one should consider the rate-limiting regime of reconstitution (a concept introduced in Ch. 10), when predicting how different scale-up criteria will influence the reconstitution of food powders. For sinking-limited reconstitution, v_p was a better scale-up criterion to preserve behavior in the larger vessel. This is because mixing characteristics related to the liquid free surface are better conserved.

For dispersing-limited reconstitution, P/V was a more appropriate scale-up criterion. This is because mixing characteristics related to shearing effects are better conserved.

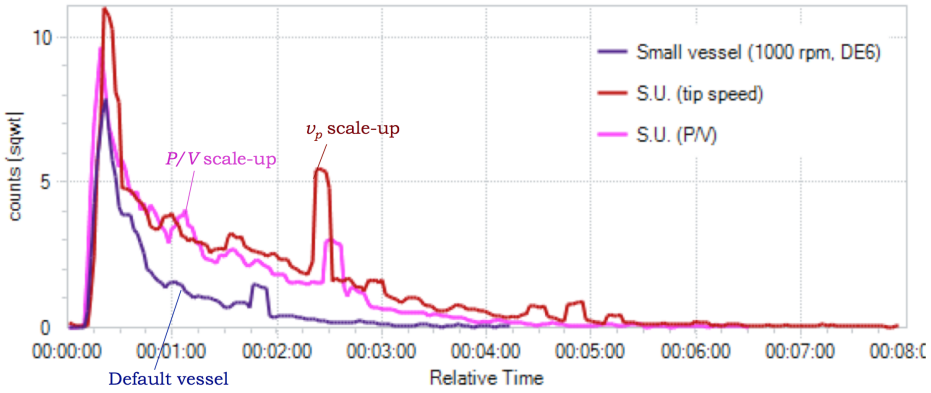

Figure 13.14: FBRM results for maltodextrin DE6 in small and large vessels (N_1 = 1000 rpm).

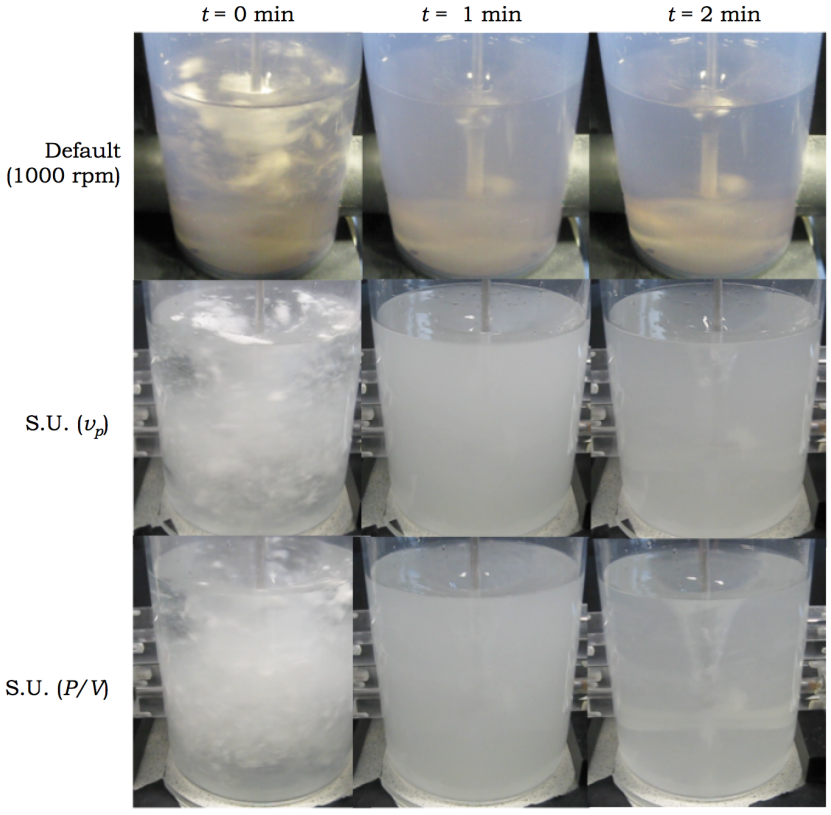

Figure 13.15: Time-lapse results for maltodextrin DE6 in small and large vessels (N_1 = 1000 rpm).

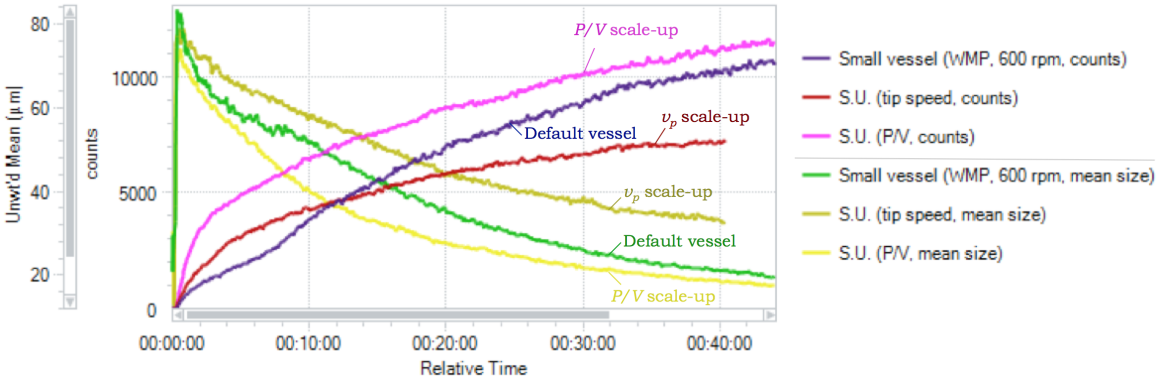

Figure 13.16: FBRM results for WMP in small and large vessels ($N_1 = 600\,\text{rpm}$).

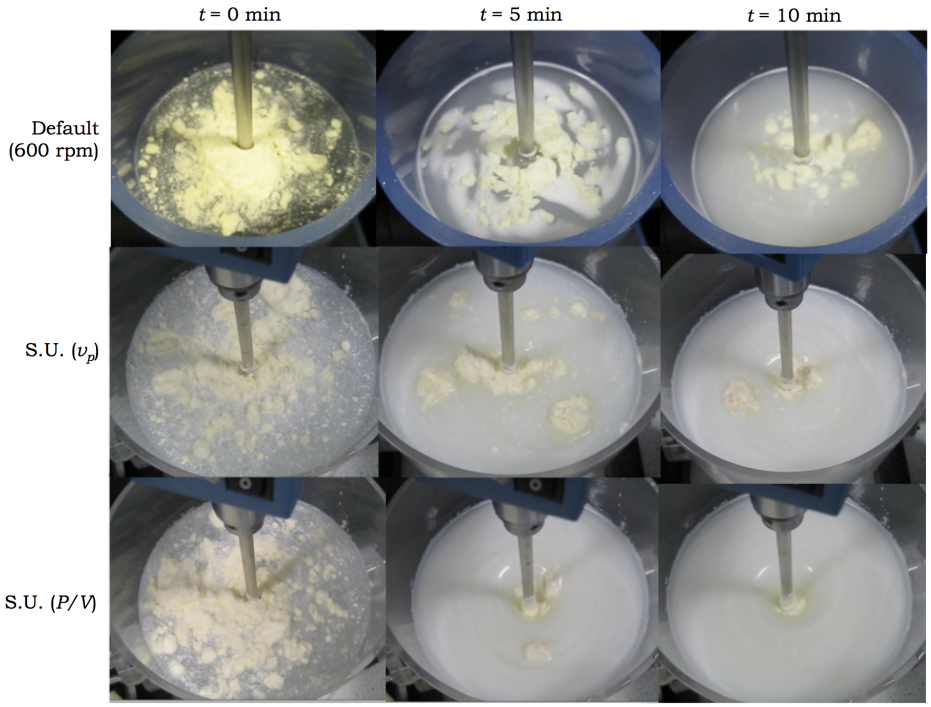

Figure 13.17: Video time-lapse results for WMP in small and large vessels ($N_1 = 600\,\text{rpm}$).

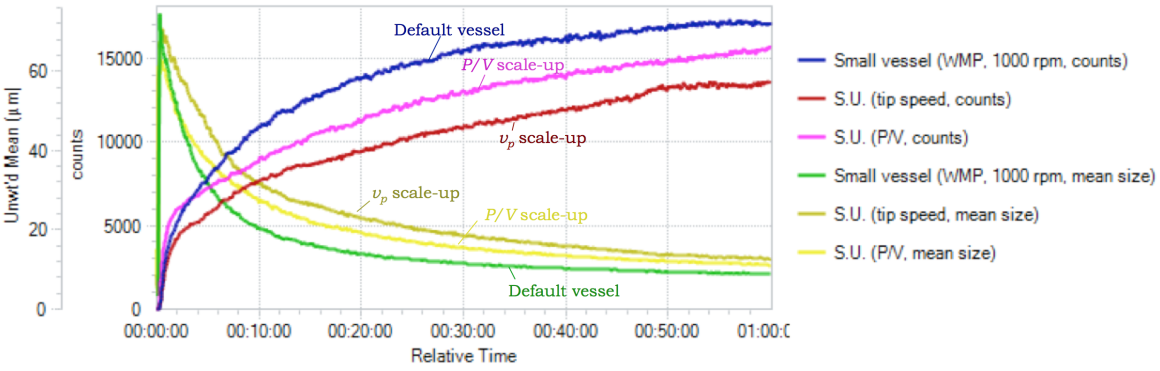

Figure 13.18: FBRM results for WMP in small and large vessels ($N_1 = 1000\,\text{rpm}$).

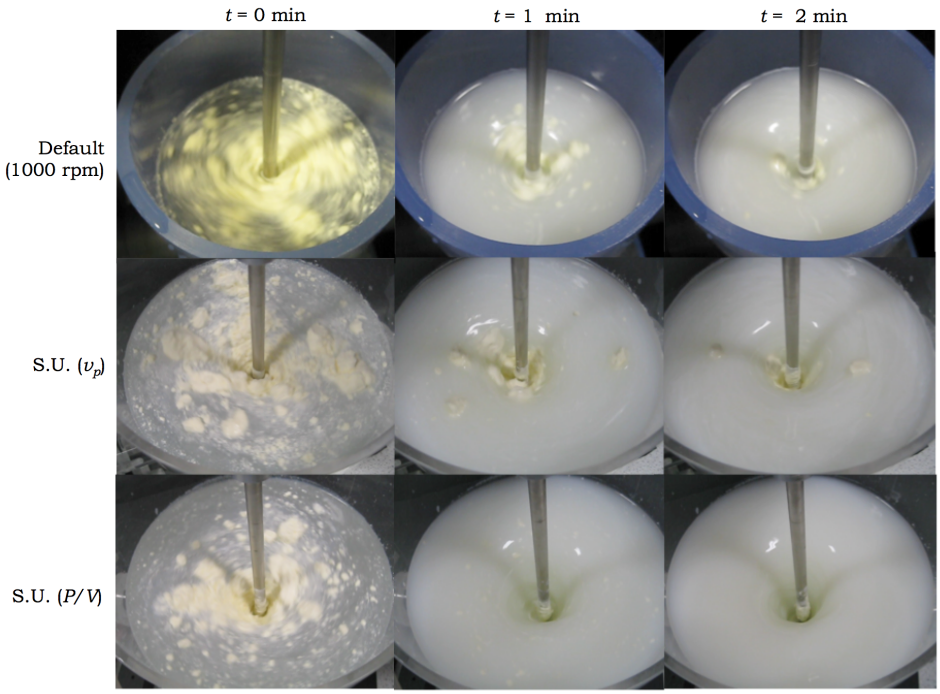

Figure 13.19: Time-lapse results for WMP in small and large vessels ($N_1 = 1000\,\mathrm{rpm}$).

Part IV

Analytical Discussion

Chapter 14

Rethinking Reconstitution Analysis

Contents

§14.1 Novel Reconstitution Rig

In the current project, a novel approach to monitoring food powder reconstitution was proposed (Ch. 7). Unlike the techniques used in the literature (Ch. 5), it allows the operator to follow *each step* of reconstitution (Ch. 1) as separate and simultaneous phenomena, thus allowing for results to be explained by physical transport phenomena. This new methodology is also applicable for *all* types of food powders.

From an analytical point of view, three different scenarios were observed for food powder reconstitution:

(1) For fast-sinking, completely water-soluble powders that completely disperse throughout the vessel, a kinetic hypothesis was proposed to model the FBRM results. This is done to describe powder dispersing and dissolving as separate phenomena (Ch. 9).

(2) For completely water-soluble powders under all conditions, rate-limiting regime maps are constructed based on video recordings, exploiting the fact that the vessel is transparent (Ch. 10).

(3) For all other powders, including those that contain components that do *not* completely dissolve, e.g. dairy powders, a slightly different mapping approach is presented, using video recordings of the liquid surface in order to characterize the sinking time and FBRM to describe the dispersing behavior (Ch. 11).

The vessel used was custom-designed to adhere to standard configurations (Fig. 3.4) for facilitated scale-up efforts, vessel characterization, and reproducibility. Probes are positioned to avoid unintended baffling effects, and feeding is performed under highly controlled conditions (§ 7.1).

FBRM

The FBRM (§ 5.9 & 7.1) probe proved to be a very versatile tool for food powder reconstitution studies. For water-soluble materials, tracking the total counts yielded important information regarding dispersing and dissolving (Ch. 9), and for more complex materials and formulations, sizing capabilities allowed for dispersing analysis, e.g. to track the number of lumps (Ch. 11). It may be worth improving the temporal resolution of the instrument, as the current version of the software only allowed one measurement every 2 s or slower, which was too slow to adequately describe powder behavior under some conditions, e.g. maltodextrin DE21 at high temperature (Ch. 9). One disadvantage of FBRM is that it can only detect particles directly in front of the probe window, thus is should not be used as the *only* technique, as phenomena such as floating and sedimentation are important to consider as well (Ch. 10). As the probe is very expensive (§ 5.9), it may not be feasible to replace quality control techniques (§ 5.1).

Videos

Videos were taken of every reconstitution trial. These provided extremely valuable information that other techniques may miss – the current author does not recommend performing reconstitution trials without video recordings. In Ch. 9, videos served to validate the kinetic hypothesis, in Ch. 10, they were used to identify rate-limiting regimes for mapping purposes, and in Ch. 11–13, the sinking time was determined. The camera was also useful for calibrating the vibratory feeder (§ 7.1) and estimating the liquid surface speed v_{surf} (§ 7.3).

Conductivity

As made clear in all of the experimental chapters, conductivity measurements were *not* particularly useful for reconstitution analysis. In Ch. 9, a direct comparison to the videos and FBRM results revealed that the "t_{90}" value corresponded to particle *sinking* – not dissolving – and thus it is likely that the rise in signal was due to the presence of impurities on the surface of the powder rather than actual material dissolving. In Ch. 11 it was shown that the t_{90} also corresponded to sinking and not dispersing/dissolving, as the probe mostly detects minerals that are not particularly interesting for studying dispersion mechanisms. *These realizations may call into question some of the conclusions of articles in the literature that used a conductivity approach* (§ 5.3).

In Ch. 12, at high ionic strength or liquid viscosities, conductivity curves were also too noisy to interpret; thus it may not even be a universal method to describe the sinking behavior – a more direct approach (videos) is thus recommended for sinking analysis. One possible alternative to conductivity may be an *in situ* UV spectrophotometer probe (Tsinman et al., 2009) or an FTIR[1] probe, e.g. the React IR 15 (Mettler Toledo, Columbus, OH, USA), as these probes may actually be able to track the dissolving of materials of interest – it could then be used in conjunction with FBRM and videos (see § 9.5).

[1] Fourier Transform Infrared

§14.2 Model and Mapping Approaches

The kinetic hypothesis/model described in Ch. 9 is, to the author's best knowledge, the first of its kind to describe the dispersing and dissolving of water-soluble powders as separate but overlapping phenomena. Additional work should be performed to calibrate the instrument, as discussed in § 9.4. This modeling approach may prove to be a promising tool for a variety of applications, and eventually information could be extracted from the empirical trials to aid in simulating dissolution, e.g. using DEM/CFD; cf. Washino et al. (2011).

The mapping approach presented in Ch. 10 and 11 was useful to obtain a more global overview on how powders will behave under different combinations of conditions – that is, a more "two-dimensional" view. A more "three-dimensional" view of powder behavior can also be obtained by comparing maps from different powders. The maps showed that qualitative information is sometimes *more important* than quantitative data obtained from measurement devices, and these maps may be useful as a diagnostic tool from a problem-solving point of view. The maps were even useful for further experimental planning – for instance in § 10.2 & 11.3, as well as Chapters 12 & 13, many of the experimental conditions were carefully chosen based on the limiting regimes desired for specific reasons. Future work should be conducted to determine if any mixing characteristic could be used as a more universal descriptor than agitation speed N (cf. Ch. 13), and also to improve the resolution to obtain a better idea of where the *regime transitions* occur.

§14.3 Defining the "End" of Reconstitution

One of the difficulties in analyzing the reconstitution of food powders is defining the "end" of rehydration. Obtaining such an end time "t_{end}" would be useful to determine the energy (E) efficiency of mixing ($E = P \cdot t_{\text{end}}$; Eq. 3.9) or, as claimed by Jeantet et al. (2010) (§ 3.6) the total number of impeller revolutions Θ may[2] be independent of N, where $\Theta = N \cdot t_{\text{end}}$.

[2]Based on the results of the experimental chapters, regardless of what "end time" value is chosen, Θ does *not* appear to be a universal defining factor for reconstitution behavior. Problems with Jeantet et al. (2010)'s approach are discussed in § 6.2.

For completely-soluble powders, t_{end} could be assigned to a “t_{90}” value, if a technique (e.g. *in situ* spectrophotometry) is used to monitor the amount of dissolved material; as discussed in § 14.1, conductivity is not appropriate. However for more complex powders, it was shown in Ch. 11 that not only the kinetics but also the *extent* of dispersing is affected by different conditions, e.g. T and N, thus normalizing the results to obtain a “t_{90}” is somewhat misleading. One possible solution would be to determine the amount of time required for the mean size to decrease to a defined value, once all the powder is sunken. As also demonstrated in Ch. 11, this defined value may depend on the powder type itself, and it may be worth consulting a sensory specialist before choosing a value (§ 1.4) to obtain the “t_{end}”.

Chapter 15

Variables affecting reconstitution

From the information obtained in the literature review and experimental chapters, a number of important trends have been identified with regards to how different variables might affect food powder reconstitution. In addition, the current author is of the opinion that there exist several opportunities for continuing the current project – suggestions are given where appropriate.

Contents

§15.1 Powder Type

One of the most obvious factors influencing reconstitution is the powder type. This is important to realize, since making broad generalizations about the behavior of food powders must be avoided. In addition, it is also important to test the behavior of *food* powders, since by using only a model material or a simple powder like maltodextrin DE21, one may miss out on important mechanisms of dispersion. Thus one should always consider the complex biochemical nature of food materials. In fact, as shown in several experiments in Part III, the rehydration behavior of maltodextrin DE21, which as discussed in § 8.1 is a material often used for granulation studies, was not particularly interesting, as reconstitution took place relatively quickly under most conditions tested. Another important consideration is that the analytical approach depends on the powder type as well; the rig described in Ch. 7 is suitable for *all* types of food powders, but the data analysis itself is powder-dependent. Future work in this area should ideally link the production/formulation aspects of powders[1] to their rehydration behaviors, paying particular attention to the microstructure (e.g. using X-ray tomography and/or SEM images (Palzer et al., 2012)) as well as *surface* characterization (Murrieta-Pazos et al., 2012a). The structuring of multicomponent powder mixes is also an interesting avenue for future study.

§15.2 Agitation

There are a number of effects that agitation has on the reconstitution behavior of food powders. Firstly, *wetting/sinking* were improved with increasing agitation rate (N) in many situations. This is due to greater downdraw and deeper vortex h' (§ 3.4) as well as faster liquid surface speed v_{surf} that helps to separate individual particles during feeding. These agitation effects on sinking are especially interesting for hard-to-sink powders, for which floating layers or powder heaps/lumps may form. Secondly, dispersing is improved with increasing N; for fast-sinking powders sedimentation was no longer a problem above a critical

[1] In the current project, powders were purchased and mostly analyzed *as is*.

N (Eq. 3.17), and the *extent* of dispersing was often improved at higher N (Ch. 11 – 13). This could be related to greater shear rates (Eq. 3.12), as well as more destructive turbulence (Eq. 1.42). Thirdly, mass transfer (i.e. the rate-limiting step of dissolving; § 1.4) is also improved with increasing agitation (Eq. 1.58).

However, in certain scenarios, increasing N did not have a dramatic impact on rehydration – particularly if reconstitution is fast anyway, e.g. for maltodextrin DE21 (Ch. 9) or at high temperature (T). In future work it may be worth performing energy efficiency studies (once a consensus about the "t_{end}" is reached; § 14.3) to see if there is an optimum N (or power draw P) for rehydration ($E = P \cdot t_{end}$), and to see if this optimum N changes with other variables, e.g. T. While not seen in the experimental chapters of the current report, in the literature review (Ch. 3) it was mentioned that if N is too high one may risk a vortex depth h' that surpasses the impeller submergence H' which may lead to undesirable air incorporation and foaming, or for fat globules, these may be disrupted, causing creaming and possibly also foaming (cf. whipped cream (Walstra et al., 2006)).

§15.3 Temperature

The water temperature (T) also has a number of effects on reconstitution. For hard-to-sink powders, sinking was generally improved with increasing T. Schubert (1993) claimed that this is due to the fact that the surface tension (γ) decreases with increasing T – however, as demonstrated in § 12.2, a decrease in γ may actually *hinder* rather than help powder sinking due to worse capillarity (Eq. 1.14). It is important to note that the *viscosity* (μ) also decreases with increasing T, according to an Arrhenius-like relationship (Ch. 12.3), and this μ depression may aid capillarity (Eq. 1.14). In fact, Saguy and Marabi (2011) demonstrated faster imbibition into freeze dried carrot particulates at increasing T values. As will be discussed in § 15.5, increasing T above the melting temperature T_m of certain materials may also improve sinking/dispersing.

The *dissolving* of materials may also improve with an increase in T. As discussed in Owusu-Apenten (2005), the solubility of food materials increases upon a rise in T, which according to Eq. 1.47 would result in faster mass transfer. As discussed in § 6.1, Klein Larsen et al.

(2003) claimed that the "dissolution rate" (using a first-order model; cf. k in Eq. 5.2 using a rheological approach (§ 5.5)) increased with T according to Arrhenius-like behavior. However it is important to note that they performed all experiments under "dispersing conditions" i.e. with much more sugar than actual polymer (§ 6.1). Thus, they did *not* consider that if "non-dispersing" conditions had been applied, i.e. if the hydrocolloid had been added by itself, then the faster dissolving of individual particles may lead to the formation of undesirable lumps (cf. Parker et al. (2000) in § 1.4).

It is also possible that a T too high can damage heat-sensitive materials in the powder, particularly proteins, that could lead to undesired effects as well (cf. whole milk powder in § 11.1). For some materials, increasing T may lead to swelling/pore collapse effects (cf. lecithinated cocoa powder in § 11.2), that may also be related to stronger hydrophobic interactions (§ 4.3) at higher T. Thus for food powders it is important not to try to oversimplify the complex relationship between rehydration and T.

§15.4 Particle Size

In § 10.1, it was also demonstrated that particle size can influence the reconstitution process. For low-molecular weight (MW) materials (e.g. maltodextrin DE21), size enlargement by agglomeration did not have a major effect on reconstitution, as wetting/sinking was good for most conditions even for small particles. Since granulation can be energetically expensive, one should thus consider if agglomeration is worthwhile, e.g. if good handling and dosing properties are required (§ 2.1). In § 2.1 it was also discussed how unnecessarily agglomerating some materials may even *worsen* reconstitution properties. However for high-MW materials (e.g. maltodextrin DE6) adding small particles to water often lead to the formation of a floating layer or lumps. However upon size enlargement, sinking was instantaneous and dispersing was greatly improved. This is because the physical separation of the primary particles allowed for greater liquid penetration (cf. $\bar{r}$ in Eq. 1.14) and concomitant water-logging effects (§ 1.2), and if material swelling occurs, there would be less "sintering" of neighboring particles that could lead to pore collapse and blockage of moisture transfer.

While not studied in the current project, as discussed in Ch. 2, Parker et al. (2000) claims

that there may be an *optimum* particle size for best reconstitution behavior. As discussed in § 1.4 (cf. Eq. 1.50), smaller particles, once submerged and dispersed, will dissolve more quickly due to greater overall surface area exposed to the liquid. However, if particles are too small, lumps can form due to swelling, etc. Particles too large may also lead to problems, because if the bulk density ρ_b is too low, if a large amount of powder is quickly added then the large bulk volume of powder (large height of the heap) may be difficult for the water to penetrate and waterlog (cf. Jurin height; Eq. 1.15). Moreover, Schubert (1993) claims that the polydispersity may also play a role; he claims that a wider span (i.e. $\frac{d_{10}-d_{90}}{d_{50}}$) in the size distribution may be preferable to a narrower span, due to pressure build-up vs. drainage, as discussed in § 1.1. In future work it would be interesting to study these effects further by using different sieve fractions, and also to see how the particle size distribution affects reconstitution under different conditions (e.g. is the optimum size temperature-dependent?).

In addition, during powder manufacturing the morphology of the material may also be changed; to the author's best knowledge these effects are not widely understood. For instance, as discussed in Ch. 2, for spray drying, depending on the conditions, particles may form that are hollow or deflated – for hollow particles one might expect higher buoyant forces (§ 1.2) resisting sinking, but deflated particles might be in closer contact to one another, which might affect water transfer (§ 1.1) or dispersing (§ 1.3) due to greater cohesivity between particles. Moreover, as discussed in § 1.1, roughness effects may also be important for wetting (and possibly overall reconstitution) – one might expect better wetting of hydrophobic materials with a *smoother* surface, and better wetting of hydrophilic materials with a *rougher* surface (see § 1.1).

§15.5 Fat content & State

While most articles in the literature (Part I) that discuss fat on food powders have associated a higher fat content with worse reconstitution (mostly related to the more hydrophobic nature of the powders, and thus worse wetting properties – see § 1.1), *this is not necessarily true.* In the current study (Ch. 11), it was found that the amount of *solid fat* (not overall fat) was a better indication of reconstitution quality. In § 11.1 it was demonstrated that the sinking (and overall behavior) was better for whole milk powder (WMP) than skim milk powder

(SMP) at $T = 45\,°C$, a T at which all of the milk fat would be expected to have melted (Kim et al., 2005b). However the reverse was true at $T = 25\,°C$, where ca. 20 % of the fat would be expected to be solid (Kim et al., 2005b). Marabi et al. (2008b), who had "dissolved" dairy powders at $T = 30\,°C$ (where ≈ 10 % of milk fat would be solid (Kim et al., 2005b)) reported slower "dissolution" (using a conductivity meter, which as discussed in § 14.1 gives a better indication of *sinking* rather than overall reconstitution) with increasing fat content. They theorized that this slower conductivity rise was due to a "less exothermic calorimetric response" (§ 5.10); however, it is important to recall that milk fat is not miscible with water, and that one would not expect a reversal in enthalpic response when the water T is increased from 25 °C to 45 °C. Thus the current author proposes that if Marabi et al. had monitored the sinking time, or had tested a range of water temperatures, they might have proposed a different mechanism. As sinking appears to be dependent on fat melting, it may be worth characterizing reconstitution of fat-containing powders as a function of $(T - T_m)$, recognizing that T_m (fat melting temperature) can actually be a *range* depending on factors such as fatty acid composition of the triacylglycerols, etc.

Another interesting consideration was that a heat treatment above the T_m of the fats of certain powders (§ 11.3) led to a lower T_m of the materials upon recrystallization – therefore less fat was solid upon reconstitution at $T = 25\,°C$, and sinking was faster. The responsible mechanisms may be related to an expulsion of lower-T_m encapsulated fat (for spray dried dairy powders – see § 2.1) and/or the solidification of crystals into less stable arrangements (dairy and cocoa powders) with lower T_m values due to polymorphicity. Possible applications (and complications) are discussed in § 11.3. One possible area of future study would be to better characterize the crystal structures pre– and post-heat treatment, e.g. using a tempermeter (Meursing, 2009).

While not studied in the current project, the processing conditions of certain liquid foods prior to drying can also affect reconstitution properties. As discussed in Ch. 2, improper homogenization may result in greater amounts of free fat on the surface of particles, which could complicate wetting/sinking, as well as other functional properties (e.g. caking). It may be interesting to further investigate such effects and how they influence different aspects of powder reconstitution.

§15.6 Material Properties

The material properties of food powders are also important to consider. While not explicitly studied in Part III, as discussed in Ch. 2, for certain materials that can exist either in an amorphous or crystalline state (e.g. sucrose or lactose), the amorphous form is preferable for reconstitution. Dupas (2012) described why the *wetting* properties of amorphous materials may be better for amorphous materials than for crystalline (related to diffusion; see § 1.1), and dissolving may be faster for amorphous materials as water can penetrate into the unstructured matrix, whereas an erosion-like dissolving would be more likely for crystals (§ 1.4).

For materials for which solid-state crystallization is *not* a concern (e.g. maltodextrin; § 8.1), in § 10.2 it was demonstrated that an increase in water activity a_w *improved* reconstitution; these results are in agreement with Dupas et al. (2013), who explained why wetting properties would be improved (§ 1.1). Results contradict Marabi et al. (2007) who had observed worse reconstitution of skim milk powder (SMP) after equilibration to a higher a_w. They noted that crystallization of lactose had occurred (using DSC; § 8.4), and they also reported a less exothermic dissolution following crystallization (the reasons for which were explained in § 1.4). They thus suggested a cause-effect relationship. However in the current report, faster reconstitution was reported at higher a_w, where a *less exothermic* response would be expected. Thus the results do *not* support a link between exothermicity and dissolving, and suggest that different mechanisms should be considered. It is also important to note that, unlike for maltodextrin, SMP normally consists of an amorphous matrix of lactose with embedded materials that could be expelled to the particle surface upon crystallization, which could further complicate matters (§ 6.2). Nevertheless, it *is* important to consider such complications (among others) before recommending increasing the a_w to improve rehydration. For instance, a powder with higher a_w may be more vulnerable to microbiological spoilage, crystallization (if crystallization is an issue), or glass transition/caking effects, depending on the material properties.

In future work it would be interesting to study more pure forms of crystalline and amorphous materials (e.g. lactose or sucrose, which *can* exist in either state) in order to see if wetting/sinking *and* dissolving are slower, using the approaches presented in Ch. 9 and 10). To obtain such powders, one could modify the drying conditions during production (Palzer

et al., 2012).

§15.7 Ionic Strength

Increasing the ionic strength (Eq. 4.8) of the reconstitution medium also appears to cause complicated effects, possibly related to interparticle interactions (Ch. 4). Electrostatic double layer repulsion (EDL; § 4.2) effects may be screened, and hydrophobic attractions may be increased, both of which may be detrimental to dispersion (Ch. 12.1). For powders high in micellar casein, an increase in Na^+ may solubilize the Ca^{2+} in calcium phosphate bridges holding micelles together (Ch. 2, § 6.2), which could lead to smaller "primary particles" (§ 12.1), in agreement with articles in the literature (§ 4.5). However, these effects may be *secondary* to processes like lump formation (Fig. 12.5), which might be undetected using techniques from the literature (Ch. 5).

For water-soluble polymers, e.g. maltodextrin, an increase in ionic strength may inhibit mass transfer during *dissolving* (§ 4.5, § 12.1), in agreement with Klein Larsen et al. (2003). While only NaCl was used in the current report to modify the ionic strength, as discussed in § 4.5, one might expect worse behavior in the presence of a divalent cation, e.g. Ca^{2+}, due to bridging effects.

§15.8 Surface Tension

The role of surface tension (γ), through the use of surfactants, has also been studied in the current report. Adding a surfactant, e.g. lecithin, can under some circumstances improve both the wetting and dispersing of hydrophobic powders (§ 11.2). In § 12.1, evidence was provided supporting the hypothesis that lecithination helps dispersing due to improved electrostatic double layer repulsion (EDL). In addition, lecithination of powders may help stabilize suspensions after reconstitution (§ 2.3).

If a surfactant is added to the *liquid* prior to powder addition (§ 12.2), the effect on

reconstitution may be "limiting regime"-dependent. For sinking-limited conditions, surfactant addition made reconstitution worse, with less powder sinking – this can be explained due to worse capillarity into the powder bed. However for dispersing-limited conditions, some particles may disperse faster if the liquid surface is saturated with tensioactive molecules – while this theory has not been tested, one possibility is that during the (fast) wetting/sinking steps, surfactant may adsorb to the particle surface, aiding with dispersing.

§15.9 Viscosity

The viscosity (μ) of the liquid medium may also play an important role in reconstitution – such effects may also be important for polymeric powders (especially those of high molecular weight (MW)) that cause an increase in μ as they dissolve in the liquid. In § 12.3 it was shown that above a critical concentration of a certain material, water transfer will be hindered, which could lead to the development of a floating layer or lumps. The increased μ could hinder capillarity effects (Eq. 1.14), and the MW of a solid may also lead to worse wetting properties (see § 1.1; cf. Dupas (2012)). Moreover, dispersing may be resisted by the action of viscous forces (Eq. 1.39). In future work, it would be interesting to see if this critical concentration is dependent on other factors, such as particle size distribution.

§15.10 Vessel Configuration

It was also shown that the configuration of the vessel plays a major role in reconstitution. This is particularly troubling, since many studies in the literature (§ 5.12) do not specify the details of their vessels (e.g. impeller type, geometry, ...), or the studies allow the measurement probes to inadvertently baffle the liquid flow. Comparing an axial and radial impeller (§ 13.1), it appears that the power draw P (not agitation speed N) was a good mixing characteristic to provide similar result for both impellers. However the radial impeller tested appears to be better at incorporating powder into the liquid (possibly due to a deeper vortex h' at the same P) as well as better dispersing (higher shear rate $\dot{\gamma}$ at the impeller blades), even if the average $\dot{\gamma}$ in the tank was lower.

The impeller submergence H' also appeared to play a role (§ 13.2) – positioning the impeller closer to the bottom of the vortex cone helped improve sinking for a hard-to-sink powder, compared to a lower off-bottom clearance H, when measurements were performed at the same N. Future studies could be performed with different impeller types, positions, etc.

Baffling the vessel with four baffles was detrimental to the quality of reconstitution (§ 13.1). For fast-sinking powders, sedimentation became an issue, and for slow-sinking powders, floating was a problem. Due to the absence of a circular flow around the impeller shaft, powder also formed a large heap that could be "transformed" into a lump if the peripheral particles became wetted. The vortex formation and swirling of unbaffled tanks appears to be important for food powder dispersion. However future work could be done to see if e.g. one baffle or half-baffle(s) help improve mixing while still allowing for circular movement (§ 3.4).

Scale-up experiments were performed in order to test if tip speed (v_p) or specific power draw (P/V) would be better at preserving behavior upon scale-up. It was found that results appeared to be limiting regime-dependent. For sinking-limited reconstitution, v_p was a better criterion as the mixing characteristics associated with the liquid free surface were better preserved. For dispersing (and dissolving)-limited conditions, preserving P/V was better at reproducing the behavior, related to more similar shear effects.

In future work it may be interesting to also test different applications such as vending (adding a jet of water to a powder), or another addition method, using an analytical technique like ultra-fast MRI (§ 5.6). Other applications could be capsules or retail reconstitution – for the latter, it may be worth performing focus groups to see if patterns exist in *how* consumer would rehydrate powders at home.

§15.11 Surface Dispersing

It was shown in § 11.4 that less hydrophobic powders had a more explosive dispersion and clump breakup when added to a static volume of water. For lecithinated cocoa powder, a Marangoni effect may be (at least partially) responsible. For skim milk (compared to whole milk) powder, the better dispersion might not be due to a Marangoni effect, but it could

be related to a stronger initial vertical capillary suction into the interface, and resultant repulsive oscillatory waves (§ 1.2). "Cheerios Effects" do not appear to be highly relevant to this phenomenon.

These surface dispersing effects may be useful for powders meant for retail applications, as consumers may add powder to a static volume of water a few seconds (the time scale of interest) before they begin the mixing process. Future work could use more advanced methods to characterize the dispersing phenomena (e.g. using PIV[2] to characterize particle speeds). Hollow glass beads could be coated with fat and/or surfactant, and the liquid properties could also be altered. It should also be determined whether such effects play a significant role in the overall beverage quality after stirring.

[2]Particle Image Velocimetry

Chapter 16

Overall Conclusions

Learn from yesterday, live for today, hope for tomorrow. The important thing is not to stop questioning.

Albert Einstein

In the current project a novel approach to studying food powder reconstitution was presented, which is applicable for all types of powders and captures all steps of reconstitution. A number of experiments were performed for different classes of food materials under wide ranges of conditions, and the influence of particle properties, liquid properties, and mixing characteristics was studied. Mechanisms of food powder dispersion were proposed, considering physical transport processes and interparticle interactions, and misconceptions in the literature regarding reconstitution were exposed. It is believed that the discussions from the current report will be useful for the industry to better understand reconstitution phenomena, in order to optimize processes related to powder production and handling.

Appendix

Preliminary work with PVM

As mentioned in § 5.10, PVM (Particle Vision Microscopy) could be an interesting tool for future studies of food powder reconstitution. At the very beginning of the current PhD in early 2012, preliminary experiments were performed using both the FBRM and PVM (during a demonstration by a representative from Mettler Toledo) in a stirred vessel. Experiments were performed with 10 – 12 % fat unlecithinated cocoa powder (§ 8.3), at temperatures T = 25 and 65 °C, and stir rates N = 400 and 700 rpm. FBRM results are shown in Fig. 1.

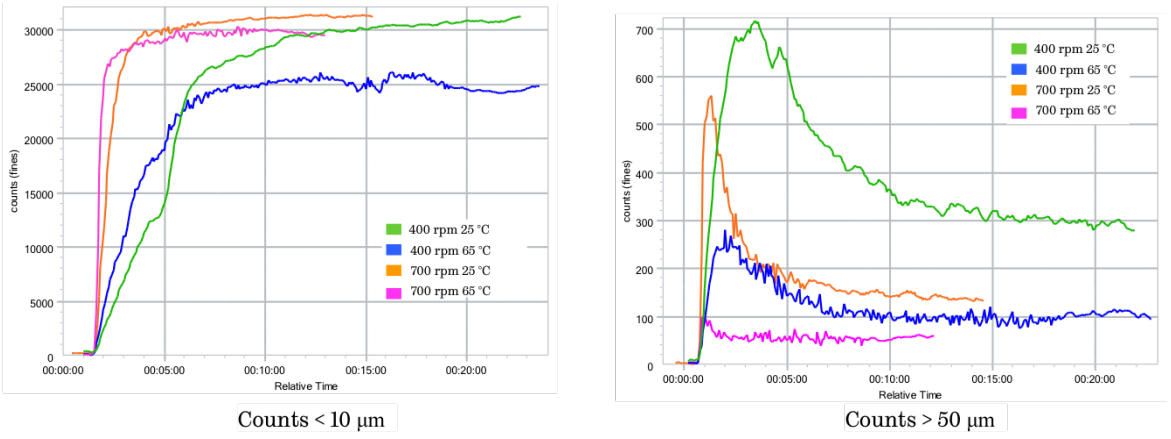

Figure 1: FBRM results of preliminary trial with cocoa powder.

It was clear that the kinetics appeared to be determined by N, but the *extent* of dispersing depended more on the water T. PVM images (Fig. 2) taken at t = 15 min provided visual confirmation of the interpretation of the FBRM results.

However, for the current project, PVM was not used, as the equipment was very expensive (§ 5.10), and it was decided that the information it yielded was not worth the cost. However, it could certainly find interesting applications for follow-up projects.

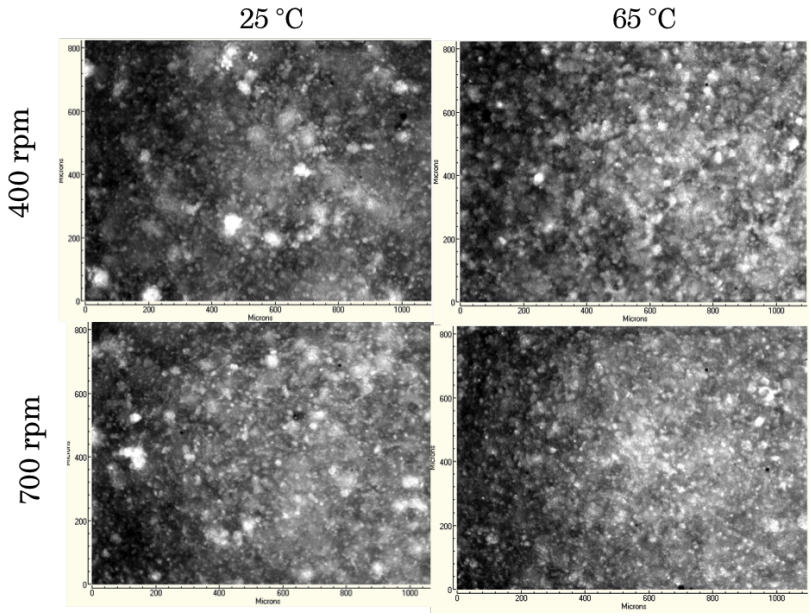

Figure 2: PVM of preliminary trial with cocoa powder.

Mathematica code for modelling

Mathematica code for model fitting
W. Robert Mitchell

File Importing

FBRM data is originally exported to an excel sheet that has four columns. The first column has the amount of powder added ($M0$), the second column is the time (t), the third column is the stir rate (N), and the fourth column is the FBRM total square weighted counts. The data is imported as four different lists in *Mathematica*.

```
SetDirectory[NotebookDirectory[]];

combined = First[Import["combined.xlsx"]];

{M0list, tlist, Nlist, countslist} = combined^T;
```

Functions for curve fitting

For symbols, see the first experimental chapter (A = heap, R = dispersed, S = dissolved, etc.). The piecewise function is used, as the differential equations are discontinuous at time T (where the FBRM counts reaches a peak value).

Concentration functions

```
CA[t_, {k1_, k2_, k3_, CA0_}] := With[{T = CA0 / (k1 + k3), CRT = k1/k2 (1 - e^-(k2 CA0/(k1+k3)))},
  Piecewise[{{CA0, t < 0}, {CA0 - (k1 + k3) t, t ≤ T}, {0, True}}]]
```

```
CR[t_, {k1_, k2_, k3_, CA0_}] := With[{T = CA0 / (k1 + k3), CRT = k1/k2 (1 - e^-(k2 CA0/(k1+k3)))},
  Piecewise[{{0, t < 0}, {k1/k2 (1 - e^(-k2 t)), t < T}, {CRT e^(-k2 (t-T)), True}}]]
```

```
CS[t_, {k1_, k2_, k3_, CA0_}] := With[{T = CA0 / (k1 + k3), CRT = k1/k2 (1 - e^-(k2 CA0/(k1+k3)))},
  Piecewise[{{0, t < 0}, {k1/k2 (e^(-k2 t) - 1) + (k1 + k3) t, t < T}, {CA0 - CRT e^(-k2 (t-T)), True}}]]
```

$t0$ is used to account for any "delay time". This is done because not all of the experiments are performed *exactly* at the same time between when the FBRM probe is turned on and the powder is added.

```
CA[t_, {k1_, k2_, k3_, CA0_, t0_}] := CA[t - t0, {k1, k2, k3, CA0}]
CR[t_, {k1_, k2_, k3_, CA0_, t0_}] := CR[t - t0, {k1, k2, k3, CA0}]
CS[t_, {k1_, k2_, k3_, CA0_, t0_}] := CS[t - t0, {k1, k2, k3, CA0}]
```

The time T is when CR(t) reaches its maximum value.

```
T[{k1_, k2_, k3_, CA0_}] := CA0 / (k1 + k3)
T[{k1_, k2_, k3_, CA0_, t0_}] := t0 + T[{k1, k2, k3, CA0}]

CRmodel[t_, M0_, N0_, α_, k1_, k2_, k3_, t0_] := CR[t, {k1, k2, k3, α M0, t0}]

CSmodel[t_, M0_, N0_, α_, k1_, k2_, k3_, t0_] := CS[t, {k1, k2, k3, α M0, t0}]
```

CR and CS are fitted for all values of $M0$ at N = 600 rpm

```
CRmodel1[t_, M0_, 600., α_, k1600_, k1800_, k11000_, k2600_, k2800_, k21000_,
  k3600_, k3800_, k31000_, t0_] := CRmodel[t, M0, 600., α, k1600, k2600, k3600, t0]

CSmodel1[t_, M0_, 600., α_, k1600_, k1800_, k11000_, k2600_, k2800_, k21000_,
  k3600_, k3800_, k31000_, t0_] := CSmodel[t, M0, 600., α, k1600, k2600, k3600, t0]
```

CR and CS are fitted for all values of $M0$ at N = 800 rpm

```
CRmodel1[t_, M0_, 800., α_, k1600_, k1800_, k11000_, k2600_, k2800_, k21000_,
  k3600_, k3800_, k31000_, t0_] := CRmodel[t, M0, 800., α, k1800, k2800, k3800, t0]

CSmodel1[t_, M0_, 800., α_, k1600_, k1800_, k11000_, k2600_, k2800_, k21000_,
  k3600_, k3800_, k31000_, t0_] := CSmodel[t, M0, 800., α, k1800, k2800, k3800, t0]
```

CR and CS are fitted for all values of $M0$ at N = 1000 rpm

```
CRmodel1[t_, M0_, 1000., α_, k1600_, k1800_, k11000_, k2600_, k2800_, k21000_,
  k3600_, k3800_, k31000_, t0_] := CRmodel[t, M0, 1000., α, k11000, k21000, k31000, t0]

CSmodel1[t_, M0_, 1000., α_, k1600_, k1800_, k11000_, k2600_, k2800_, k21000_,
  k3600_, k3800_, k31000_, t0_] := CSmodel[t, M0, 1000., α, k11000, k21000, k31000, t0]
```

Model Fitting

```
nlm = NonlinearModelFit[combined,
   CRmodel1[t, M0, N0, α, k1600, k1800, k11000, k2600, k2800, k21000, k3600, k3800, k31000, t0],
   {{k1600, 0.5}, {k1800, 0.5}, {k11000, 0.5}, {k2600, 0.05}, {k2800, 0.05}, {k21000, 0.05},
    {k3600, 10}, {k3800, 10}, {k31000, 10}}, {M0, t, N0}, MaxIterations → 100];

nlm["RSquared"]

0.859479

nlm["ParameterTable"]
```

	Estimate	Standard Error	t-Statistic	P-Value
k1600	0.680616	0.0147957	46.0008	$1.05197848071\times10^{-401}$
k1800	1.13064	0.0209855	53.8769	$4.5068667391\times10^{-526}$
k11000	1.04885	0.020908	50.1651	$2.3891867798\times10^{-466}$
k2600	0.0434132	0.000895523	48.478	$7.8236878166\times10^{-440}$
k2800	0.061008	0.00109635	55.6464	$3.8123851263\times10^{-555}$
k21000	0.0566369	0.0010652	53.1701	$1.45626423729\times10^{-514}$
k3600	0.426904	0.015825	26.9766	3.02817×10^{-152}
k3800	0.202698	0.0162178	12.4985	1.88896×10^{-35}
k31000	0.29869	0.0169448	17.6272	5.14849×10^{-68}

Fitted Parameters

k_1

```
ListPlot[{{600, 800, 1000}, {k1600, k1800, k11000} /. nlm["BestFitParameters"]}^T,
 PlotMarkers → Automatic, PlotRange → {0, All}, AxesLabel → {"Speed (rpm)", "k1 (counts/s)"}]
```

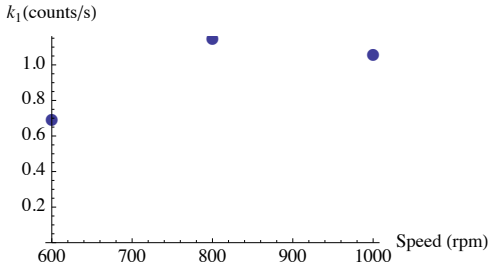

k_2

```
ListPlot[{{600, 800, 1000}, {k2600, k2800, k21000} /. nlm["BestFitParameters"]}^T,
 PlotMarkers → Automatic, PlotRange → {0, All}, AxesLabel → {"Speed (rpm)", "k2 (s^-1)"}]
```

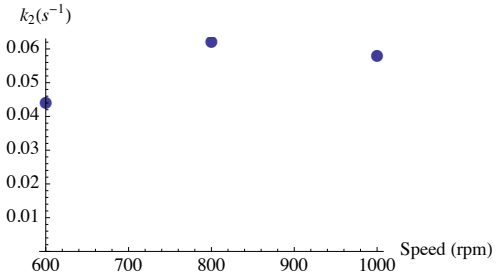

k_3

```
ListPlot[{{600, 800, 1000}, {k3600, k3800, k31000} /. nlm["BestFitParameters"]}^T,
 PlotMarkers → Automatic, PlotRange → {0, All}, AxesLabel → {"Speed (rpm)", "k3 (counts/s)"}]
```

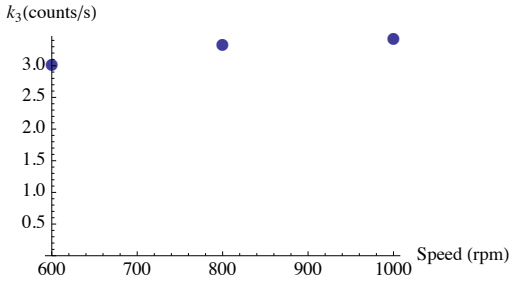

Listplots of raw data along with model fits

```
M0fn[M0_] := Switch[1, M0 == 5., 2, M0 == 10., 3, M0 == 20., 4, M0 == 40.]; SetAttributes[M0fn, Listable]

countplot[N0_] := ListPointPlot3D[{{tspeedlist[N0], M0fn[M0speedlist[N0]], countsspeedlist[N0]}^T,
   Flatten[Table[{t, i + 2, nlm[10 × 2.^i, t, N0]}, {i, -1, 2}, {t, 0, 150, 0.1}], 1]},
  PlotRange → All, AxesLabel → {"time (s)", "M0 (kg m^-3)", "Counts"},
  Ticks → {Automatic, {{1, 5}, {2, 10}, {3, 20}, {4, 40}}, Automatic}]
```

- **600 rpm**

```
selectspeed[600.];

countplot[600.]
```

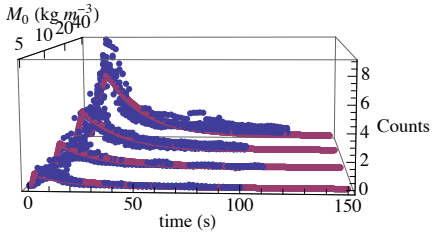

- **800 rpm**

```
selectspeed[800.];

countplot[800.]
```

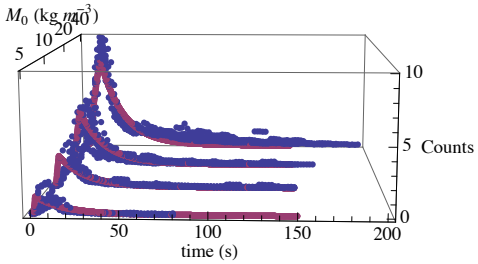

- **1000 rpm**

```
selectspeed[1000.];
```

```
countplot[1000.]
```

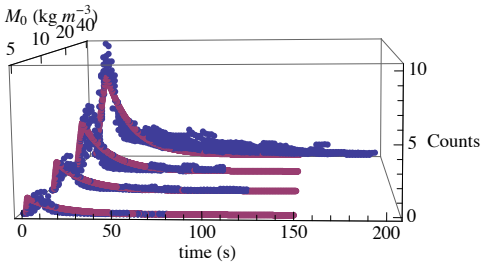


```
params = Join[kp, nlm["BestFitParameters"]]
```

```
{t0 → 1, α → 0.3`, k1600 → 0.6806156280901254`, k1800 → 1.1306358192911878`,
 k11000 → 1.0488544708163312`, k2600 → 0.04341320479963936`,
 k2800 → 0.06100799951090119`, k21000 → 0.05663694313090603`,
 k3600 → 0.4269043333588486`, k3800 → 0.20269751343542475`, k31000 → 0.2986899332112539`}
```

```
CSmodel2[t_, M0_, N0_, ps_] := CSmodel1[t, M0, N0, α /. ps, k1600 /. ps, k1800 /. ps, k11000 /. ps,
  k2600 /. ps, k2800 /. ps, k21000 /. ps, k3600 /. ps, k3800 /. ps, k31000 /. ps, t0 /. ps]
```

As discussed in the first experimental chapter, the fitting parameters from CR(t) (i.e. the FBRM results) were used to estimate the CS(t), which is what we had theorized the conductivity results would resemble. However, it turned out that conductivity is not a good indication of dissolved fraction of maltodextrin, and that the technique itself is flawed. Below is an example of how CS(t) was predicted (e.g. determining the "t_{90}" values, given in seconds).

```
Plot[CSmodel2[t, 5, 600., params], {t, 0, 100}, PlotRange → All]
```

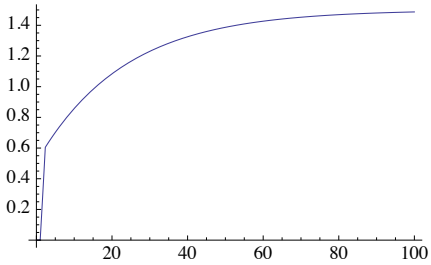


```
CSmx[M0_, N0_, ps_] := CSmodel2[100, M0, N0, ps]
```

```
CSmx[5, 600., params]
```

```
1.48709
```

```
t90[M0_, N0_, ps_] := t /. FindRoot[CSmodel2[t, M0, N0, ps] == 0.9 CSmx[M0, N0, ps], {t, 20, 90}]
```

```
t90[5, 600., params]
```

```
41.7858
```

Dimensions of Vessels

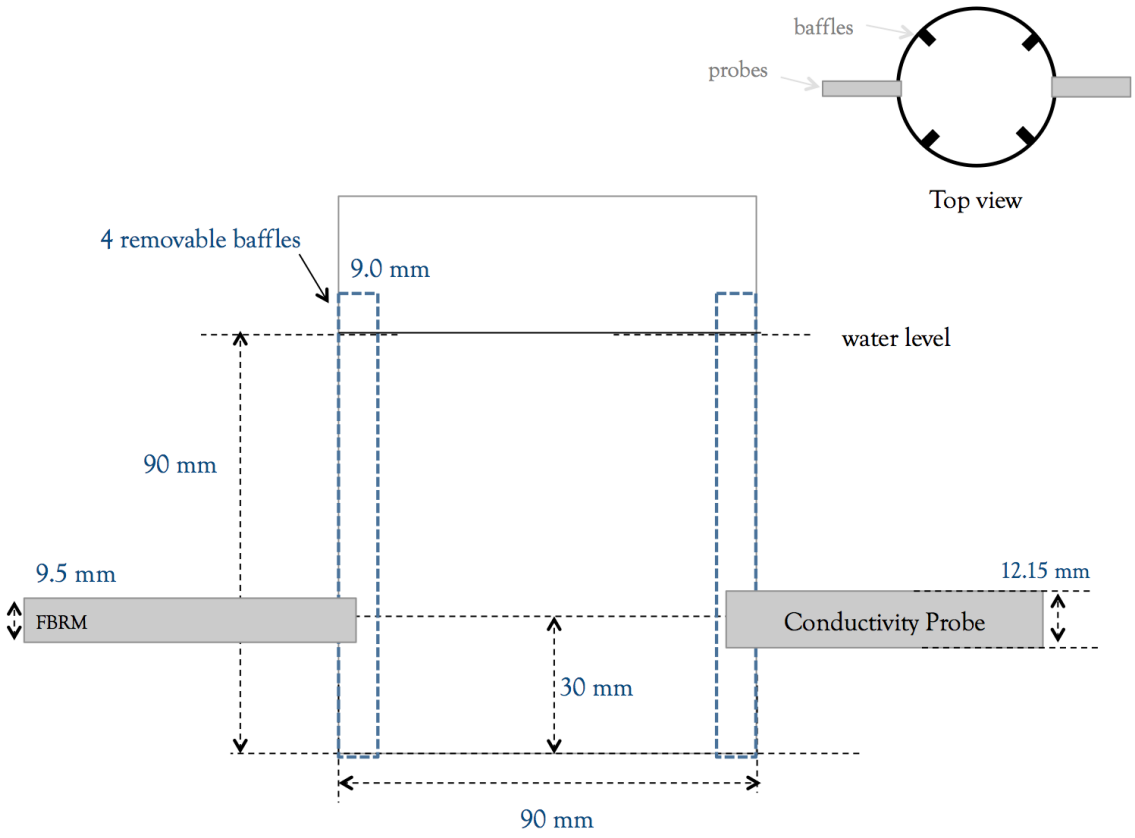

Figure 3: Dimensions of default vessel.

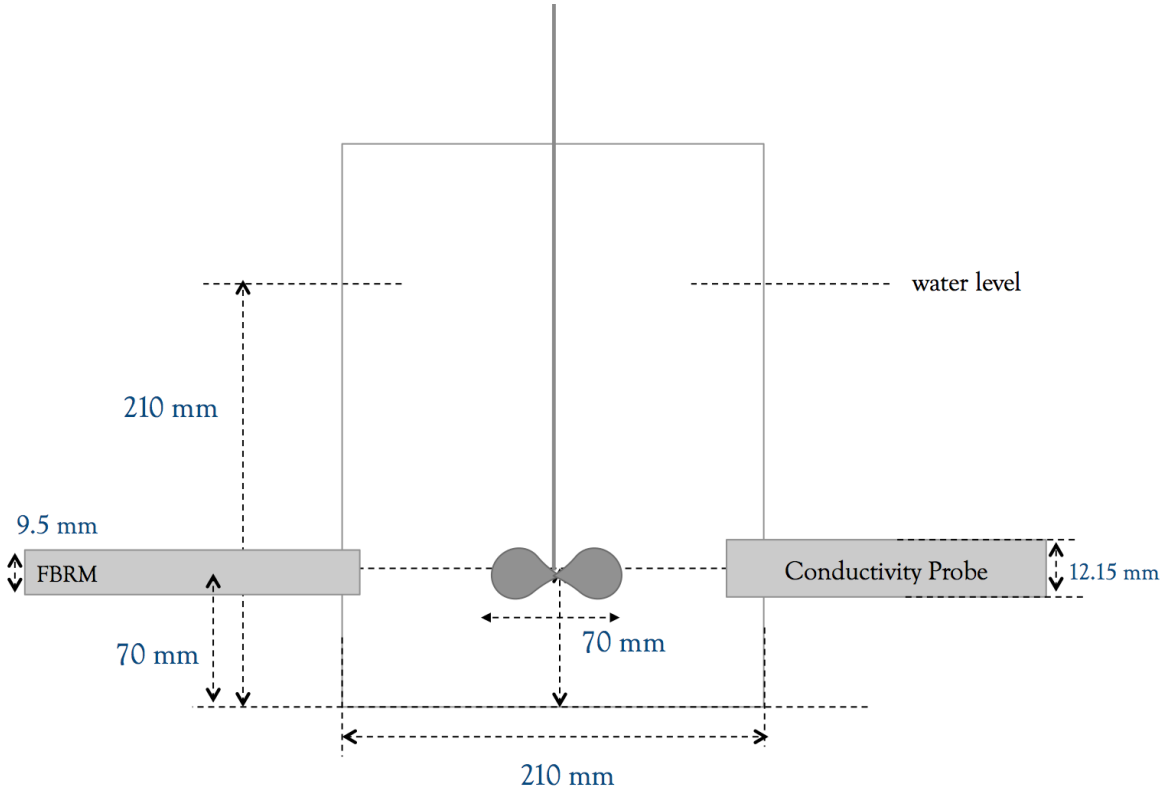

Figure 4: Dimensions of scaled-up vessel.

References

F. Abbès, M. Masmoudi, W. Kchaou, S. Danthine, C. Blecker, H. Attia, and S. Besbes. Effect of enzymatic treatment on rheological properties, glass temperature transition and microstructure of date syrup. *LWT - Food Science and Technology*, 60(1):339 – 345, 2015.

I. B. Abdelaziz, A. Sahli, S. Bornaz, J. Scher, and C. Gaiani. Dynamic method to characterize rehydration of powdered cocoa beverage: Influence of sugar nature, quantity and size. *Powder Technology*, 264:184 – 189, 2014.

C. Achebe. Mathematical determination of the critical absolute hamaker constant of the serum (as an intervening medium) which favours repulsion in the human immunodeficiency virus (HIV)- blood interactions mechanism. In *Proceedings of the World Congress on Engineering, London.*, 2013.

L. Afferrante and G. Carbone. Microstructured superhydrorepellent surfaces: effect of drop pressure on fakir-state stability and apparent contact angles. *Journal of Physics: Condensed Matter*, 22(32):325107, 2010.

W. Albarracín, I. C. Sánchez, R. Grau, and J. M. Barat. Salt in food processing; usage and reduction: a review. *International Journal of Food Science & Technology*, 46(7):1329 – 1336, 2011.

L. Albright. *Albright's Chemical Engineering Handbook.* CRC Press, 2009.

T. Allen. *Powder sampling and particle size determination.* Elsevier B.V., 2003.

T. O. Althaus, E. J. Windhab, and N. Scheuble. Effect of pendular liquid bridges on the flow behavior of wet powders. *Powder Technology*, 217:599 – 606, 2012.

D. am Ende. *Chemical engineering in the pharmaceutical industry: R&D to manufacturing.* John Wiley & Sons, Inc., 2011.

C. Anandharamakrishnan, C. D. Rielly, and A. G. F. Stapley. Effects of process variables on the denaturation of whey proteins during spray drying. *Drying Technology*, 25(5):799 – 807, 2007.

S. Anema, D. Pinder, R. Hunter, and Y. Hemar. Effects of storage temperature on the solubility of milk protein concentrate (MPC85). *Food Hydrocolloids*, 20:386 – 393, 2006.

M. Arellano, H. Benkhelifa, D. Flick, and G. Alvarez. Online ice crystal size measurements during sorbet

freezing by means of the focused beam reflectance measurement (FBRM) technology. Influence of operating conditions. *Journal of Food Engineering*, 113(2):351 – 359, 2012.

M. Ash and I. Ash. *Handbook of Fillers, Extenders, and Diluents: Second Edition*. Synapse Information Resources, Inc., 2007.

M. A. Augustin, P. Sanguansri, R. Williams, and H. Andrews. High shear treatment of concentrates and drying conditions influence the solubility of milk protein concentrate powders. *Journal of Dairy Research*, 79(4):459 – 468, 2012.

F. Avaltroni, P. Bouquerand, and V. Normand. Maltodextrin molecular weight distribution influence on the glass transition temperature and viscosity in aqueous solutions. *Carbohydrate Polymers*, 58(3):323 – 334, 2004.

S. Azarmi, W. Roa, and R. Löbenberg. Current perspectives in dissolution testing of conventional and novel dosage forms. *International Journal of Pharmaceutics*, 328(1):12 – 21, 2007.

D. Bagster and D. Tomi. The stresses within a sphere in simple flow fields. *Chemical Engineering Science*, 29 (8):1773 – 1783, 1974.

A. Baldwin. Insolubility of milk powder products – a minireview. *Dairy Science & Technology*, pages 169 – 179, 2010.

A. Baldwin and G. Truong. Development of insolubility in dehydration of dairy milk powders. *Food and Bioproducts Processing*, 85(3):202 – 208, 2007.

M. Barigou. Chapter 10: Solid-liquid mixing. In P. Cullen, editor, *Food Mixing: Principles and Applications*. Wiley-Blackwell, 2009.

S. C. Barthe, M. A. Grover, and R. W. Rousseau. Observation of polymorphic change through analysis of FBRM data: Transformation of paracetamol from form II to form I. *Crystal Growth & Design*, 8(9):3316 – 3322, 2008.

M. Benković and I. Bauman. Agglomeration of cocoa powder mixtures – influence of process conditions on physical properties of the agglomerates. *Journal on Processing and Energy in Agriculture*, 15(1):46 – 49, 2011.

A. Bertsch. Surface tension of whole and skim-milk between 18 and 135 °C. *Journal of Dairy Research*, 50: 259 – 267, 1983.

B. Bhandari and Y. Roos. *Food Materials Science and Engineering*. Wiley-Blackwell, 2012.

S. N. Bhattachar, L. A. Deschenes, and J. A. Wesley. Solubility: it's not just for physical chemists. *Drug Discovery Today*, 11(21–22):1012 – 1018, 2006.

W. Bisig, D. Guggisberg, R. Badertscher, U. Bütikofer, J. Meyer, and B. Rehberger. *Milchproteinpulver und ihre technologischen Eigenschaften: Methodik und Untersuchung. Technisch-wissenschaftliche Informationen*. ALP Science, Nr. 488, 2005.

G. Bonacucina, M. Cespi, and G. F. Palmieri. Evaluation of dissolution kinetics of hydrophilic polymers by use of acoustic spectroscopy. *International Journal of Pharmaceutics*, 377(1–2):153 – 158, 2009.

E. Börjesson, F. Innings, C. Trägårdh, B. Bergenståhl, and M. Paulsson. The dissolution behavior of individual powder particles. *Dairy Science & Technology*, 93(4-5):357 – 371, 2013.

M. Boström, V. Deniz, G. Franks, and B. Ninham. Extended DLVO theory: Electrostatic and non-electrostatic forces in oxide suspensions. *Advances in Colloid and Interface Science*, 123–126:5 – 15, 2006.

J. Boxall, C. Koh, E. Sloan, A. Sum, and D. Wu. Droplet size scaling of water-in-oil emulsions under turbulent flow. *Langmuir*, 28(1):104 – 110, 2011.

J. F. Boyle, I. Manas-Zloczower, and D. L. Feke. Hydrodynamic analysis of the mechanisms of agglomerate dispersion. *Powder Technology*, 153(2):127 – 133, 2005.

N. Brielles, F. Chantraine, M. Viana, D. Chulia, P. Branlard, G. Rubinstenn, F. Lequeux, and O. Mondain-Monval. Dissolution of a surfactant-containing active porous material. *Journal of Colloid and Interface Science*, 328(2):344 – 352, 2008.

W. Briscoe. Chapter 16: Surface forces. In T. Cosgrove, editor, *Colloid Science: Principles, Methods, and Applications*. Wiley-Blackwell, 2010.

M. Brown and R. Semelka. *MRI – Basic Principles and Applications: Fourth Edition.* Wiley-Blackwell, 2010.

V. Buckin, B. O'Driscoll, C. Smyth, A. Alting, and R. Visschers. Ultrasonic spectroscopy for material analysis. Recent advances. *Spectroscopy Europe*, 15(1):20 – 25, 2003.

A. Busciglio, F. Grisafi, F. Scargiali, and A. Brucato. On vortex shape in unbaffled stirred vessels as measured by digital image analysis. In *Proceedings of the 14th European Conference on Mixing, Warsaw.*, 2012.

A. Busciglio, G. Caputo, and F. Scargiali. Free-surface shape in unbaffled stirred vessels: Experimental study via digital image analysis. *Chemical Engineering Science*, 104:868 – 880, 2013.

J. W. Bye and R. J. Falconer. Thermal stability of lysozyme as a function of ion concentration: A reappraisal of the relationship between the Hofmeister series and protein stability. *Protein Science*, 22(11):1563 – 1570, 2013.

G. Caliskan and S. N. Dirim. The effects of the different drying conditions and the amounts of maltodextrin addition during spray drying of sumac extract. *Food and Bioproducts Processing*, 91(4):539 – 548, 2013.

G. Calvert, M. Ghadiri, and R. Tweedie. Aerodynamic dispersion of cohesive powders: A review of understanding and technology. *Advanced Powder Technology*, 20(1):4 – 16, 2009.

G. Calvert, A. Hassanpour, and M. Ghadiri. Analysis of aerodynamic dispersion of cohesive clusters. *Chemical Engineering Science*, 86:146 – 150, 2013.

S. Capaccioli and K. L. Ngai. Resolving the controversy on the glass transition temperature of water? *The Journal of Chemical Physics*, 135(10):104504–1 – 104504–12, 2011.

P. Carman. Fluid flow through granular beds. *Transactions, Institution of Chemical Engineers, London*, 15: 150 – 166, 1937.

G. Cartland Glover and J. Fitzpatrick. Modelling vortex formation in an unbaffled stirred tank reactors. *Chemical Engineering Journal*, 127:11 – 22, 2007.

A. B. D. Cassie and S. Baxter. Wettability of porous surfaces. *Trans. Faraday Soc.*, 40:546 – 551, 1944.

M. Cavinato. *High Shear Wet Granulation: Process understanding and scale up*. PhD thesis, Università degli studi di Padova, 2010.

J. Chandrapala, G. J. O. Martin, B. Zisu, S. E. Kentish, and M. Ashokkumar. The effect of ultrasound on casein micelle integrity. *Journal of Dairy Science*, 95(12):6882 – 6890, 2012.

J. Chandrapala, B. Zisu, M. Palmer, S. E. Kentish, and M. Ashokkumar. Sonication of milk protein solutions prior to spray drying and the subsequent effects on powders during storage. *Journal of Food Engineering*, 141:122 – 127, 2014.

E. Chávez Montes, N. Ardila Santamaría, J.-C. Gumy, and P. Marchal. Moisture-induced caking of beverage powders. *Journal of the Science of Food and Agriculture*, 91(14):2582 – 2586, 2011a.

E. Chávez Montes, N. Dogan, R. Nelissen, A. Marabi, L. Ducasse, and G. Ricard. Effects of drying and agglomeration on the dissolution of multi-component food powders. *Chemical Engineering & Technology*, 34(7):1159 – 1163, 2011b.

Y. Y. Chen, L. Hughes, L. Gladden, and M. Mantle. Quantitative ultra-fast MRI of HPMC swelling and dissolution. *Journal of Pharmaceutical Sciences*, 99(8):3462 – 3472, 2010.

Y. Cheong, G. Reynolds, A. Salman, and M. Hounslow. Modelling fragment size distribution using two-parameter Weibull equation. *International Journal of Mineral Processing*, 74S:S227 – S237, 2004.

M. W. Chudacek. Impeller power numbers and impeller flow numbers in profiled bottom tanks. *Industrial & Engineering Chemistry Process Design and Development*, 24(3):858 – 867, 1985.

M. Ciofalo, A. Brucato, F. Grisafi, and N. Torraca. Turbulent flow in closed and free-surface unbaffled tanks stirred by radial impellers. *Chemical Engineering Science*, 51(14):3557 – 3573, 1996.

J. Claude and J. Ubbink. Thermal degradation of carbohydrate polymers in amorphous states: A physical study including colorimetry. *Food Chemistry*, 96(3):402 – 410, 2006.

L. Colarow. US Patent 0226562 A1 Modified cocoa product and process for its manufacture, 2009.

K. D. Collins. Why continuum electrostatics theories cannot explain biological structure, polyelectrolytes or ionic strength effects in ion–protein interactions. *Biophysical Chemistry*, 167:43 – 59, 2012.

S. Conti, S. Gaisford, G. Buckton, and U. Conte. Solution calorimetry to monitor swelling and dissolution of polymers and polymer blends. *Thermochimica Acta*, 450(1 – 2):56 – 60, 2006.

C. Coutant, M. Skibic, G. Doddridge, C. Kemp, and D. Sperry. *In vitro* monitoring of an immediate release tablet by Focused Beam Reflectance Measurement. *Molecular Pharmaceutics*, 7(5):1508 – 1515, 2010.

P. Cullen and R. K. Connelly. Chapter 4: Rheology and mixing. In P. Cullen, editor, *Food Mixing: Principles and Applications*. Wiley-Blackwell, 2009.

B. Cuq, E. Rondet, and J. Abecassis. Food powders engineering, between knowhow and science: constraints, stakes and opportunities. *Powder Technology*, 208(2):244–251, 2011.

D. Dalgleish. On the structural models of bovine casein micelles – review and possible improvements. *Soft Matter*, 7(6):22650 – 2272, 2011.

S. Damodaran, K. Parkin, and O. Fennema. *Fennema's Food Chemistry: Fourth Edition*. CRC Press, 2008.

D. M. D'arcy and T. Persoons. Mechanistic modelling and mechanistic monitoring: Simulation and shadowgraph imaging of particulate dissolution in the flow-through apparatus. *Journal of Pharmaceutical Sciences*, 100 (3):1102 – 1115, 2011.

H. Darcy. *Les fontaines publiques de la ville de Dijon*. Dalmont, 1856.

A. Davenel, P. Schuck, and P. Marchal. A NMR relaxometry method for determining the reconstitutability and the water-holding capacity of protein-rich milk powders. *Milchwissenschaft*, 52(1):35–39, 1997.

A. Davenel, P. Schuck, F. Mariette, and G. Brulé. NMR relaxometry as a non-invasive tool to characterize milk powders. *Lait*, 82(4):465–473, 2002.

G. Davidov-Pardo and D. J. McClements. Nutraceutical delivery systems: Resveratrol encapsulation in grape seed oil nanoemulsions formed by spontaneous emulsification. *Food Chemistry*, 167:205 – 212, 2015.

M. J. de Ruijter, J. De Coninck, and G. Oshanin. Droplet spreading: partial wetting regime revisited. *Langmuir*, 15(6):2209 – 2216, 1999.

B. Derjaguin and L. Landau. Theory of the stability of strongly charged lyophobic sols and of the adhesion of strongly charged particles in solutions of electrolytes. *Acta Physico Chemica URSS*, 14(633), 1941.

N. Descamps, S. Palzer, and U. Zuercher. The amorphous state of spray-dried maltodextrin: sub–T_g enthalpy relaxation and impact of temperature and water annealing. *Carbohydrate Research*, 344(1):85 – 90, 2009.

N. Descamps, S. Palzer, Y. H. Roos, and J. J. Fitzpatrick. Glass transition and flowability/caking behaviour of maltodextrin DE 21. *Journal of Food Engineering*, 119(4):809 – 813, 2013.

R. M. Dhenge, K. Washino, J. J. Cartwright, M. J. Hounslow, and A. D. Salman. Twin screw granulation using conveying screws: Effects of viscosity of granulation liquids and flow of powders. *Powder Technology*, 238:77 – 90, 2013.

D. Dickey. Chapter 6: Mixing scale-up. In P. Cullen, editor, *Food Mixing: Principles and Applications*. Wiley-Blackwell, 2009a.

D. S. Dickey. Chapter 5: Equipment design. In P. Cullen, editor, *Food Mixing: Principles and Applications*. Wiley-Blackwell, 2009b.

H. Dogan and J. L. Kokini. Chapter 1: Rheological properties of foods. In D. Heldman and D. Lund, editors, *Handbook of Food Engineering: Second Edition*. CRC Press, 2007.

N. Dogan and F. Doleac. US Patent 0186498 A1 Capsule for use in a beverage preparation machine, 2014.

P. Dokic, J. Jakovljevic, and L. Dokic-Baucal. Molecular characteristics of maltodextrins and rheological behaviour of diluted and concentrated solutions. *Colloids and Surfaces A: Physicochemical and Engineering Aspects*, 141(3):435 – 440, 1998.

A. Dokoumetzidis and P. Macheras. A century of dissolution research: From Noyes and Whitney to the biopharmaceutics classification system. *International Journal of Pharmaceutics*, 321(1–2):1 – 11, 2006.

P. Doran. *Bioprocess Engineering Principles: Second Edition*. Academic Press, 2013.

S. Drusch, S. Hamann, A. Berger, Y. Serfert, and K. Schwarz. Surface accumulation of milk proteins and milk protein hydrolysates at the air–water interface on a time-scale relevant for spray-drying. *Food Research International*, 47(2):140 – 145, 2012.

J. Dupas. *Mouillage de polymères solubles*. PhD thesis, Université Pierre et Marie Curie, 2012.

J. Dupas, E. Verneuil, M. Ramaioli, L. Forny, L. Talini, and F. Lequeux. Dynamic wetting on a thin film of soluble polymer: Effects of nonlinearities in the sorption isotherm. *Langmuir*, 29(40):12572–12578, 2013.

J. Dupas, E. Verneuil, M. van Landeghem, B. Bresson, L. Forny, M. Ramaioli, F. Lequeux, and L. Talini. Glass transition accelerates the spreading of polar solvents on a soluble polymer. *Physical Review Letters*, 112:188302–1–5, 2014.

M. Dupas-Langlet, M. Benali, I. Pezron, K. Saleh, and L. Metlas-Komunjer. The impact of deliquescence lowering on the caking of powder mixtures. *Powder Technology*, 270, Part B:502 – 509, 2015.

N. Ewing and J. Fisher. US Patent 4318932 Instant milk process, 1982.

C. C. Fagan, P. Cullen, and C. P. O'Donnell. Chapter 7: Monitoring and control of mixing operations. In P. Cullen, editor, *Food Mixing: Principles and Applications*. Wiley-Blackwell, 2009.

Y. Fang, C. Selomulya, and X. Chen. On measurement of food powder reconstitution properties. *Drying Technology*, 26(1):3–14, 2007.

Y. Fang, C. Selomulya, and X. Chen. Characterization of milk protein concentrate solubility using focused beam reflectance measurement. *Dairy Science Technology*, 90:253–270, 2010.

Y. Fang, C. Selomulya, S. Ainsworth, M. Palmer, and X. Chen. On quantifying the dissolution behaviour of milk protein concentrate. *Food Hydrocolloids*, 25(3):503–510, 2011.

Y. Fang, S. Rogers, C. Selomulya, and X. Chen. Functionality of milk protein concentrate: Effect of spray drying temperature. *Biochemical Engineering Journal*, 62:101–105, 2012.

L. Figura and A. Teixeira. *Food Physics: Physical properties, measurement and applications*. Springer, 2007.

R. Fisher. On the capillary forces in an ideal soil; correction of formulae given by W. B. Haines. *The Journal of Agricultural Science*, 16(3):492–505, 1926.

J. Fitzpatrick, K. Weidendorfer, and E. Teunou. Reconstitution of dairy powders to high solids content in a stirred-tank: the effect of agitation. *Milchwissenschaft*, 55(8):437–440, 2000.

J. Fitzpatrick, K. Weidendorfer, M. Weber, and E. Teunou. Practical considerations for reconstituting dairy powders to high solids contents in a stirred-tank. *Milchwissenschaft*, 56(9):512–516, 2001.

J. Fitzpatrick, T. Iqbal, C. Delaney, T. Twomey, and M. Keogh. Effect of powder properties and storage conditions on the flowability of milk powders with different fat contents. *Journal of Food Engineering*, 64: 435 – 444, 2004.

J. Fitzpatrick, K. Barry, P. Cerqueira, T. Iqbal, J. O'Neill, and Y. Roos. Effect of composition and storage conditions on the flowability of dairy powders. *International Dairy Journal*, 17(4):383 – 392, 2007.

J. Fitzpatrick, E. O'Callaghan, and J. O'Flynn. Application of a novel cake strength tester for investigating caking of skim milk powder. *Food and Bioproducts Processing*, 86(3):198 – 203, 2008.

J. Fitzpatrick, N. Descamps, K. O'Meara, C. Jones, D. Walsh, and M. Spitere. Comparing the caking behaviours of skim milk powder, amorphous maltodextrin and crystalline common salt. *Powder Technology*, 204(1):131 – 137, 2010.

C. Flemmer. On the regime boundaries of moisture in granular materials. *Powder Technology*, 66(2):191 – 194, 1991.

L. Forny, I. Pezron, K. Saleh, P. Guigon, and L. Komunjer. Peculiar absorption of water by hydrophobized glass beads. *Colloids and Surfaces A: Physicochemical and Engineering Aspects*, 270–271:263 – 269, 2005.

L. Forny, K. Saleh, I. Pezron, L. Komunjer, and P. Guigon. Influence of mixing characteristics for water encapsulation by self-assembling hydrophobic silica nanoparticles. *Powder Technology*, 189(2):263 – 269, 2009.

L. Forny, A. Marabi, and S. Palzer. Wetting, disintegration and dissolution of agglomerated water soluble powders. *Powder Technology*, 206(1 – 2):72 – 78, 2011.

G. Fountain and W. Gundle, A. Kang. UK patent 2496265 Coffee products and related processes, 2014.

T. G. Fox and P. J. Flory. 2^{nd}-order transition temperatures and related properties of polystyrene. 1. Influence of molecular weight. *Journal of Applied Physics*, 21:581–591, 1950.

B. Freudig, S. Hogekamp, and H. Schubert. Dispersion of powders in liquids in a stirred vessel. *Chemical Engineering and Processing*, 38(4 - 6):525 – 532, 1999.

L. Fries, S. Antonyuk, S. Heinrich, D. Dopfer, and S. Palzer. Collision dynamics in fluidised bed granulators: A DEM-CFD study. *Chemical Engineering Science*, 86:108 – 123, 2013.

N. Fu, M. W. Woo, and X. D. Chen. Colloidal transport phenomena of milk components during convective droplet drying. *Colloids and Surfaces B: Biointerfaces*, 87(2):255 – 266, 2011.

K. Fyfe, O. Kravchuk, A. V. Nguyen, H. Deeth, and B. Bhandari. Influence of dryer type on surface characteristics of milk powders. *Drying Technology*, 29(7):758 – 769, 2011.

E. Gaddis. N3: Heat transfer and power consumption in stirred vessels. In V. Gesellschaft Verfahrenstechnik und Chemieingenieurwesen, editor, *VDI Heat Atlas, Second Edition*. Springer, 2010.

C. Gaiani. *Etude des mécanismes de réhydratation des poudres laitières : influence de la structure et de la composition des poudres*. PhD thesis, l'Institut National Polytechnique de Lorraine, 2006.

C. Gaiani, S. Banon, J. Scher, P. Schuck, and J. Hardy. Use of a turbidity sensor to characterize micellar casein powder rehydration: influence of some technological effects. *Journal of Dairy Science*, 88(8):2700–2706, 2005.

C. Gaiani, J. Scher, P. Schuck, J. Hardy, S. Desobry, and S. Banon. The dissolution behaviour of native phosphocaseinate as a function of concentration and temperature using a rheological approach. *International Dairy Journal*, 16(12):1427 – 1434, 2006.

C. Gaiani, P. Schuck, J. Scher, S. Desobry, and S. Banon. Dairy powder rehydration: Influence of protein state, incorporation mode, and agglomeration. *Journal of Dairy Science*, 90(2):570 – 581, 2007.

C. Gaiani, J. Scher, P. Schuck, S. Desobry, and S. Banon. Use of a turbidity sensor to determine dairy powder rehydration properties. *Powder Technology*, 190(1 – 2):2–5, 2009.

C. Gaiani, M. Morand, C. Sanchez, E. A. Tehrany, M. Jacquot, P. Schuck, R. Jeantet, and J. Scher. How surface composition of high milk proteins powders is influenced by spray-drying temperature. *Colloids and Surfaces B: Biointerfaces*, 75(1):377 – 384, 2010.

C. Gaiani, M. Mullet, E. Arab-Tehrany, M. Jacquot, C. Perroud, A. Renard, and J. Scher. Milk proteins differentiation and competitive adsorption during spray-drying. *Food Hydrocolloids*, 25(5):983 – 990, 2011.

S. Gaisford and M. Saunders. Chapter 7: Physical form I – Crystalline materials. In *Essentials of Pharmaceutical Preformulation*. John Wiley & Sons, Ltd, 2012.

L. Galet, T. Vu, D. Oulahna, and J. Fages. The wetting behaviour and dispersion rate of cocoa powder in water. *Food and Bioproducts Processing*, 82(4):298 – 303, 2004.

L. Galet, C. Goalard, and J. Dodds. The importance of surface energy in the dispersion behaviour of talc particles in aqueous media. *Powder Technology*, 190(1 – 2):242 – 246, 2009.

N. Garti and D. McClements. *Encapsulation Technologies and Delivery Systems for Food Ingredients and Nutraceuticals*. Elsevier, 2012.

N. Gavish and K. Promislow. Dependence of the dielectric constant of electrolyte solutions on ionic concentration. *ArXiv e-prints*, pages 1–5, 2012.

C. Gerhardt and M. Tasker. US Patent 7618648 B2 Satiety inducing composition, 2009.

S. Ghosal, T. Indira, and S. Bhattacharya. Agglomeration of a model food powder: Effect of maltodextrin and gum Arabic dispersions on flow behavior and compacted mass. *Journal of Food Engineering*, 96(2):222 – 228, 2010.

A. Gianfrancesco, C. Turchiuli, D. Flick, and E. Dumoulin. CFD modeling and simulation of maltodextrin solutions spray drying to control stickiness. *Food Bioprocess Technology*, 3:946–955, 2010.

A. Gianfrancesco, C. Casteran, J. Andrieux, M. Giardiello, and G. Vuataz. Assessment of physical characteristics

and dissolution behavior of protein based powders. In *International Congress on Engineering and Food*, 2011.

A. Gianfrancesco, C. Smarrito-Menozzi, G. Niederreiter, and S. Palzer. Freeze drying as a food structuring process: a scientific approach based on drying kinetics and material properties. *Drying Technology*, 30:1160 – 1166, 2012.

C. Goalard, A. Samimi, L. Galet, J. A. Dodds, and M. Ghadiri. Characterization of the dispersion behavior of powders in liquids. *Particle & Particle Systems Characterization*, 23(2):154 – 158, 2006.

P. Gopalkrishnan, I. Manas-Zloczower, and D. L. Feke. Investigating dispersion mechanisms in partially infiltrated agglomerates: Interstitial fluid effects. *Powder Technology*, 156(2 – 3):111 – 119, 2005.

P. Gopalkrishnan, I. Manas-Zloczower, and D. Feke. Effect of morphology and extent of infiltration on the cohesivity and dispersion mechanisms of particle agglomerates. *Chemical Engineering Science*, 62(14):3740 – 3747, 2007.

M. Gordon and T. Taylor. Ideal copolymers and the second-order transitions of synthetic rubbers. i. non-crystalline copolymers. *Journal of Applied Chemistry 2*, pages 493 – 500, 1952.

D. Granizo, B. Reuhs, R. Stroshine, and L. Mauer. Evaluating the solubility of powdered food ingredients using dynamic nuclear magnetic resonance (NMR) relaxometry. *LWT - Food Science and Technology*, 40(1): 36 – 42, 2007.

E. Guggenheim. *Applications of statistical mechanics*. Clarendon press, 1966.

M. Gulzar, S. Bouhallab, R. Jeantet, P. Schuck, and T. Croguennec. Influence of pH on the dry heat-induced denaturation/aggregation of whey proteins. *Food Chemistry*, 129(1):110 – 116, 2011.

S. Gurupatham, B. Dalal, M. Hossain, I. Fischer, P. Singh, and D. Joseph. Particles dispersion on fluid-liquid interfaces. *Particuology*, 9(1):1 – 13, 2011.

S. Gurupatham, M. Hossain, B. Dalal, I. Fischer, P. Singh, and D. Joseph. Breakup of particle clumps on liquid surfaces. *Powder Technology*, 217:288 – 297, 2012.

M. Hadnadev, T. D. Hadnadev, L. Dokić, B. Pajin, A. Torbica, L. Šarić, and P. Ikonić. Physical and sensory aspects of maltodextrin gel addition used as fat replacers in confectionery filling systems. *LWT - Food Science and Technology*, 59(1):495 – 503, 2014.

C. Hahn, T. Wachter, J. Weiss, and J. Hinrichs. Application of an inline particle size device to microgel particles during post-processing of fresh cheese. *International Dairy Journal*, 29(2):75 – 81, 2013.

C. I. Haider, T. Althaus, G. Niederreiter, M. J. Hounslow, S. Palzer, and A. D. Salman. A micromanipulation particle tester for agglomeration contact mechanism studies in a controlled environment. *Measurement Science and Technology*, 23(10):105904–1–12, 2012.

C. I. Haider, M. J. Hounslow, A. D. Salman, T. O. Althaus, G. Niederreiter, and S. Palzer. Influence of environmental conditions on caking mechanisms in individual amorphous food particle contacts. *AIChE Journal*, 60(8):2774–2787, 2014.

X. Han, C. Ghoroi, D. To, Y. Chen, and R. Davé. Simultaneous micronization and surface modification for improvement of flow and dissolution of drug particles. *International Journal of Pharmaceutics*, 415(1 – 2): 185 – 195, 2011.

E. Haque, B. Bhandari, M. Gidley, H. Deeth, and A. Whittaker. Ageing-induced solubility loss in milk protein concentrate powder: Effect of protein conformational modifications and interactions with water. *Journal of the Science of Food and Agriculture*, 91(14):2576–2581, 2011.

E. Haque, A. K. Whittaker, M. J. Gidley, H. C. Deeth, K. Fibrianto, and B. R. Bhandari. Kinetics of enthalpy relaxation of milk protein concentrate powder upon ageing and its effect on solubility. *Food Chemistry*, 134 (3):1368 – 1373, 2012.

M. K. Haque and Y. H. Roos. Differences in the physical state and thermal behavior of spray-dried and freeze-dried lactose and lactose/protein mixtures. *Innovative Food Science & Emerging Technologies*, 7(1 – 2):62 – 73, 2006.

H. Hartmann, J. Derksen, and H. van den Akker. Numerical simulation of a dissolution process in a stirred tank reactor. *Chemical Engineering Science*, 61(9):3025 – 3032, 2006.

M. Hartmann and S. Palzer. Caking of amorphous powders — material aspects, modelling and applications. *Powder Technology*, 206(1–2):112 – 121, 2011.

P. Havea. Protein interactions in milk protein concentrate powders. *International Dairy Journal*, 16(5):415 – 422, 2006.

M. Heine, S. Antonyuk, L. Fries, G. Niederreiter, S. Heinrich, and S. Palzer. Modeling of the spray zone for particle wetting in a fluidized bed. *Chemie Ingenieur Technik*, 85(3):280–289, 2013.

D. Hellborg, B. Bergenståhl, and C. Trägårdh. The influence of powder properties on the imbibation rate. *Colloids and Surfaces B: Biointerfaces*, 93:108–115, 2012.

A. W. Hixson and J. H. Crowell. Dependence of reaction velocity upon surface and agitation. *Industrial & Engineering Chemistry*, 23(8):923–931, 1931.

E. M. Hoek and G. K. Agarwal. Extended DLVO interactions between spherical particles and rough surfaces. *Journal of Colloid and Interface Science*, 298(1):50 – 58, 2006.

S. Hogan and G. Buckton. The quantification of small degrees of disorder in lactose using solution calorimetry. *International Journal of Pharmaceutics*, 207(1–2):57–64, 2000.

S. Hogan, M. Famelart, D. O'Callaghan, and P. Schuck. A novel technique for determining glass–rubber transition in dairy powders. *Journal of Food Engineering*, 99(1):76 – 82, 2010.

S. Hogekamp and H. Schubert. Rehydration of food powders. *Food Science and Technology International*, 9 (3):223–235, 2003.

T. Höpfner, A. Bluma, G. Rudolph, P. Lindner, and T. Scheper. A review of non-invasive optical-based image analysis systems for continuous bioprocess monitoring. *Bioprocess and Biosystems Engineering*, 33(2): 247–256, 2010.

T. Hörmann, D. Suzzi, and J. G. Khinast. Mixing and dissolution processes of pharmaceutical bulk materials in stirred tanks: Experimental and numerical investigations. *Industrial & Engineering Chemistry Research*, 50(21):12011–12025, 2011.

S. Hosseini, D. Patel, F. Ein-Mozaffari, and M. Mehrvar. Study of solid–liquid mixing in agitated tanks through electrical resistance tomography. *Chemical Engineering Science*, 65:1374–1384, 2010.

J. Huang, G. Kaul, J. Utz, P. Hernandez, V. Wong, D. Bradley, A. Nagi, and D. O'Grady. A PAT approach to improve process understanding of high shear wet granulation through in-line particle measurement using FBRM C35. *Journal of Pharmaceutical Sciences*, 99(7):3205–3212, 2010.

Y. Hui. *Handbook of Food Science, Technology, and Engineering*, volume 1. Taylor & Francis, 2006.

T. Huppertz and C. de Kruif. Disruption and reassociation of casein micelles during high pressure treatment: influence of whey proteins. *Journal of Dairy Research*, 74(2):194–197, 2007.

T. Huppertz and P. F. Fox. Effect of NaCl on some physico-chemical properties of concentrated bovine milk. *International Dairy Journal*, 16(10):1142 – 1148, 2006.

R. Hussain, C. Gaiani, L. Aberkane, and J. Scher. Characterization of high-milk-protein powders upon rehydration under various salt concentrations. *Journal of Dairy Science*, 94(1):14–23, 2011.

R. Hussain, C. Gaiani, and J. Scher. From high milk protein powders to the rehydrated dispersions in variable ionic environments: A review. *Journal of Food Engineering*, 113(3):486 – 503, 2012.

S. Ibrahim and A. Nienow. Comparing impeller performance for solid-suspension in the transitional flow regime with Newtonian fluids. *Trans IChemE*, 77(A):721 – 727, 1999.

IDF. Standard 87: Instant dried milk – determination of the dispersibility & wettability. *International Dairy Federation*, 1979.

IDF. Standard 129A: Dried milk and dried milk products. Determination of insolubility index. *International Dairy Federation*, 1988.

IDF. Standard 173: Dried milk protein products. Determination of nitrogen solubility index. *International Dairy Federation*, 1995.

T. Imison, B. Zeller, and I. Fisk. UK Patent 2486487 Instant coffee, 2012.

S. P. Ishwarya and C. Anandharamakrishnan. Spray-freeze-drying approach for soluble coffee processing and its effect on quality characteristics. *Journal of Food Engineering*, 149:171 – 180, 2015.

J. Israelachvili. *Intermolecular and Surface Forces, Third Edition.* Academic Press, 2011.

S. M. Iveson and J. D. Litster. Growth regime map for liquid-bound granules. *AIChE Journal*, 44(7):1510–1518, 1998.

S. M. Iveson, P. A. Wauters, S. Forrest, J. D. Litster, G. M. Meesters, and B. Scarlett. Growth regime map for liquid-bound granules: further development and experimental validation. *Powder Technology*, 117(1–2): 83 – 97, 2001.

R. Jeantet, P. Schuck, T. Six, C. Andre, and G. Delaplace. The influence of stirring speed, temperature and solid concentration on the rehydration time of micellar casein powder. *Dairy Science & Technology*, 90(2): 225–236, 2010.

J. Jurin. An account of some experiments shown before the royal society; with an enquiry into the cause of the ascent and suspension of water in capillary. *Philosophical Transactions of the Royal Society of London*, 1718.

H. Kamphuis. Chapter 6: Production and quality standards of cocoa mass, cocoa butter and cocoa powder. In S. Beckett, editor, *Industrial Chocolate Manufacture and Use*. Blackwell Publishing Inc, 2009.

E. Katainen, P. Niemelä, P. Harjunen, J. Suhonen, and K. Järvinen. Evaluation of the amorphous content of lactose by solution calorimetry and raman spectroscopy. *Talanta*, 68(1):1–5, 2005.

P. Kayaert, B. Li, I. Jimidar, P. Rombaut, F. Ahssini, and G. V. den Mooter. Solution calorimetry as an alternative approach for dissolution testing of nanosuspensions. *European Journal of Pharmaceutics and Biopharmaceutics*, 76(3):507 – 513, 2010.

B. A. Kerwin. Polysorbates 20 and 80 used in the formulation of protein biotherapeutics: Structure and degradation pathways. *Journal of Pharmaceutical Sciences*, 97(8):2924–2935, 2008.

J. Kestin, E. Khalifa, and R. Correia. Tables of the dynamic and kinematic viscosity of aqueous NaCl solutions in the temperature range 20 – 150 °C and the pressure range 0.1 – 35 MPa. *Journal of Physical Chemistry Reference Data*, 10(1):71 – 87, 1981.

O. Khazam and S. M. Kresta. Mechanisms of solids drawdown in stirred tanks. *The Canadian Journal of Chemical Engineering*, 86(4):622–634, 2008.

O. Khazam and S. M. Kresta. A novel geometry for solids drawdown in stirred tanks. *Chemical Engineering Research and Design*, 87(3):280 – 290, 2009.

E. H.-J. Kim, X. Chen, and D. Pearce. Surface characterization of four industrial spray-dried dairy powders in relation to chemical composition, structure and wetting property. *Colloids and Surfaces B: Biointerfaces*, 26(3):197 – 212, 2002.

E. H.-J. Kim, X. D. Chen, and D. Pearce. Effect of surface composition on the flowability of industrial spray-dried dairy powders. *Colloids and Surfaces B: Biointerfaces*, 46(3):182 – 187, 2005a.

E. H. J. Kim, X. D. Chen, and D. Pearce. Melting characteristics of fat present on the surface of industrial spray-dried dairy powders. *Colloids and Surfaces B: Biointerfaces*, 42(1):1 – 8, 2005b.

E. H.-J. Kim, X. D. Chen, and D. Pearce. Surface composition of industrial spray-dried milk powders. 1. Development of surface composition during manufacture. *Journal of Food Engineering*, 94(2):163 – 168, 2009a.

E. H.-J. Kim, X. D. Chen, and D. Pearce. Surface composition of industrial spray-dried milk powders. 2. Effects of spray drying conditions on the surface composition. *Journal of Food Engineering*, 94(2):169 – 181, 2009b.

E. H.-J. Kim, X. D. Chen, and D. Pearce. Surface composition of industrial spray-dried milk powders. 3. Changes in the surface composition during long-term storage. *Journal of Food Engineering*, 94(2):182 – 191, 2009c.

N. King. Dispersibility and reconstitutability of dried milk. *Dairy Science & Technology*, 28:105–118, 1966.

C. Klein Larsen, O. Gaserod, and O. Smidsrod. A novel method for measuring hydration and dissolution kinetics of alginate powders. *Carbohydrate Polymers*, 51(2):125–134, 2003.

V. Koganti, F. Carroll, R. Ferraina, R. Falk, Y. Waghmare, M. Berry, Y. Liu, K. Norris, R. Leasure, and J. Gaudio. Application of modeling to scale-up dissolution in pharmaceutical manufacturing. *AAPS PharmSciTech*, 11(4):1541–1548, 2010.

A. Kolmogorov. The local structure of turbulence in incompressible viscous fluid for very large Reynolds numbers. *Doklady Akademii Nauk SSR*, 30:301–305, 1941.

J. Kowalska and A. Lenart. The influence of ingredients distribution on properties of agglomerated cocoa products. *Journal of Food Engineering*, 68(2):155 – 161, 2005.

J. Kowalska, E. Majewska, and A. Lenart. Sorption properties of a modified powdered cocoa beverage. *Chemical and Process Engineering*, 32(1):21–31, 2011.

A. Kowalski, J. Davidson, M. Flanagan, and T. York. Electrical Resistance Tomography for characterisation of physical stability in liquid compositions. *Chemical Engineering Journal*, 158:69–77, 2010.

J. Kozeny. Über kapillare Leitung des Wassers im Boden. *Akademie der Wissenschaften in Wien. Sitzungsberichte.*, 1927.

P. Kralchevsky and N. Denkov. Capillary forces and structuring in layers of colloid particles. *Current Opinion in Colloid & Interface Science*, 6(4):383 – 401, 2001.

T. Kravtchenko, J. Renoir, A. Parker, and G. Brigand. A novel method for determining the dissolution kinetics of hydrocolloid powders. *Food Hydrocolloids*, 13(3):219–225, 1999.

C. Kumar, M. Karim, and M. U. Joardder. Intermittent drying of food products: A critical review. *Journal of Food Engineering*, 121:48 – 57, 2014.

K. A. Kusters, S. E. Pratsinis, S. G. Thoma, and D. M. Smith. Ultrasonic fragmentation of agglomerate powders. *Chemical Engineering Science*, 48(24):4119 – 4127, 1993.

P. Kyaw Hla and S. Hogekamp. Wetting behaviour of instantized cocoa beverage powders. *International Journal of Food Science & Technology*, 34(4):335–342, 1999.

T. Laaman. *Hydrocolloids in food procesing.* John Wiley & Sons, Inc., 2011.

Z. A. Langham, J. Booth, L. P. Hughes, G. K. Reynolds, and S. A. C. Wren. Mechanistic insights into the dissolution of spray-dried amorphous solid dispersions. *Journal of Pharmaceutical Sciences*, 101(8): 2798–2810, 2012.

M. Langlet, M. Benali, I. Pezron, K. Saleh, P. Guigon, and L. Metlas-Komunjer. Caking of sodium chloride:

Role of ambient relative humidity in dissolution and recrystallization process. *Chemical Engineering Science*, 86:78 – 86, 2013.

P. Laplace. Theory of capillary attraction. *Supplements to the 10^{th} book of Celestial Mechanics*, 1806.

P. Larsen, J. Rawlings, and N. Ferrier. Model-based object recognition to measure crystal size and shape distributions from *in situ* video images. *Chemical Engineering Science*, 62(5):1430 – 1441, 2007.

H. Lawless and H. Heymann. *Sensory Evaluation of Food: Principles and Practices*. Springer, 2010.

M. Lazghab, K. Saleh, I. Pezron, P. Guigon, and L. Komunjer. Wettability assessment of finely divided solids. *Powder Technology*, 157(1–3):79–91, 2005.

G. Lefebvre. *Modification de surface de particules de talc par de la silice nanométrique hydrophobe (par enrobage à sec) : influence sur leurs propriétés physicochimiques et leur dispersibilité dans une phase aqueuse*. PhD thesis, L'université de Toulouse, 2010.

G. Lefebvre, L. Galet, and A. Chamayou. Dry coating of talc particles: Effect of material and process modifications on their wettability and dispersibility. *AIChE Journal*, 57(1):79–86, 2011a.

G. Lefebvre, L. Galet, and A. Chamayou. Dry coating of talc particles with fumed silica: Influence of the silica concentration on the wettability and dispersibility of the composite particles. *Powder Technology*, 208 (2):372–377, 2011b.

O. Levenspiel. *Chemical reaction engineering*. Wiley, 1999.

T. Leyssens, C. Baudry, and M. Escudero-Hernandez. Optimization of a crystallization by online FBRM analysis of needle-shaped crystals. *Organic Process Research & Development*, 15(2):413–426, 2011.

H. Li, M. A. Grover, Y. Kawajiri, and R. W. Rousseau. Development of an empirical method relating crystal size distributions and FBRM measurements. *Chemical Engineering Science*, 89:142 – 151, 2013.

G. Lian, C. Thornton, and M. J. Adams. A theoretical study of the liquid bridge forces between two rigid spherical bodies. *Journal of Colloid and Interface Science*, 161(1):138 – 147, 1993.

Y. Liang, N. Hilal, P. Langston, and V. Starov. Interaction forces between colloidal particles in liquid: Theory and experiment. *Advances in Colloid and Interface Science*, 134-135:151–166, 2007.

R. A. Lipasek, J. C. Ortiz, L. S. Taylor, and L. J. Mauer. Effects of anticaking agents and storage conditions on the moisture sorption, caking, and flowability of deliquescent ingredients. *Food Research International*, 45(1):369 – 380, 2012.

Z. Liu, P. Juliano, R. Williams, J. Niere, and M. Augustin. Ultrasound effects on the assembly of casein micelles in reconstituted skim milk. *Journal of Dairy Research*, 81(2):146–155, 2014.

C. Loret, V. Meunier, W. J. Frith, and P. J. Fryer. Rheological characterisation of the gelation behaviour of maltodextrin aqueous solutions. *Carbohydrate Polymers*, 57(2):153 – 163, 2004.

C. Malmberg and A. Maryott. Dielectric constant of water from 0 ° to 100 °C. *Journal of Research of the National Bureau of Standards*, 56(1):1–8, 1956.

I. Manas-Zloczower. *Mixing and compounding of polymers, Second Edition*. Hanser GmbH, 2009.

L. Mao. *Application of Extended DLVO Theory: Modeling of Flotation and Hydrophobicity of Dodecane*. PhD thesis, Virginia Polytechnic Institute and State University, 1998.

A. Marabi, S. Livings, M. Jacobson, and I. Saguy. Normalized Weibull distribution for modeling rehydration of food particulates. *European Food Research and Technology*, 217(4):311–318, 2003.

A. Marabi, G. Mayor, A. Raemy, I. Bauwens, J. Claude, A. Burbidge, R. Wallach, and I. Saguy. Solution calorimetry: A novel perspective into the dissolution process of food powders. *Food Research International*, 40(10):1286–1298, 2007.

A. Marabi, G. Mayor, A. Burbidge, R. Wallach, and I. Saguy. Assessing dissolution kinetics of powders by a single particle approach. *Chemical Engineering Journal*, 139(1):118–127, 2008a.

A. Marabi, A. Raemy, I. Bauwens, A. Burbidge, R. Wallach, and I. Saguy. Effect of fat content on the dissolution enthalpy and kinetics of a model food powder. *Journal of Food Engineering*, 85(4):518–527, 2008b.

A. Marabi, A. Burbidge, and A. Raemy. US Patent 0098811 A1 Particulate structuration for improving the dissolution kinetics of food powders, 2010.

L. Marchal, H. Beeftink, and J. Tramper. Towards a rational design of commercial maltodextrins. *Trends in Food Science & Technology*, 10(11):345 – 355, 1999.

M. F. Marcone, S. Wang, W. Albabish, S. Nie, D. Somnarain, and A. Hill. Diverse food-based applications of nuclear magnetic resonance (NMR) technology. *Food Research International*, 51(2):729 – 747, 2013.

A. Markande, J. Fitzpatrick, A. Nezzal, L. Aerts, and A. Redl. Application of in-line monitoring for aiding interpretation and control of dextrose monohydrate crystallization. *Journal of Food Engineering*, 114(1):8 – 13, 2013.

S. I. Martins, W. M. Jongen, and M. A. van Boekel. A review of Maillard reaction in food and implications to kinetic modelling. *Trends in Food Science & Technology*, 11(9–10):364 – 373, 2000.

A. Massey and A. Massey. US Patent 8529973 B2 Coffee composition and method of making a three-layered coffee drink, 2013.

D. Mather and H. Hollender. The influence of some surfactants upon the self-dispersion and churning of whole milk powder. *Journal of Dairy Science*, 38(2):217–223, 1955.

J. Mauger, J. Ballard, R. Brockson, S. De, V. Gray, and D. Robinson. Intrinsic dissolution performance testing of the USP dissolution apparatus 2 (rotating paddle) using modified salicylic acid calibrator tablets: Proof of principle. *Dissolution Technologies*, 10:6–15, 2003.

N. A. McCarthy, P. M. Kelly, P. G. Maher, and M. A. Fenelon. Dissolution of milk protein concentrate (MPC) powders by ultrasonication. *Journal of Food Engineering*, 126:142 – 148, 2014.

D. J. McClements. Principles of ultrasonic droplet size determination in emulsions. *Langmuir*, 12(14):3454–3461, 1996.

H. Merkus. *Particle size measurements: fundamentals, practice, quality*. Springer Science + Business Media B.V., 2009.

A. B. Metzner and R. E. Otto. Agitation of non-Newtonian fluids. *AIChE Journal*, 3(1):3–10, 1957.

E. Meursing. *de Zaan Cocoa & Chocolate Manual*. ADM, 2009.

S. Meyer, S. Berrut, T. I. J. Goodenough, V. S. Rajendram, V. J. Pinfield, and M. J. W. Povey. A comparative study of ultrasound and laser light diffraction techniques for particle size determination in dairy beverages. *Measurement Science and Technology*, 17(2):289–297, 2006a.

S. Meyer, V. S. Rajendram, and M. J. Povey. Characterization of reconstituted milk powder by ultrasound spectroscopy. *Journal of Food Quality*, 29(4):405–418, 2006b.

A. Millqvist-Fureby and P. Smith. *In-situ* lecithination of dairy powders in spray-drying for confectionery applications. *Food Hydrocolloids*, 21(5–6):920 – 927, 2007.

A. Millqvist-Fureby, U. Elofsson, and B. Bergenståhl. Surface composition of spray-dried milk protein-stabilised emulsions in relation to pre-heat treatment of proteins. *Colloids and Surfaces B: Biointerfaces*, 21(1–3): 47–58, 2001.

A. Mimouni, H. Deeth, A. Whittaker, M. Gidley, and B. Bhandari. Rehydration process of milk protein concentrate powder monitored by static light scattering. *Food Hydrocolloids*, 23(7):1958–1965, 2009.

A. Mimouni, H. Deeth, A. Whittaker, M. Gidley, and B. Bhandari. Investigation of the microstructure of milk protein concentrate powders during rehydration: Alterations during storage. *Journal of Dairy Science*, 93 (2):463–472, 2010.

A. P. Minoja and C. Napoli. NMR screening in the quality control of food and nutraceuticals. *Food Research International*, 63, Part B:126 – 131, 2014.

W. Mitchell, D. Dopfer, L. Forny, T. Althaus, G. Niederreiter, and S. Palzer. Compaction of food powders: The influence of material properties and process parameters on tablet structure, strength, and dissolution. *Nestlé Research Internal Document*, 2011.

A. Muñoz-Herrera, V. Tejeda-Hernández, A. Jiménez-Aparicio, J. Welti-Chanes, J. Chanona-Pérez, and G. Guttiérrez. Microstructural, physical, and rehydration properties of maltodextrin. In D. Reid, T. Sajjaanantakul, P. Lillford, and S. Charoenrein, editors, *Water properties in food, health, pharmaceutical, and biological systems: ISOPOW 10*, pages 673–679. Wiley-Blackwell, 2010.

I. Murrieta-Pazos, C. Gaiani, L. Galet, R. Calvet, B. Cuq, and J. Scher. Food powders: Surface and form characterization revisited. *Journal of Food Engineering*, 112(1–2):1 – 21, 2012a.

I. Murrieta-Pazos, C. Gaiani, L. Galet, and J. Scher. Composition gradient from surface to core in dairy powders: Agglomeration effect. *Food Hydrocolloids*, 26(1):149 – 158, 2012b.

K. Muthukumarappan. Chapter 2: Mixing fundamentals. In P. Cullen, editor, *Food Mixing: Principles and Application*. Wiley-Blackwell, 2009.

W. Nernst. Theorie der Reaktionsgeschwindigkeit in heterogenen Systemen. *Zeitschrift für Physikalische Chemie*, 47:52–55, 1904.

K. A. Newman and K. D. Stolzenbach. Kinetics of aggregation and disaggregation of titanium dioxide particles and glass beads in a sheared fluid suspension. *Colloids and Surfaces A: Physicochemical and Engineering Aspects*, 107:189 – 203, 1996.

S. Nielsen. *Food Analysis*. Springer, 2014.

J. Nijdam and T. Langrish. The effect of surface composition on the functional properties of milk powders. *Journal of Food Engineering*, 77(4):919 – 925, 2006.

T. Nijhuis, T. Gusek, B. Jirjis, and I. Purtle. US Patent 7201934 B2 Dispersible cocoa products, 2007.

Y. Nikolova, J. Petit, C. Sanders, A. Gianfrancesco, N. Desbenoit, G. Frache, G. Francius, J. Scher, and C. Gaiani. Is it possible to modulate the structure of skim milk particle through drying process and parameters? *Journal of Food Engineering*, 142:179 – 189, 2014.

A. Noyes and W. Whitney. The rate of solution of solid substances in their own solutions. *Journal of the American Chemical Society*, 19(930–934), 1897.

M. R. Okos, O. Campanella, G. Narsimhan, R. K. Singh, and A. Weitnauer. Chapter 10: Food dehydration. In D. Heldman and D. Lund, editors, *Handbook of Food Engineering: Second Edition*. CRC Press, 2007.

D. Oldfield, C. Teehan, and P. Kelly. The effect of preheat treatment and other process parameters on the coffee stability of instant whole milk powder. *International Dairy Journal*, pages 659–667, 2000.

D. Oldfield, M. Taylor, and H. Singh. Effect of preheating and other process parameters on whey protein reactions during skim milk powder manufacture. *International Dairy Journal*, 15(5):501 – 511, 2005.

T. Omobuwajo, O. Busari, and A. Osemwegie. Thermal agglomeration of chocolate drink powder. *Journal of Food Engineering*, 46(2):73 – 81, 2000.

M. A. O'Neill and S. Gaisford. Application and use of isothermal calorimetry in pharmaceutical development. *International Journal of Pharmaceutics*, 417(1–2):83 – 93, 2011.

J. D. Osborne, T. Althaus, L. Forny, G. Niederreiter, S. Palzer, M. J. Hounslow, and A. D. Salman. Investigating the influence of moisture content and pressure on the bonding mechanisms during roller compaction of an amorphous material. *Chemical Engineering Science*, 86:61 – 69, 2013.

R. Owusu-Apenten. *Introduction to Food Chemistry*. CRC Press, 2005.

G. Özcan-Taşkin. Effect of scale on the draw down of floating solids. *Chemical Engineering Science*, 61(9): 2871 – 2879, 2006.

L. Pakzad, F. Ein-Mozaffari, and P. Chan. Using electrical resistance tomography and computational fluid dynamics modeling to study the formation of cavern in the mixing of pseudoplastic fluids possessing yield stress. *Chemical Engineering Science*, 63(9):2508–2522, 2008.

L. Pakzad, F. Ein-Mozaffari, S. R. Upreti, and A. Lohi. Characterisation of the mixing of non-Newtonian fluids

with a scaba 6SRGT impeller through ERT and CFD. *The Canadian Journal of Chemical Engineering*, 91 (1):90–100, 2013.

S. Palzer. The effect of glass transition on the desired and undesired agglomeration of amorphous food powders. *Chemical Engineering Science*, 60(14):3959 – 3968, 2005.

S. Palzer. Chapter 13: Agglomeration of dehydrated consumer foods. In A. D. Salman, M. J. Hounslow, and J. Seville, editors, *Handbook of Powder Technology: Granulation*. Elsevier, 2007.

S. Palzer. Influence of material properties on the agglomeration of water-soluble amorphous particles. *Powder Technology*, 189(2):318 – 326, 2009.

S. Palzer. Agglomeration of pharmaceutical, detergent, chemical and food powders — similarities and differences of materials and processes. *Powder Technology*, 206(1–2):2–17, 2011.

S. Palzer. Plenary lecture: Food structures for nutrition, health and wellness. In *Proceedings of the 6th International Workshop on Granulation, Sheffield, UK*, 2013.

S. Palzer, C. Dubois, and A. Gianfrancesco. Generation of product structures during drying of food products. *Drying Technology*, 30(1):97–105, 2012.

J. Parada and J. Aguilera. Food microstructure affects the bioavailability of several nutrients. *Journal of Food Science*, 72(2):R21–R32, 2007.

D. Park, J. Imm, and K. Ku. Improved dispersibility of green tea powder by microparticulation and formulation. *Journal of Food Science*, 66(6):793–798, 2001.

A. Parker, F. Vigouroux, and W. Reed. Dissolution kinetics of polymer powders. *Fluid Mechanics and Transport Phenomena*, 46(7):1290–1299, 2000.

D. F. Parsons, M. Boström, P. L. Nostro, and B. W. Ninham. Hofmeister effects: interplay of hydration, nonelectrostatic potentials, and ion size. *Physical Chemistry Chemical Physics*, 13:12352—12367, 2011.

K. S. Parvathy, N. S. Susheelamma, and R. N. Tharanathan. Hydration characteristics of guar gum samples and their fractions. *Food Hydrocolloids*, 21(4):630 – 637, 2007.

E. Paul, V. Atlemo-Obeng, and S. Kresta. *Handbook of Industrial Mixing: Science and Practice*. John Wiley & Sons, Inc., 2004.

S. Peda, M. Smieszek, C. Stollberg, and P. Ay. Interpretation of FBRM and 3D ORM SMF data via simulated nucleation and crystal growth. In *Proceedings of the 17th International Workshop on Industrial Crystallization, Rouen*, 2010.

S. Peda, U. Bröckel, P. Ay, and C. Stollberg. Anwendbarkeit der Lasermessverfahren FBRM und 3D ORM SMF in Batch-Kristallisationen. *Chemie Ingenieur Technik*, 83(4):558 – 562, 2011.

L. M. Pegram and M. T. Record. Hofmeister salt effects on surface tension arise from partitioning of anions and cations between bulk water and the air–water interface. *The Journal of Physical Chemistry B*, 111(19): 5411–5417, 2007.

L. M. Pegram, T. Wendorff, R. Erdmann, I. Shkel, D. Bellissimo, D. J. Felitsky, and M. T. Record. Why Hofmeister effects of many salts favor protein folding but not DNA helix formation. *Proceedings of the National Academy of Sciences*, 107(17):7716–7721, 2010.

Y. Peng, M. Mantle, A. Sederman, M. Ramaioli, E. Hughes, and L. Gladden. Quantitative ultra-fast MRI of powder dispersion. In *Proceedings of the 12th International Conference on Magnetic Resonance Microscopy, Cambridge*, 2013.

J. S. Pérez, E. R. Porcel, J. C. López, J. F. Sevilla, and Y. Chisti. Shear rate in stirred tank and bubble column bioreactors. *Chemical Engineering Journal*, 124(1–3):1 – 5, 2006.

W. Pietsch. *Agglomeration Processes*. Wiley-VCH, 2002.

V. J. Pinfield. Advances in ultrasonic monitoring of oil-in-water emulsions. *Food Hydrocolloids*, 42, Part 1:48 – 55, 2014.

N. Potes, J. P. Kerry, and Y. H. Roos. Additivity of water sorption, alpha-relaxations and crystallization inhibition in lactose–maltodextrin systems. *Carbohydrate Polymers*, 89(4):1050 – 1059, 2012.

M. Povey, M. Golding, D. Higgs, and Y. Wang. Ultrasonic spectroscopy studies of casein in water. *International Dairy Journal*, 9(3–6):299–303, 1999.

L. Pray and R. Scott. US Patent 5264228 Preparation of compositions for making cocoa beverages, 1993.

M. X. Quintanilla-Carvajal, H. Hernández-Sánchez, L. Alamilla-Beltrán, G. Zepeda-Vallejo, M. E. Jaramillo-Flores, M. de Jesús Perea-Flores, A. Jimenez-Aparicio, and G. F. Gutiérrez-López. Effects of microfluidisation process on the amounts and distribution of encapsulated and non-encapsulated α-tocopherol microcapsules obtained by spray drying. *Food Research International*, 63, Part A:2 – 8, 2014.

M. Rao. *Rheology of Fluids and Semisolid Foods: Principles and Applications*. Springer, 2007.

P. S. Raux, H. Cockenpot, M. Ramaioli, D. Quéré, and C. Clanet. Wicking in a powder. *Langmuir*, 29(11): 3636–3644, 2013.

J. Ren, W. Wang, S. Lu, J. Shen, and F. Tang. Characteristics of dispersion behavior of fine particles in different liquid media. *Powder Technology*, 137(1–2):91 – 94, 2003.

B. Richard, M. Toubal, J.-F. Le Page, G. Nassar, E. Radziszewski, B. Nongaillard, P. Debreyne, P. Schuck, R. Jeantet, and G. Delaplace. Ultrasound tests in a stirred vessel to evaluate the reconstitution ability of dairy powders. *Innovative Food Science & Emerging Technologies*, 16:233–242, 2012.

B. Richard, J. L. Page, P. Schuck, C. Andre, R. Jeantet, and G. Delaplace. Towards a better control of dairy powder rehydration processes. *International Dairy Journal*, 31(1):18 – 28, 2013.

F. Rieger, P. Ditl, and O. Havelkova. Suspension of solid particles – concentration profiles and particle layer on the vessel bottom. In *Proceedings of the 6th European Conference on Mixing, Pavia, Italy*, 1988.

C. D. Rielly and J. Gimbun. Chapter 8: Computational fluid mixing. In P. Cullen, editor, *Food Mixing: Principles and Applications*. Wiley-Blackwell, 2009.

D. Ring, J. Oliveira, and A. Crean. Evaluation of the influence of granulation processing parameters on the granule properties and dissolution characteristics of a modified release drug. *Advanced Powder Technology*, 22(2):245 – 252, 2011.

A. Rogers. US Patent 0070354 A1 Instantized whey protein concentrate/isolate with egg lecithin, 2011.

S. Rogers, Y. Fang, S. Qi Lin, C. Selomulya, and X. Dong Chen. A monodisperse spray dryer for milk powder: Modelling the formation of insoluble material. *Chemical Engineering Science*, 71:75–84, 2012.

Y. Rong, M. Sillick, and C. Gregson. Determination of dextrose equivalent value and number average molecular weight of maltodextrin by osmometry. *Journal of Food Science*, 74(1):C33–C40, 2009.

Y. Roos. Glass transition temperature and its relevance in food processing. *Annual Review of Food Science and Technology*, 1(1):469–496, 2010.

T. Rosanke and C. Brown. Chapter 7: Dissolution studies. In C. Riley and T. Rosanke, editors, *Development and validation of analytical methods*. Elsevier Science B.V., 1996.

M. Roustan, J. Pharamond, and A. Line. Agitation. Mélange. Concepts théorique de base. *Technique de l'ingénieur*, J 3 800:1 – 22, 1999.

H. Rumpf. Zur Theorie der Zugfestigkeit von Agglomeraten bei Kraftübertragung an Kontaktpunkten. *Chemie-Ingenieur-Technik*, 42:538–540, 1970.

J. Rushton, E. Costich, and H. Everett. Power characteristics of mixing impellers. *Chemical Engineering Progress*, 46(8):395–476, 1950.

R. Saggin and J. Couplan. Ultrasonic monitoring of powder dissolution. *Journal of Food Science*, 67(4): 1473–1477, 2002.

I. Saguy and A. Marabi. Rehydration of dried food particulates. In D. Heldman and C. Moraru, editors, *Encyclopedia of agricultural, food, and biological engineering, Second Edition*. Taylor & Francis, 2011.

D. Saha and S. Bhattacharya. Hydrocolloids as thickening and gelling agents in food: a critical review. *Journal of Food Science and Technology*, 47(6):587–597, 2010.

I. Schmitz-Schug, A. Gianfrancesco, U. Kulozik, and P. Foerst. Physical state, molecular mobility and chemical stability of powdered dairy formulations. *Food Research International*, 53(1):268 – 277, 2013.

C. Schober and J. Fitzpatrick. Effect of vortex formation on powder sinkability for reconstituting milk powders in water to high solids content in a stirred-tank. *Journal of Food Engineering*, 71(1):1–8, 2005.

E. Schokker, J. Church, J. Mata, E. Gilbert, A. Puvanenthiran, and P. Udabage. Reconstitution properties of micellar casein powder: Effects of composition and storage. *International Dairy Journal*, 21(11):877–886, 2011.

H. Schubert. Instantization of powdered food products. *International Chemical Engineering*, 33(1):28–45, 1993.

P. Schuck, A. Davenel, F. Mariette, V. Briard, S. Méjean, and M. Piot. Rehydration of casein powders: effects

of added mineral salts and salt addition methods on water transfer. *International Dairy Journal*, 12(1): 51–57, 2002.

P. Schuck, S. Mejean, A. Dolivet, C. Gaiani, S. Banon, J. Scher, and R. Jeantet. Water transfer during rehydration of micellar casein powders. *Lait*, 87(4–5):425–432, 2007.

P. Schuck, R. Jeantet, and A. Dolivet. *Analytical Methods for Food and Dairy Powders*. Wiley-Blackwell, 2012.

J. Selamat, N. Hussin, A. M. Zain, and Y. B. C. Man. Effects of alkalized cocoa powder and soy lecithin on physical characteristics of chocolate beverage powders. *Journal of Food Processing and Preservation*, 22(3): 241–254, 1998.

M. Sharifi and B. Young. 3-Dimensional spatial monitoring of tanks for the milk processing industry using Electrical Resistance Tomography. *Journal of Food Engineering*, 105:312–319, 2011.

M. Sharifi and B. Young. Electrical resistance tomography (ERT) applications to chemical engineering. *Chemical Engineering Research and Design*, 91(9):1625 – 1645, 2013.

A. Sharma, A. H. Jana, and R. S. Chavan. Functionality of milk powders and milk-based powders for end use applications—a review. *Comprehensive Reviews in Food Science and Food Safety*, 11(5):518–528, 2012.

Y. Shimada, Y. Yonezawa, H. Sunada, R. Nonaka, K. Katou, and H. Morishita. Development of an apparatus for measuring adhesive force between fine particles. *KONA Powder and Particle Journal*, (20):223 – 230, 2002.

V. Shirhatti, M. Wang, and R. Williams. Visualisation of dispersion, dissolution and settling of powders in a stirred mixing vessel by Electrical Resistance Tomography. In 4^{th} *World Congress on Industrial Process Tomography*, Aizu, Japan, 2005.

T. Shittu and M. Lawal. Factors affecting instant properties of powdered cocoa beverages. *Food Chemistry*, 100(1):91–98, 2007.

J. Siepmann and F. Siepmann. Mathematical modeling of drug delivery. *International Journal of Pharmaceutics*, 364(2):328 – 343, 2008.

V. Sikand, P. S. Tong, and J. Walker. Effect of adding salt during the diafiltration step of milk protein concentrate powder manufacture on mineral and soluble protein composition. *Dairy Science & Technology*, 93(4–5):401–413, 2013.

S. Simons, J. Seville, and M. Adams. An analysis of the rupture energy of pendular liquid bridges. *Chemical Engineering Science*, 49(14):2331 – 2339, 1994.

H. Singh and J. Flanagan. Chapter 26: Milk proteins. In Y. Hui, editor, *Handbook of Food Science, Technology, and Engineering*. CRC Press, 2006.

H. Singh and A. Ye. Controlling milk protein interactions to enhance the reconstitution properties of whole milk powders — a minireview. *Dairy Science & Technology*, 90(2–3):123–136, 2010.

P. Singh, D. Joseph, S. Gurupatham, B. Dalal, and S. Nudurupati. Spontaneous dispersion of particles

sprinkled onto a liquid surface. In *Proceedings of the National Academy of Sciences*, pages 19761–19764, 2009.

P. Singh, D. Joseph, and N. Aubry. Dispersion and attraction of particles floating on fluid-liquid surfaces. *Soft Matter*, 6(18):4310–4325, 2010.

K. Smith. *Dried Dairy Ingredients.* Wisconsin Center for Dairy Research, 2008.

P. Somasundaran, S. C. Mehta, X. Yu, and S. Krishnakumar. Chapter 6: Colloid systems and interfaces stability of dispersions through polymer and surfactant adsorption. In K. Birdi, editor, *Handbook of Surface and Colloid Chemistry: Third Edition.* Taylor & Francis, 2009.

H. Swaisgood. Chapter 15: Characteristics of milk. In S. Damodaran, K. Parkin, and O. Fennema, editors, *Fennema's Food Chemistry: Fourth Edition.* CRC Press, 2007.

O. Syll, B. Richard, J. F. Willart, M. Descamps, P. Schuck, G. Delaplace, and R. Jeantet. Rehydration behaviour and ageing of dairy powders assessed by calorimetric measurements. *Innovative Food Science & Emerging Technologies*, 14:139 – 145, 2012.

A. S. Szczesniak. Texture is a sensory property. *Food Quality and Preference*, 13(4):215 – 225, 2002.

K. Szulc and A. Lenart. Surface modification of dairy powders: Effects of fluid-bed agglomeration and coating. *International Dairy Journal*, 33(1):55 – 61, 2013.

T. Tadros. Interparticle interactions in concentrated suspensions and their bulk (rheological) properties. *Advances in Colloid and Interface Science*, 168(1–2):263–277, 2011.

P. Tahvildarian, H. Ng, M. D'Amato, S. Drappel, F. Ein-Mozaffari, and S. R. Upreti. Using electrical resistance tomography images to characterize the mixing of micron-sized polymeric particles in a slurry reactor. *Chemical Engineering Journal*, 172(1):517 – 525, 2011.

C. Takeiti, T. Kieckbusch, and F. Collares-Queiroz. Optimization of the jet steam instantizing process of commercial maltodextrins powders. *Journal of Food Engineering*, 86(3):444 – 452, 2008.

W. Tam. MEng thesis: Influence of material properties on the dispersing behaviour of bulk food powders in a liquid (University of Sheffield), 2013.

A. Tamime. *Dairy powders and concentrated products.* Wiley-Blackwell, 2009.

G. M. Tavares, T. Croguennec, A. F. Carvalho, and S. Bouhallab. Milk proteins as encapsulation devices and delivery vehicles: Applications and trends. *Trends in Food Science & Technology*, 37(1):5 – 20, 2014.

K. Terada, H. Kitano, Y. Yoshihashi, and E. Yonemochi. Quantitative correlation between initial dissolution rate and heat of solution of drug. *Pharmaceutical Research*, 17(8):920–924, 2000.

P. Tervasmäki, J. Tiihonen, and H. Ojamo. Comparison of solids suspension criteria based on electrical impedance tomography and visual measurements. *Chemical Engineering Science*, 116:128 – 135, 2014.

M. E. C. Thomas, J. Scher, S. Desobry-Banon, and S. Desorby. Milk powders ageing: Effect on physical and functional properties. *Critical Reviews in Food Science and Nutrition*, 44(5):297–322, 2004.

R. W. Thring and M. F. Edwards. An experimental investigation into the complete suspension of floating solids in an agitated tank. *Industrial & Engineering Chemistry Research*, 29(4):676–682, 1990.

Y. Tian, N. Fu, W. D. Wu, D. Zhu, J. Huang, S. Yun, and X. D. Chen. Effects of co-spray drying of surfactants with high solids milk on milk powder wettability. *Food Bioprocess Technology*, 7:3121–3135, 2014.

A. Tinke, R. Govoreanu, I. Weuts, K. Vanhoutte, and D. D. Smaele. A review of underlying fundamentals in a wet dispersion size analysis of powders. *Powder Technology*, 196(2):102 – 114, 2009.

B. Tiwari and P. Cullen. Chapter 3: Kinematics of flow and mixing mechanisms. In P. Cullen, editor, *Food Mixing: Principles and Applications*. Wiley-Blackwell, 2009.

K. To, J. Mitchell, S. Hill, L. Bardon, and P. Matthews. Measurements of hydration of polysaccharides. *Food Hydrocolloids*, 8:243–249, 1994.

A. T. Tok, X. Goh, W. K. Ng, and R. B. H. Tan. Monitoring granulation rate processes using three PAT tools in a pilot-scale fluidized bed. *American Association of Pharmaceutical Scientists PharmSciTech*, 9(4): 1083–1091, 2008.

K. Tsinman, A. Avdeef, O. Tsinman, and D. Voloboy. Powder dissolution method for estimating rotating disk intrinsic dissolution rates of low solubility drugs. *Pharmaceutical Research*, 26(9):2093–2100, 2009.

P. Tyle. Effect of size, shape and hardness of particles in suspension on oral texture and palatability. *Acta Psychol (Amst)*, 84(1):111–118, 1993.

P. Udabage, A. Puvanenthiran, J. Yoo, C. Versteeg, and M. Augustin. Modified water solubility of milk protein concentrate powders through the application of static high pressure treatment. *Journal of Dairy Research*, 79(1):76–83, 2012.

V. Vaclavik and E. Christian. *Essentials of Food Science*. Springer, 2008.

S. Vallar, D. Houivet, J. E. Fallah, D. Kervadec, and J.-M. Haussonne. Oxide slurries stability and powders dispersion: optimization with zeta potential and rheological measurements. *Journal of the European Ceramic Society*, 19(6–7):1017 – 1021, 1999.

J. van Duynhoven, G. Goudappel, W. Weglarz, C. Windt, P. Cabrer, A. Mohoric, and H. van As. Chapter 21. Noninvasive assessment of moisture migration in food products by MRI. In S. Codd and J. Seymour, editors, *Magnetic Resonance Microscopy: Spatially Resolved NMR techniques and applications*. Wiley-VCH, Weinheim, 2009.

C. van Oss. *Interfacial Forces in Aqueous Media, Second Edition*. CRC Press, 2006.

D. Vella and H. Huppert. The waterlogging of floating objects. *Journal of Fluid Mechanics*, 585:245–254, 2007.

D. Vella and L. Mahadevan. The "Cheerios effect". *American Journal of Physics*, 73(9):817–825, 2005.

D. Vella and P. D. Metcalfe. Surface tension dominated impact. *Physics of Fluids*, 19(7):072108–1–11, 2007.

D. Vella, D.-G. Lee, and H.-Y. Kim. The load supported by small floating objects. *Langmuir*, 22(14):5979–5981, 2006.

B. C. Venneker, J. J. Derksen, and H. E. V. den Akker. Turbulent flow of shear-thinning liquids in stirred tanks—the effects of Reynolds number and flow index. *Chemical Engineering Research and Design*, 88(7): 827 – 843, 2010.

F. Vergeldt, G. van Dalen, A. Duijster, A. Voda, S. Khalloufi, L. van Vliet, H. V. As, J. van Duynhoven, and R. van der Sman. Rehydration kinetics of freeze-dried carrots. *Innovative Food Science & Emerging Technologies*, 24:40 – 47, 2014.

E. Verwey and J. Overbeek. *Theory of the stability of lyophobic colloids*. Elsevier, 1948.

M. L. Vignolles, C. Lopez, M. N. Madec, J. J. Ehrhardt, S. Méjean, P. Schuck, and R. Jeantet. Fat properties during homogenization, spray-drying, and storage affect the physical properties of dairy powders. *Journal of Dairy Science*, 92(1):58–70, 2009.

F. Vissotto, L. Jorge, G. Makita, M. Rodrigues, and F. Menegalli. Influence of the process parameters and sugar granulometry on cocoa beverage powder steam agglomeration. *Journal of Food Engineering*, 97(3): 283 – 291, 2010.

F. Z. Vissotto, F. M. Montenegro, J. M. dos Santos, and S. J. R. de Oliveira. Avaliação da influência dos processos de lecitinação e de aglomeração nas propriedades físicas de achocolatado em pó. *Revista Ciência e Tecnologia de Alimentos*, 26(3):666–671, 2006.

T. Vu, L. Galet, J. Fages, and D. Oulahna. Improving the dispersion kinetics of a cocoa powder by size enlargement. *Powder Technology*, 130(1):400–406, 2003.

G. Vuataz. The phase diagram of milk: a new tool for optimising the drying process. *Lait*, 82(4):485–500, 2002.

Y. Waghmare, R. Falk, L. Graham, and V. Koganti. Drawdown of floating solids in stirred tanks: Scale-up study using CFD modeling. *International Journal of Pharmaceutics*, 418(2):243 – 253, 2011.

P. Walstra. *Physical Chemistry of Foods*. Marcel Dekker, Inc., 2003.

P. Walstra, J. Wouters, and T. Geurts. *Dairy Science and Technology: Second Edition*. Taylor & Francis, 2006.

J. Wang and D. Flanagan. Chapter 13: Fundamentals of dissolution. In Y. Qiu, Y. Chen, and G. Zhang, editors, *Developing Oral Dosage Forms: Pharmaceutical Theory and Practice*. Academic Press, 2009.

J. Wang and D. R. Flanagan. General solution for diffusion-controlled dissolution of spherical particles. 2. Evaluation of experimental data. *Journal of Pharmaceutical Sciences*, 91(2):534–542, 2002.

Q. Wang, P. Ellis, and S. Ross-Murphy. Dissolution kinetics of guar gum powders–II. Effects of concentration and molecular weight. *Carbohydrate Polymers*, 53(1):75 – 83, 2003.

Q. Wang, P. R. Ellis, and S. B. Ross-Murphy. Dissolution kinetics of water-soluble polymers: The guar gum paradigm. *Carbohydrate Polymers*, 74(3):519 – 526, 2008a.

Z. Wang, G. Narsimhan, and D. Kim. Characterization of the effect of food emulsifiers on contact angle

and dispersibility of lipid coated neutrally buoyant particles. *LWT - Food Science and Technology*, 41(7): 1232–1238, 2008b.

E. Washburn. The dynamics of capillary flow. *The Physical Review*, 17(3):273 – 283, 1921.

K. Washino, H. Tan, A. Salman, and M. Hounslow. Direct numerical simulation of solid–liquid–gas three-phase flow: Fluid–solid interaction. *Powder Technology*, 206(1–2):161 – 169, 2011.

C. Weiler, M. Wolkenhauer, M. Trunk, and P. Langguth. New model describing the total dispersion of dry powder agglomerates. *Powder Technology*, 203(2):248 – 253, 2010.

R. N. Wenzel. Resistance of solid surfaces to wetting by water. *Industrial & Engineering Chemistry*, 28(8): 988–994, 1936.

R. Weser, S. Wöckel, B. Wessely, and U. Hempel. Particle characterisation in highly concentrated dispersions using ultrasonic backscattering method. *Ultrasonics*, 53(3):706 – 716, 2013.

R. Weser, S. Wöckel, B. Wessely, U. Steinmann, F. Babick, and M. Stintz. Ultrasonic backscattering method for *in situ* characterisation of concentrated dispersions. *Powder Technology*, 268:177 – 190, 2014.

V. Westergaard. *Milk powder technology: Evaporation and spray drying*. Niro A/S, 2004.

J. Whelan, E. Murphy, A. Pearson, P. Jeffers, P. Kieran, S. McDonnell, and B. Glennon. Use of focused beam reflectance measurement (FBRM) for monitoring changes in biomass concentration. *Bioprocess and Biosystems Engineering*, pages 1–13, 2012.

WHO. *Sodium in Drinking-water. Background document for development of WHO Guidelines for Drinking-water Quality*. World Health Organization (United Nations), 2003.

D. Wilson, S. Wren, and G. Reynolds. Linking dissolution to disintegration in immediate release tablets using image analysis and a population balance modelling approach. *Pharmaceutical Research*, 29(1):198–208, 2012.

E. Windhab. Chapter 13: Tempering. In S. Beckett, editor, *Industrial Chocolate Manufacture and Use*. Blackwell Publishing Ltd., 2009.

J. Wu, Y. Zhu, and L. Pullum. Impeller geometry effect on velocity and solids suspension. *Chemical Engineering Research and Design*, 79(8):989 – 997, 2001.

W. D. Wu, W. Liu, T. Gengenbach, M. W. Woo, C. Selomulya, X. D. Chen, and M. Weeks. Towards spray drying of high solids dairy liquid: Effects of feed solid content on particle structure and functionality. *Journal of Food Engineering*, 123:130 – 135, 2014.

E. Wynn. Relationship between particle-size and chord-length distributions in focused beam reflectance measurement: stability of direct inversion and weighting. *Powder Technology*, 133(1–3):125 – 133, 2003.

N. Yazdanpanah and T. A. Langrish. Comparative study of deteriorative changes in the ageing of milk powder. *Journal of Food Engineering*, 114(1):14 – 21, 2013.

T. Young. An essay on the cohesion of fluids. *Philosophical Transactions of the Royal Society of London*, 95: 65 – 87, 1805.

U. Yucel and J. N. Coupland. Ultrasonic characterization of lactose dissolution. *Journal of Food Engineering*, 98(1):28 – 33, 2010.

J. Zhao, M. Wang, B. Dong, Q. Feng, and C. Xu. Monitoring the polymorphic transformation of imidacloprid using *in situ* FBRM and PVM. *Organic Process Research & Development*, 17(3):375–381, 2013.

H.-X. Zhou. Interactions of macromolecules with salt ions: An electrostatic theory for the Hofmeister effect. *PROTEINS: Structure, Function, and Bioinformatics*, 61:69–78, 2005.

P. Zhou and T. P. Labuza. Effect of water content on glass transition and protein aggregation of whey protein powders during short-term storage. *Food Biophysics*, 2(2–3):108–116, 2007.

L. Ziyani and N. Fatah. Use of experimental designs to optimize fluidized bed granulation of maltodextrin. *Advanced Powder Technology*, 25(3):1069 – 1075, 2014.

M. Zlokarnik. Trombentiefe beim Rühren in unbewehrten Behältern. *Chemie Ingenieur Technik*, 43:1028 – 1030, 1971.

T. Zwietering. Suspending of solid particles in liquid by agitators. *Chemical Engineering Science*, 8(3–4): 244–253, 1958.